

**AMINO-TERMINAL REGULATION OF K<sub>v</sub> CHANNEL INACTIVATION**

by

HARLEY TAKATSUNA KURATA

B.Sc. (Hons.), University of British Columbia, 1999

A THESIS SUBMITTED IN PARTIAL FULFILLMENT OF  
THE REQUIREMENTS FOR THE DEGREE OF

DOCTOR OF PHILOSOPHY

in

THE FACULTY OF MEDICINE

Department of Physiology

We accept this thesis as conforming to the required standard

THE UNIVERSITY OF BRITISH COLUMBIA

July, 2004

© Harley T. Kurata, 2004

## ABSTRACT

C-type inactivation of Kv channels is thought to involve conformational changes in the outer pore of the channel, culminating in partial constriction of the selectivity filter. Through biophysical characterization of an N-terminally truncated form of Kv1.5, we have demonstrated that the cytoplasmic N-terminus exerts an important regulatory role in this process. Deletion of the N-terminus significantly alters the inactivation properties of Kv1.5, resulting most remarkably in a U-shaped inactivation-voltage relationship, excessive cumulative inactivation (in which more inactivation is observed during multiple repetitive depolarization than during a continuous pulse of the same duration), and markedly enhanced voltage-dependence of recovery from inactivation. These changes were attributed to a shift in the state-dependence of inactivation in N-terminally truncated forms of Kv1.5, suggesting that the N-terminus limits the propensity for closed-state inactivation in full-length channels. Using a deletion scan of the Kv1.5 N-terminus, and analysis of several chimeric channels, we have delimited this effect to the T1 domain, a segment of the N-terminus that is very highly conserved among Kv channels.

Interactions between the Kv1.4 N-terminal inactivation domain and the pore of Kv channels have also been investigated. In experiments using  $\text{Na}^+$  as the primary permeant ion, Kv1.4 and Kv1.5 channels exhibit a pronounced  $\text{Na}^+$  tail current during recovery from C-type inactivation, as channels transiently occupy one or more states that are highly permeable to  $\text{Na}^+$ . In the presence of the Kv1.4 N-terminal inactivation domain, or intracellular quaternary ammonium ions, the properties of this C-type inactivated tail current are dramatically altered: the magnitude of inward tail current is reduced, and the kinetics of tail current rise and decay are slowed considerably. These observations parallel previously

documented effects of the N-terminal inactivation ball on deactivation of open channels. These effects can be explained by stable binding of the N-terminal inactivation domain to C-type inactivated channels, therefore we conclude that the inner pore remains a patent receptor for the inactivation ball after the onset of C-type inactivation. These results constrain the view of conformational changes that take place during C-type inactivation at the inner pore of Kv channels.

## TABLE OF CONTENTS

<b>ABSTRACT .....</b>	<b>II</b>
<b>TABLE OF CONTENTS .....</b>	<b>IV</b>
<b>LIST OF FIGURES.....</b>	<b>VII</b>
<b>LIST OF TABLES.....</b>	<b>VIII</b>
<b>ABBREVIATIONS.....</b>	<b>VIII</b>
<b>ACKNOWLEDGEMENTS .....</b>	<b>IX</b>
<b>PREFACE .....</b>	<b>X</b>
<b>CHAPTER 1: INTRODUCTION.....</b>	<b>1</b>
<b>I:OVERVIEW.....</b>	<b>2</b>
<b>II:GENERAL STRUCTURE .....</b>	<b>3</b>
<i>Broad features of Kv channel architecture .....</i>	<i>3</i>
<i>Macromolecular view of Kv channel structure .....</i>	<i>5</i>
<b>III: DETAILED FEATURES OF K<sup>+</sup> CHANNEL PORES .....</b>	<b>6</b>
<i>KcsA- A prokaryotic potassium-selective channel .....</i>	<i>6</i>
<i>Conformational changes of the pore during activation .....</i>	<i>11</i>
<i>Voltage-dependent gating .....</i>	<i>15</i>
<b>IV: MECHANISMS OF Kv CHANNEL INACTIVATION.....</b>	<b>17</b>
<i>N-type inactivation.....</i>	<i>18</i>
<i>Structural determinants of N-type inactivation .....</i>	<i>19</i>
<i>C-type inactivation.....</i>	<i>22</i>
<i>Alternative inactivation phenotypes.....</i>	<i>25</i>
<i>Synergistic interactions of N-type and C-type inactivation.....</i>	<i>27</i>
<i>Allosteric coupling of N-type and C-type mechanisms.....</i>	<i>28</i>
<i>The Role of the Selectivity Filter in C-type Inactivation .....</i>	<i>29</i>
<i>Conformational changes underlying C-type inactivation .....</i>	<i>33</i>
<i>A structural conception of conformational changes during C-type inactivation .....</i>	<i>35</i>
<i>Voltage-sensor interactions with the pore during C-type inactivation .....</i>	<i>37</i>
<i>Summary .....</i>	<i>40</i>
<b>V: Kv CHANNEL REGULATION BY THE CYTOPLASMIC T1 DOMAIN .....</b>	<b>41</b>
<i>Detailed structures of Kv channel T1 domains .....</i>	<i>41</i>
<i>Roles of the T1 domain in channel assembly .....</i>	<i>43</i>
<i>Gating effects of the T1 domain .....</i>	<i>45</i>
<b>VI: SCOPE OF THESIS INVESTIGATION .....</b>	<b>47</b>
<b>CHAPTER 2: MATERIALS AND METHODS .....</b>	<b>50</b>
<i>Cell preparation and transfection.....</i>	<i>51</i>
<i>Recording Solutions .....</i>	<i>52</i>
<i>Electrophysiological procedures.....</i>	<i>53</i>
<i>Data analysis and modeling.....</i>	<i>53</i>
<i>Molecular Biology and Channel Mutations .....</i>	<i>54</i>
<i>N-terminal deletions of Kv1.5 .....</i>	<i>54</i>
<i>N-terminal deletions of Kv2.1 .....</i>	<i>55</i>
<i>Kv1.XN/Kv1.5 Chimeric Constructs.....</i>	<i>55</i>
<i>Kv1.5/Kv2.1 Chimeric Constructs.....</i>	<i>56</i>
<i>Site-directed mutagenesis.....</i>	<i>57</i>

<b>CHAPTER 3: ALTERED STATE-DEPENDENCE OF SLOW INACTIVATION IN LONG AND SHORT FORMS OF KV1.5 .....</b>	<b>58</b>
CHAPTER SUMMARY .....	59
BACKGROUND .....	60
RESULTS .....	62
<i>Amino acids 1-209 modulate the activation properties of Kv1.5 .....</i>	<i>62</i>
<i>Inactivation-voltage relationship of Kv1.5 <math>\Delta</math>N209.....</i>	<i>65</i>
<i>Closed-state inactivation and excessive cumulative inactivation.....</i>	<i>70</i>
<i>Voltage-dependent recovery from inactivation in Kv1.5<math>\Delta</math>N209.....</i>	<i>77</i>
<i>Excessive inactivation of Kv1.5<math>\Delta</math>N209 under cardiac action potential clamp.....</i>	<i>79</i>
<i>Kinetic Models of Inactivation: Models Describing a U-shaped Inactivation-Voltage Relationship .....</i>	<i>81</i>
<i>Building a kinetic model of inactivation in Kv1.5 and Kv1.5<math>\Delta</math>N209.....</i>	<i>84</i>
<i>Incorporating the U-shaped voltage-dependence of inactivation .....</i>	<i>86</i>
<i>Simulation of excessive cumulative inactivation .....</i>	<i>89</i>
DISCUSSION.....	92
<i>Altered state-dependence of inactivation in the short form of human Kv1.5 .....</i>	<i>92</i>
<i>Model of Kv1.5<math>\Delta</math>N209 inactivation.....</i>	<i>95</i>
<i>Mechanisms of closed-state inactivation.....</i>	<i>98</i>
<i>Conclusions.....</i>	<i>99</i>
<b>CHAPTER 4: AMINO-TERMINAL REGULATION OF SLOW INACTIVATION IN VOLTAGE-GATED K<sup>+</sup> CHANNELS .....</b>	<b>100</b>
CHAPTER SUMMARY .....	101
BACKGROUND .....	102
RESULTS .....	104
<i>Recapitulation of C-type and U-type inactivation phenotypes in Kv1.5 .....</i>	<i>104</i>
<i>Modulation of inactivation by extracellular cations .....</i>	<i>105</i>
<i>The Kv1.5 T1 domain influences the slow inactivation phenotype.....</i>	<i>112</i>
<i>N-termini of Kv1.1 and Kv1.3 channels restore wild-type inactivation in Kv1.5.....</i>	<i>116</i>
<i>Disruption of the intersubunit T1 interface influences slow inactivation in Kv1.5.....</i>	<i>118</i>
<i>Reciprocal influences of the Kv2.1 and Kv1.5 N-termini.....</i>	<i>120</i>
DISCUSSION.....	123
<i>Multiple inactivation phenotypes in Kv1 channels.....</i>	<i>123</i>
<i>N-terminal regulation of inactivation in other Kv channels.....</i>	<i>126</i>
<i>Coupling mechanisms between the T1 and transmembrane domains.....</i>	<i>127</i>
<i>Conclusions.....</i>	<i>128</i>
<b>CHAPTER 5: N-TERMINAL INACTIVATION DOMAIN BINDING TO C-TYPE INACTIVATED KV CHANNELS.....</b>	<b>129</b>
CHAPTER SUMMARY .....	130
BACKGROUND .....	131
RESULTS .....	133
<i>Multiple mechanisms of K<sup>+</sup> channel inactivation.....</i>	<i>133</i>
<i>Inactivation and recovery in Na<sup>+</sup> conditions .....</i>	<i>135</i>
<i>Two types of recovery tails in Kv channels.....</i>	<i>136</i>
<i>Slowing of recovery tails by the N-terminal inactivation domain .....</i>	<i>139</i>
<i>Blockade of inward Na<sup>+</sup> tails by the N-terminal inactivation domain .....</i>	<i>142</i>
<i>Delayed peak of the slow Na<sup>+</sup> tail.....</i>	<i>143</i>
<i>Common effects of the N-terminal inactivation domain in Kv1.5 and Kv1.4.....</i>	<i>145</i>
<i>C-type inactivation deficient channels exhibit incomplete N-type inactivation in Na<sup>+</sup> recording conditions .....</i>	<i>148</i>
<i>Summary and model of the slow Na<sup>+</sup> tail.....</i>	<i>155</i>
<i>Simulation of tail currents in C-type deficient channels .....</i>	<i>158</i>
<i>Interactions of the N-terminal inactivation domain with the R state.....</i>	<i>161</i>

DISCUSSION.....	164
<i>Mechanism of slowing of the Na<sup>+</sup> tail by the N-terminal inactivation domain</i> .....	164
<i>Inactivation ball binding to the C-type inactivated state – structural considerations</i> .....	165
<i>Inactivation domain binding to the C-type inactivated state – gating considerations</i> .....	167
<i>Kinetic effects of binding of the N-terminal inactivation domain</i> .....	169
<i>Conclusion</i> .....	171
<b>CHAPTER 6: CONCLUSIONS AND GENERAL DISCUSSION.....</b>	<b>172</b>
<i>Regulation of state-dependence of inactivation by the Kv1.5 N-terminus</i> .....	173
<i>Potential physiological roles of N-terminally truncated channels</i> .....	173
<i>Regulation of channel gating by the T1 domain</i> .....	175
<i>Structural determinants of state-dependent inactivation</i> .....	181
<i>Mechanisms of Kv Channel Slow Inactivation</i> .....	183
<i>N-terminal regulation of Kv channel expression</i> .....	186
<i>Conformational changes of the inner pore during C-type inactivation</i> .....	187
<i>Steps in recovery from inactivation</i> .....	191
<i>Summary</i> .....	192
<b>APPENDICES.....</b>	<b>193</b>
APPENDIX A1: SOURCE CODE FOR CLOSED-STATE INACTIVATION MODEL OF Kv1.5 AND Kv1.5ΔN209 .....	194
APPENDIX A2: SOURCE CODE FOR MODEL OF NA <sup>+</sup> TAILS THROUGH Kv1.5.....	196
<b>REFERENCES .....</b>	<b>199</b>

## LIST OF FIGURES

Figure 1.1. Overview of Kv channel structure.....	4
Figure 1.2. Detailed features of the KcsA channel. ....	8
Figure 1.3. KcsA and MthK structures. ....	12
Figure 1.4. Cartoon representation of N-type inactivation. ....	22
Figure 1.5. Detailed molecular model of extracellular residues involved in C-type inactivation. ....	37
Figure 3.1. Construction of Kv1.5ΔN209.....	63
Figure 3.2. Activation properties of Kv1.5ΔN209.....	64
Figure 3.3. Inactivation properties of Kv1.5ΔN209.....	67
Figure 3.4. Inactivation properties of Kv1.5ΔN209 expressed in Mouse <i>ltk</i> cells.....	69
Figure 3.5. Voltage-dependence of inactivation behavior of full-length Kv1.5, Kv1.5ΔN209 and Kv2.1.....	71
Figure 3.6. Excessive cumulative inactivation in Kv1.5ΔN209. ....	73
Figure 3.7. Excessive cumulative inactivation in Kv1.5ΔN209 depends on pulse duration.....	76
Figure 3.8. Voltage-dependence of recovery from inactivation. ....	78
Figure 3.9. Excessive cumulative inactivation in Kv1.5ΔN209 subjected to a human cardiac action potential clamp.....	80
Figure 3.10. Schematic representation of inactivation in full-length Kv1.5 and Kv1.5ΔN209. ....	84
Figure 3.11. Simulated effects of alterations to closed and open state inactivation rates. ....	88
Figure 3.12. Simulations generated from the kinetic model of inactivation in Kv1.5ΔN209 and full-length Kv1.5.....	91
Figure 4.1. Inactivation properties of Kv1.5, Kv1.5ΔN209, and Kv2.1. ....	105
Figure 4.2. Differential effects of extracellular K <sup>+</sup> on Kv1.5 and Kv1.5ΔN209 inactivation.....	108
Figure 4.3. Inactivation voltage-relationships for full-length Kv1.5 and Kv1.5ΔN209 in K <sup>+</sup> and Cs <sup>+</sup> recording conditions.....	109
Figure 4.4. Effects of extracellular TEA <sup>+</sup> on Kv1.5R487T ΔN209 inactivation. ....	111
Figure 4.5. N-terminal deletion mutants of Kv1.5.....	112
Figure 4.6. Activation and inactivation properties of N-terminal deletion mutants of Kv1.5. ....	115
Figure 4.7. N-termini of Kv1 channels rescue the inactivation properties of full-length Kv1.5.....	117
Figure 4.8. Point mutations at the intersubunit T1 interface influence Kv1.5 inactivation. ....	119
Figure 4.9. The N-termini of Kv1.5 and Kv2.1 exert reciprocal influences on Kv channel inactivation. ....	122
Figure 5.1. Mechanisms of N- and C-type inactivation in K <sup>+</sup> and Na <sup>+</sup> recording conditions. ....	134
Figure 5.2. Two types of recovery tails through Kv channels. ....	138
Figure 5.3. Slowing of Na <sup>+</sup> tail current decay by the Kv1.4 inactivation domain. ....	141
Figure 5.4. Blockade and delay of peak tail current by the Kv1.4 inactivation domain. ....	144
Figure 5.5. Common effects of the N-terminal inactivation domain and quaternary ammonium ions in Kv1.4 and Kv1.5.....	146
Figure 5.6. A Kv1.4 C-type inactivation deficient channel mutant. ....	150
Figure 5.7. N-type inactivation in C-type inactivation-deficient Kv channels. ....	154
Figure 5.8. Kinetic model of Na <sup>+</sup> permeation through N- and C-type inactivated K <sup>+</sup> channels. ....	156
Figure 5.9. Interactions between the R state and the N-terminal inactivation domain. ....	162
Figure 6.1. Schematic diagram illustrating a potential mechanism of communication between the cytosolic and membrane bound domains of a Kv channel. ....	180

## LIST OF TABLES

Table 3.1. Inactivation time constants for full-length Kv1.5 and Kv1.5ΔN209..... 71

## ABBREVIATIONS

<u>Amino Acid</u>	<u>3 Letter Code</u>	<u>1 Letter Code</u>
Alanine	Ala	A
Arginine	Arg	R
Asparagine	Asn	N
Aspartate	Asp	D
Cysteine	Cys	C
Glutamine	Gln	Q
Glutamate	Glu	E
Glycine	Gly	G
Histidine	His	H
Isoleucine	Ile	I
Leucine	Leu	L
Lysine	Lys	K
Methionine	Met	M
Phenylalanine	Phe	F
Proline	Pro	P
Serine	Ser	S
Threonine	Thr	T
Tryptophan	Try	W
Tyrosine	Tyr	Y
Valine	Val	V

QA – quaternary ammonium

TEA<sup>+</sup> - tetraethylammonium

TBA<sup>+</sup> - tetrabutylammonium

4-AP – 4-aminopyridine

CNG – cyclic-nucleotide gated

HCN – Hyperpolarization-activated and cyclic-nucleotide gated

K<sub>v</sub> – voltage-gated potassium

K<sub>ir</sub> – inwardly-rectifying potassium

PKA - protein kinase A

PKC – protein kinase C

K<sub>ATP</sub> – ATP-sensitive potassium channel

BTB/POZ – Broad-complex, Tramtrack, and Bric-a-brac, Poxvirus and Zinc finger domain

KChIP – K<sup>+</sup> channel interacting protein

s – seconds

ms - milliseconds

mV – millivolts

nA – nanoamperes

pA – picoamperes

subscript 'i' – intracellular

subscript 'o' – extracellular

subscript 'i/o' – intracellular and extracellular

## **ACKNOWLEDGEMENTS**

I would like to express my sincere gratitude to several individuals who have contributed to my graduate student experience at UBC. My graduate supervisor, David Fedida, and other members of my supervisory committee, Steve Kehl, Eric Accili and Tony Pearson, have all provided helpful insights over the years, and during the preparation of this thesis. I have also shared many unforgettable experiences with a few special friends/roommates (MS, KB, KL, AP, JE). I am very appreciative of their boundless patience and consideration, especially over the past few months. I don't mean to leave out other friends and fellow graduate students – all of you have contributed to the fantastic social environment in the department. I cherish all of the Friday nights and grad retreats we've spent as a gang. Finally, to my loving and supportive family, I am eternally grateful for your encouragement, generosity and patience over the past few years.

## **PREFACE**

Parts of the following work have been published as follows:

**Kurata, H.T.**, G.S. Soon, and D. Fedida. 2001. Altered state dependence of C-type inactivation in long and short forms of Kv1.5. *J. Gen. Physiol.* 118(3):315-332.

**Kurata, H.T.**, Soon, G.S., Eldstrom, J.R., Lu, G.W.K., Steele, D.F., and D. Fedida. 2002. Amino-terminal determinants of U-type inactivation in voltage-gated K<sup>+</sup> channels. *J. Biol. Chem.* 277(32):29045-29053.

**Kurata, H.T.**, Z. Wang, and D. Fedida. 2004. NH<sub>2</sub>-terminal inactivation peptide binding to C-type inactivated Kv channels. *J. Gen. Physiol.* 123(5): 505-520.

## **CHAPTER 1: INTRODUCTION**

## **I:OVERVIEW**

Voltage-gated potassium (Kv) channels are transmembrane proteins that underlie membrane repolarization and termination of excitation in many tissues, including muscle and neurons. To fulfill their role in excitation, Kv channels possess several critical properties. Firstly, they exhibit a defined selectivity between cations, combined with a very high ion throughput rate. These properties, together with the transmembrane  $K^+$  concentration gradient established by various pumps and transporters, cause Kv channel opening to exert a repolarizing influence on the transmembrane voltage due to outward-flowing potassium currents. By definition, Kv channels possess the ability to open or close in response to changes in the transmembrane voltage. In addition, many Kv channels exhibit one or more additional mechanisms of closure, collectively termed inactivation, when subjected to prolonged depolarizations. Mechanisms underlying and regulating Kv channel inactivation are the principal focus of the experimental work presented in this thesis.

Kv channels are a widely studied prototype of the voltage-gated cation channel family, and remain the only cation channel subtype with a pore structure known at atomic resolution. Years of biophysical experimentation have contributed to our understanding of Kv channel behaviour, and dramatic recent advances have illuminated the structural elements underlying specific channel functions. This introductory chapter provides an overview of these elements in isolation, together with the gating processes they underlie, and their spatial and functional relationships to one another in an intact channel.

## II:GENERAL STRUCTURE

### *Broad features of Kv channel architecture*

Each Kv channel gene encodes a single  $\alpha$ -subunit consisting of 6 transmembrane domains numbered S1-S6. The minimal requirement for a functional Kv channel is a tetrameric assembly of these subunits, which may assemble as homo- or heteromultimers (Isacoff *et al.*, 1990; MacKinnon, 1991; Sheng *et al.*, 1993). A generalized topology of a single Kv channel subunit is illustrated in Figure 1, showing the presence of 6 transmembrane domains, with cytosolic N- and C-termini (Fig. 1A). The S5 and S6 transmembrane helices, and a connecting re-entrant loop termed H5 or P-region comprise the pore-forming module of the channel. This ion permeation pathway is lined by the cytoplasmic side of S6, and specific residues within the P-region (discussed in detail in Section III; Hartmann *et al.*, 1991; Yellen *et al.*, 1991; Yool & Schwarz, 1991; Heginbotham *et al.*, 1994; Taglialatela *et al.*, 1994). The S4 transmembrane helix contains a series of regularly spaced basic (Arg or Lys) amino acids. These positively charged residues span the transmembrane electric field, and so their position and motion are influenced by changes in transmembrane voltage. The S4 helix provides a mechanism for voltage-gated channels to respond to changes in membrane potential, and is generally referred to as the voltage sensor (Bezannilla, 2000). With the exception of the highly conserved N-terminal T1 domain (discussed in detail in Section V; Shen & Pfaffinger, 1995; Kreuzsch *et al.*, 1998), the cytosolic N- and C-termini of Kv channels exhibit considerable variability, and subserve a diverse range of functions. In some channels, the N-terminus contains a subset of amino acids critical for inactivation (Hoshi *et al.*, 1990; Antz *et al.*, 1999; Wissmann *et al.*, 2003). Other functions attributed to the cytosolic Kv channel domains are channel assembly and

subfamily recognition (Shen *et al.*, 1993; Xu *et al.*, 1995), association with auxiliary subunits (Rettig *et al.*, 1994; Xu *et al.*, 1998; Gulbis *et al.*, 2000), and channel modulation by various intracellular signaling molecules (Huang *et al.*, 1993; Drain *et al.*, 1994; Huang *et al.*, 1994; Holmes *et al.*, 1996).

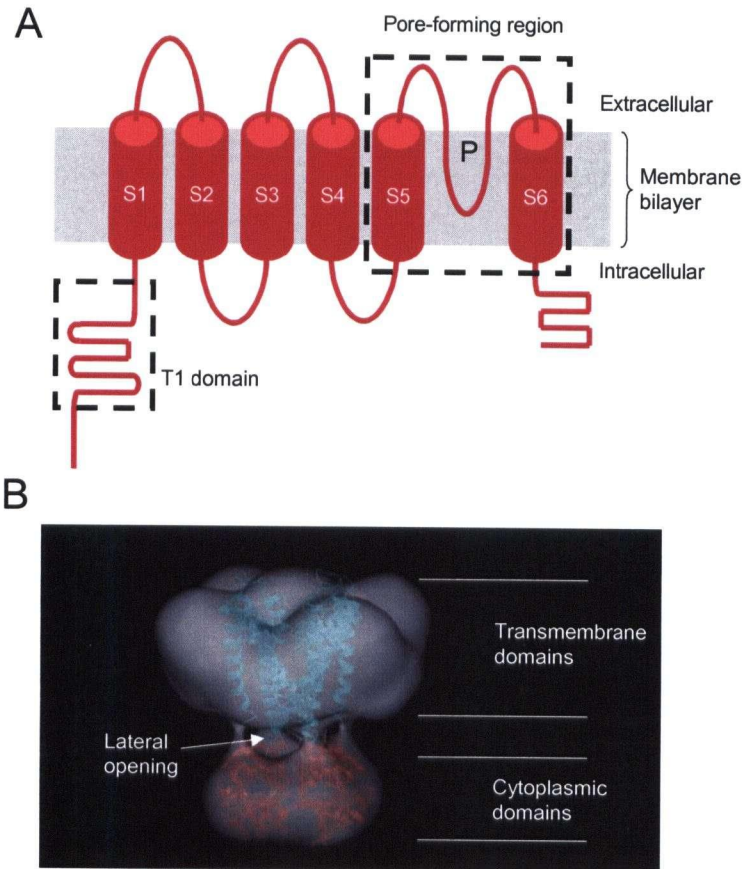


Figure 1.1. Overview of Kv channel structure. (A) Transmembrane topology of a Kv channel subunit. Transmembrane domains are labeled S1-S6, with 'P' indicating the H5 or P-region linking the S5 and S6 segments. Boxed segments of the channel represent the highly conserved cytosolic N-terminal T1 domain, and the pore-forming region of the channel, as indicated. (B) Single molecule electron microscope reconstruction of recombinant *Shaker* channels (Sokolova *et al.*, 2001). The EM structure illustrates that the channel is divided into two distinct regions of mass. The large mass is believed to correspond to the transmembrane domains of the channel, containing the voltage-sensor and pore-forming channel domains. The smaller mass likely corresponds to the cytoplasmic channel domains, consisting of the T1 domain, and possibly other N- or C-terminal amino acids. Atomic resolution structures of the KcsA channel (cyan) and the T1 domain (red) are superimposed on the EM structure in their hypothesized locations (the image in Panel B has been reproduced with kind permission of Dr. N. Grigorieff, HHMI, Brandeis University).

### ***Macromolecular view of Kv channel structure***

The structures of several bacterial K<sup>+</sup> channels and isolated eukaryotic Kv channel domains have been determined at atomic resolution. However, it is instructive to first consider how the vague transmembrane topology just described is organized in an intact channel. Recent advances in single-molecule electron microscopy have provided interesting new insights into the overall organization of K<sup>+</sup> channels and their auxiliary subunits (Sokolova *et al.*, 2001; Sokolova *et al.*, 2003; Orlova *et al.*, 2003). Single molecule electron microscope images of the *Shaker* channel suggest that the tetrameric assembly of the pore-forming  $\alpha$ -subunits is arranged into two distinct domains connected by thin linkers 2-3 nm in length (Fig. 1.1B; Sokolova *et al.*, 2001). This overall organization of the channel is now frequently described as the ‘hanging gondola’ model of channel structure (Kobertz *et al.*, 2000). The larger of the two domains likely corresponds to the membrane-bound portion of the channel, formed by the transmembrane helices S1-S6. Again, these helices comprise the pore-forming region and the voltage-sensing machinery of the channel. The smaller domain, the ‘gondola’, corresponds to segments of the channel residing within the cytoplasm, consisting of the T1 domain and some extra mass which may arise from the channel C-terminus and/or N-terminal residues preceding the T1 domain (Sokolova *et al.*, 2003). In the single molecule EM structure, these two domains are clearly structurally distinct, and linkers between them form four lateral openings through which ions or blockers likely must pass to gain access to the channel pore (Fig. 1.1B). This modular arrangement of Kv channel structure has also been observed in single electron microscope images of *Shaker* and mammalian Kv1 channels in complex with auxiliary  $\beta$ -subunits (Sokolova *et al.*, 2003;

Orlova *et al.*, 2003), and most recently in Kv4.2 channels in complex with KChIP2 (Kim *et al.*, 2004).

### III: DETAILED FEATURES OF K<sup>+</sup> CHANNEL PORES

In all K<sup>+</sup> channel structures determined to date, the pore-forming regions, and particularly the selectivity filter, exhibit remarkable similarity (Doyle *et al.*, 1998; Zhou *et al.*, 2001b; Jiang *et al.*, 2002a; Kuo *et al.*, 2003). The K<sup>+</sup> channel pore provides a hospitable permeation pathway for the dehydration, diffusion, and rehydration of potassium ions as they move between the extracellular and intracellular sides of the plasma membrane. The ion-conducting pore contains structural elements conferring ion selectivity, and also elements that can gate the pathway and regulate ion conduction through the channel.

#### *KcsA- A prokaryotic potassium-selective channel*

Determination of the structure of the *Streptomyces lividans* K<sup>+</sup> channel KcsA at atomic resolution has proven to be a landmark achievement in the study of ion channels (Fig. 1.2A; Doyle *et al.*, 1998; Zhou *et al.*, 2001b). The structure illuminates several important properties of K<sup>+</sup> channel pores underlying their high selectivity and K<sup>+</sup> throughput, and confirms several fundamental predictions arising through years of biophysical studies of K<sup>+</sup> channels. An image of two opposing KcsA subunits is illustrated in Fig. 1.2A. Each subunit of the KcsA channel consists of two transmembrane helices (M1 and M2), arranged with a four-fold axis of symmetry along the center of the permeation pathway, perpendicular to the plane of the plasma membrane. The M1 and M2 transmembrane helices exhibit relatively weak primary sequence identity with the corresponding S5 and S6 helices of voltage-gated K<sup>+</sup> channels (see alignment in Fig. 1.2D). However there is much stronger sequence identity within the P-region, and chimeric substitution of this region in *Shaker* with homologous

sequence from KcsA allows the formation of functional  $K^+$  selective and voltage-gated channels, suggesting that the KcsA structure provides a reasonable approximation of a Kv channel pore (Lu *et al.*, 2001).

The P-region of *Shaker* and its mammalian Kv1 homologues contains the TMTTVGYGD sequence, a subset of the TXXTXGYGD  $K^+$  channel signature sequence, which forms the selectivity filter of the channel (Heginbotham *et al.*, 1994). Amino acids forming the selectivity filter are highlighted in 'ball-and-stick' in Fig. 1.2A, and are magnified in Fig. 1.2B. This structural element of the channel allows selective permeation of  $K^+$  ions, and excludes the other predominant physiological cation,  $Na^+$ . As discussed in Section IV, the selectivity filter is also likely a dynamic structure that contributes to the C-type inactivation gating mechanism of Kv channels (Kiss *et al.*, 1999). The selectivity filter is lined with backbone carbonyl oxygen atoms contributed by each channel subunit (Fig. 2B; Doyle *et al.*, 1998), a structural arrangement of the protein backbone that depends critically on the flexibility of the glycine residues within the  $K^+$  channel signature sequence (MacKinnon, 2003). Selectivity for  $K^+$  over  $Na^+$  arises from close octahedral coordination of each  $K^+$  ion in the filter by eight backbone carbonyl oxygen atoms, which closely match the dimensions of the hydration sphere of  $K^+$  in solution (Zhou *et al.*, 2001b). Thus, the selectivity filter provides a very hospitable milieu for  $K^+$  ions in transit, resembling the hydrated conditions of bulk solution.

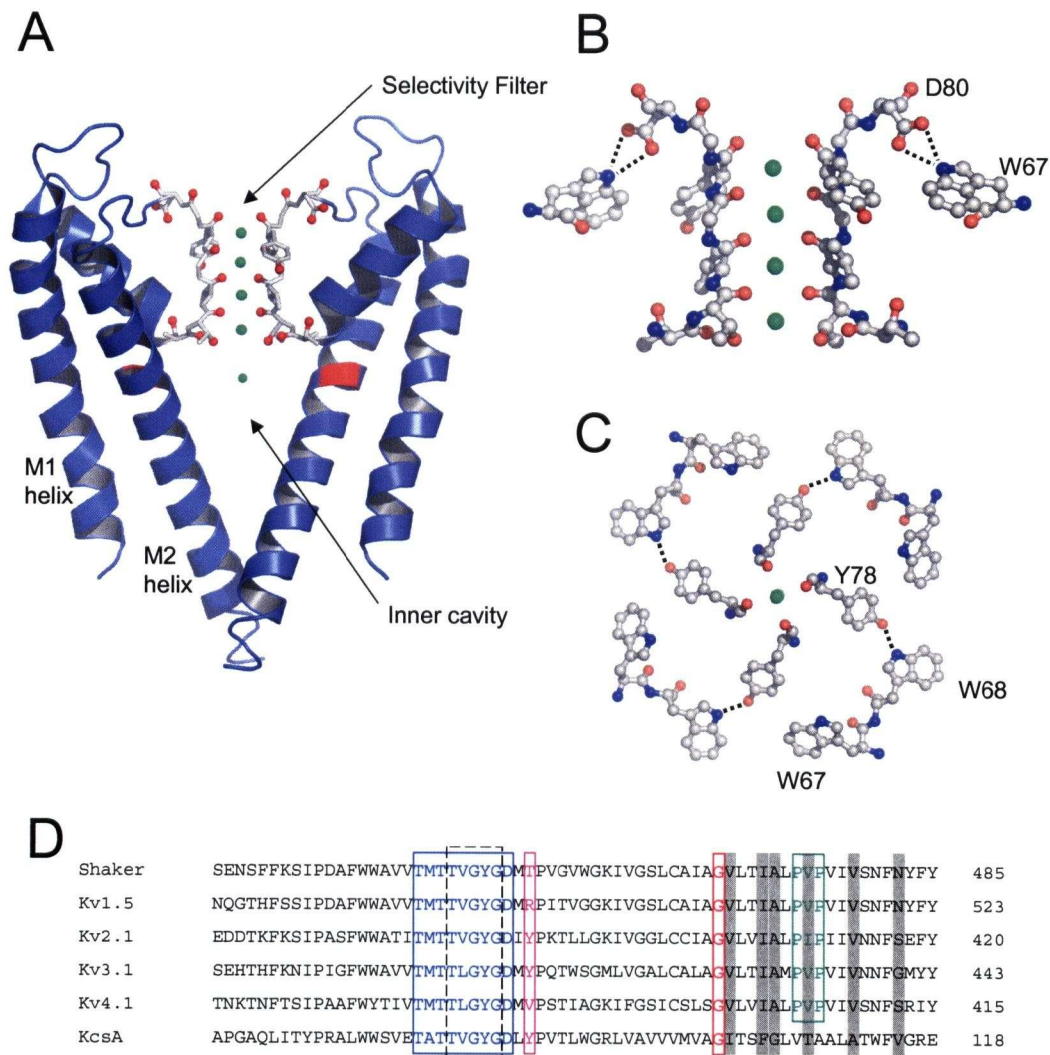


Figure 1.2. Detailed features of the KcsA channel. (A) Side view of two opposing subunits of KcsA. Residues within the selectivity filter are illustrated in ‘ball-and-stick’ format, and magnified in panel (B). Potassium ions are represented as green spheres. Panels (B) and (C) also illustrate stabilizing interactions between residues in the selectivity filter and elsewhere in the channel. (B) Sidechain carboxyl oxygen atoms of KcsA residue D80 (*Shaker* D447) are in very close proximity to the W67 (*Shaker* W434) sidechain, and these two residues may form an intra-subunit hydrogen bond. (C) The side chain hydroxyl group of Y78 in KcsA (Y445 in *Shaker* GYG sequence) is stabilized by hydrogen bonding with W68 (*Shaker* W435) in an adjacent subunit, and van der Waals interactions with W67 (*Shaker* W434) within the same subunit. (D) Amino acid sequence alignment for KcsA, *Shaker*, and multiple mammalian Kv channel clones. Blue amino acids comprise the K<sup>+</sup> channel signature sequence, while those enclosed within the dashed line contribute backbone carbonyl oxygen atoms to the channel selectivity filter. The red box demarcates a conserved glycine termed the ‘gating hinge’, and the green box demarcates the Pro-X-Pro motif present in voltage-gated K<sup>+</sup> channels, but absent in KcsA and MthK. The purple box demarcates residues equivalent to *Shaker* T449. Grey shading indicates pore-lining amino acids in the S6 segment, which are predominantly hydrophobic in nature.

The geometry of the selectivity filter shown in Fig. 1.2B is optimal for coordination of  $K^+$  ions, and is maintained by several critical interactions between residues in the  $K^+$  channel signature sequence and residues elsewhere in the protein (Fig. 1.2B, C). Firstly, the planar arrangement of two adjacent tryptophan residues (W67 and W68 in KcsA, W434 and W435 in *Shaker*) forms an 'aromatic cuff' that interacts with the tyrosine residue in the  $K^+$  channel selectivity filter (Fig. 1.2B, C). This residue (Y78 in KcsA, Y445 in *Shaker*) contributes a carbonyl oxygen near the extracellular entrance to the selectivity filter (Fig. 1.2B, C; Doyle *et al.*, 1998). In the KcsA structure, the hydroxyl group of Y78 forms an intersubunit hydrogen bond with the sidechain nitrogen of W68. In addition, significant intrasubunit van der Waals interactions are likely between Y78 and W67 (Fig. 1.2C; Doyle *et al.*, 1998). Figure 1.2B illustrates the relative positions of residues D80 and W67 in KcsA (*Shaker* residues D447 and W434, respectively), showing the close proximity of the carboxyl group of D80 with the sidechain nitrogen atom in W67 (Doyle *et al.*, 1998). A critical role for these amino acids is corroborated by numerous mutagenesis studies of Kv channels. In various cases, disruption of residues within the selectivity filter or the aromatic cuff have been shown to accelerate inactivation, render channels non-conducting, alter pore selectivity, and alter gating (Perozo *et al.*, 1993; Heginbotham *et al.*, 1994; Kirsch *et al.*, 1995; Yang *et al.*, 1997).

The channel also contains a large aqueous cavity on the cytosolic side of the selectivity filter (labeled 'inner cavity' in Fig. 1.2A). Importantly, the  $\alpha$ -helices formed within the P-region are arranged such that the negative end of their intrinsic dipole moment is directed towards the center of the intracellular aqueous cavity of the channel (Doyle *et al.*,

1998). High-resolution structures of KcsA demonstrate the presence of a  $K^+$  ion bound in the cavity of the channel, and it has been suggested that the dipoles of the pore helices are critical in stabilizing this  $K^+$  binding site (Roux & MacKinnon, 1999; Zhou *et al.*, 2001b; Zhou & MacKinnon, 2004). Although this structural arrangement does not suggest a mechanism for selectivity of  $K^+$  over  $Na^+$  in the aqueous cavity, it does provide a mechanism for cation selectivity, and for concentration of cations near the entrance to the selectivity filter.

The arrangement of  $K^+$  ions in the KcsA structure also confirms the prediction that  $K^+$  channels can simultaneously contain multiple  $K^+$  ions arranged in single file (Hodgkin & Keynes, 1955; Neyton & Miller, 1988a; Zhou *et al.*, 2001b). Other experiments suggesting multi-ion pores of  $K^+$  channels include (but are not limited to), consistent demonstration of Ussing flux exponents  $> 1$  in voltage-gated and inwardly rectifying  $K^+$  channels (Stampe & Begenisich, 1996; Stampe *et al.*, 1998), effective valences  $> 1$  for monovalent cationic  $K^+$  channel blockers such as  $Cs^+$  (Hille & Schwarz, 1978), and the anomalous mole fraction effect (Eisenman *et al.*, 1986; Wagoner & Oxford, 1987; Heginbotham & MacKinnon, 1993). With respect to  $K^+$  permeation, the presence of multiple  $K^+$  ions in the permeation pathway is thought to be critical for high  $K^+$  throughput. Electrostatic repulsion between multiple  $K^+$  ions destabilizes otherwise favorable binding sites, effectively reducing the  $K^+$  affinity of the selectivity filter, and preventing very stable binding of  $K^+$  ions from slowing ion permeation (Eisenman *et al.*, 1986; Neyton & Miller, 1988b; Heginbotham & MacKinnon, 1993; Vergara *et al.*, 1999; Miller, 2000; Berneche & Roux, 2001).

### ***Conformational changes of the pore during activation***

Like KcsA, the MthK channel (from *Methanobacterium thermoautotrophicum*) is formed by a rotationally symmetric tetramer of a 2 transmembrane domain subunit. Functional experiments have demonstrated that opening of the MthK channel is promoted by elevation of intracellular  $\text{Ca}^{2+}$ , and the determination of the MthK structure in the presence of  $\text{Ca}^{2+}$  has provided a plausible model for a gating mechanism of Kv channels (Jiang *et al.*, 2002a). The KcsA and MthK structures exhibit a significant difference in the arrangement of the transmembrane M2 helices (Fig. 1.3). In the KcsA channel, the M2 helices form a constriction near the cytosolic side of the channel, referred to as the inner helix bundle, or bundle-crossing (Doyle *et al.*, 1998). In stark contrast, the M2 helices in MthK are wide open – no bundle-crossing is apparent, and the aqueous central cavity of the channel is accessible to what would be the intracellular medium. These differences between the KcsA and MthK channel structures suggest a structural interpretation of channel opening, with the KcsA structure representing a closed/resting pore conformation, and the MthK structure representing an open pore (Doyle *et al.*, 1998; Jiang *et al.*, 2002a; Jiang *et al.*, 2002b). Under conditions that promote channel opening, it has been suggested that the M2 helices (corresponding to the S6 helix of a Kv channel) undergo a conformational change dependent on the flexibility of a highly conserved glycine residue referred to as the ‘gating hinge’ (Gly 83 in MthK, red residues in Fig. 1.2D), in which the helices swing open and expose the internal cavity to the intracellular solution (Jiang *et al.*, 2002b). The location of the ‘gating hinge’ is colored red in the KcsA and MthK structures in Fig. 1.3.

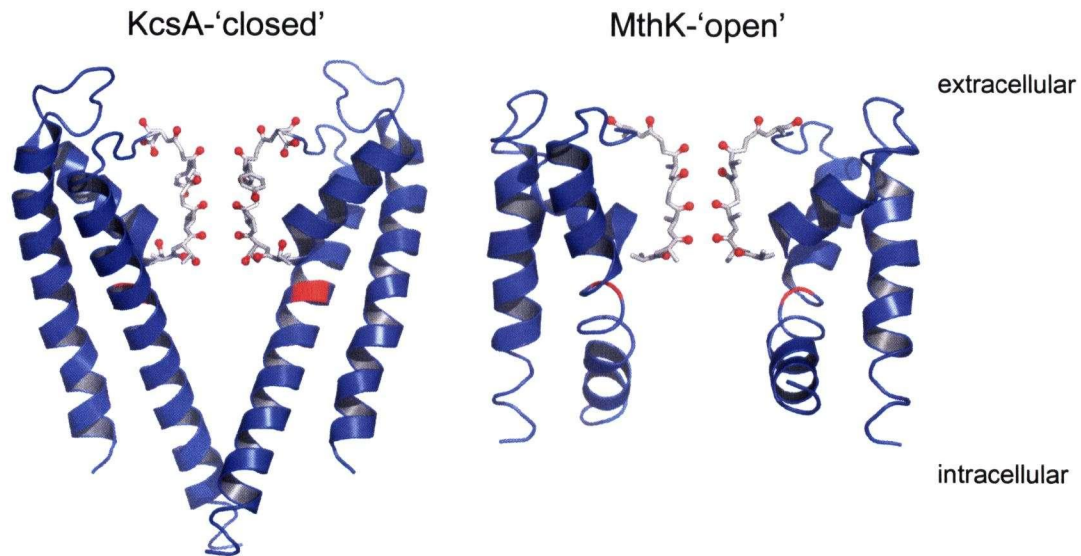


Figure 1.3. KcsA and MthK structures. In the KcsA structure, the M2 helices form a constriction at the cytoplasmic entrance to the channel, called the inner helix bundle, or ‘bundle-crossing’. In the MthK structure, the M2 helices are splayed open around residue Gly83, the ‘gating hinge’, colored red in both structures. Motion of the M2 helix around the gating hinge has been suggested to underlie channel activation (Jiang *et al.*, 2002b).

Can this gating model, based on the bacterial MthK and KcsA channels, be generalized to suggest a pore opening mechanism for Kv channels? In *Shaker* channels, accessibility studies of substituted cysteine residues in the channel pore clearly suggest the presence of a functional intracellular gate between residues 474 and 478, at a position corresponding to the KcsA bundle crossing (Holmgren *et al.*, 1997; Liu *et al.*, 1997; Del Camino *et al.*, 2000; Del Camino & Yellen, 2001). In the closed state, pore-lining residues above and including *Shaker* residue 474 remain inaccessible to cations as small as  $\text{Cd}^{2+}$  or  $\text{Ag}^+$ , and to uncharged (MTSACE) or negatively charged (MTSES) thiol-reactive MTS

reagents, suggesting the presence of a steric intracellular gate regulating ion flux. In addition, there is a conserved glycine residue analogous to MthK Gly-83 in the S6 segment of *Shaker* and other Kv channels (Fig. 1.2D, red residues). However, the presence of a conserved helix-breaking Pro-X-Pro motif in the S6 segment of Kv channels (Fig. 1.2D, green residues) suggests a kinked or bent S6 helix in both the open and closed channel conformations (Del Camino *et al.*, 2000; Webster *et al.*, 2004). This structural detail of the S6 helix differs from the  $\alpha$ -helical arrangement of the M2 helices in the KcsA structure (Fig. 1.3), and below the 'gating hinge' in the MthK structure, since the Pro-X-Pro motif is absent in both KcsA and MthK. Interestingly, there is not an absolute requirement for the position or number of prolines in the S6 helix of Kv1.5 in order to maintain voltage-dependent gating (Labro *et al.*, 2003), and it remains unclear whether the S6 proline residues in Kv channels provide an alternative hinge for channel opening, or whether they position S6 to allow coupling to voltage-sensing modules of the channel (Yellen, 2002).

Despite these important differences and uncertainties, both models espouse the general concept of a functional gate at the cytoplasmic entrance of the channel, formed by the S6 helices of Kv channels (Del Camino & Yellen, 2001; Jiang *et al.*, 2002b). This picture of gating by the S6 helix is also generally consistent with the understanding of channel interactions with open-state channel blockers, such as quaternary ammonium ions. That is, the constriction formed at the intracellular entrance to the channel (by the M2 helices in the KcsA structure) occludes entry of quaternary ammonium ions into the permeation pathway. However, opening of the gate at the cytoplasmic entrance exposes the internal cavity of the channel, allowing the entry of organic cations. Rapid closure of the activation gate, as is

possible in Kv channels, can also trap cations in the internal vestibule of the channel (Armstrong, 1971; Holmgren *et al.*, 1997).

It should be noted that in other channel types, the establishment of a cytoplasmic gate analogous to the KcsA bundle crossing remains controversial. One prominent example is the cyclic-nucleotide gated (CNG) family of channels, in which accessibility of cysteine residues substituted within the pore appears to be essentially independent of whether the channel is open or closed (Flynn & Zagotta, 2001). Although conformational rearrangements of S6 likely take place during CNG channel activation (Johnson, Jr. & Zagotta, 2001), this observation argues against the existence of a tight steric gate on the cytosolic side of CNG channels. Similar suggestions have been made for inwardly-rectifying potassium (Kir) channels. For instance, some reports suggest that Ba<sup>2+</sup> blockade of the ATP sensitive K<sup>+</sup> channel (K<sub>ATP</sub>) is also essentially state-independent (Proks *et al.*, 2003), and similar suggestions have been made for the strong inward-rectifier Kir2.1 (Xiao *et al.*, 2003). However, others have clearly demonstrated trapping of intracellular organic blockers such as spermine by ATP-mediated channel closure of Kir 6.2 (Phillips & Nichols, 2003), analogous to the 'blocker-trapping' experiments described above for Kv channels, and have also demonstrated gated accessibility of MTS reagents to the inner cavity of K<sub>ATP</sub> channels (Phillips *et al.*, 2003).

In addition to the steric gate on the intracellular side of Kv channels, some evidence suggests that Kv channel activation may also involve conformational changes of the selectivity filter (Chapman *et al.*, 1997). Most notable are single channel studies demonstrating altered ionic selectivity in subconductance levels that appear during activation and deactivation (Zheng & Sigworth, 1997; Zheng & Sigworth, 1998). In particular,

subconductance states of T442S mutant *Shaker* channels, or WT *Shaker* and T442S heteromultimers, exhibit enhanced selectivity for  $K^+$  over  $Rb^+$  or  $NH_4^+$  relative to the fully open state (Zheng & Sigworth, 1997; Zheng & Sigworth, 1998). Others have also observed activation-dependent changes in accessibility of cysteine residues substituted in the pore-helix of CNG channels (Sun *et al.*, 1996; Liu & Siegelbaum, 2000), although this observation has not been confirmed in a Kv channel. Collectively, these observations suggest that Kv channel opening at the cytoplasmic bundle-crossing may also be accompanied by conformational changes around the selectivity filter.

### ***Voltage-dependent gating***

In Kv channels, transmembrane voltage controls the opening and closing of the S6 activation gate. The voltage-sensing structures of Kv channels underlie their hallmark property of regulated open probability in response to changes in the transmembrane voltage. Early primary sequence analysis of the first cloned voltage-gated cation channels led to the suggestion that a high density of basic residues within the fourth transmembrane domain (S4) of *Shaker* or  $Na^+$  channels form a voltage-sensing component of the channel (Noda *et al.*, 1984; Papazian *et al.*, 1987; Tempel *et al.*, 1987). Several neutralizing mutations of positively charged residues in the S4 segment of *Shaker* and other Kv channels have been shown to alter the total gating charge movement upon depolarization, supporting the notion that the S4 segment underlies part of the voltage-sensing mechanism of the channel (Liman *et al.*, 1991; Papazian *et al.*, 1991; Schoppa *et al.*, 1992; Perozo *et al.*, 1994; Aggarwal & MacKinnon, 1996). Other experiments, notably accessibility studies of cysteine residues substituted within the S4 segment of *Shaker* and  $Na^+$  channels (Yang & Horn, 1995; Larsson *et al.*, 1996; Yang *et al.*, 1996; Baker *et al.*, 1998), and fluorescence studies employing dyes

introduced *in situ* at different residues within the S4 segment (Mannuzzu *et al.*, 1996; Cha & Bezanilla, 1997; Cha *et al.*, 1998; Glauner *et al.*, 1999; Cha *et al.*, 1999a; Cha *et al.*, 1999b; Chanda & Bezanilla, 2002), confirmed motion of the S4 segment with voltage and time-dependence that correspond to electrophysiological gating current measurements. Additionally, acidic residues within the S2 and S3 transmembrane domains were found to be critical for voltage-dependent gating in *Shaker* channels, likely through formation of stabilizing hydrogen bonds with basic S4 residues (Papazian *et al.*, 1995; Seoh *et al.*, 1996; Tiwari-Woodruff *et al.*, 1997; Tiwari-Woodruff *et al.*, 2000). Fluorescently tagged *Shaker* S2 residues also report rapid environmental changes (Cha & Bezanilla, 1997), and various studies have suggested molecular motions around the S2 and S3 segments of voltage-gated cation channels upon depolarization (Milligan & Wray, 2000; Nguyen & Horn, 2002).

Despite a huge amount of experimental effort, a thorough understanding of the molecular motions underlying the voltage-sensing mechanism of Kv channels remains elusive (Cohen *et al.*, 2003; Laine *et al.*, 2004; Ahern & Horn, 2004b). Most published work has supported a ‘conventional’ model of voltage-sensing movement, suggesting that the voltage-sensor is at least partially shielded from the hydrophobic environment of the lipid bilayer by a proteinaceous envelope formed by other transmembrane domains (Starace *et al.*, 1997; Cha & Bezanilla, 1998; Clapham, 1999; Starace & Bezanilla, 2004; Ahern & Horn, 2004a). It has been suggested that the transmembrane segments of the channel form gating canals or ‘canaliculi’: aqueous crevasses within which basic S4 residues can reside and remain shielded from the hydrophobic lipid environment (Goldstein, 1996; Islas & Sigworth, 2001). Recent crystallographic work and accessibility studies of the bacterial KvAP channel have suggested a very different model of organization of the Kv channel transmembrane

domains, and a revision of current structural models of voltage sensor movement, referred to as the 'paddle' hypothesis (Ruta *et al.*, 2003; Jiang *et al.*, 2003b; Jiang *et al.*, 2003c). The paddle model of voltage-sensor orientation and movement diverges most significantly from more conventional models in its proposal that charged residues in the S4 segments are actually lipid accessible.

Whatever the exact molecular location and motions of the voltage sensor turn out to be, they are likely coupled to gating motions in the channel pore in at least two ways. Firstly, movement of the voltage sensors into their activated conformation favors opening of the cytoplasmic activation gate, formed by the S6 helices, and various hypotheses have been suggested to explain this coupling. These include a repacking of transmembrane helices, allowing for reorientation of the pore-forming S5 and S6 helices, or by some association of the S4-S5 linker and the S6 helix (Horn, 2000; Li-Smerin *et al.*, 2000; Yellen, 2002; Lu *et al.*, 2002; Tristani-Firouzi *et al.*, 2002). Secondly, there is considerable evidence that residues at the extracellular end of the S4 helix reside near the pore-forming domain of the channel, and play a role in triggering conformational changes underlying C-type inactivation (Loots & Isacoff, 1998; Gandhi *et al.*, 2000; Loots & Isacoff, 2000).

#### **IV: MECHANISMS OF K<sub>v</sub> CHANNEL INACTIVATION**

After channel activation, and in some cases with subthreshold stimuli, K<sub>v</sub> channels undergo a time-dependent current decay by a family of mechanisms termed inactivation. Inactivation entails entry of channels into a stable, non-conducting state, and thereby functionally reduces the availability of channels for opening. That is, if a channel has inactivated, some time must expire after repolarization of the membrane voltage to allow the channel to recover and become available to open again. A variety of inactivation

mechanisms exhibited by different Kv channels provide important physiological means by which the duration of action potentials in many excitable tissues can be regulated at different frequencies and potentials. Inactivation of Kv channels has historically been divided into two categories, fast (N-type) inactivation which involves occlusion of the inner pore by an N-terminal ball, and slow (C-type) inactivation which involves a concerted constriction of the outer mouth of the channel pore (Hoshi *et al.*, 1991; Panyi *et al.*, 1995; Ogielska & Aldrich, 1998). These are discussed in detail in the sections that follow.

### ***N-type inactivation***

N-type inactivation is frequently described as the 'ball-and-chain' mechanism of inactivation, in which a sequence of amino acids (the inactivation domain) at the N-terminus of the channel occludes the intracellular channel pore and prevents ion permeation. The N-type inactivation mechanism underlies a very rapid inactivation process in *Shaker* channels, and several mammalian Kv channels including Kv1.4 and Kv3.4 (Hoshi *et al.*, 1990; Rasmusson *et al.*, 1995; Beck *et al.*, 1998). In addition, the association of Kv1 channels with certain auxiliary Kv $\beta$  subunits can also confer rapid inactivation by an N-type mechanism (Morales *et al.*, 1995; Sewing *et al.*, 1996; Accili *et al.*, 1997). This 'ball and chain' model of inactivation is illustrated in cartoon form in Fig. 1.4 and has been confirmed by several lines of evidence. Most importantly, N-type inactivation is abolished by deletion or enzymatic removal of the N-terminus, and restored by subsequent application of exogenous peptides derived from the N-terminus of one of many N-type inactivating channels (Zagotta *et al.*, 1990; Murrell-Lagnado & Aldrich, 1993b; Antz *et al.*, 1999). A tetrameric K<sup>+</sup> channel can contain multiple inactivation domains, and these are thought to behave roughly independently (Gomez-Lagunas & Armstrong, 1995), although some reports have suggested

a small degree of negative cooperativity (Hashimoto *et al.*, 2000). A single inactivation domain is sufficient to confer N-type inactivation (MacKinnon *et al.*, 1993; Lee *et al.*, 1996).

Another important characteristic of N-type inactivation is sensitivity to intracellular pore blockers, notably TEA<sup>+</sup> and its derivatives (Choi *et al.*, 1991). This effect arises because the N-terminal inactivation domain and cytosolically applied QA ions compete for identical or overlapping binding sites, and so their pore occupancy is mutually exclusive (Choi *et al.*, 1991; Choi *et al.*, 1993; Baukrowitz & Yellen, 1996a; Zhou *et al.*, 2001a). Therefore, intracellular QA ions generally slow the process of N-type inactivation, whereas application of extracellular TEA<sup>+</sup> has no effect on this process (Choi *et al.*, 1991).

### ***Structural determinants of N-type inactivation***

Early detailed studies of the efficacy of isolated N-terminal inactivation domains (inactivation peptides) from multiple channels, and several synthetic inactivation peptides, revealed fairly non-specific requirements for effective blockade of ionic currents. The basic requirements were a series of ~10 hydrophobic amino acids, followed by a series of amino acids with a net positive charge. Furthermore, modification of the charged amino acids generally altered the binding rate of the inactivation peptide, whereas mutations of the hydrophobic amino acids predominantly affect unbinding (Murrell-Lagnado & Aldrich, 1993a; Murrell-Lagnado & Aldrich, 1993b). These data led to speculation that hydrophobic residues within the inactivation domain interact directly with hydrophobic regions of the channel, while long-range electrostatic interactions between charged residues might effectively increase the local concentration of the inactivation domain and promote entry to its binding site (Murrell-Lagnado & Aldrich, 1993a; Murrell-Lagnado & Aldrich, 1993b; Aldrich, 2001). These results are also consistent with the identification of several cellular

mechanisms of modulation of N-type inactivation that act by altering the net charge of the inactivation domain. For instance, protein kinase C phosphorylation of multiple serine residues in the Kv3.4 N-terminus dramatically attenuates the N-type inactivation normally observed in this channel (Beck *et al.*, 1998; Antz *et al.*, 1999). Similar effects have been attributed to protein kinase A phosphorylation of serine 24 in the N-terminus of the Kv $\beta$ 1.3 subunit (Kwak *et al.*, 1999). Although some of these effects have been attributed to altered secondary structure of the N-terminal domain (Antz *et al.*, 1999), in both instances the site of phosphorylation is distinct from the hydrophobic N-terminal residues currently thought to interact with the inner cavity of Kv channels (Zhou *et al.*, 2001a). In what may be a complimentary mechanism, others have demonstrated that PKA phosphorylation of the C-terminus of *Shaker* stabilizes N-type inactivation (Drain *et al.*, 1994). This effect may arise by the addition of negative charge near the inactivation domain receptor, in a location able to interact with positively charged residues in the *Shaker* N-terminus. Other examples of chemical modifications of the channel N-terminus impacting N-type inactivation include the inhibitory effect of Src tyrosine kinase phosphorylation of tyrosine 8 in the *Shaker* N-terminus (Encinar *et al.*, 2002), and the stimulatory effects of intracellular acidification on Kv1.4 inactivation gating due to protonation of N-terminal histidine residue 16 (Padanilam *et al.*, 2002).

How do these structural determinants of the N-terminal inactivation domain fit into current models of channel structure? Firstly, N-type inactivation is generally described as being dependent on channel opening, although some apparent exceptions have been identified (Murrell-Lagnado & Aldrich, 1993a; Murrell-Lagnado & Aldrich, 1993b; Ayer, Jr. & Sigworth, 1997). This view of the inactivation peptide as an open channel blocker that

binds to the intracellular cavity of the channel (Demo & Yellen, 1991) is consistent with the presence of a cytoplasmic gate formed by the S6 helices in K<sup>+</sup> channels (Section II). As suggested by the KcsA and MthK structures (Doyle *et al.*, 1998; Jiang *et al.*, 2002b), and scanning cysteine accessibility studies (Liu *et al.*, 1997; Del Camino *et al.*, 2000), channel opening exposes the large intracellular cavity that can readily accommodate large intracellular agents such as the N-terminal inactivation domain, or bulky QA compounds (Holmgren *et al.*, 1997). Pore-lining residues in KcsA and other K<sup>+</sup> channels are predominantly hydrophobic, and therefore may form a binding partner for the hydrophobic residues in the N-terminal inactivation domain (Zhou *et al.*, 2001a). In addition, several studies clearly suggest that the inactivation domain must be located at the immediate N-terminus of the channel to effectively confer N-type inactivation, as inactivation domains are non-functional if buried within the N-terminal sequence (Kondoh *et al.*, 1997; Hollerer-Beitz *et al.*, 1999; Wissmann *et al.*, 2003). This is consistent with results of a thermodynamic mutant cycle analysis between the Kvβ1 N-terminus and the inner pore of Kv1.4, which suggested that the N-terminal inactivation domain enters the pore as an extended peptide with minimal secondary structure (Gulbis *et al.*, 2000; Zhou *et al.*, 2001a). Finally, a role for positively charged residues in the inactivation domain has emerged from recent work demonstrating the likely presence of complementary acidic residues in the linkers between the T1 domain and the S1 transmembrane segment (Figs. 1.1B, 1.4; Gulbis *et al.*, 2000). As described, these linkers form four fenestrations that likely constitute an obligatory pathway for the N-terminus to reach the intracellular mouth of the channel pore (Gulbis *et al.*, 2000; Sokolova *et al.*, 2001; Aldrich, 2001). Based on thermodynamic mutant cycle analysis, interactions between N-terminal basic residues and acidic residues in the T1-S1 linker have

been suggested to promote entry and thereby effectively stabilize binding of the inactivation domain (shown in cartoon form in Fig. 1.4; Gulbis *et al.*, 2000).

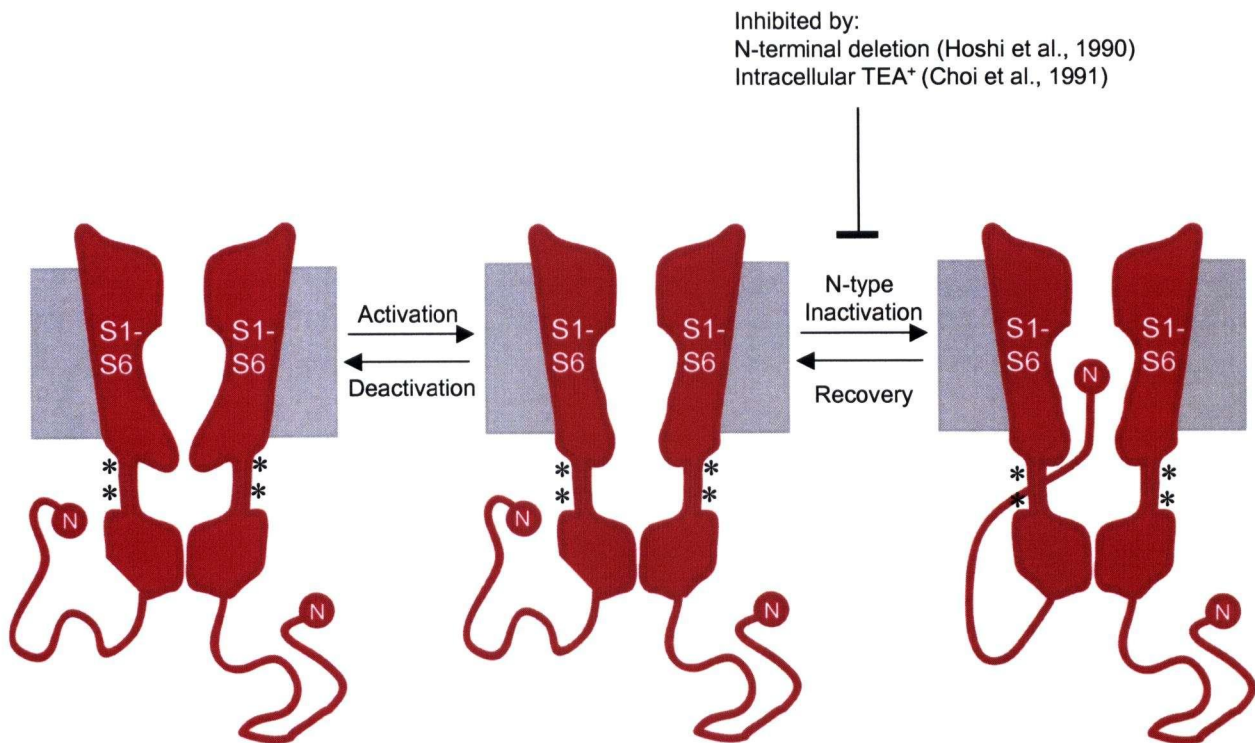


Figure 1.4. Cartoon representation of N-type inactivation. Upon channel opening, the N-terminal inactivation domain is able to access its binding site within the inner cavity of the channel. To access this site, the N-terminal inactivation domain must pass through one of four lateral openings, or fenestrations, formed by T1-S1 linkers (Sokolova *et al.*, 2001). Interactions between positively charged residues in the inactivation domain, and negatively charged acidic residues in the T1-S1 linker sequence (shown as asterisks) promote entry of the inactivation domain into the channel pore (Gulbis *et al.*, 2000).

### ***C-type inactivation***

Early studies of *Shaker* channel inactivation clearly demonstrated that elimination of fast N-type inactivation by deletion of the *Shaker* N-terminal inactivation domain revealed a residual slow inactivation process (Hoshi *et al.*, 1990). This slower inactivation was termed C-type inactivation, because its rate depended upon the identity of C-terminal *Shaker* splice

variants, and particularly upon the identity of *Shaker* residue 463 (Hoshi *et al.*, 1991). However, as described below, it is now thought that C-type inactivation primarily involves conformational changes around the selectivity filter and extracellular entrance to the channel. The C-type inactivation mechanism in *Shaker* can be clearly distinguished from N-type inactivation, because C-type inactivation is not abolished by deletion of N-terminal residues, nor is it substantially inhibited by intracellular TEA<sup>+</sup> (Choi *et al.*, 1991). C-type inactivation is inhibited by elevated concentrations of extracellular K<sup>+</sup> (Hoshi *et al.*, 1990; Lopez-Barneo *et al.*, 1993), and this observation has been confirmed in several mammalian *Shaker* homologues (Rasmusson *et al.*, 1995; Fedida *et al.*, 1999). Also, in channels with pore residues permissive for TEA<sup>+</sup> binding, extracellular TEA<sup>+</sup> is also able to inhibit C-type inactivation (Grissmer & Cahalan, 1989; Choi *et al.*, 1991; Molina *et al.*, 1997). Collectively, these observations have been interpreted as a 'foot in the door' mechanism, in which occupancy of an ion binding site on the extracellular side of the channel by K<sup>+</sup> or TEA<sup>+</sup> slows or prevents the conformational changes required for C-type inactivation (Rasmusson *et al.*, 1998). As mentioned, this effect contrasts significantly with the N-type mechanism, which is insensitive to extracellular K<sup>+</sup> or TEA<sup>+</sup> (Choi *et al.*, 1991).

C-type inactivation in *Shaker* channels can also be dramatically altered by mutations in the extracellular pore region (Lopez-Barneo *et al.*, 1993). Mutagenesis studies of the extracellular mouth of the *Shaker* pore identified an important role for residue T449 (Fig. 1.2D, purple box) in the regulation of the inactivation rate in *Shaker*. Substitution of certain residues (arginine, lysine, glutamate, alanine) at this site dramatically accelerated the inactivation rate (Lopez-Barneo *et al.*, 1993). In contrast, substitution at this site with valine or tyrosine dramatically inhibited inactivation. These effects contrast with the N-type

inactivation mechanism, as studies in multiple channels have demonstrated that mutations at *Shaker* T449 or its equivalent residue in other Kv1 channels does not significantly affect the time course of N-type inactivation (Baukrowitz & Yellen, 1995; Rasmusson *et al.*, 1995).

Importantly, the effects of mutations at T449 (or equivalent residues) as determined for *Shaker* are not universal among Kv1 channels. As an example, Kv1.4 and Kv1.5 possess a lysine and an arginine at this site, respectively, and both exhibit much slower rates of C-type inactivation than the T449R or T449K *Shaker* mutants (Rasmusson *et al.*, 1995; Fedida *et al.*, 1999). Also, mutation of this residue to either a valine or a tyrosine has small effects on the C-type inactivation rates in Kv1.4 or Kv1.5 (Rasmusson *et al.*, 1995; Fedida *et al.*, 1999). Furthermore, in Kv1.2 a valine is present at the *Shaker* T449 equivalent position, yet at physiological pH this channel exhibits inactivation rates comparable to those observed in Kv1.5 (Russell *et al.*, 1994; Steidl & Yool, 1999). Thus, among the mammalian Kv1 channels, the identity of the *Shaker* T449 equivalent residue exerts weaker effects on the C-type inactivation rate than in the *Shaker* channel itself, and may not be a universally good predictor of the C-type inactivation rate.

Another distinction between C-type and N-type inactivation arises from their respective functional stoichiometry. As described previously, multiple N-terminal inactivation domains in a K<sup>+</sup> channel behave essentially independently, and only one is necessary to confer N-type inactivation (MacKinnon *et al.*, 1993; Lee *et al.*, 1996). In contrast, experiments in both *Shaker* and Kv1.3 suggest that the C-type inactivation transition is a cooperative transition of all four channel subunits. Using chimeras or coexpression of channels with different rates of C-type inactivation (*Shaker* A463 or V463, and equivalent mutations in Kv1.3), several groups demonstrated that all four subunits of a channel

contribute to the activation energy of the C-type inactivation transition (Ogielska *et al.*, 1995; Panyi *et al.*, 1995). This demonstration of cooperativity has also been confirmed with mutations at other locations in the *Shaker* channel (Ogielska *et al.*, 1995; Larsson & Elinder, 2000). These findings suggest that C-type inactivation does not arise from independent gates in individual subunits (as for the N-type mechanism), but rather a cooperative rearrangement of all four subunits of the channel.

### ***Alternative inactivation phenotypes***

Essentially by default, inactivation mechanisms that persist after N-terminal deletion are frequently categorized as C-type mechanisms. However, the properties characterized for C-type inactivation in *Shaker* channels do not generalize to many Kv channels. A notable and well-described example is Kv2.1, in which inactivation actually appears to be accelerated by increasing extracellular TEA<sup>+</sup> or K<sup>+</sup> (Klemic *et al.*, 1998). In addition, the inactivation-voltage relationship of Kv2.1 exhibits a very prominent 'U-shape', such that intermediate voltages (eg. 0 mV) result in more rapid and profound inactivation than higher voltages (eg. +60 mV). This apparent voltage-dependence of inactivation contrasts with C-type inactivation in *Shaker* and its mammalian Kv1 homologues, which exhibit relatively voltage-independent inactivation at voltages that saturate channel open probability (Hoshi *et al.*, 1991; Fedida *et al.*, 1999; Kurata *et al.*, 2001). In addition, this inactivation behavior of Kv2.1 has been attributed to preferential inactivation from partially-activated closed states of the channel, whereas C-type inactivation of *Shaker* is thought to occur primarily from the open state (Olcese *et al.*, 1997; Klemic *et al.*, 1998). Other channels also exhibit divergent inactivation properties from *Shaker*. In rapidly inactivating Kv4 channels, elevation of extracellular K<sup>+</sup> concentration promotes inactivation and inhibits recovery, and these

channels also exhibit a significant component of closed-state inactivation (Jerng & Covarrubias, 1997; Jerng *et al.*, 1999; Bähring *et al.*, 2001). In hERG, inactivation is inhibited by extracellular TEA<sup>+</sup>, but unlike *Shaker*, hERG inactivation exhibits considerable voltage-dependence (Smith *et al.*, 1996; Zhang *et al.*, 2003a).

These differences in the voltage-dependence and sensitivity of inactivation to extracellular cations raise the difficult issue of whether their classification as distinct inactivation mechanisms is merited. At present, the bulk of our understanding of the conformational changes of non N-type mechanisms of inactivation has arisen from studies of C-type inactivation in *Shaker*, reviewed in some detail in the sections that follow, but whether similar conformational changes underlie inactivation in other channels is unclear. It is of relevance to the experimental work presented here that distinctions between the properties of Kv2.1 and *Shaker* C-type inactivation have led one group to introduce the term ‘U-type’ inactivation (Klemic *et al.*, 2001). Various properties ascribed to ‘U-type’ inactivation of Kv2.1 have also been described in other channels, and in Chapters 3 and 4, we report several manipulations of channel structure that can impart a U-shaped inactivation-voltage relationship to the *Shaker* homologue Kv1.5 (Kurata *et al.*, 2002). Importantly, ‘U-type’ inactivation remains a phenotypic description of channel behaviour, as the mechanism underlying this process is poorly understood, and it is unclear whether it differs significantly from C-type inactivation. Because of this uncertainty, the term ‘slow inactivation’ is occasionally used here to collectively include non N-type mechanisms of Kv channel inactivation, that do not necessarily exhibit classical features associated with C-type inactivation in *Shaker*.

### *Synergistic interactions of N-type and C-type inactivation*

An important conclusion arising from N-terminal deletion studies of *Shaker* channel inactivation is that multiple mechanisms of inactivation can co-exist and interact in Kv channels, and studies examining these interactions have contributed significantly to our understanding of C-type inactivation. Characterization of both *Shaker* and Kv1.4 has demonstrated that despite causing a much more rapid inactivation rate, recovery from inactivation is unaffected by the presence of the N-type inactivation domain (Baukrowitz & Yellen, 1995; Rasmusson *et al.*, 1995), showing that it is the C-type mechanism that governs the time course of recovery in channels with both N-type and C-type inactivation. Additionally, Baukrowitz and Yellen (1995) made the important observation that use-dependent reductions of peak current in *Shaker* could be abolished either by removal of N-type inactivation (through N-terminal truncation of the channel), or by slowing of C-type inactivation (by the T449V point mutation in the extracellular pore). They reasoned that use-dependent current reduction in *Shaker* arose from an interaction between the N-type and C-type mechanisms, and suggested that N-type inactivation actually promotes and accelerates the onset of the C-type inactivation process. A further critical observation was that use-dependent current reduction in *Shaker* was strongly dependent on the concentration of extracellular  $K^+$ . This observation was extended to demonstrate that quaternary ammonium ions, which are intracellular open pore blockers of  $K^+$  channels, also promoted C-type inactivation when applied intracellularly, in a manner highly dependent on extracellular  $K^+$  concentration (Baukrowitz & Yellen, 1995; Baukrowitz & Yellen, 1996b).

These experiments culminated with the proposal that C-type inactivation depends on the occupancy of a highly  $K^+$  selective 'control site' located near the extracellular mouth of

the channel, and likely within the selectivity filter of the channel (Baukrowitz & Yellen, 1995). It was hypothesized that certain permeant ions including  $K^+$  or  $Rb^+$ , but not  $Na^+$ , can occupy this site and stabilize the open state, preventing C-type inactivation (Baukrowitz & Yellen, 1995; Yellen, 1998). In the simplest conception of this model, blockade of outward  $K^+$  permeation by N-type inactivation allows  $K^+$  ions to evacuate the  $K^+$  channel pore and ‘control site’, and prevents outward flowing  $K^+$  ions from replenishing this binding site. If extracellular  $K^+$  concentration is high, prolonged evacuation of  $K^+$  from the pore is unlikely, and so the onset of C-type inactivation is delayed or eliminated. In contrast, in minimal concentrations of extracellular  $K^+$ , ions are absent from the control site for longer durations, and C-type inactivation is accelerated (Baukrowitz & Yellen, 1996b). Delineation of this mechanism of interaction between the N- and C-type mechanisms of inactivation provided a critical foundation for the current understanding of the C-type inactivation process, with the realization that C-type inactivation is fundamentally affected by ion occupancy of the pore (Baukrowitz & Yellen, 1995; Baukrowitz & Yellen, 1996b).

#### *Allosteric coupling of N-type and C-type mechanisms*

An ‘allosteric’ mechanism of coupling between N- and C-type inactivation has also been suggested, in which direct structural interactions between the N-terminal inactivation domain (or intracellular blockers such as quinidine) and the inner pore of the channel govern the onset of C-type inactivation, and outweigh the effects of  $K^+$  depletion (Rasmusson *et al.*, 1998; Wang *et al.*, 2003; Bett & Rasmusson, 2004). At present, the relative importance of this mechanism, and the channels in which it acts, have not been clearly delineated. Another significant drawback of the allosteric hypothesis of coupling between N-type and C-type inactivation is that a detailed structural model of the mechanism has yet to be developed. At

various times, it has been proposed that binding of the N-terminal inactivation domain immobilizes the voltage-sensors for as long as the N-terminus remains bound to the channel, and that this immobilization of the voltage-sensors in their activated conformation promotes C-type inactivation (Rasmusson *et al.*, 1998). More recently, it has been proposed that lipophilic interactions between the Kv channel inner cavity and the inactivation domain causes a reorientation of the S6 transmembrane domain into a conformation that resembles or promotes C-type inactivation (Bett & Rasmusson, 2004). While allosteric interactions between the pore and the N-type inactivation domain or other intracellular blockers seem likely (Baukrowitz & Yellen, 1996a; Baukrowitz & Yellen, 1996b; Rasmusson *et al.*, 1998), structural interpretations of this process remain vague, and have not yet provided detailed insights into the mechanism of C-type inactivation.

#### ***The Role of the Selectivity Filter in C-type Inactivation***

The role of the selectivity filter in C-type inactivation has been highlighted and refined by studies of Na<sup>+</sup> permeation through Kv channels during channel inactivation. In particular, when K<sup>+</sup> ions are absent from recording solutions, and replaced with Na<sup>+</sup> ions, *Shaker* inactivation is significantly accelerated, and its inactivated state retains a significant permeability to Na<sup>+</sup> ions. This is apparent as a Na<sup>+</sup> current that persists after the onset of inactivation (Starkus *et al.*, 1997). These findings, and similar results in other channels, have many important implications regarding the conformational changes associated with C-type inactivation (Starkus *et al.*, 1997; Wang *et al.*, 2000a; Wang *et al.*, 2000b). Firstly, the rapid rate of inactivation observed with Na<sup>+</sup> as the permeant ion suggests that Na<sup>+</sup> does not inhibit C-type inactivation with nearly the potency of K<sup>+</sup>, consistent with the results of Baukrowitz and Yellen (1995). This may arise either because Na<sup>+</sup> does not interfere with (or may

promote) closure of the C-type inactivation gate, or because  $\text{Na}^+$  has a relatively weak affinity and/or brief dwell time at the ion binding site regulating C-type inactivation (Starkus *et al.*, 1997; Ogielska & Aldrich, 1999). In addition, the persistent  $\text{Na}^+$  current through inactivated channels suggested that C-type inactivation does not entail a complete closure/collapse of the permeation pathway, but involves a conformational change at or near the selectivity filter that remains permissive for  $\text{Na}^+$  permeation (Yellen, 1998).

Careful examination of the effects of extracellular  $\text{K}^+$  ions on the  $\text{Na}^+$  permeation properties of Kv channels has yielded further insight into the role of the selectivity filter in C-type inactivation (Kiss & Korn, 1998). In general, extracellular  $\text{K}^+$  exerts two very significant effects on  $\text{Na}^+$  permeation. Firstly, addition of micromolar concentrations of extracellular  $\text{K}^+$  results in a reduction of  $\text{Na}^+$  currents through the channel. This is a reflection of competition for binding sites within the selectivity filter. Tightly binding  $\text{K}^+$  ions are able to exclude more weakly binding  $\text{Na}^+$  ions, and thereby impede  $\text{Na}^+$  permeation through the channel (Korn & Ikeda, 1995; Kiss *et al.*, 1998). Secondly, addition of extracellular  $\text{K}^+$  results in slower inactivation of macroscopic currents (Kiss & Korn, 1998). Importantly, Kiss and Korn observed that the  $\text{K}^+$  concentration dependence of these two effects were superimposable, and highly  $\text{K}^+$  selective, as both effects exhibited a  $K_d$  for  $\text{K}^+$  of roughly 30  $\mu\text{M}$  in the presence of 145 mM extracellular  $\text{Na}^+$ . These experiments, conducted in a chimeric channel consisting of the Kv1.3 pore fused into the Kv2.1 channel (Gross *et al.*, 1994), suggested that a high affinity  $\text{K}^+$  binding site(s) underlying selectivity for  $\text{K}^+$  over  $\text{Na}^+$  (eg. within the selectivity filter) also underlies  $\text{K}^+$  inhibition of C-type inactivation (Kiss & Korn, 1998). Similar results from Kv1.5 also support this conclusion, although addition of small concentrations of extracellular  $\text{K}^+$  actually results in mild potentiation of  $\text{Na}^+$  through

Kv1.5, masking any blockade of Na<sup>+</sup> current by K<sup>+</sup> competition in the pore. However, small concentrations of K<sup>+</sup> are again sufficient to inhibit C-type inactivation, even in the presence of much larger concentrations of Na<sup>+</sup> ions (Wang *et al.*, 2000b).

Additional support for the role of the selectivity filter arises from apparent changes in ionic selectivity during inactivation (Kiss *et al.*, 1999). In particular, prolonged depolarizations can generate significant changes in the reversal potential of macroscopic ionic currents through Kv channels, as they shift from an open state that is highly K<sup>+</sup> selective to an inactivated state that conducts Na<sup>+</sup> ions with greater facility (Kiss *et al.*, 1999). Under appropriate ionic conditions, it is possible to observe complete reversal of the direction of ionic current during a single depolarization, due to relative changes in the K<sup>+</sup>/Na<sup>+</sup> permeabilities during inactivation. Although most of these experiments were performed using Kv2.1 as a model channel, Kiss *et al.* (1999) reported similar results for a *Shaker* mutant (A463C), and the Kv1.3/Kv2.1 chimeric construct mentioned above (Gross *et al.*, 1994), suggesting that conformational changes of the selectivity filter underlying C-type inactivation may be conserved in multiple Kv channel subtypes (Kiss *et al.*, 1999). Importantly, interpretation of these results has been met with some criticism, as significant intracellular K<sup>+</sup> depletion or accumulation during whole-cell recordings have also been shown to alter the reversal potential (Frazier *et al.*, 2000). Nevertheless, similar changes in selectivity have been reported in C-type inactivated *Shaker* channels, using the inside-out patch clamp configuration, which is likely much less prone to artifacts resulting from ion accumulation or depletion (Starkus *et al.*, 1997; Starkus *et al.*, 1998).

In *Shaker*, it should be noted that the K<sup>+</sup> concentrations required for inhibition of C-type inactivation are somewhat larger than the concentrations required for blockade of Na<sup>+</sup>

current. In *Shaker* A463C channels, 50  $\mu\text{M}$  extracellular  $\text{K}^+$  can significantly block  $\text{Na}^+$  permeation, without slowing the time course of inactivation (Ogielska & Aldrich, 1998; Ogielska & Aldrich, 1999). This diverges somewhat from the reports described earlier, in which the  $\text{K}^+$  affinities for  $\text{Na}^+$  current blockade and inhibition of C-type inactivation were identical (Kiss & Korn, 1998), but the basis for this difference is unresolved. In contrast to the 30-50  $\mu\text{M}$  value reported by Kiss et al. (1998), Ogielska and Aldrich (1998) report a  $\text{K}^+$  affinity for inhibition of C-type inactivation closer to 2 mM, which is similar to the earlier estimate of Baukrowitz and Yellen in *Shaker* (Baukrowitz & Yellen, 1995). This observation implies that  $\text{K}^+$  may occupy a very high affinity binding site (presumably within the selectivity filter) without inhibiting C-type inactivation, prompting the suggestion that conformational changes of the selectivity filter underlying C-type inactivation may be extremely localized (Ogielska & Aldrich, 1999).

Other experimental data also support the notion that C-type inactivation involves a highly localized change in the conformation of the selectivity filter. Firstly, channel blockade by  $\text{Ba}^{2+}$  does not impede C-type inactivation, and it has been shown that C-type inactivation can actually trap  $\text{Ba}^{2+}$  within the *Shaker* channel pore (Harris *et al.*, 1998). Since the high affinity  $\text{Ba}^{2+}$  binding site is thought to overlap with a  $\text{K}^+$  binding site at the cytoplasmic end of the selectivity filter (Jiang & MacKinnon, 2000), these data suggest that C-type inactivation may require only a very localized constriction of the selectivity filter. Also, C-type inactivated channels, while impermeant to  $\text{K}^+$ , seem to maintain some elements of  $\text{K}^+$  selectivity. As evidence for this, sub-millimolar concentrations of  $\text{K}^+$ , particularly in the intracellular medium, are able to inhibit  $\text{Na}^+$  permeation through C-type inactivated *Shaker* channels (Starkus *et al.*, 1997), suggesting that the C-type inactivated pore retains the

ability to bind at least one  $K^+$  ion with high affinity over  $Na^+$ . These observations suggest that constriction of the filter during C-type inactivation may occur in only a restricted segment, possibly near the extracellular side of the filter (Harris *et al.*, 1998; Yellen, 1998; Ogielska & Aldrich, 1999).

X-ray structures of the KcsA channel solved in different ionic conditions have also demonstrated multiple conformations of the selectivity filter. Of particular interest to this discussion of C-type inactivation is the 'low potassium' structure of KcsA, solved with  $Na^+$  as the predominant cation. In the presence of low concentrations of  $K^+$ , the KcsA selectivity filter exhibits a distorted structure, with the backbone carbonyls no longer directed towards the central axis of the pore (Zhou *et al.*, 2001b). It has been suggested that this partially collapsed structure of the selectivity filter may resemble the C-type inactivated  $K^+$  channel pore, although there is no definitive data correlating C-type inactivation with the low  $K^+$  structure (Yellen, 2001; Yellen, 2002). Nevertheless, this structure suggests that the selectivity filter is a dynamic, non-rigid element of the channel, with a detailed structure determined by the balance of stabilizing interactions with other residues in the channel (Fig. 1.2B, C), and the occupant ions.

### ***Conformational changes underlying C-type inactivation***

Other experimental approaches have also added to our understanding of conformational changes at the extracellular mouth of the channel during C-type inactivation. Yellen *et al.* (1994) demonstrated that substitution of a cysteine for *Shaker* residue T449, at the extracellular entrance to the selectivity filter, allowed modulation of slow inactivation by the addition of extracellular divalent cations including  $Zn^{2+}$  and  $Cd^{2+}$ . The onset of C-type inactivation resulted in a dramatic increase in the affinity for metal binding in the T449C

*Shaker* mutant, and therefore stabilization of inactivation in this mutant in the presence of extracellular  $\text{Cd}^{2+}$  (Yellen *et al.*, 1994). These results clearly suggested a conformational rearrangement around the T449 residue during C-type inactivation. In an extension of this study, Liu *et al.* (1996) examined changes in accessibility of several substituted cysteine residues in the extracellular pore mouth during various gating states, and demonstrated a dramatically accelerated rate of cysteine modification by thiol-reactive MTS reagents of *Shaker* pore residues 448-450, after channels had undergone C-type inactivation. This modification rate was relatively insensitive to activation and deactivation transitions of the channel, and these results further suggested a conformational rearrangement of the outer mouth of the  $\text{K}^+$  channel pore during inactivation (Liu *et al.*, 1996). Also consistent with conformational changes of the extracellular pore mouth, is the demonstration that the rate of chloramine T oxidation of *Shaker* residue M448 depends upon the rate of C-type inactivation, as determined by residues substituted at position 449 (Schlief *et al.*, 1996).

Others have also examined the time-dependence of conformational changes around the extracellular entrance to the channel pore by tagging introduced cysteine residues with fluorescent reporter dyes. Conformational changes that alter environmental quenching of the dye affect the fluorescence emission, and these changes can be tracked with various optical methods. Fluorescent dyes introduced immediately above the selectivity filter at residue 449 (Cha & Bezanilla, 1997), and in several other residues throughout the extracellular mouth of the channel (Loots & Isacoff, 1998; Gandhi *et al.*, 2000; Loots & Isacoff, 2000) exhibit changes in emission upon depolarization, with kinetics that approximate the time course of C-type inactivation in these mutants.

Conformational changes at the intracellular side of the channel remain poorly understood and have been less widely studied, especially among Kv channels. However, conformational changes of this region may be of considerable interest in the context of state-dependent drug interactions in the inner channel pore. This is particularly true in the hERG channel, where conformational changes of the S6 helix during C-type inactivation have been suggested to underlie high affinity methanesulfonanilide drug binding (Mitcheson *et al.*, 2000; Chen *et al.*, 2002). In addition, one recently published study has demonstrated that elevation of intracellular tonicity results in acceleration of C-type inactivation in Kv1.4, suggesting that C-type inactivation is accompanied by a significant constriction of the inner cavity (Jiang *et al.*, 2003a). Although it is difficult to rule out conformational changes of the inner pore, we present data in Chapter 5 that suggest that a significant constriction of this region during C-type inactivation is unlikely (Kurata *et al.*, 2004).

#### ***A structural conception of conformational changes during C-type inactivation***

Most recently, Larsson and Elinder have delineated the importance of *Shaker* residue E418 in the regulation of C-type inactivation (Larsson & Elinder, 2000). They demonstrated that disulfide linkage between cysteine residues substituted at E418 (in the *Shaker* S5 segment) and V451 (in the P-region) was found to stabilize C-type inactivation. In contrast, disulfide linkage of E418C to G452C appeared to slow inactivation and favor the open state of the channel. These observations have led to speculation of possible conformational changes of the outer pore during C-type inactivation, illustrated in detail in Fig. 1.5A and B. Based on the KcsA structure, it is likely that in an intact *Shaker* channel the sidechain of residue E418 forms a hydrogen bond with the backbone carbonyl atoms of residue V451 and/or G452. Carbon atoms from *Shaker* residues E418, V451, and G452 are colored white

in Fig. 1.5A and B, illustrating the close proximity of these residues. It is predicted that breakage of this intra-subunit hydrogen bond is an important step during C-type inactivation, permitting a rotation of residues 448-452, with the side chain of V451 turning towards the E418 residue: this conformational state would resemble a disulfide bonded conformation of E418C and V451C (Larsson & Elinder, 2000).

Conformational rearrangement of the outer pore associated with disulfide linkage of cysteines substituted at residues 418 and 451 may be transmitted to the selectivity filter of the channel as follows. Residue P450 lies wedged between the W434 and W435 residues (aromatic cuff residues) from adjacent channel subunits (green residues in Fig. 1.5B), and it is known that the P450 side chain undergoes significant changes in accessibility during inactivation (Liu *et al.*, 1996). Rotation of residues 448-452 would alter the position of residue P450 and may allow the aromatic cuff residues to approach one another and constrict the selectivity filter (Larsson & Elinder, 2000). A second possible influence on the selectivity filter may arise from slight changes in the position of residue D447 (KcsA residue D80), which also likely stabilizes the selectivity filter structure through interactions with W435 in the aromatic cuff (Fig. 1.2C, yellow residues in Fig. 1.5A, B; Kirsch *et al.*, 1995). This interpretation provides a plausible structural model of the rearrangements occurring at the outer pore mouth during inactivation, and the proposed rotation of residues 448-452 is consistent with the previously demonstrated changes in the accessibility of *Shaker* residues 448-450 during inactivation (Liu *et al.*, 1996). Interestingly, many of these residues (particularly those in the aromatic cuff, and Y445 in the selectivity filter, see Fig. 1.2B, C) are involved in both intra- and inter-subunit contacts, which may underlie a structural basis for cooperativity in C-type inactivation.

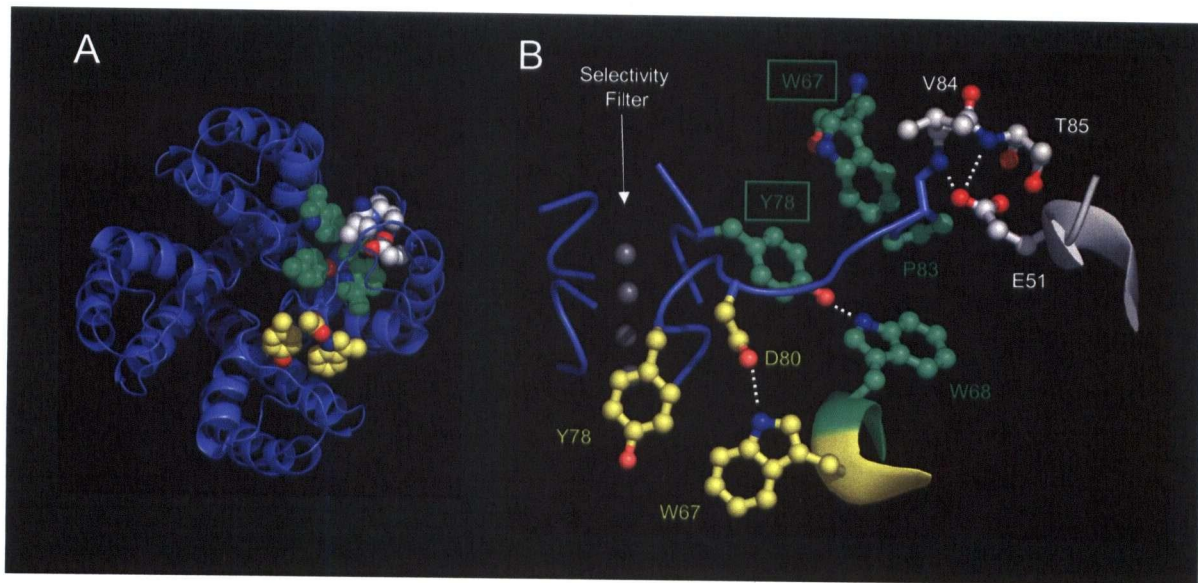


Figure 1.5. Detailed molecular model of extracellular residues involved in C-type inactivation. (A), (B) The KcsA structure has been used to highlight residues proposed to be involved in C-type inactivation of *Shaker* channels (Larsson and Elinder, 2000). For clarity of discussion, carbon atoms in discrete groups of interacting residues have been color-coded (either green, yellow, or white). It is proposed that C-type inactivation requires breaking of hydrogen bonds between E51 (*Shaker* E418) and the backbone nitrogen atoms of V84 and T85 (*Shaker* V451 and T452, white residues). This may precipitate a conformational change in the extracellular pore leading to destabilization of the selectivity filter. Residue P83 (*Shaker* P450) is wedged between residues in the aromatic cuff (green residues). Movement of *Shaker* P450 may allow the aromatic cuff to constrict slightly, leading to conformational changes within the selectivity filter. Alternatively, movement of residue D80 (*Shaker* D447) may also affect a network of stabilizing interactions around the selectivity filter (yellow residues). In panel (B), all residues depicted are from a single subunit, except those with boxed labels, which arise from an adjacent subunit.

### ***Voltage-sensor interactions with the pore during C-type inactivation***

There is evidence that the voltage sensor is intimately involved in C-type inactivation, potentially as a trigger for the process, and also likely undergoes some form of conformational rearrangement in concert with C-type inactivation. As previously described, fluorescent probes introduced at residue T424C and other sites in the outer pore of *Shaker* channels exhibit a slow change in fluorescence intensity that matches the time course of

macroscopic inactivation (Loots & Isacoff, 1998; Gandhi *et al.*, 2000; Loots & Isacoff, 2000). Importantly, after the onset of inactivation (but not when channels are open), T424C conjugated fluorophores appear to detect rapid molecular motions of the voltage sensor. Complementary observations were made for the fluorescence signal observed from tags conjugated to the extracellular end of the S4 transmembrane helix (A359C). That is, two components were observed from the A359C conjugated fluorophore upon depolarization: a fast component attributed to rapid motion of the voltage sensor, and a slow component with kinetics equal to the inactivation rate (Loots & Isacoff, 1998). A subsequent scan of residues in the S5 segment demonstrated that fluorophores conjugated to the *Shaker* channel pore, particularly at residue 419, can detect conformational changes of the voltage sensor (S4) (Loots & Isacoff, 2000). Together, these observations strongly suggest that localized regions of the pore and S4 segment may lie in close proximity in an intact channel. This idea has also been suggested by many recent studies designed to examine the location of S4 relative to the pore. Specific evidence includes the demonstration of disulfide bond formation between cysteine residues substituted in the extracellular ends of the *Shaker* S4 and S5 segments, and the suggestion that residue E418 may act as a surface charge and modulate voltage sensor movement in *Shaker* (Elinder & Århem, 1999; Gandhi *et al.*, 2000; Elinder *et al.*, 2001a; Elinder *et al.*, 2001b; Laine *et al.*, 2003; Gandhi *et al.*, 2003). Consequently, it has been suggested by several groups that movement of the voltage sensor into its activated conformation alters voltage sensor-pore interactions. The ability of fluorophores conjugated to *Shaker* residue 419 to detect movement of the S4 segment has led to the suggestion that interactions in this region might promote breakage of hydrogen bonds around the adjacent

E418 residue (Loots & Isacoff, 2000), precipitating the conformational twisting of residues 448-452, and C-type inactivation, as described previously (Fig. 1.5B).

Functional changes in voltage sensor behaviour are also observed during C-type inactivation, made apparent through characterization of the effects of inactivation on gating charge movement. In particular, it has been demonstrated that the onset of C-type inactivation causes apparent 'immobilization' of gating charge movement (Olcese *et al.*, 1997; Olcese *et al.*, 2001). For example, depolarizations to 0 mV from a holding potential of -60mV (where channels are at rest) displace substantially more gating charge than repolarizations to -60 mV from a holding potential of 0 mV (where channels have C-type inactivated). This asymmetry reflects a hyperpolarizing shift of the voltage-dependence of gating charge movement in channels that have undergone C-type inactivation (Olcese *et al.*, 1997), and has also been confirmed with fluorescence measurements of conformational changes of the voltage sensor (Loots & Isacoff, 1998). The shift is probably better described as a hysteresis of the voltage-dependence of gating charge movement, and suggests that the energetics of voltage-sensor movement are altered significantly after the onset of slow inactivation (Olcese *et al.*, 1997).

Gating current studies in Kv1.5 have provided the important insight that gating charge immobilization can be profoundly decelerated or prevented by permeating cations or the channel blocker 4-aminopyridine (but not quaternary ammonium ions, Fedida *et al.*, 1996; Chen *et al.*, 1997; Wang & Fedida, 2001). For instance, inclusion of weakly permeant Cs<sup>+</sup> ions in the intracellular recording solutions accelerates off gating currents observed upon repolarization, and thereby abolishes any apparent shift of the Q-V relationship. These observations correlate with previously described studies of the effects of permeant ion

binding within the pore on C-type inactivation (Kiss & Korn, 1998; Wang *et al.*, 2000b). That is, these experiments suggest that high affinity binding of permeant ions within the selectivity filter is able to stabilize the open pore structure and somehow prevent the charge immobilization that accompanies C-type inactivation (Chen *et al.*, 1997).

A further interesting observation, although lacking a clear interpretation at present, is that charge immobilization functionally reduces the number of charge systems involved in gating charge movement. That is, the gating charge-voltage relationship measured from negative holding potentials is described by a two-component Boltzmann function, which is thought to reflect the movement of two distinct charge systems (Q1 and Q2) during activation (Bezanilla *et al.*, 1994; Stefani *et al.*, 1994). However, the gating charge-voltage relationship measured from positive holding potentials (favoring charge immobilization), essentially collapses onto a single Boltzmann function, with a  $V_{1/2}$  equal to the *Shaker* Q1 charge system but encompassing a total gating charge equivalent to Q1 and Q2 (Olcese *et al.*, 1997).

### ***Summary***

Inactivation of Kv channels can occur by multiple mechanisms that vary in their time- and state-dependence, and sensitivity to permeant ions and blockers. N-type inactivation arises through blockade of the channel by an inactivation domain tethered to the N-terminus of the channel. C-type inactivation is clearly a very complex, and more poorly understood mechanism of channel closure. The structural basis for the C-type inactivation 'gate' appears to be a localized constriction of the selectivity filter. However, this constriction is likely accompanied by conformational changes throughout the channel, including multiple residues

in the extracellular channel mouth, residues affecting movement of the voltage-sensor, and potentially even residues in the inner pore of the channel.

## **V: Kv CHANNEL REGULATION BY THE CYTOPLASMIC T1 DOMAIN**

Based on EM reconstructions of ion channels, it seems clear that K<sup>+</sup> channel architecture consists of a membrane bound gating domain, and a distinct cytosolic domain (Sokolova *et al.*, 2001). Contributing to the cytosolic mass of the channel is the T1 domain, a very highly conserved domain present in the N-terminus of Kv channels. While early studies demonstrated an important role of the N-terminal T1 domain in channel assembly, it has now become apparent that the T1 domain also plays a significant role in the regulation of channel gating. Much of the experimental work in this thesis revolves around the regulation of slow inactivation of a *Shaker* homologue by the N-terminal T1 domain. The various roles of the T1 domain in Kv channel function are reviewed briefly in the sections that follow.

### ***Detailed structures of Kv channel T1 domains***

Atomic resolution structures of the Kv channel T1 domain have been determined for representative members of the *Shaker*/Kv1 (Kreusch *et al.*, 1998; Gulbis *et al.*, 2000; Minor *et al.*, 2000), *Shaw*/Kv3 (Bixby *et al.*, 1999) and *Shal*/Kv4 (Zhou *et al.*, 2004; Scannevin *et al.*, 2004) channel subfamilies. Interestingly, despite fairly significant divergence of primary amino acid sequence, the T1 domains of all Kv channel subfamilies exhibit the same structural scaffold, with the primary difference being the presence of Zn<sup>2+</sup> binding domains in the Kv2, Kv3 and Kv4 T1 domains, that are absent in the *Shaker* T1 structure (Bixby *et al.*, 1999). The T1 domain exhibits a rotational fourfold axis of symmetry, mirroring the symmetrical arrangement of the channel pore (Kreusch *et al.*, 1998; Doyle *et al.*, 1998). In addition, the T1 domain possesses a central pore (~3.2 Å in diameter at its narrowest

constriction) that is thought to lie in alignment with the central cavity of the channel (Kreusch *et al.*, 1998). The intersubunit interface between the T1 domains exhibits an unusually large number of polar interactions (Minor *et al.*, 2000). Thus, tetramerization of the T1 domain appears to be driven by hydrogen bonding and electrostatic interactions between hydrophilic amino acids, rather than by hydrophobic stabilization of non-polar amino acid side chains. The central pore of the T1 tetramer provoked early speculation that the T1 domain may comprise a portion of the permeation pathway (Kreusch *et al.*, 1998), however, it is now considered unlikely to play a direct role in ion conduction (Kobertz & Miller, 1999).

Do the structures determined for isolated T1 domains reflect their structure in an intact channel? The 'hanging gondola' model of Kv channel structure suggests that the T1 domain exists as a tetramer in the intact channel, resembling the X-ray structure of the isolated domain. Based on the isolated T1 domain structure, pairs of cysteine residues were introduced at sites in close proximity near the intersubunit T1 domain interface in *Shaker*, designed to crosslink T1 domains from separate channel subunits (Kobertz *et al.*, 2000). Multiple introduced cysteine pairs were indeed able to crosslink channel subunits, suggesting that the organization of the T1 domain in the native channel structure resembles the atomic resolution structure determined for the isolated T1 domain. Given that the central pore of the T1 domain is too narrow to allow entry of known pore blockers, several groups inferred that the T1 domain must hang away from the transmembrane domains of the channel, and this seems to be confirmed by the single molecule structural studies of Kv channels described earlier (Gulbis *et al.*, 2000; Kobertz *et al.*, 2000; Sokolova *et al.*, 2001; Sokolova *et al.*, 2003; Orlova *et al.*, 2003). Finally, trypsin cleavage of assembled channels releases a tetrameric N-

terminal fragment that is recognized by antibodies directed against the T1 domain, again suggesting that the T1 domain exists as a tetramer in native Kv channels (Strang *et al.*, 2001).

### ***Roles of the T1 domain in channel assembly***

The T1 domain provides the molecular basis for two important aspects of channel biosynthesis: driving efficient channel assembly, and preventing promiscuous assembly of channels from different subfamilies. Tetramerization of the T1 domains is thought to be a very early step in channel biosynthesis, and has been demonstrated to occur while channels are still attached to ribosomes during protein synthesis (Tu *et al.*, 2000). Multiple studies have demonstrated that N-terminal deletions extending into the T1 domain significantly reduce channel expression in heterologous systems, and this has been attributed to a role of the T1 domain in channel assembly (Tu *et al.*, 1996; Sheng *et al.*, 1997; Kobertz & Miller, 1999; Zerangue *et al.*, 2000). Importantly, deletions within the T1 domain frequently do not completely abolish expression, and interactions between transmembrane segments have been identified as additional determinants of channel assembly, particularly in T1-deleted channels (Tu *et al.*, 1996; Sheng *et al.*, 1997). In addition, Zerangue *et al.* (2000) observed that a *Shaker* construct containing an artificial tetramerization domain (GCN4-LI) in place of the native T1 domain partially rescued expression of T1-deleted channels, and formed functional, voltage-gated, K<sup>+</sup>-selective channels. These observations led to the suggestion that early tetramerization of the T1 domain drives channel assembly, but is not required for later folding and assembly steps of transmembrane domains of the channel (Zerangue *et al.*, 2000).

The second important role of the T1 domain in channel assembly is to prevent promiscuous interfamily multimerization of channel subunits. It has been well demonstrated

that Kv1 family subunits will only multimerize with other Kv1 subunits, Kv2 family subunits will only assemble with other Kv2 subunits, etc. (Li *et al.*, 1992; Li *et al.*, 1993; Shen *et al.*, 1993; Shen & Pfaffinger, 1995; Xu *et al.*, 1995). The molecular basis of this subfamily recognition is encoded at the intersubunit interface of the T1 domain (Bixby *et al.*, 1999). Early studies of *Shaker* channel assembly demonstrated that the T1 domain drives this specificity in channel assembly, and several reports suggest that the T1 domain is the only significant determinant of subfamily specificity in Kv channel assembly (Li *et al.*, 1992; Li *et al.*, 1993). Importantly, chimeric channels consisting of the *Shaker* N-terminal sequence fused to the membrane core of Kv2.1 exhibited functional voltage-gated, K<sup>+</sup>-selective currents, demonstrating functional compatibility between the cytosolic and membrane bound regions of *Shaker* and Kv2.1 (Li *et al.*, 1992). This compatibility/modularity between the transmembrane domains and N-termini of different channel subfamilies has been confirmed in several chimeric studies (Li *et al.*, 1992; Xu *et al.*, 1995; Kurata *et al.*, 2002; Gebauer *et al.*, 2004). Furthermore, chimeric channels consisting of the *Shaker* N-terminus and the Kv2.1 transmembrane domains can successfully heteromultimerize with WT *Shaker* channels, demonstrating that incompatibility between the transmembrane domains cannot underlie the subfamily specificity of channel assembly (Li *et al.*, 1992). Additionally, T1 deleted forms of Kv2.1 and Kv1.4 have been shown to coassemble into hybrid channels (Lee *et al.*, 1994). A final illustration of promiscuous assembly of Kv channel transmembrane domains arises from the demonstration that subfragments of the transmembrane domains of Kv1.3 are able to suppress expression of T1-deleted Kv2.1, suggesting that in the absence of the T1 domain, the transmembrane domains of Kv1.3 and Kv2.1 can interact (Tu *et al.*,

1996). Collectively, these data suggest that the T1 domain is the most important determinant of subfamily specificity in Kv channel assembly.

A final role for the T1 domain in Kv channel biosynthesis is the direction of channel assembly with auxiliary subunits. Various protein binding experiments have illustrated that residues in the T1 domain were critical for association of Kv1 channels with cytosolic  $\beta$ -subunits (Yu *et al.*, 1996). In addition, residues in the Kv1 T1 domain directed the specificity of this assembly, such that Kv1 channels were found to assemble with  $\beta$ -subunits, whereas other Kv channel subfamily members did not (Yu *et al.*, 1996). This role of the T1 domain in the Kv $\alpha$ -Kv $\beta$  assembly has been confirmed by the structural determination of a complex of the T1 domain and Kv $\beta$ 2, which demonstrated specific contacts between a single loop formed at the cytosolic face of the T1 domain, with the C-terminal core of Kv $\beta$ 2 (Gulbis *et al.*, 2000). Mutations of residues on either side of this interacting surface disrupted association of the  $\beta$ -subunit with the channel. Very recently, similar results have been demonstrated in the Kv4 channel subfamily, in which mutations in the analogous cytosolic loop of the Kv4.2 T1 domain appear to disrupt association of Kv4 channels with KChIP subunits (Zhou *et al.*, 2004; Scannevin *et al.*, 2004).

#### ***Gating effects of the T1 domain***

The role of the T1 domain in channel gating has been examined by a true combination of structural and electrophysiological techniques. Atomic resolution structures have been determined for several mutant forms of the *Shaker* family T1 domain, and through characterization of these mutants with patch clamp techniques, several groups have attempted to correlate the structural effects of T1 mutations with alterations of channel function (Minor *et al.*, 2000; Cushman *et al.*, 2000). Mutations throughout the T1 domain can clearly exert

effects on channel gating, and structures have been determined for mutations near the central pore of the T1 tetramer, at the C-terminal face of the tetramer (which is thought to face the membrane bound channel core), and at the intersubunit interface of the T1 domain.

Overall, it has proven difficult to understand the effects of altered T1 structure on changes in channel function. Several mutations in the *Aplysia* Kv1.1 T1 domain exert very innocuous effects on T1 domain structure, but vary in their effects on activation gating of the channel (Cushman *et al.*, 2000). Similarly, through a scan of residues lying at the intersubunit interface of the Kv1.2 T1 domain, Minor *et al.* (2000) identified several mutations that cause significant (between  $-10$  mV and  $+30$  mV) shifts in the Kv1.2 activation  $V_{1/2}$ . However, crystallization of one of these T1 mutants (Kv1.2 T46V) revealed a structure essentially indistinguishable from the WT T1 structure, in spite of a significant  $+20$  mV depolarizing shift of Kv1.2 activation. In general, published results have demonstrated gating effects of mutations with fairly insignificant effects on T1 structure, leading to the proposal that the T1 domain undergoes conformational changes during channel gating, and is conformationally coupled to the activation process (Minor *et al.*, 2000; Cushman *et al.*, 2000). While most studies have concentrated on the role of the T1 domain in channel activation, data presented in this thesis also demonstrates a significant role for the Kv channel T1 domain in the regulation of slow inactivation in the *Shaker* homologue Kv1.5 (Chapters 3 and 4; Kurata *et al.*, 2001; Kurata *et al.*, 2002).

The apparent sensitivity of channel gating to small changes in T1 domain structure is of interest, because the T1 domain forms a segment of the cytosolic domain of the channel (Sokolova *et al.*, 2001), and thus may frequently encounter a number of intracellular signaling molecules. In addition the T1 domain fold is classified in the BTB/POZ family, a

widely conserved protein-protein interaction domain, and so the likelihood of interaction with other proteins or channel domains seems high, but remains undetermined (Albagli *et al.*, 1995; Collins *et al.*, 2001; Jahng *et al.*, 2002). Given the significant gating effects observed for relatively innocuous point mutations, post-translational modification of residues within or near the T1 domain could conceivably alter the structure of this domain sufficiently to cause measurable changes in gating. In addition, RNA editing mechanisms have been demonstrated to alter a number of residues in the T1 domain of the squid giant axon delayed rectifier Kv channel (SqKv1.1A), with variable but often significant effects on channel gating and expression (Rosenthal & Bezanilla, 2002). However, our understanding of a coupling mechanism between the T1 domain and the transmembrane channel core remains incomplete.

## **VI: SCOPE OF THESIS INVESTIGATION**

The primary focus of the experimental work included in this thesis is the mechanism(s) of slow inactivation in Kv channels, with a particular focus on the hKv1.5 channel. Kv1.5 is a mammalian homologue of *Shaker* that is widely expressed throughout the cardiovascular system and elsewhere. It is found in human adult and fetal heart (Tamkun *et al.*, 1991; Fedida *et al.*, 1993), in mouse and rabbit heart (Attali *et al.*, 1993; Sasaki *et al.*, 1995; Dobrzynski *et al.*, 2000), in vascular and intestinal smooth muscles (Overturf *et al.*, 1994; Clément-Chomienne *et al.*, 1999), and also in airways (Adda *et al.*, 1996). The homomeric channel expresses as a rapidly-activating delayed rectifier K<sup>+</sup> current with an intermediate rate of inactivation, that is modulated by the activity of  $\beta$ -subunits (Sewing *et al.*, 1996). In excitable tissues this channel is often proposed to have an important function during repolarization in the termination of excitation events, which has been best defined in human atrium (Fedida *et al.*, 1993; Wang *et al.*, 1993; Schaffer *et al.*, 1998), and vascular

smooth muscle. Clinically, down-regulation of the channel may play a role in the ionic remodeling that accompanies disease states like atrial fibrillation and hypertension (Van Wagoner *et al.*, 1997; Brandt *et al.*, 2000).

Specifically, the work presented here examines multiple mechanisms by which the cytosolic N-terminus of Kv channels interacts with slow inactivation processes. In the first results chapter (Chapter 3), we describe a detailed biophysical study of the inactivation properties of an N-terminally truncated form of Kv1.5. Kv1.5 does not possess an N-type mechanism of inactivation, instead inactivating by a C-type mechanism with properties similar to those observed in *Shaker*. Using electrophysiological experiments combined with kinetic modeling, we provide a mechanistic interpretation of the role of the Kv1.5 N-terminus in the regulation of channel inactivation, suggesting that the cytosolic N-terminus regulates the extent of inactivation observed from closed-states of the channel. This study is the first clear demonstration of N-terminal modulation of slow inactivation in a *Shaker* family Kv channel (Kurata *et al.*, 2001).

Chapter 4 describes several molecular manipulations of the Kv1.5 channel, with a goal of examining the molecular determinants underlying the N-terminal regulation of inactivation in this channel. These manipulations include a deletion analysis spanning most of the cytoplasmic Kv1.5 N-terminus, chimeric substitution of residues from other Kv1 channels and Kv2.1, and analysis of point mutations lying near the T1 intersubunit interface. This study delineates a critical role for the T1 domain in the regulation of closed-state inactivation in Kv1.5 (Kurata *et al.*, 2002).

The final study presented as Chapter 5 offers a new perspective on the most well-defined mechanism of interaction between the N-terminus and the pore: N-type inactivation.

In this study, we have exploited the properties of Na<sup>+</sup> permeation through Kv1.4 and Kv1.5, and particularly the development of a high permeability to Na<sup>+</sup> during recovery from C-type inactivation, to examine interactions between the Kv1.4 N-terminal inactivation domain and the pore of Kv1 channels, before after the onset of C-type inactivation. The study demonstrates two potentially important features of C-type inactivated K<sup>+</sup> channel pores. Firstly, this study demonstrates that after C-type inactivation, the channel pore remains a patent receptor for the N-terminal inactivation domain, suggesting that the inner cavity of the channel remains accessible to cytosolic compounds after the onset of C-type inactivation. Secondly, the study demonstrates what appears to be a slightly enhanced interaction between the Kv1.4 N-terminal inactivation domain and the C-type inactivated pore, suggesting that the inactivation domain dissociates slowly from the pore of a C-type inactivated channel (Kurata *et al.*, 2004).

## **CHAPTER 2: MATERIALS AND METHODS**

### ***Cell preparation and transfection***

All cells were grown in Minimal Essential Medium (MEM) with 10% fetal bovine serum, at 37° C in an air/5% CO<sub>2</sub> incubator. Most experiments reported were carried out using HEK 293 cells as a transient expression system. In some experiments, a Mouse *ltk*<sup>-</sup> cell line was used as a transient expression system due to its lack of endogenous voltage-gated K<sup>+</sup> channel subunits (Chapters 3,4). One day before transfection, cells were plated on glass coverslips in 35 mm Petri dishes to achieve 20-30% confluence. On the day of transfection, cells were washed once with MEM with 10% fetal bovine serum. In order to identify the transfected cells efficiently, channel DNA was co-transfected with the vector pHook-1 (Invitrogen, San Diego, CA, USA). This plasmid encodes the production of an antibody to the hapten phOX, which when expressed is displayed on the cell surface. Channel DNA was mixed with pHook-1 (1 µg of pHook, 1-3µg of channel DNA) and 2 µL of LipofectAMINE 2000 (Gibco-BRL, Gaithersburg, MD, USA) in 100 µL of serum-free MEM, incubated for 20-30 minutes at room temperature then added to the Petri dishes. Cells were allowed to grow overnight before recording. One hour prior to experiments, cells were treated with Capture-tec beads coated with phOX (Invitrogen, San Diego, CA, USA). After 15 min, excess beads were washed off with cell culture medium, and cells which had beads stuck to them were used for electrophysiological recordings.

In later experiments, the pHook vector was abandoned for the identification of transfected cells, and substituted with a vector encoding green fluorescent protein (GFP). As with the pHook vector (above), channel DNA was mixed with the GFP vector (1 µg of GFP, 1-3 µg of channel DNA) in 100 µL of serum-free MEM, incubated for 20-30 minutes at room temperature, then added to the Petri dishes containing cells. Transfected cells were

allowed to grow overnight before recording, and successful transfectants were identified by illumination with a Xenon arc lamp fluorescence attachment (CAIRN research, Kent, UK) on the patch clamp apparatus.

HEK293 cell lines stably expressing full-length human Kv1.5 or the short form of human Kv1.5, hKv1.5 $\Delta$ N209, were developed and used in the experiments presented in the Chapter 3. For the generation of stable cell lines, HEK-293 cells were stably transfected with linearized plasmids carrying full-length hKv1.5 or Kv1.5 $\Delta$ N209 cDNAs using LipofectACE reagent (Canadian Life Technologies, Bramalea, ON, Canada). Transfectants were selected and maintained using a 0.5 mg/mL dose of G418 antibiotic, which exploits a selection marker present within the vector used to carry both cDNAs.

### ***Recording Solutions***

All chemicals were purchase from Sigma Aldrich Chemical Co. (Mississauga, Ont., Canada). Recording solutions were prepared as follows.

#### I) Standard K<sup>+</sup> recording solutions:

Patch pipettes contained (in mM): NaCl, 5; KCl, 135; Na<sub>2</sub>ATP, 4; GTP, 0.1; MgCl<sub>2</sub>, 1; EGTA, 5; HEPES, 10; and was adjusted to pH 7.2 with KOH. The bath solution contained (in mM): NaCl, 135; KCl, 5; HEPES, 10; sodium acetate, 2.8; MgCl<sub>2</sub>, 1; CaCl<sub>2</sub>, 1; and was adjusted to pH 7.4 with NaOH. For recordings in high extracellular K<sup>+</sup> (135 mM) conditions, the bath solution contained (in mM): KCl, 135; HEPES, 10; MgCl<sub>2</sub>; Dextrose, 10; adjusted to pH 7.4 with KOH.

#### II) Standard Na<sup>+</sup> recording solutions:

Patch pipettes contained (in mM): NaCl, 135; Na<sub>2</sub>ATP, 4; GTP, 0.1; MgCl<sub>2</sub>, 1; EGTA, 10; HEPES, 5; and was adjusted to pH 7.2 with NaOH. Na<sup>+</sup> bath solution contained

(in mM): NaCl, 135; HEPES, 10; Dextrose, 10; MgCl<sub>2</sub>, 1; CaCl<sub>2</sub>, 1; and was adjusted to pH 7.4 with NaOH.

III) Standard Cs<sup>+</sup> recording solutions:

Patch pipettes contained (in mM): CsCl, 135; MgCl<sub>2</sub>, 1; EGTA, 10; HEPES, 5; and was adjusted to pH 7.2 with CsOH. Cs<sup>+</sup> bath solution contained (in mM): CsCl, 135; HEPES, 10; Dextrose, 10; MgCl<sub>2</sub>, 1; CaCl<sub>2</sub>, 1; and was adjusted to pH 7.4 with CsOH.

### ***Electrophysiological procedures***

Coverslips containing cells were removed from the incubator before experiments and placed in a superfusion chamber (volume ~250 µl) containing the control bath solution at room temperature, and perfused with bathing solution throughout the experiments. Whole-cell current recordings and data analysis were done using an Axopatch 200A amplifier and pClamp (v. 8 or 9) software (Axon Instruments, Foster City, CA, USA). Patch electrodes were fabricated using thin-walled borosilicate glass (World Precision Instruments; FL, USA). Electrodes had resistances of 1-3 MΩ when filled with control filling solution. Capacity compensation and 80% series resistance compensation were used in all whole cell recordings. Data were sampled at 10-20 kHz and filtered at 5-10 kHz. Membrane potentials have not been corrected for small junctional potentials between bath and pipette solutions.

### ***Data analysis and modeling***

Throughout the text, the voltage-dependence of activation and inactivation are fit with Boltzmann functions of the form:  $y = 1/(1+\exp[(V_{1/2}-V)/k])$  and  $y = 1/(1+\exp[(V-V_{1/2})/k]) + C$ , respectively, where  $V_{1/2}$  represents the voltage at which 50% activation or inactivation occurred,  $V$  is the membrane potential, and  $k$  is a slope factor that reflects the steepness of the

voltage dependence.  $C$  represents the fraction of non-inactivating channels at potentials where inactivation was most complete.

Kinetic models in Chapters 3 and 5 were constructed using ScoP and ScoPfit (version 3.51, Simulation Resources, Berrien Springs, MI, USA). The number of channels moving between different states was described by a series of first-order differential equations and solved numerically. The transition rates between states in the activation pathway were exponential functions of voltage of the form:  $\text{rate} = k_o \cdot \exp[z_i \cdot e_0 \cdot V/kT]$ , where  $k_o$  represents the rate at 0 mV,  $z_i$  refers to the effective valency ( $z\delta$ ) for the transition, and  $e_0$ ,  $V$ ,  $k$ , and  $T$  have their usual meanings. Annotated source code for the models presented in the text are included in Appendices 1 and 2.

### ***Molecular Biology and Channel Mutations***

The mammalian expression vector pcDNA3 (Invitrogen, San Diego, CA, USA) was used for expression of all channel constructs used in this study. All primers used were synthesized by SigmaGenosys (Oakville, Ont., Canada). All constructs have been sequenced to check for sequence errors, and to ensure the correct reading frame (NAPS Unit, University of British Columbia, Vancouver, Canada).

### ***N-terminal deletions of Kv1.5***

The Kv1.5 $\Delta$ N19, Kv1.5 $\Delta$ N91 and Kv1.5 $\Delta$ N162 (Fig. 4.5) mutants were generated by Bal31 exonuclease digestion from the 5' end of hKv1.5. Resulting fragments were ultimately subcloned into a pcDNA3 vector cut with *NcoI* (blunted with Klenow fragment to introduce a start codon) and *XbaI* restriction enzymes. The Kv1.5 $\Delta$ N119 and Kv1.5 $\Delta$ N140 mutants (Fig. 4.5) were generated by PCR amplification of the cDNA encoding residues 120 or 141 to the C-terminus of hKv1.5. The 5' primers used were

5'-CCCAAGCTTATGCAGCGCGTCCACATCAACATC-3' for Kv1.5ΔN119, and 5'-CCCAAGCTTATGGGCACCCTGGCGCAGTTTCC-3' for Kv1.5ΔN140 (introduced restriction sites are underlined). The resulting channels were ultimately subcloned in a pcDNA3 vector using *HindIII* and *NotI* restriction sites. Kv1.5T19+163 (Fig. 4.5) was generated with a PCR-based protocol. Using FL Kv1.5 as template, two PCR fragments were generated using 5'-CCCAAGCTTATGGGCACCCTGGCGCAGTTC-3' and 5'-CGCCAGGGTGCCAGCTG-3' for one of the fragments, and 5'-CAGCTGGGCACCCTGGCGCTACTTCTTCGACCGCAACCG-3' and 5'-AAGACCGAGACGATGGCGATG-3'. These two fragments were mixed together as the template for a third PCR reaction, using 5'-CCCAAGCTTATGGGCACCCTGGCGCAGTTC-3' and 5'-AAGACCGAGACGATGGCGATG-3'. The Kv1.5ΔN188 mutant was generated by removal of the *NcoI-HincII* fragment of Kv1.5 (Fig. 4.5). Kv1.5ΔN209 was generated by removal of the *NcoI-NcoI* fragment of Kv1.5.

### ***N-terminal deletions of Kv2.1***

Kv2.1ΔN101 was generated by removal of sequence up to the *NarI* restriction site in rKv2.1. Residue 101 in Kv2.1 is equivalent to Kv1.5 residue 181.

### ***Kv1.XN/Kv1.5 Chimeric Constructs***

For preparation of the Kv1.1N/Kv1.5 and Kv1.3N/Kv1.5 chimeric channels, DNA encoding the Kv1.5 channel core beginning at the *NcoI* site encoding residue M210 was subcloned into homologous *NcoI* sites in pGBT9 vectors encoding the N-termini of Kv1.1 and Kv1.3 (gift of Dr. Barbara Wible, Rammelkamp Health Science Centre, Cleveland, OH, USA) using *NcoI* and *XbaI* restriction sites. The resulting fusion protein was then subcloned

into the pcDNA3 vector for mammalian expression as an *EcoRI/EcoRI* fragment, and screened for correct orientation of the insert.

The Kv1.4N/Kv1.5 and Kv1.4N/Kv1.5R487V chimeric constructs were generated by PCR amplification of the Kv1.4 N-terminus using the T7 primer and 5'-GGAATTCTCCGGATATTCAAAGAGGAGC-3', which introduced a *BspEI* restriction site (underlined) at Kv1.4 residue E301, and allowed fusion of the Kv1.4 N-terminus to the Kv1.5 channel just before the initiation of the S1 transmembrane segment. The resulting PCR fragment was subcloned into pcDNA3 vectors carrying either full-length Kv1.5 or Kv1.5R487V, using *HindIII* and *BspEI* restriction sites.

#### ***Kv1.5/Kv2.1 Chimeric Constructs***

For preparation of Kv1.5N/Kv2.1 T19+163/Kv2.1, DNA encoding amino acids 180 to the C-terminus of rKv2.1 were amplified by PCR, such that a *BspEI* restriction site at P180 of rKv2.1, and a *XbaI* site following the termination codon were introduced. The primers used were 5'-ATCGTCCGGAGTCGTCGGTGGCCGCCAAG-3' for the 5' end, and 5'-GCTCTAGACCCTCTGTGGTAGGGAGC-3' for the 3' end (introduced restriction sites are underlined). The resulting fragment was used to replace the analogous region of Kv1.5 encoding amino acids 243 to the C-terminus of Kv1.5, in a pcDNA3 vector containing either Kv1.5 or the Kv1.5T19+163 deletion, using *BspEI* and *XbaI* restriction sites.

For preparation of Kv2.1N/Kv1.5, the N-terminus of rKv2.1 was amplified by PCR, introducing a *EcoRI* restriction site preceding the start codon, and a *BspEI* restriction site at residue 180 of rKv2.1. The primers employed were 5'-CGGAATTCGGCATGACGAAGCATGGC-3' as the 5' primer and 5'-GCTGTCCGGATACTCCAGCAGATCCCAGAG-3' as the 3' primer (introduced

restriction sites are underlined). The resulting fragment was used to replace analogous Kv1.5 sequence encoding amino acids of the Kv1.5 N-terminus up to residue 243, by subcloning into a pcDNA3 vector encoding Kv1.5 using *HindIII* and *BspEI* restriction sites.

### ***Site-directed mutagenesis***

Site-directed mutagenesis of Kv1.5 was performed using the Stratagene Quikchange kit (La Jolla, CA, USA). For preparation of the Kv1.5AAQL mutant, the primers used were 5'-GGGCTGCGCTTTGCGGCGCAGCTGGGCACCCTG-3' and its complement (mutated codons are underlined). For preparation of the Kv1.5R487V mutant, the primers used were 5'- GCTACGGGGACATGGTTCCCATCACTGTTGG -3' and its complement. For preparation of the Kv1.5 R487T mutant the, the primers were 5'- GCTACGGGGACATGACGCCCATCACTGTTGG -3' and its complement. For preparation of Kv1.4 K533V, the primers used were 5'GGGCTATGGGGACATGGTGCCCA-TCACTGTAGGG-3' and its complement.

**CHAPTER 3: ALTERED STATE-DEPENDENCE OF SLOW INACTIVATION IN  
LONG AND SHORT FORMS OF Kv1.5**

## CHAPTER SUMMARY

Evidence from both human and murine cardiomyocytes suggests that truncated isoforms of Kv1.5 can be expressed *in vivo*. In this chapter, we have characterized the activation and inactivation properties of Kv1.5 $\Delta$ N209, a naturally-occurring short form of human Kv1.5 that is lacking 75% of the T1 domain. When expressed in HEK 293 cells, this truncated channel exhibited a  $V_{1/2}$  of  $-19.5 \pm 0.9$  mV for activation and  $-35.7 \pm 0.7$  mV for inactivation, compared with a  $V_{1/2}$  of  $-11.2 \pm 0.3$  mV for activation and  $-20.9 \pm 1.6$  mV for inactivation in full-length Kv1.5. Kv1.5 $\Delta$ N209 channels exhibited several features rarely reported in voltage-gated K<sup>+</sup> channels and absent in full-length Kv1.5, including a U-shaped voltage-dependence of inactivation and 'excessive cumulative inactivation', in which a train of repetitive depolarizations resulted in greater inactivation than a continuous pulse. Kv1.5 $\Delta$ N209 also exhibited a stronger voltage dependence of recovery from inactivation, with the time to half-recovery changing roughly 15-fold between recovery potentials of  $-50$  mV and  $-110$  mV, while this parameter varied only 3-fold over the same voltage range in full-length Kv1.5. During trains of human action potential voltage clamps, Kv1.5 $\Delta$ N209 showed 30-35% greater accumulated inactivation than full-length Kv1.5. These results are explained with a model based on an allosteric model used previously to describe inactivation of Kv2.1 (Klemic *et al.*, 1998), in which deletion of the N-terminus results in inactivation from partially-activated closed states that is accelerated relative to full-length Kv1.5.

## BACKGROUND

It is not generally appreciated that Kv1.5 channels, like KvLQT1 (Jiang *et al.*, 1997), appear to exist in at least two isoforms, including an N-terminally truncated form, in murine and human cardiac myocytes. A methionine residue at hKv1.5 residue 210 provides an alternative start codon for expression of an N-terminally truncated 'short form' of the channel. In the mouse, it appears that this isoform arises from an unusual splicing mechanism within the exonic structure of the Kv1.5 gene (Attali *et al.*, 1993). Northern blot analysis has also previously revealed two distinct bands of Kv1.5 RNA of appropriate size in human atrium, both neonatal and adult (Tamkun *et al.*, 1991; Fedida *et al.*, 1993). Apart from alternative splicing, other mechanisms may also exist that generate truncated channel isoforms, as it has been recently suggested that an unidentified mechanism of post-translational proteolysis can result in the generation of tetrameric N-terminally truncated channels in some mammalian cell lines (Strang *et al.*, 2001).

The region of the N-terminus that is absent in the short form of Kv1.5 (Kv1.5 $\Delta$ N209) is important for a number of fundamental properties, as described in Chapter 1 (Attali *et al.*, 1993). The first 200 amino acids mediate the interaction of the channel with  $\beta$  subunits, which can alter the extent and rate of inactivation in this channel by introducing an N-type mechanism of inactivation (Rehm & Lazdunski, 1988; Rettig *et al.*, 1994; Sewing *et al.*, 1996; Pongs *et al.*, 1999; Gulbis *et al.*, 2000). The N-terminus also contains multiple potential phosphorylation and interaction sites, including a proline-rich domain required for channel modulation by Src tyrosine kinase, and a binding site for  $\alpha$ -actinin-2 (Holmes *et al.*, 1996; Maruoka *et al.*, 2000; Nitabach *et al.*, 2001). Also within the N-terminus, the T1 domain prevents heteromultimerization of different Kv channel subfamilies (Li *et al.*, 1992;

Xu et al., 1995; Shen and Pfaffinger, 1995), although it is now known that the T1 domain is not absolutely required for channel assembly, as T1 deleted mutants of Kv2.1, *Shaker*, Kv1.3, Kv1.4 and Kv1.5 have all been shown to assemble into functional channels (VanDongen et al., 1990; Lee et al., 1994; Tu et al., 1996; Fedida et al., 1999; Kobertz & Miller, 1999). The T1 domain also influences channel gating, as several studies have shown that deletion mutations and point mutations in the N-terminus can substantially alter the voltage-dependence and/or kinetics of channel activation (Kobertz and Miller, 1999; Minor et al., 2000; Cushman et al., 2000). However, the mechanism by which these effects arise remains uncertain, particularly given recent crystallographic and biochemical evidence suggesting that in intact channels, the T1 domain tetramerizes and adopts a “hanging gondola” structure, structurally distinct from the transmembrane regions of the channel (Kreusch et al., 1998; Gulbis et al., 2000; Kobertz et al., 2000; Sokolova et al., 2001; Sokolova et al., 2003; Orlova et al., 2003).

Prompted by multiple reports of altered activation properties by mutations or deletions within the Kv channel N-terminus, we have characterized the gating properties of Kv1.5 $\Delta$ N209, the short form of human Kv1.5. This study shows that the N-terminus of Kv1.5 exerts effects both on channel activation and inactivation. Of particular interest is that truncation of the N-terminus results in a U-shaped voltage-dependence of inactivation, and other features attributed to mechanisms of closed-state inactivation, all of which are absent in the full-length Kv1.5 channel. We show that this is related to a shift in the state-dependence of channel inactivation, resulting in accelerated inactivation from partially-activated closed states in Kv1.5 $\Delta$ N209. To our knowledge, this study represents the first characterization of modulation of C-type inactivation by the N-terminus of a *Shaker* family K<sup>+</sup> channel.

## RESULTS

### *Amino acids 1-209 modulate the activation properties of Kv1.5*

The loss of the first 209 amino acid residues in the short form of Kv1.5 corresponds to elimination of the N-terminus nearly to the S1 transmembrane domain, including roughly 75% of the T1 domain (see Fig. 3.1A, the T1A, T1B, and T1C regions correspond to residues 121-150, 156-225, and 233-260 respectively, based on alignments with *Shaker*) (Shen *et al.*, 1993; Shen & Pfaffinger, 1995). This deletion eliminates all sequence preceding the T1 domain, and virtually the entire portion of T1 solved by X-ray crystallography (Kreusch *et al.*, 1998; Minor *et al.*, 2000). Since the crystallized structure of the T1 domain can account for most of the cytoplasmic mass apparent in single EM structures of *Shaker*, it is likely that this deletion eliminates most, if not all of the cytoplasmic 'gondola' (cartoon in Fig. 3.1B; Sokolova *et al.*, 2001; Sokolova *et al.*, 2003).

Importantly, this manipulation does not preclude formation of functional channels, as shown by our generation of a stable HEK 293 cell line expressing the short form of Kv1.5 (Kv1.5 $\Delta$ N209), as well as the expression of similar T1 deleted channels in *Xenopus oocytes* (Kobertz & Miller, 1999). Currents from Kv1.5 $\Delta$ N209 appeared very similar to those seen in the full-length Kv1.5 channels (Fig. 3.2A, B), although single exponential fits of the activation time course in Kv1.5 $\Delta$ N209 reveal slightly faster time constants of activation than in the full-length channel (Fig. 3.2D). Also, the activation curve of Kv1.5 $\Delta$ N209 channels exhibits a leftward shift relative to the full-length channel. The half-activation voltage ( $V_{1/2}$ ) was shifted from  $-11.2 \pm 0.3$  mV in full-length Kv1.5 channels to  $-20.9 \pm 1.6$  mV in Kv1.5 $\Delta$ N209 (Fig. 3.2C).

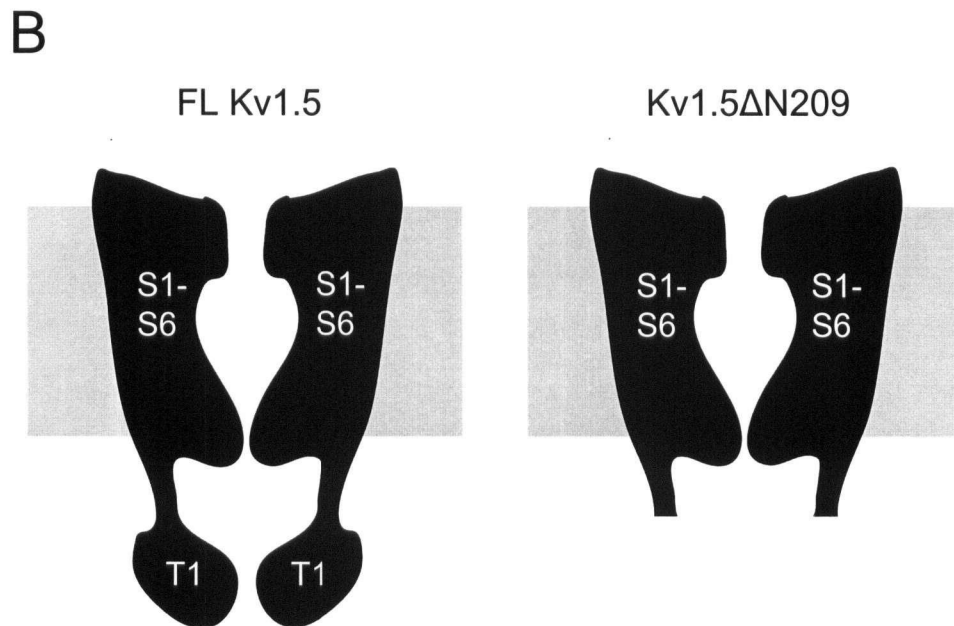
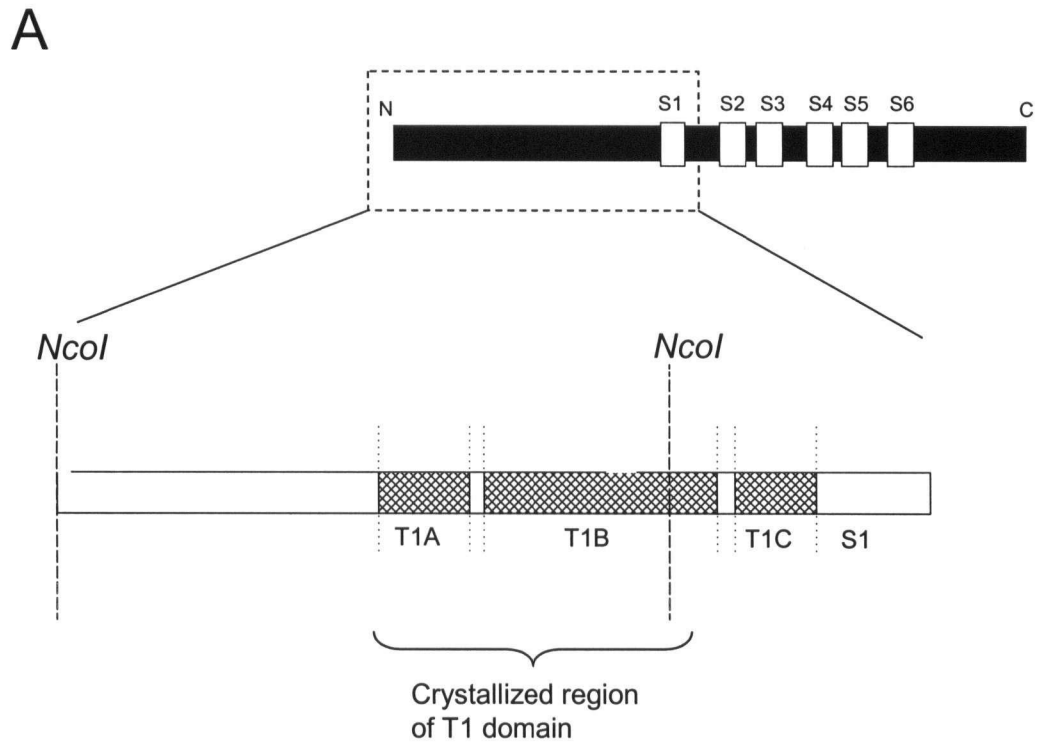


Figure 3.1. Construction of Kv1.5 $\Delta$ N209. (A) The Kv1.5 $\Delta$ N209 construct was generated by deleting the sequence between the two *NcoI* restriction enzyme sites in Kv1.5. S1 denotes the first transmembrane domain as determined by hydropathy analysis. (B) Cartoon representation of the Kv1.5 $\Delta$ N209 deletion, in which the entire known structure of the cytosolic T1 domain has been removed from the coding sequence.

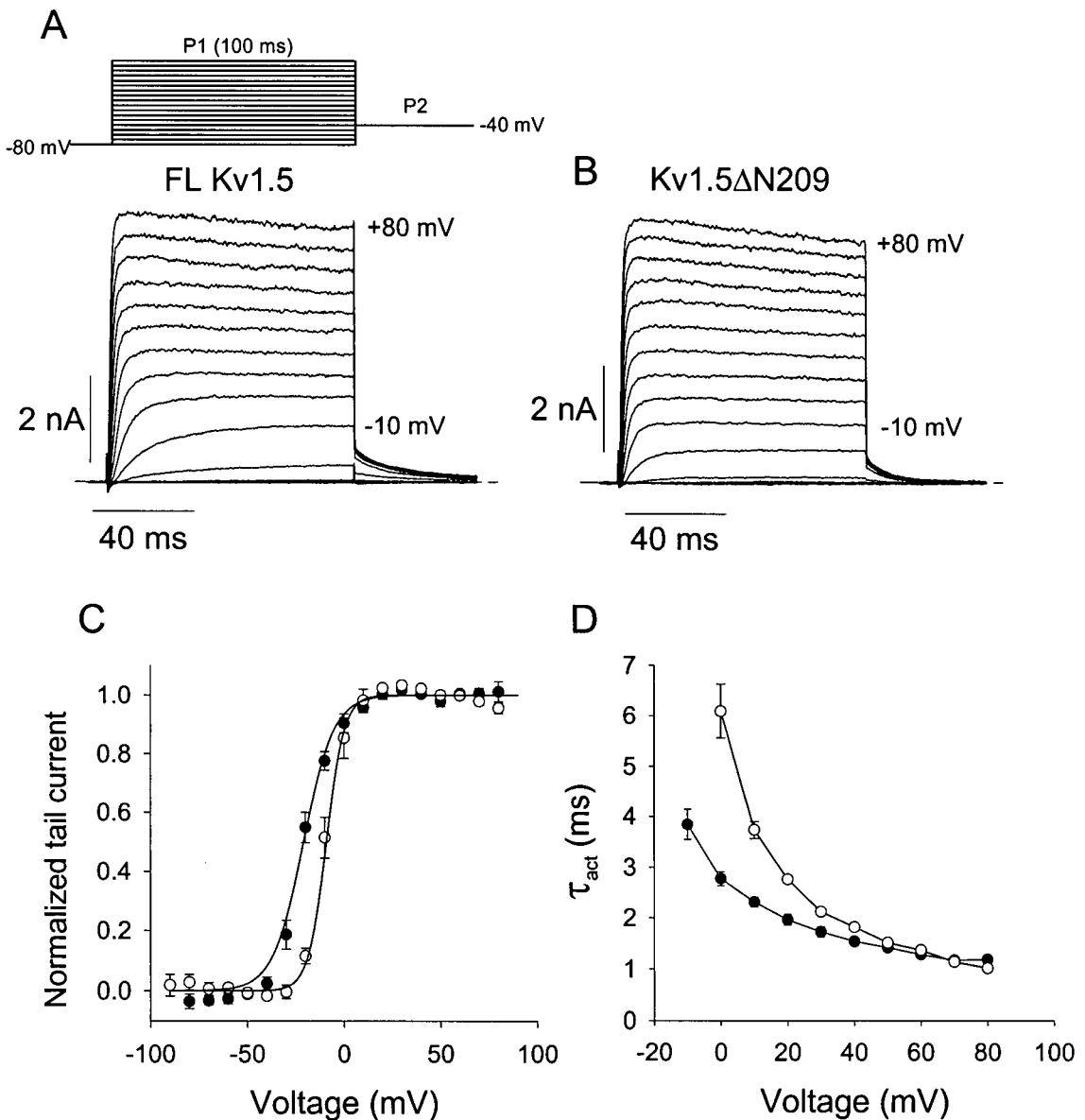


Figure 3.2. Activation properties of Kv1.5ΔN209. Activation curves were measured in HEK293 cells stably expressing (A) full-length (FL) Kv1.5 or (B) Kv1.5ΔN209. From a holding potential of -80 mV, cells were stepped to voltages between -80 mV and +80 mV (P1) in 10 mV steps for 100 ms, followed by a 20 ms repolarization to -40 mV (P2). (C) Tail current amplitudes were measured isochronally shortly after repolarization to -40 mV, normalized and fit with single Boltzmann equations (○, full-length Kv1.5; ●, Kv1.5ΔN209). The  $V_{1/2}$  for activation was  $-11.2 \pm 0.3$  mV in full-length Kv1.5 ( $n = 5$ ) and  $-20.9 \pm 1.6$  mV in Kv1.5ΔN209 ( $n = 5$ ). The slope factor,  $k$ , was  $4.3 \pm 1.0$  mV in full-length Kv1.5 and  $7.9 \pm 1.6$  mV in Kv1.5ΔN209. (D) Time constants of activation were determined at various potentials by fitting the 50%-100% rise time of the activation time courses with single exponential equations (○, full-length; ●, Kv1.5ΔN209). Dashed lines in this, as in all other figures, denote the zero current level.

### ***Inactivation-voltage relationship of Kv1.5 $\Delta$ N209***

The most striking difference between full-length Kv1.5 and the shorter Kv1.5 $\Delta$ N209 channels lies in their inactivation properties (Fig. 3.3). Inactivation-voltage relationships were measured isochronally with a standard double pulse protocol (inset in Fig. 3.3A), consisting of a 5 s conditioning pulse (P1) to various potentials to inactivate the channel, followed by a brief test pulse to +60 mV (P2), where the conductance-voltage relationship is saturated (Fig. 3.3A,B). Thus, the measured amplitude of the test pulse current is proportional to the number of available (non-inactivated) channels remaining after the conditioning pulse. Each sweep was preceded by a brief 100 ms pulse to +60 mV (not shown in the sample traces) which was not long enough to cause significant inactivation, but allowed us to ensure that changes in pipette access resistance and channel rundown during the lengthy protocol did not significantly affect the measured inactivation-voltage relationships. The half-inactivation voltage was shifted from  $-19.5 \pm 0.9$  mV in full-length channels to  $-35.7 \pm 0.7$  mV in Kv1.5 $\Delta$ N209. Importantly, this  $\sim 16$  mV shift of the inactivation  $V_{1/2}$  is greater than the  $\sim 9$  mV shift of the activation  $V_{1/2}$  in Kv1.5 $\Delta$ N209 (Fig. 3.2C), suggesting that the inactivation process has become dissociated from channel opening. Furthermore, lack of residues 1-209 imparts a significant U-shaped voltage dependence to the inactivation-voltage relationship (Fig. 3.3C). The conditioning pulses used in these experiments, as illustrated in Fig. 3.3A and 3.3B, were limited to 5 s, as longer pulses made completion of the entire protocol impractical. Since inactivation remains incomplete even following depolarizations up to 20 s in duration (Fig. 3.3D), the inactivation-voltage relationships presented do not represent a true steady-state inactivation curve. However, as

shown in Figure 3.3D, the observed U-shaped voltage dependence of inactivation is preserved even after 20 s inactivating pulses. Two 20 s voltage pulses to +60 mV or 0 mV were given to full-length Kv1.5 channels (Fig. 3.3D, upper traces) and Kv1.5 $\Delta$ N209 channels (Fig. 3.3D, lower traces). These were followed by a brief pulse to +60 mV to measure the residual current (indicated with an arrow and asterisk in Fig. 3.3D). In the Kv1.5 $\Delta$ N209 channels the test pulse current after the 0 mV prepulse falls below that after the +60 mV prepulse, indicating more inactivation at 0 mV in Kv1.5 $\Delta$ N209 (Fig. 3.3D, lower traces). This again indicates a U-shaped inactivation-voltage relationship in the short form of Kv1.5. In full-length Kv1.5 channels, the test pulse currents were essentially identical after prepulses to either 0 mV or +60 mV (Fig. 3.3D, upper traces).

Over the time courses examined, Kv1.5 $\Delta$ N209 channels appear to inactivate more completely than full-length Kv1.5 channels. There is an increase in the maximum level of inactivation during 5 s depolarizations, from a mean of  $49 \pm 2\%$  in full-length Kv1.5 to  $79 \pm 2\%$  (at  $-20$  mV) in Kv1.5 $\Delta$ N209 (Fig. 3.3C). In a previous study of full-length Kv1.5, it was reported that 10 s depolarizations gave a mean reduction of 60% at +60 mV (Fedida *et al.*, 1999), and during the 20 s depolarizations shown in Fig. 3.3D the amount of inactivation in full-length channels did not exceed 70%. It appears that the Kv1.5 $\Delta$ N209 short form can inactivate more completely than the full-length channel, and the half-inactivation voltage of the channel is modified, as well as the overall shape of the inactivation-voltage relationship. These findings suggest alternative or additional pathways for inactivation in the short form of the channel.

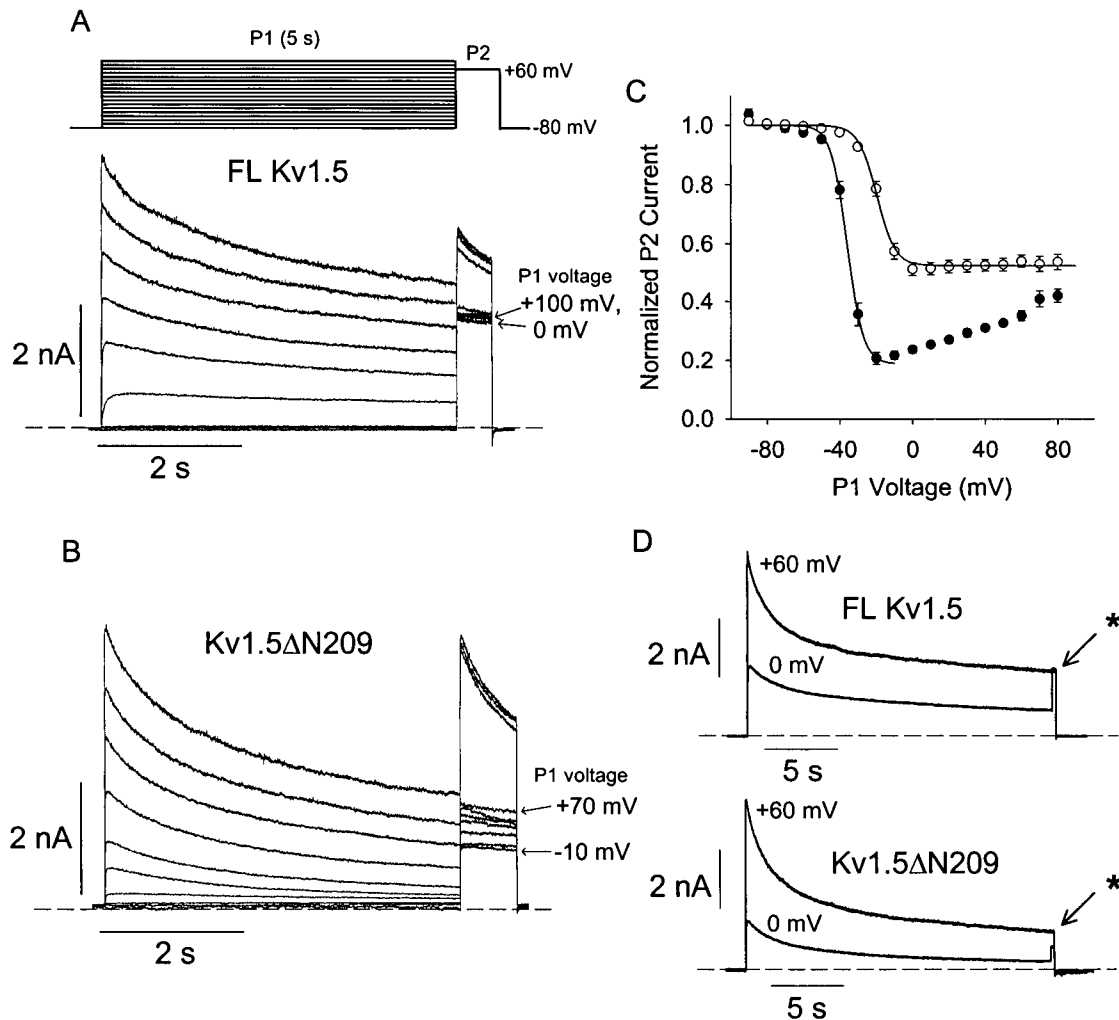


Figure 3.3. Inactivation properties of Kv1.5ΔN209. Inactivation-voltage relationships were measured in HEK293 cells expressing full-length (FL) Kv1.5 (A) or Kv1.5ΔN209 (B) with a double pulse protocol. In the conditioning (P1) pulse, cells were stepped over a range of voltages in 10 mV steps for 5s, followed by a brief test (P2) pulse to +60 mV (for clarity, the sample traces only depict every second sweep). The size of the test pulse current reflects the number of available (non-inactivated) channels after the P1 pulse. The holding potential was -80 mV. (C) Peak test pulse currents (P2) for full-length Kv1.5 (○, n = 5) and Kv1.5 ΔN209 (●, n = 5), were normalized, plotted against the voltage of the P1 pulse, and fit with single Boltzmann equations. The  $V_{1/2}$  was  $-19.5 \pm 0.9$  mV in full-length Kv1.5 and  $-35.7 \pm 0.7$  mV in Kv1.5ΔN209.  $k$  was  $5.1 \pm 0.8$  in full-length channels and  $4.3 \pm 0.1$  in Kv1.5ΔN209. Panel (D) illustrates current inactivation properties over a much longer time scale. Cells were pulsed to either +60 mV or 0 mV for 20 s, followed by a brief test pulse to +60 mV.

As noted earlier, the T1 domains have been implicated in prevention of inter-family subunit heteromultimerization (Li *et al.*, 1992; Shen & Pfaffinger, 1995; Xu *et al.*, 1995; Bixby *et al.*, 1999), and it is known that HEK 293 cells express an endogenous delayed rectifier K<sup>+</sup> current in small amounts. In our parent HEK cell line the endogenous current amplitude was ~300 pA at +60 mV so that for the size of currents illustrated in Figures 3.2 and 3.3, 90-95% of the observed current should be accounted for by Kv1.5ΔN209 channel subunits. To confirm that the currents elicited in HEK 293 cells arose from homotetramers of the Kv1.5ΔN209 subunit, as opposed to heterotetramers containing HEK 293 cell endogenous channel subunits, we transiently expressed Kv1.5ΔN209 in Mouse *ltk* cells, which we observed express little or no endogenous voltage-gated K<sup>+</sup> current (Fig. 3.4D). The measured inactivation-voltage relationship of Kv1.5ΔN209 exhibited the same features observed in the HEK cell expression system: an upturn of the relationship, and a leftward shift of the half-inactivation voltage. The maximum percentage inactivation attained during 5s pulses is  $75.3 \pm 3\%$  at -10 mV, compared with  $46 \pm 5\%$  inactivation at +60 mV. The half-inactivation potential is  $-18.5 \pm 1.1$  mV in full-length Kv1.5, and shifted to  $-30.2 \pm 0.9$  mV in Kv1.5ΔN209 when expressed in Mouse *ltk* cells (Fig. 3.4C). These data support the conclusion that the altered inactivation behavior of Kv1.5ΔN209 is an intrinsic property of the short form of the channel, and is not cell-type dependent or due to heteromultimerization with channel subunits endogenous to the HEK 293 expression system.

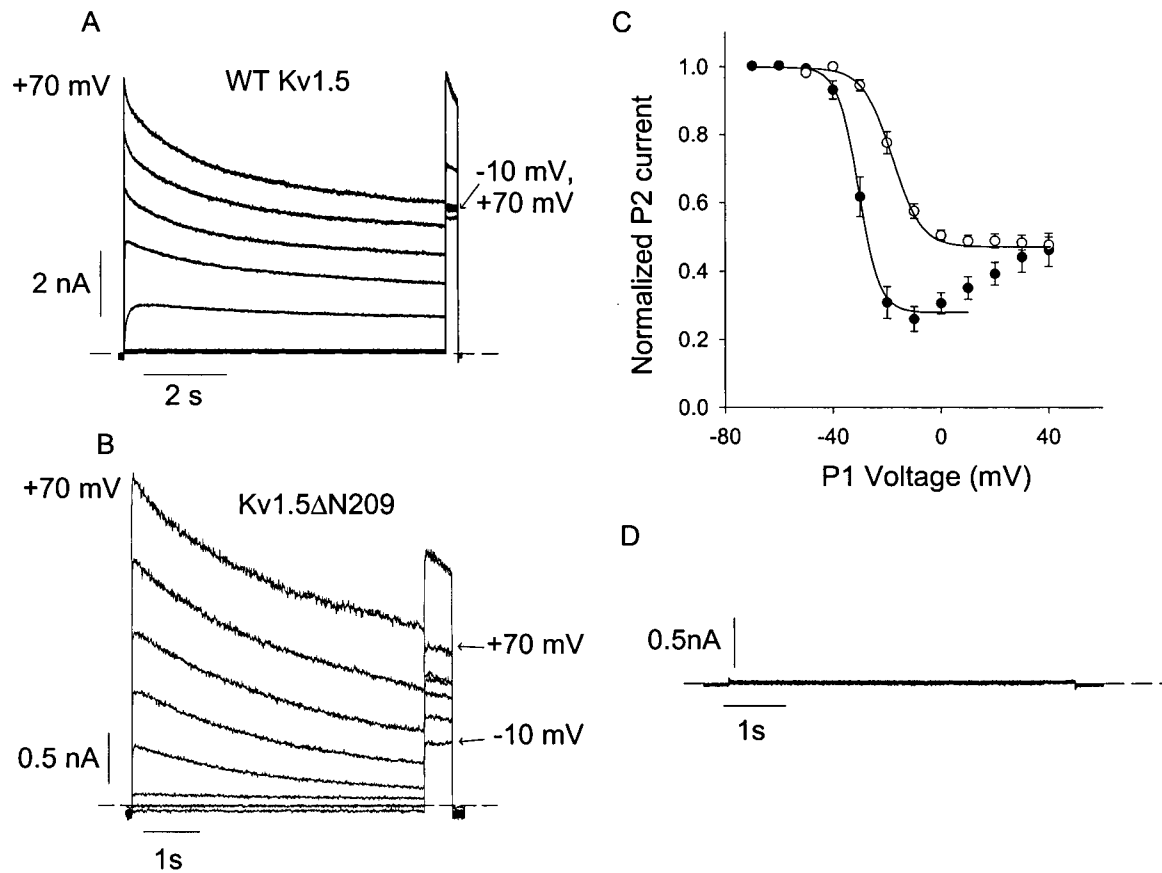


Figure 3.4. Inactivation properties of Kv1.5 $\Delta$ N209 expressed in Mouse *ltk* cells. Steady-state inactivation curves were measured for (A) WT Kv1.5 and (B) Kv1.5 $\Delta$ N209 using the pulse protocol described in Figure 3.3, with conditioning (P1) voltages between  $-70$  mV and  $+70$  mV, and test pulses (P2) to  $+60$  mV. (C) Peak test pulse currents for WT Kv1.5 ( $\circ$ ,  $n=5$ ) and Kv1.5  $\Delta$ N209 ( $\bullet$ ,  $n=5$ ), were normalized and fit with single Boltzmann equations. (D) Typical endogenous current expressed in untransfected Mouse *ltk* cells. The traces presented are non-leak subtracted 5 s pulses to 60 mV and 0 mV, with the same scaling as shown in panel (B)

### ***Closed-state inactivation and excessive cumulative inactivation***

At the time this study was initiated, the only detailed analysis of a U-shaped voltage dependence of inactivation in cloned Kv channels was for homomeric Kv2.1 channels or heteromers of Kv2.1 with either Kv5.1 or Kv9.3 (Klemic *et al.*, 1998; Kramer *et al.*, 1998; Kerscheneiner & Stocker, 1999). To explain this relationship, Klemic *et al.* proposed a model in which inactivation is fastest from partially-activated closed states, in which most or all of the voltage sensors are in an activated conformation, but the channel has yet to open. One consequence of this model of state-dependent inactivation is that the time course of inactivation during a long voltage step exhibits a clear voltage-dependence, as observed in Kv2.1 (Klemic *et al.*, 1998). Data in Fig. 3.5 shows a series of 5 s inactivating pulses recorded at multiple voltages in full-length Kv1.5, Kv1.5 $\Delta$ N209, and Kv2.1, normalized to the peak current at each voltage. The currents evoked in Kv2.1 and Kv1.5 $\Delta$ N209 are qualitatively very similar, with the extent of inactivation clearly dependent on voltage in both cases. In agreement with the inactivation-voltage relations (Fig. 3.3C) there is a greater relative amount of inactivation at 0 mV than at more positive potentials. Full-length Kv1.5 channels do not exhibit such a voltage-dependence, and mean data are summarized in Table 3.1. Here, inactivation of full-length Kv1.5 or Kv1.5 $\Delta$ N209 during 20 s depolarizations (Fig. 3.3D) has been fit to a bi-exponential decay function with fast ( $\tau_1$ ) and slow ( $\tau_2$ ) time constants. The difference between inactivation rates in the two channels arises at 0 mV by the almost two-fold faster rate of  $\tau_2$  in Kv1.5 $\Delta$ N209 than in Kv1.5.

Table 3.1

	Full-length Kv1.5		Kv1.5ΔN209	
	0 mV	60 mV	0 mV	60 mV
$\tau_1$ (s)	$1.4 \pm 0.2$	$1.1 \pm 0.1$	$1.5 \pm 0.2$	$1.1 \pm 0.1$
$\tau_2$ (s)	$11.7 \pm 1.5$	$9.0 \pm 0.9$	* $6.8 \pm 0.6$	$8.8 \pm 0.7$
$a_1$	$0.32 \pm 0.01$	$0.36 \pm 0.02$	* $0.35 \pm 0.01$	$0.34 \pm 0.03$
$a_2$	$0.43 \pm 0.01$	$0.32 \pm 0.02$	* $0.53 \pm 0.01$	* $0.44 \pm 0.02$
$c$	$0.25 \pm 0.01$	$0.30 \pm 0.02$	* $0.11 \pm 0.01$	* $0.20 \pm 0.01$

Table 3.1. Inactivation time constants for full-length Kv1.5 and Kv1.5ΔN209. Current decay during 20 s depolarizations to either +60 mV or 0 mV was fit with a biexponential decay equation ( $y = a_1 \cdot \exp(-t/\tau_1) + a_2 \cdot \exp(-t/\tau_2) + C$ ). Data are mean  $\pm$  S.E.,  $n = 4$ . An asterisk in the Kv1.5ΔN209 column denotes a significant difference (\*) from the corresponding value in full-length Kv1.5,  $p < 0.05$ .

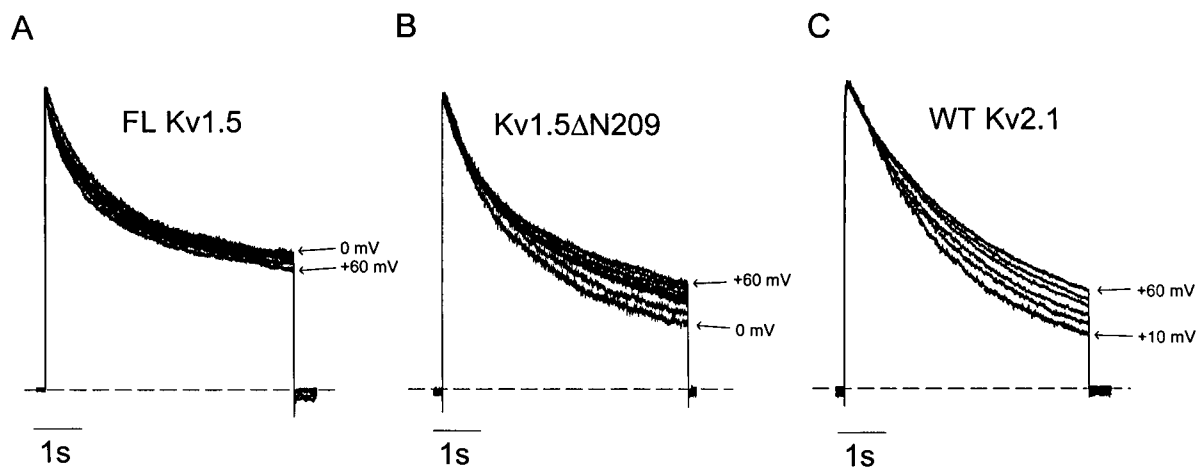


Figure 3.5. Voltage-dependence of inactivation behavior of full-length Kv1.5, Kv1.5ΔN209 and Kv2.1. Depolarizing pulses to between +60 and 0 mV, 5 s in duration, were applied to HEK293 cells stably expressing full-length (FL) Kv1.5 (A), Kv1.5ΔN209 (B), or WT Kv2.1 (C). The evoked currents have been normalized to the peak current during each voltage step to illustrate the voltage-dependence of the inactivation time course in WT Kv2.1 and Kv1.5ΔN209.

A second possible consequence of preferential inactivation from partially-activated closed states is the observation of 'excessive cumulative inactivation'. This phenomenon is similar to cumulative inactivation first described by Aldrich (1981), but reflects more complete inactivation observed when channels are repeatedly shuttled between positive and negative voltages, rather than held continuously at a depolarized voltage (Klemic *et al.*, 1998). This allows channels to repeatedly pass through partially-activated closed states in the activation pathway, and results in more complete inactivation than would be observed if channels were held continuously in the open state. We have tested for 'excessive cumulative inactivation' in full-length Kv1.5 and Kv1.5ΔN209, to ascertain whether closed state inactivation in the Kv1.5ΔN209 short form may explain the U-shaped inactivation-voltage relation. Representative records are shown in Fig. 3.6, in which cells were repetitively pulsed to a test potential (+60 or 0 mV) for 90 ms followed by a 10 ms repolarization period at -80 mV (a 90:10 duty ratio). The peak currents during each test pulse were compiled and their decay (shown as open symbols) compared with the current decay observed during a continuous pulse to the test potential (solid line, Fig. 3.6). Clearly, in Kv1.5ΔN209, rapid shuttling with a 90:10 duty ratio between 60 mV and -80 mV (Fig. 3.6B) results in 'excessive cumulative inactivation', in that the peak current measured during the repetitive pulses falls below the current level during the continuous pulse at +60 mV. It is of note that shuttling the potential between 0 mV and -80 mV does not lead to excessive inactivation (Fig. 3.6D), which is consistent with this potential being close to the nadir of the inactivation-voltage relationship, where channel occupancy of partially activated states is already likely

substantial (Fig. 3.3C). Full-length Kv1.5, in contrast, exhibits no 'excessive cumulative inactivation' under either condition (Fig. 3.6A, C).

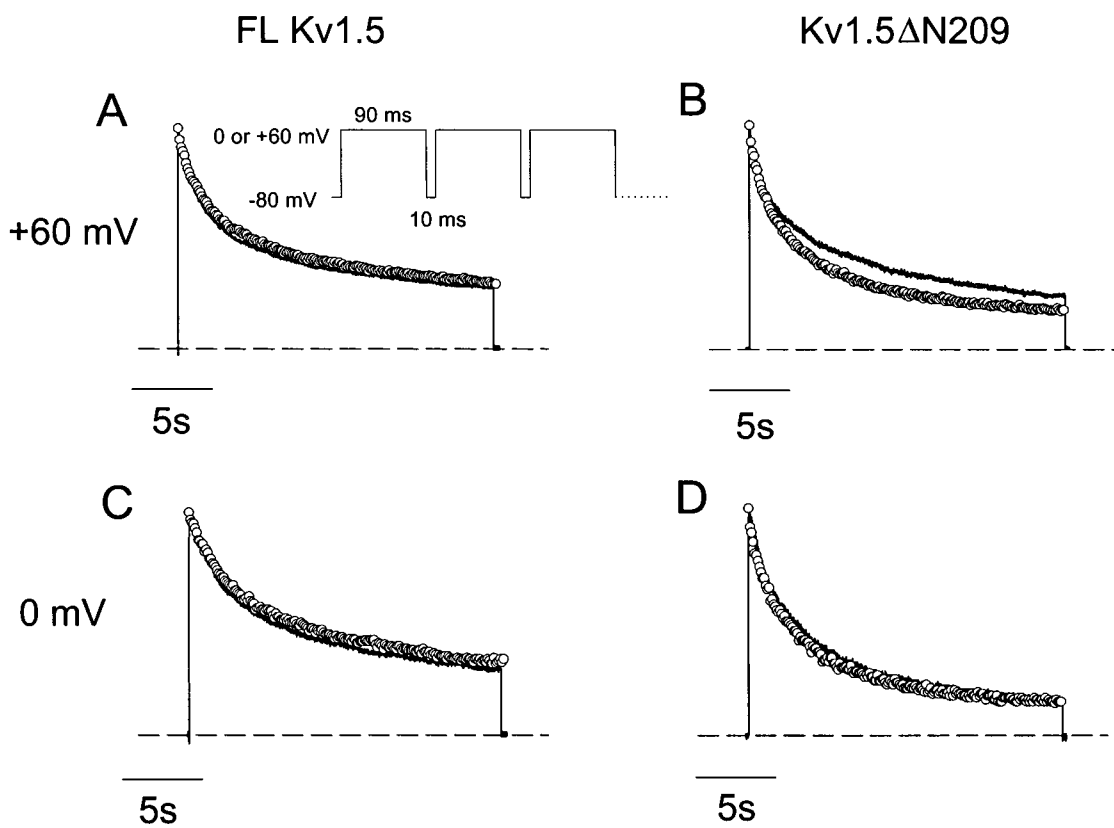


Figure 3.6. Excessive cumulative inactivation in Kv1.5ΔN209. Cells expressing full-length (FL) Kv1.5 (A and C) or Kv1.5ΔN209 (B and D) were subjected to a 20 s depolarizing pulse to either 0 or + 60 mV (continuous traces in all panels). Subsequently, cells were subjected to a train of 200 pulses, each 90 ms in duration to either 0 (C and D) or + 60 mV (A and B), and interspersed by 10 ms repolarizations to -80 mV. Normalized peak currents of the repetitive depolarizing pulses are plotted as open circles in each panel (similar observations were made in 6 cells of each type).

To further characterize 'excessive cumulative inactivation' in this channel, cells expressing full-length Kv1.5 or Kv1.5 $\Delta$ N209 were subjected to repetitive depolarizations (-80 mV to 0 or +60 mV) in which the interpulse interval was held constant at 20 ms, but the pulse duration and number of pulses were varied such that the total depolarization time was 5 s (Fig. 3.7A). The residual current observed following each pulse train was normalized to the current remaining at the end of a continuous 5 s pulse. In full-length channels, data denoted by the filled circles indicates that the amount of inactivation during a train of repetitive depolarizations from -80 mV to +60 mV never significantly exceeds the amount of inactivation that occurs during a continuous pulse (ie. normalized current doesn't fall below 1.0). This observation is consistent with the amount of inactivation observed being related to the total time spent depolarized, implying that in full-length Kv1.5, inactivation occurs primarily from the open state. Also, when pulsed repetitively between -80 mV and 0 mV, the relationship was shifted to longer pulse durations (Fig. 3.7A, open circles) than for the pulse trains between -80 mV and +60 mV. This observation is most likely due to the slower activation kinetics at 0 mV relative to +60 mV (Fig. 3.2D), and again supports the idea that closed-state inactivation does not contribute substantially to full-length Kv1.5 inactivation, since channels would be expected to dwell longer in closed states when pulsed to 0 mV than when pulsed to +60 mV.

When the same protocol was applied to Kv1.5 $\Delta$ N209, pulse trains to +60 mV with intermediate pulse durations (10 to 200 ms) resulted in substantially more inactivation than a continuous 5 s pulse. This finding suggests that the amount of inactivation observed is related to the number of times a channel shuttles between open and closed states: a high pulse

frequency passes channels through closed states more often, and results in a greater amount of inactivation. This experiment suggests a shift in the state-dependence of inactivation in the short form of Kv1.5, as a significant component of inactivation in Kv1.5 $\Delta$ N209 appears to occur from closed states. Importantly, this experiment does not directly inform us of the relative contribution of closed-state inactivation to the overall time course of inactivation, but suggests that the inactivation rate is faster from one or more closed states compared with the open state. An examination of individual data tracings during 90 ms depolarizations in Kv1.5 $\Delta$ N209 (using the 90:10 duty cycle in Fig. 3.6) shows that, after the first pulse, currents rise more rapidly in subsequent pulses (Fig. 3.7B). The instantaneous rising phase of the second pulse current in Fig 3.7B is a driving force effect on the fraction of channels that have failed to close, however there is also a reduction in the delay preceding channel opening, which indicates that channels lack the time to completely deactivate during the interpulse interval, and only reach partially activated closed states in the deactivation pathway. If channels are inactivating from closed states, this observation suggests that these closed states are late in the activation pathway, very near to the open state.

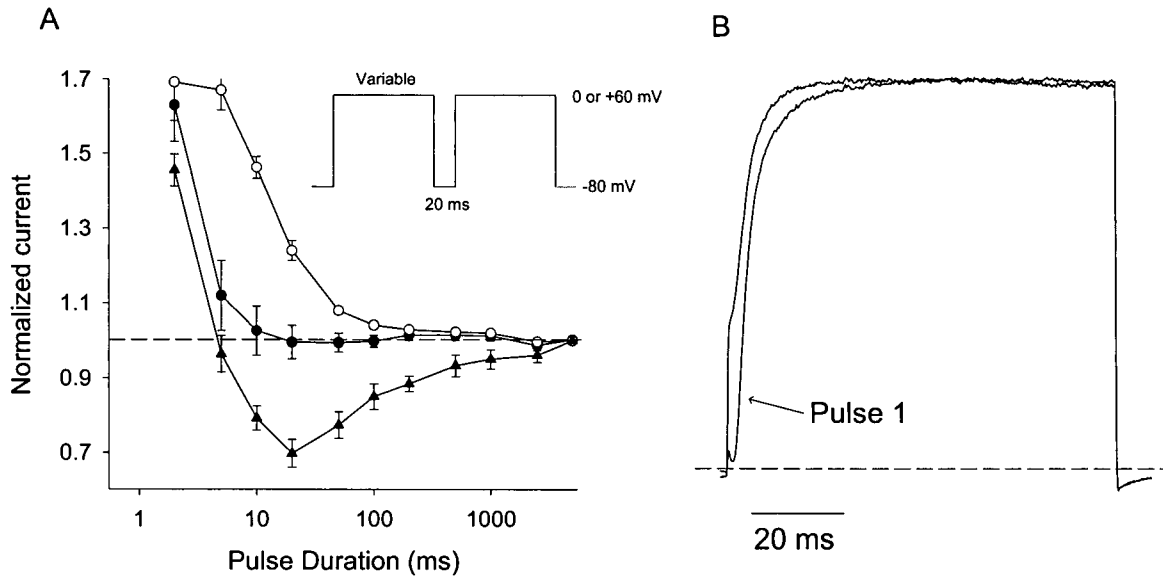


Figure 3.7. Excessive cumulative inactivation in Kv1.5 $\Delta$ N209 depends on pulse duration. (A) A series of repetitive depolarizations to either 0 mV (open symbols) or +60 mV (filled symbols) was applied to HEK293 cells expressing full-length (FL) Kv1.5 ( $\circ$ ,  $\bullet$ ) or Kv1.5 $\Delta$ N209 ( $\blacktriangle$ ). Pulses were interspersed by 20 ms repolarizations to -80 mV, but the number of pulses and their duration were varied to generate a total depolarization time of 5 s. The residual current following each pulse train was normalized to the current remaining after a continuous 5 s pulse ( $n = 5-11$  per data point). (B) Representative currents from Kv1.5 $\Delta$ N209 during 90 ms pulses from -80 mV to 0 mV, with a 10 ms interpulse interval (as in Fig. 3.6). The currents during the first and second pulses of the train are illustrated and the second current shows the rapid rising phase of currents at this interpulse interval.

### ***Voltage-dependent recovery from inactivation in Kv1.5ΔN209***

We also observed that the voltage-dependence of recovery from inactivation is markedly altered in Kv1.5ΔN209 channels (Fig. 3.8). To measure recovery from inactivation, HEK 293 cells expressing full-length Kv1.5 or Kv1.5ΔN209 were subjected to 7 s inactivating pulses at +60 mV, returned to a recovery potential (voltages between -50 mV and -110 mV) for a variable duration, then pulsed again briefly to +60 mV to assess the extent of recovery. A significant difference in the voltage-dependence of recovery is immediately evident upon examination of the representative traces presented in Fig. 3.8A. In Kv1.5ΔN209, recovery is nearly complete within 2 s at -110 mV but is extremely slow with a holding potential of -50 mV (Fig. 3.8A, lower traces). In full-length Kv1.5, the time course of recovery appears to vary far less over the same voltage range (Fig. 3.8A, upper traces). Summary data are shown for a range of recovery potentials between -50 and -110 mV for full-length Kv1.5 in Fig. 3.8B, and Kv1.5ΔN209 in Fig. 3.8C. The holding potential has a fairly minor effect on recovery from inactivation in full-length Kv1.5 (Fig. 3.8B). However in Kv1.5ΔN209, recovery from inactivation exhibits a much stronger voltage-dependence, as the data is scattered over a wider time interval (Fig. 3.8C). Also, the time course of recovery exhibits multiple components, depending on the recovery potential. In Kv1.5ΔN209, the recovery time course is fit very well with a single exponential equation at negative voltages (-95 mV, -110 mV), but requires multiple components at more positive voltages (between -50 mV and -80 mV). To facilitate comparison, we have plotted the time required for 50% recovery of the inactivated fraction of channels, at multiple voltages in full-length Kv1.5 and Kv1.5ΔN209 (Fig. 3.8D). Overall, the  $t_{1/2}$  for channel recovery in

Kv1.5 $\Delta$ N209 was found to vary roughly 15-fold over the voltage range examined, whereas recovery of full-length Kv1.5 was found to vary only approximately 3-fold. This difference in the  $t_{1/2}$  for recovery was found to be significant at potentials of -50, -65, -95, and -110 mV (Fig. 3.8D,  $p < 0.05$ ).

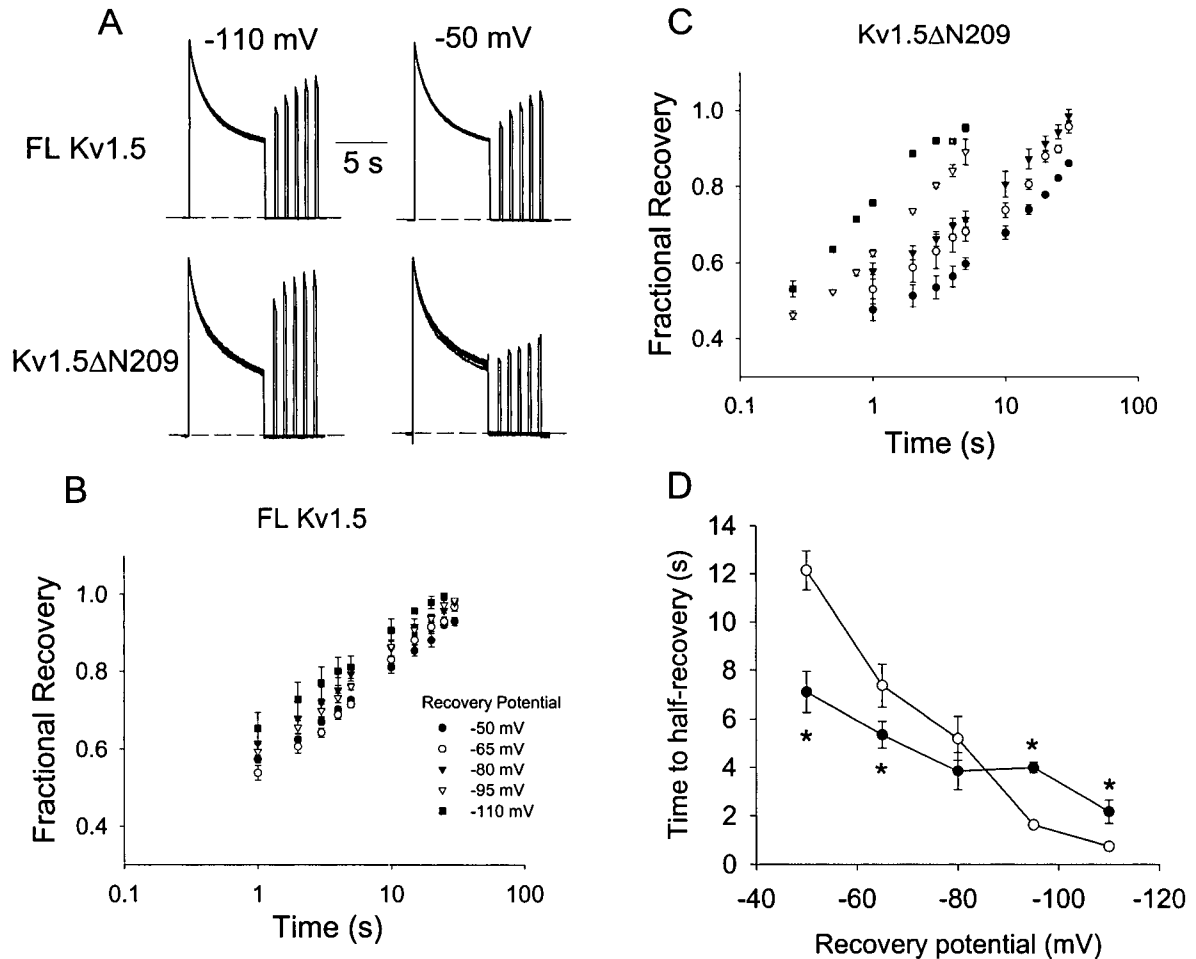


Figure 3.8. Voltage-dependence of recovery from inactivation. (A) Cells expressing full-length (FL) Kv1.5 or Kv1.5 $\Delta$ N209 were subjected to 7 s inactivating pulses at +60 mV and tracings show recovery from inactivation at -110 and -50 mV. (B, C) Recovery in Kv1.5 $\Delta$ N209 and full-length Kv1.5 was measured during 250 ms test pulses to +60 mV, after holding at recovery potentials between -50 and -110 mV for 0.25 to 30 s. (D) Time to half-recovery for Kv1.5 $\Delta$ N209 ( $\circ$ ) and full-length Kv1.5 ( $\bullet$ ) at various recovery potentials illustrates the time required for recovery of 50% of the inactivated fraction of channels.

### *Excessive inactivation of Kv1.5 $\Delta$ N209 under cardiac action potential clamp*

To compare cumulative inactivation in full-length Kv1.5 and Kv1.5 $\Delta$ N209 using a more physiological stimulus, we obtained an action potential waveform recorded from a human ventricular myocyte (stimulated at 1 Hz, room temperature) and subjected transfected HEK cells to this waveform repetitively at frequencies of either 1 Hz or 1.67 Hz. The waveform is shown in the inset to Fig. 3.9A. In both channels, inactivation accumulates over the course of the pulse trains, seen as a progressive decrease in the peak current during trains of action potential clamps (Fig. 3.9A and B). Peak current during each pulse has been normalized to the current during the first pulse and plotted against the respective pulse number to illustrate the relative current decay over time at the two pulse frequencies (Fig. 3.9C and D). At both pulse frequencies, peak currents decrease substantially more in Kv1.5 $\Delta$ N209 than in full-length Kv1.5, suggesting that in the physiological setting of the human heart, inactivation is likely to accumulate to a greater degree in Kv1.5 $\Delta$ N209 than in the long form of the channel.

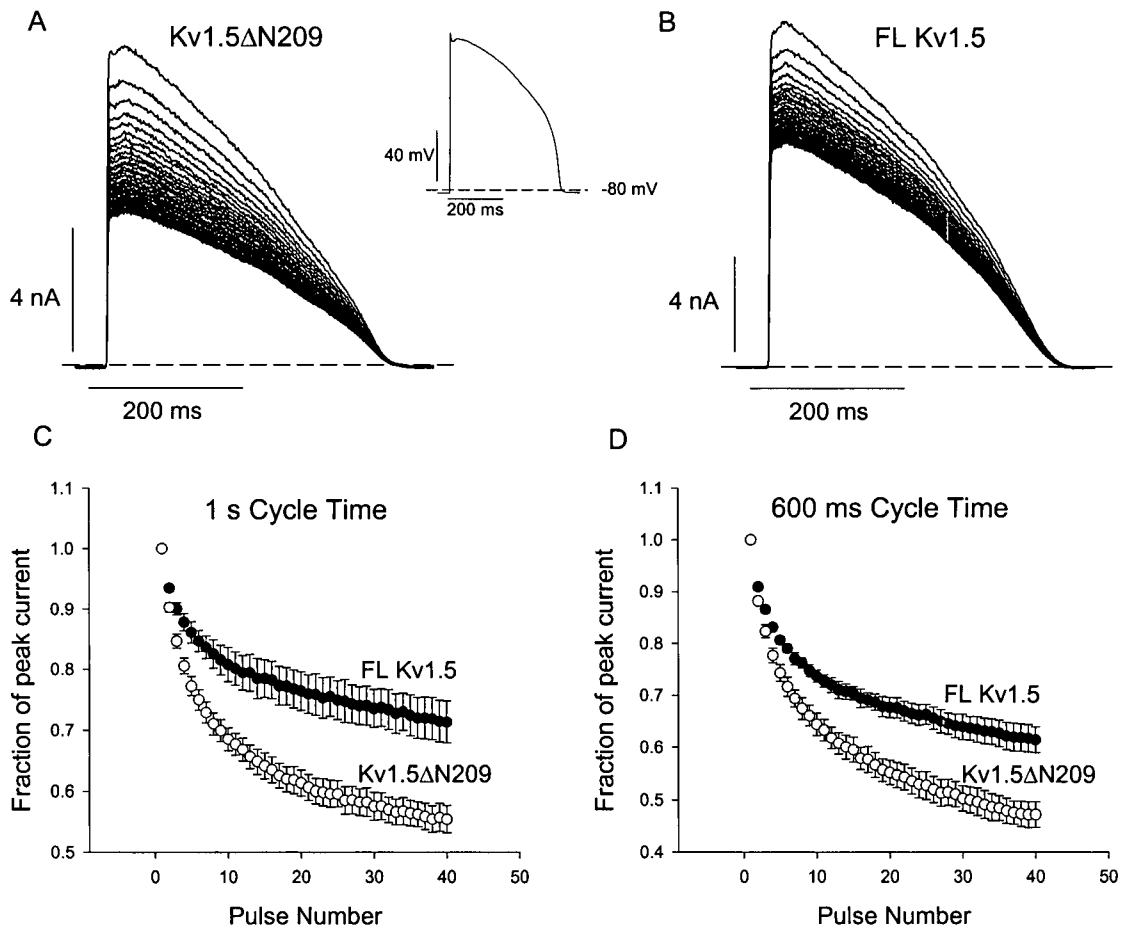
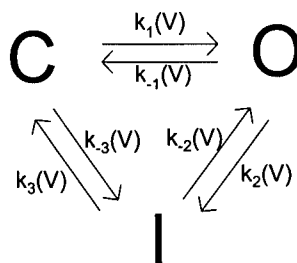


Figure 3.9. Excessive cumulative inactivation in Kv1.5ΔN209 subjected to a human cardiac action potential clamp. A human ventricular cardiac action potential was recorded during stimulation at 1 Hz as shown in the inset in panel (A). This waveform was then used as the stimulus waveform to voltage clamp HEK cells expressing Kv1.5ΔN209 (A) or full-length (FL) Kv1.5 (B). Currents are shown to decrease in both cases during constant stimulation from rest at 1 Hz. The peak currents during each pulse have been normalized to the peak current in the first pulse, and plotted in (C) and (D) for stimulation at 1 Hz and at 1.67 Hz, respectively. In both cases, a significantly greater decrease in Kv1.5ΔN209 current was observed. Data are means of 5-8 cells.

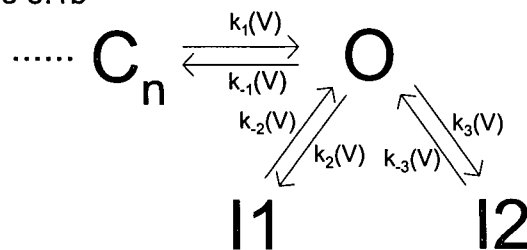
***Kinetic Models of Inactivation: Models Describing a U-shaped Inactivation-Voltage Relationship***

Excluding the  $\text{Ca}^{2+}$ -current dependent inactivation of certain  $\text{Ca}^{2+}$  channels (Brehm & Eckert, 1978; Peterson *et al.*, 1999), models that predict a U-shaped inactivation-voltage relationship can be divided into two classes. The first of these is characterized by voltage-dependent microscopic inactivation rates between the open state and one or more inactivated states (Schemes 3.1a and 3.1b). An example is the three-state cyclic model in Scheme 3.1a, formulated to describe the U-shaped inactivation-voltage relationship of  $\text{Ca}^{2+}$ -currents in bullfrog sympathetic neurons (Jones & Marks, 1989). The primary feature of these models are that the microscopic inactivation rates are voltage-dependent, which itself confers a voltage-dependence to inactivation, or causes disparate entry into one or more inactivated states. The model structures in Schemes 3.1a and 3.1b require the postulation of a voltage-sensor for inactivation.

Scheme 3.1a



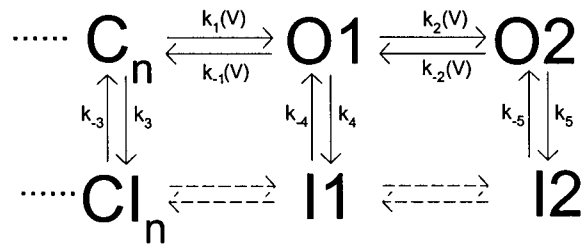
Scheme 3.1b



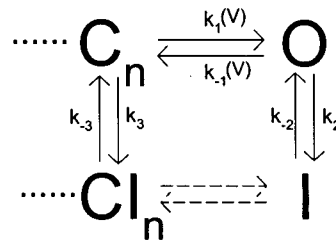
The second class of model describing a U-shaped inactivation-voltage relationship is characterized by accelerated inactivation from an intermediate state in the activation pathway. Several examples include the models of Klemic *et al.* (1998, 2001) describing the inactivation of Kv2.1, and later *Shaker* and Kv3.1, and a model describing inactivation of N-type Ca<sup>2+</sup> channels (Patil *et al.*, 1998). In this class of model, the voltage-dependence of transitions through the activation pathway results in enhanced occupancy of partially-activated, rapidly-inactivating states with moderate depolarizations, and hence an accelerated time course of inactivation at these intermediate voltages. Importantly, the second class of model is unique among published models in its ease of prediction of 'excessive cumulative inactivation' (described below). Finally, the second class of model does not require the postulation of a voltage-dependent inactivation process, which is significant because inactivation in full-length Kv1.5 does not exhibit any apparent voltage-dependence.

We considered two specific models in this second class, shown in Schemes 3.2a and 3.2b. In Scheme 3.2a, the channel is proposed to occupy multiple open states in a voltage-dependent manner, with inactivation occurring most readily from the 1st open state. That is,  $k_3$ ,  $k_4$ , and  $k_5$  are voltage-independent rates, but  $k_4$  is  $> k_5$ . If depolarization favors occupancy of the 2<sup>nd</sup> open state, the model could predict a U-shaped voltage-dependence of inactivation, and 'excessive cumulative inactivation', because trains of repetitive depolarizations could allow channels to repeatedly pass through the first open state (O1, rapidly inactivating), causing an increased likelihood of inactivating. However, this model does not necessarily predict a dissociation of the  $V_{1/2}$ s of activation and inactivation as we observed in Kv1.5 $\Delta$ N209 (Figs. 3.2, 3.3).

Scheme 3.2a



Scheme 3.2b



In Scheme 3.2b (see also Fig. 3.10), the model structure parallels that of Scheme 3.2a, but the model contains a single open state. Voltage-dependent microscopic activation ( $k_1$ ) and deactivation rates ( $k_{-1}$ ) then predict greater occupancy of a partially-activated closed-state at intermediate potentials. If  $k_3 > k_2$ , the model predicts more rapid inactivation at intermediate potentials. This model also predicts ‘excessive cumulative inactivation’, as channels will repeatedly pass through a more rapidly inactivating closed state during repetitive depolarizations. In the context of Scheme 3.2b, we would hypothesize that deletion of the N-terminus of Kv1.5 somehow allows accelerated inactivation from partially-activated closed states, similar to the model proposed for inactivation of Kv2.1. The model of Klemic *et al.* (1998) is of this form and proposes allosteric coupling of closed-state inactivation to transitions throughout the activation pathway as a mechanism to account for accelerated inactivation from late closed states. It is a particularly attractive way to describe

our results, because this model predicts a strong voltage-dependence of recovery from inactivation, in addition to a U-shaped inactivation-voltage relationship and excessive cumulative inactivation, as was observed in Kv1.5 $\Delta$ N209. As well, it is in agreement with a single open state for *Shaker* channels (Hoshi *et al.*, 1994).

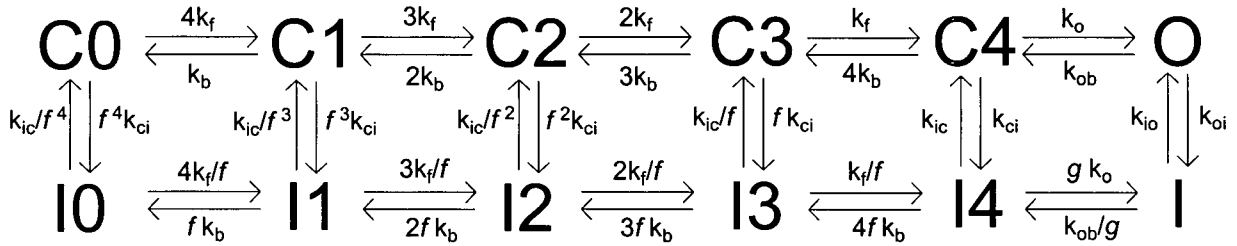


Figure 3.10. Schematic representation of inactivation in full-length Kv1.5 and Kv1.5 $\Delta$ N209. The rate constants in the activation pathway (horizontal transitions) were governed by exponential functions of voltage (see Methods). The factor  $g$  was included to preserve microscopic reversibility, and was defined as  $\sqrt{[(k_{oi} * k_{ic}) / (k_{io} * k_{ci})]}$ . At 0 mV, the rate constants were ( $\text{ms}^{-1}$ )  $k_f = 0.4$ ,  $k_b = 0.065$ ,  $k_o = 0.31$ , and  $k_{ob} = 0.017$ , with associated valences of  $z = 1.4$  for  $k_f$ ,  $z = -0.35$  for  $k_b$ ,  $z = 0.38$  for  $k_o$  and  $z = -0.70$  for  $k_{ob}$ . Vertical transitions were voltage independent. Rate constants of vertical transitions for simulation of full-length Kv1.5 were ( $\text{ms}^{-1}$ )  $k_{ci} = 0.00008$ ,  $k_{ic} = 0.000055$ ,  $k_{oi} = 0.00017$ ,  $k_{io} = 0.000061$ ,  $g = 1.39$ , and the allosteric factor  $f$  was 0.64. For simulations of Kv1.5 $\Delta$ N209, parameters were ( $\text{ms}^{-1}$ )  $k_{ci} = 0.0013$ ,  $k_{ic} = 0.0000054$ ,  $k_{oi} = 0.00017$ ,  $k_{io} = 0.000061$ ,  $g = 0.11$ , and the allosteric factor  $f$  was 0.3.

### ***Building a kinetic model of inactivation in Kv1.5 and Kv1.5 $\Delta$ N209***

With the above considerations in mind, we constructed a model based upon the previously published model of Kv2.1 inactivation (Klemic *et al.*, 1998). The model consists of 12 states: 5 closed states, 5 closed-inactivated states, 1 open state, and 1 inactivated state (see Fig. 3.10). Horizontal transitions between states are governed by exponential functions of voltage, and the model assumes four independent transitions along the activation pathway, followed by a concerted opening transition. Vertical transitions in Fig. 3.10 were assumed to be independent of voltage. Forwards ( $k_o$ ) and backwards ( $k_{ob}$ ) rates between the open state

and final closed state were governed by exponential functions of voltage, and were estimated by fitting the voltage-dependence of time constants of single exponential fits of deactivation and activation rates. The resulting activation transitions reasonably approximate the experimentally observed kinetics and voltage-dependence of activation in the full-length channel (Fig. 3.11A), with simulations yielding a  $V_{1/2}$  of activation of  $-12$  mV. It is widely held that the steps involved in Kv1 channel activation are far more complex than those depicted here (Zagotta *et al.*, 1994a; Zagotta *et al.*, 1994b; Schoppa & Sigworth, 1998a; Schoppa & Sigworth, 1998b). Although the model generates reasonable reproductions of the activation relationships and activation kinetics of Kv1.5 (Fig. 3.11A), it is not intended to provide a quantitative description of the gating pathways in Kv1.5 in all details.

Current records from long 20 s pulses to  $+60$  mV (Fig. 3.3D) in the full-length channel were used to estimate the forwards and backwards rates of inactivation from the open state ( $k_{oi}$ ,  $k_{io}$ ), based on the assumption that most inactivation was occurring from the open state in the full-length channel. The parameter  $g$  is included to preserve microscopic reversibility. Using this model construction, we have systematically varied the rates of inactivation from the open state and closed states, in order to investigate the potential influence of closed-state inactivation in the different forms of Kv1.5.

We found that the rate of inactivation from the open state was the prime determinant of the time course of inactivation at depolarized potentials. This is expected, due to the strong bias towards the open state with strong depolarizations predicted by our activation parameters (Fig. 3.11B). Our simulations predict that above  $10$  mV, greater than 90% of channels are fully activated (Fig. 3.11B). In the formulation of the model presented in Figure 3.10, simulations of the inactivation-voltage relationships (using the protocol described in

Fig. 3.3A,B) resulted in behaviour qualitatively resembling the full-length channel, as long as the closed-state inactivation rate  $k_{ci}$  was roughly equal to or less than the rate of open-state inactivation  $k_{oi}$ . However, the model produces essentially monoexponential kinetics of inactivation, in contrast to the biexponential kinetics observed experimentally. The only noted alteration of the inactivation-voltage relationship upon deceleration of the closed-state inactivation rate is a slight depolarizing shift of the  $V_{1/2}$  of inactivation (see Fig. 3.11D). To adequately describe the dissociation between the half-activation and half-inactivation potentials (roughly an 8 mV difference) in full-length Kv1.5, we estimated a closed-state inactivation rate of  $0.00008 \text{ ms}^{-1}$  ( $k_{ci}$ , see Fig. 3.10). The inactivation-voltage relationship derived from this simulation (Fig. 3.11A) was fit with a Boltzmann function to yield a  $V_{1/2}$  of -20 mV, which is close to the value observed experimentally in the full-length channel ( $-19.5 \pm 0.9 \text{ mV}$  in full-length Kv1.5, Fig. 3.3).

#### ***Incorporating the U-shaped voltage-dependence of inactivation***

A number of possible changes to the model can result in a U-shaped inactivation-voltage relationship. Initially, we examined the effects of destabilization of inactivation from the open state. Deceleration of the rate of open-state inactivation results in a U-shaped inactivation-voltage relationship (Fig. 3.11C, inset), but also results in very slow inactivation that poorly reproduces the time course of inactivation observed at depolarized potentials (Fig. 3.11C, solid lines). In addition, a far more significant acceleration of closed-state inactivation is required to approximate the time course of inactivation experimentally observed with strong depolarizations. For example, deceleration of inactivation from the open state by 10-fold (chosen because it is sufficient to generate a mildly U-shaped inactivation-voltage relationship) required acceleration of closed-state inactivation by

roughly 250-fold or more in order to reproduce the experimentally observed time course of inactivation at +60 mV (Fig. 3.11C, broken lines). The result of this acceleration is more profound inactivation at intermediate potentials – in our example, we see complete inactivation within 2.5 s at 0 mV (Fig. 3.11C) - and consequently an exaggerated U-shape of the inactivation-voltage relationship.

The explanation that we prefer for the U-shaped inactivation-voltage relationship in Kv1.5 $\Delta$ N209 is that deletion of the N-terminus results primarily in acceleration of inactivation from closed states relative to full-length Kv1.5 (with minimal effects on inactivation from the open state). This possibility was supported by unique insights gained through comparisons of the Kv1.5 $\Delta$ N209 channel with the full-length channel. As noted, inactivation of Kv1.5 $\Delta$ N209 was more complete than for full-length Kv1.5 at intermediate potentials, but gradually approached the level observed in the full-length channel at more positive potentials (Figs. 3.3C, 3.4C). This can be explained by the presence or enhancement of an inactivation pathway in addition to the primarily open-state inactivation observed in full-length Kv1.5. More importantly, deeper inactivation at intermediate voltages in Kv1.5 $\Delta$ N209 is a rigid outcome of such a model, and is not necessarily predicted by a model based on deceleration of inactivation from the open state.

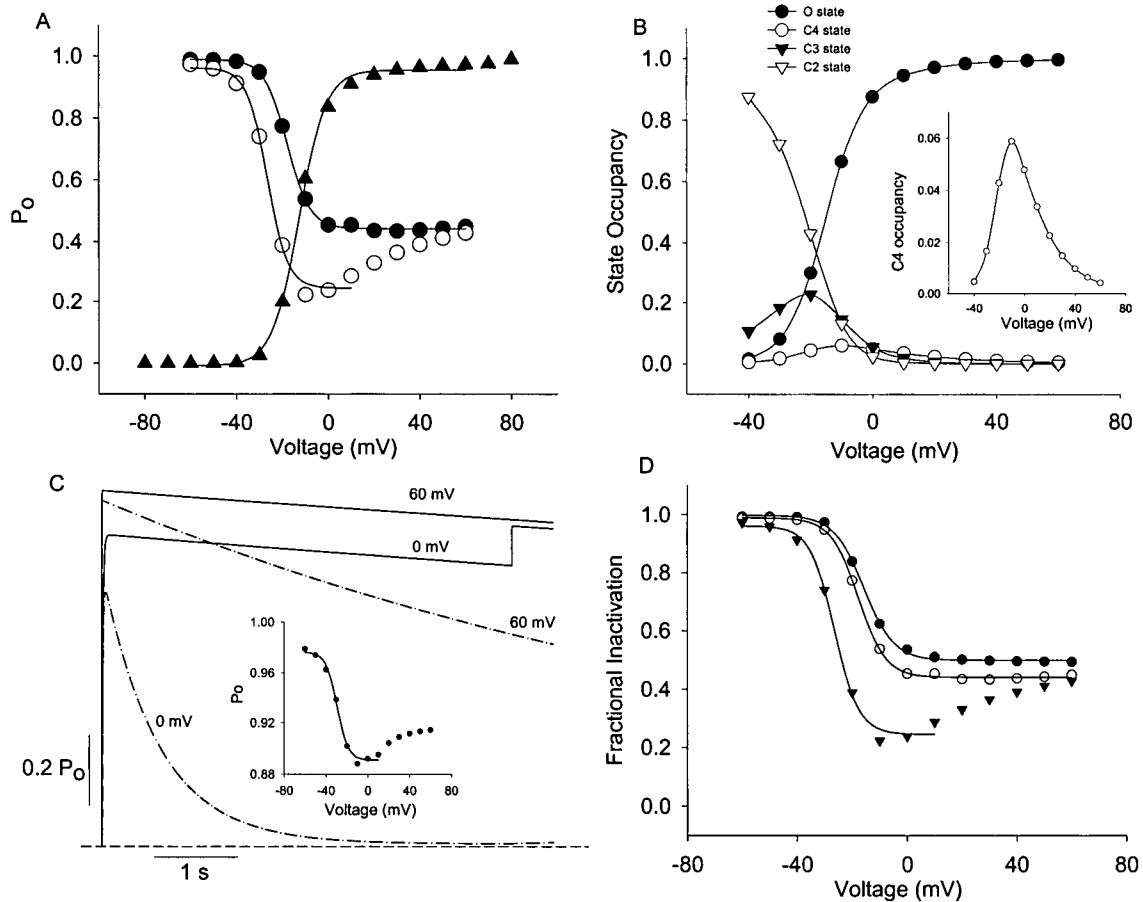


Figure 3.11. Simulated effects of alterations to closed and open state inactivation rates. (A) Activation curve ( $\blacktriangle$ ) and inactivation-voltage relationships simulated for full-length (FL) Kv1.5 ( $\circ$ ) and Kv1.5 $\Delta$ N209 ( $\bullet$ ), using the parameters presented in Fig. 3.10, and the protocols described in Figs 3.2 and 3.3. (B) Predicted voltage-dependent state-occupancy in full-length Kv1.5 and Kv1.5 $\Delta$ N209, measured after 60 ms simulated depolarizations to each potential, with parameters from Fig. 3.10. In panels (C) and (D),  $k_{ic}$  was set to  $0.0000054 \text{ ms}^{-1}$ ,  $f$  was set to 0.3, and  $k_{ci}$  was altered as noted. (C) Simulated currents after deceleration of inactivation from the open state ( $k_{oi}$  in Fig 3.10) to  $0.000017 \text{ ms}^{-1}$  (solid lines) exhibit extremely slow inactivation, but result in a U-shaped inactivation-voltage relationship (inset panel). Acceleration of  $k_{ci}$  (Fig. 3.10) to  $0.02 \text{ ms}^{-1}$  (dotted lines) results in a more accurate reproduction of inactivation at +60 mV, but extremely exaggerated inactivation at 0 mV. (D) Alterations of the closed state inactivation rates shift the inactivation  $V_{1/2}$ . Steady-state inactivation relationships were simulated using the protocol described in Figure 3.3, with  $k_{ci}$  rates of  $0.000000017$  ( $\bullet$ ),  $0.00008$  ( $\circ$ ), and  $0.0013$  ( $\blacktriangledown$ ) (see Fig. 3.10) yielding inactivation  $V_{1/2}$ s of  $-17 \text{ mV}$ ,  $-19 \text{ mV}$ , and  $-29 \text{ mV}$  respectively.

Acceleration of inactivation transitions from closed-states of the channel (without changing the inactivation rate from the open state) results in a progressive leftward shift of the inactivation-voltage relationship, without affecting the voltage-dependence of activation (Figure 3.11D). When the closed-state inactivation rate exceeds the rate of inactivation from the open state, simulations begin to generate U-shaped inactivation-voltage relationships, and this becomes more pronounced as the closed-state inactivation rate is accelerated further (Figure 3.11D). Acceleration of closed-state inactivation to  $0.0013 \text{ ms}^{-1}$  results in a 17 mV dissociation between the  $V_{1/2}$ s of activation and inactivation, and a marked U-shaped inactivation-voltage relationship (Fig. 3.11A; it is important to note that we have not considered the 10 mV hyperpolarizing activation shift in Kv1.5 $\Delta$ N209, and hence the  $V_{1/2}$  of the Boltzmann fit in Figure 3.11D reproduces the enhanced dissociation of inactivation from activation, but not the true half-inactivation potential in Kv1.5 $\Delta$ N209).

#### ***Simulation of excessive cumulative inactivation***

The parameters derived using the approach described above also allowed for effective simulation of ‘excessive cumulative inactivation’ in full-length Kv1.5 and Kv1.5 $\Delta$ N209. Simulations of the repetitive 90 ms depolarizations (+60 mV) and 10 ms repolarizations (-80 mV) described in Fig. 3.6 are shown in Fig. 3.12A. Clearly, the parameters derived for the full-length channel predict little or no ‘excessive cumulative inactivation’. In contrast, the parameters derived for Kv1.5 $\Delta$ N209 predict ‘excessive cumulative inactivation’ which is maintained throughout the 20 s pulse train with the absence of any crossover with the continuous 20 s depolarization, as observed experimentally (Fig. 3.6B).

The allosteric factor,  $f$ , reflects the extent to which inactivation is favored by transitions through the activation pathway (Fig. 3.10). It affects the half-inactivation voltage,

since  $f$  governs the relative rates of inactivation and recovery at potentials where few or no channels reach the open state. For the same reason,  $f$  also has a significant effect on the voltage-dependence of recovery from inactivation. Having roughly determined the rates of inactivation from partially-activated closed states, we used the rates of recovery at extremely negative potentials (ie.  $-110$  mV, see Fig. 3.8) to fix a rate for recovery from the earliest closed state. This line of reasoning was based on the assumption that very hyperpolarized recovery potentials would result in the vast majority of channels dwelling in the earliest closed state (C0 in Fig. 3.10), and is corroborated by our observation of a single-exponential recovery time course at hyperpolarized recovery potentials. Finally, the allosteric factor  $f$  was estimated by studying its effects on the predicted voltage-dependence of recovery.

This approach can be used to roughly fit the voltage-dependence of recovery in both full-length Kv1.5 and Kv1.5 $\Delta$ N209, however it does not predict the crossover of their respective recovery rates around  $-80$  mV, as was observed experimentally (Fig. 3.8D). In order to reproduce this feature of our experimental data, slight changes were made to the modeled rates of recovery from inactivation (compare  $k_{ic}$  for full-length Kv1.5 and Kv1.5 $\Delta$ N209 in the legend for Fig. 3.10, and the simulations shown in Fig. 3.12B, C). Finally, while this model predicts a strong voltage-dependence of recovery in Kv1.5 $\Delta$ N209 (Fig. 3.12B, C), it does not identically reproduce the voltage-dependence of recovery observed experimentally (Figs. 3.12C; 3.8B, C). Most likely, this difficulty arises because of our simplification of the Kv1.5 activation pathway, as the model implies that the voltage-dependent occupancy of different closed-inactivated states governs the voltage-dependence of the recovery pathway.

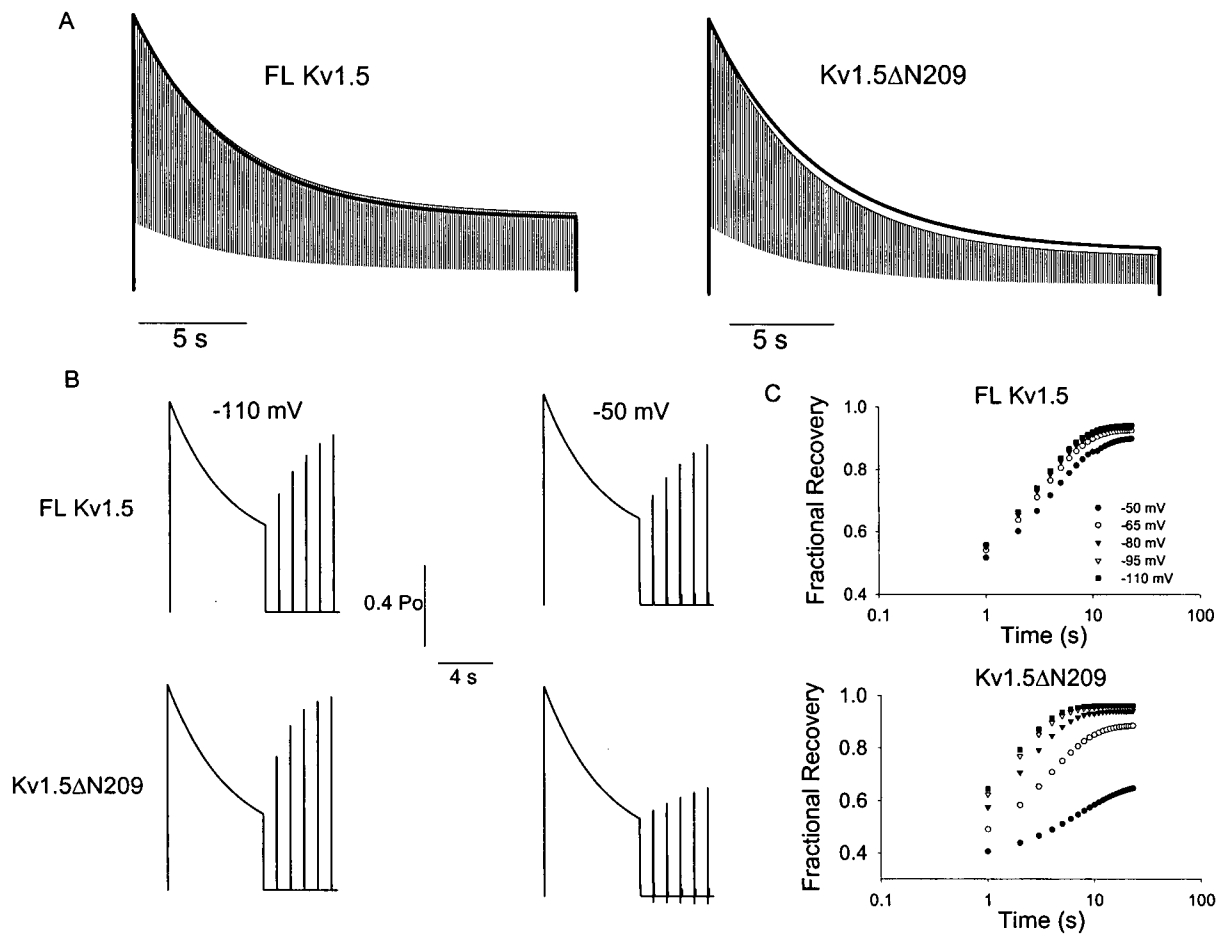


Figure 3.12. Simulations generated from the kinetic model of inactivation in Kv1.5ΔN209 and full-length Kv1.5. (A) Simulated excessive cumulative inactivation in full-length (FL) Kv1.5 and Kv1.5ΔN209. Currents were simulated with a 20 s continuous depolarizing pulse to +60 mV (heavy line) or with a 20 s train of 90 ms depolarizations to +60 mV separated by 10 ms repolarizations to -80 mV (same protocol as Fig. 3.6). (B) Voltage-dependent recovery from inactivation in full-length (FL) Kv1.5 and Kv1.5ΔN209. Currents were simulated with a 7 s depolarizing pulse to +60 mV followed by recovery at -110 mV or -50 mV for up to 5 s. (C) The time course of recovery in full-length Kv1.5 and Kv1.5ΔN209 was simulated at -50 mV, -65 mV, -80 mV, -95 mV, -110 mV with test pulses at 1 s intervals (up to 30 s) following 7 s depolarizing pulses to +60 mV (same protocol as Fig. 3.8).

## DISCUSSION

### *Altered state-dependence of inactivation in the short form of human Kv1.5*

Experiments in this chapter demonstrate that the activation, inactivation and recovery properties of Kv1.5 $\Delta$ N209 are significantly modified from those of the long form, or full-length Kv1.5. Activation is affected only in a minor way, with a small but significant hyperpolarizing shift in the half activation potential, and a decrease in the slope (Fig. 3.2). The Kv1.5 $\Delta$ N209 channel lacks almost the entire cytoplasmic N-terminal domain and a significant portion of the T1 inter-subunit assembly domains, including all of T1A and most of the T1B portion (Shen & Pfaffinger, 1995). The deletion removes essentially the entire region of the T1 domain determined by X-ray crystallography (Kreusch *et al.*, 1998; Minor *et al.*, 2000). The small changes in channel steady-state activation properties are consistent with those that have been described for a similar extensive *Shaker* T1 deletion mutant (Kobertz & Miller, 1999), although we found that current activation rate was mildly accelerated in the truncated form, whereas activation was significantly slower in T1 deleted forms of *Shaker* (Kobertz & Miller, 1999). The most important changes that we have observed in the kinetic properties of the short form of Kv1.5 are related to the inactivation properties of this channel. Kobertz and Miller (1999) found that the effects of exogenously applied N-type inactivation domains were relatively unaffected by T1 deletion in *Shaker*, but did not examine the effects on slow inactivation that we report in this study.

The critical observation that we have made here is that Kv1.5 $\Delta$ N209 shows a marked shift in the state-dependence of inactivation compared to the full-length Kv1.5 channel. Our experimental data show that inactivation in full-length Kv1.5, as in most voltage-gated K<sup>+</sup> channels, increases with voltage and eventually stabilizes, so that the inactivation-voltage

relationship reaches a steady level at depolarized potentials. In Kv1.5, for long pulses, this is about 40% of the maximum current (Fedida *et al.*, 1999), and roughly 50% with the 5 s depolarizations employed in this study, although it should be noted that inactivation can be almost complete when Na<sup>+</sup> permeates the channel (Wang *et al.*, 2000a). In Kv1.5ΔN209, there is a prominent upturn of the inactivation-voltage relationship when expressed in both HEK 293 cells and Mouse *ltk-* cells (Figs. 3.3, 3.4). In Kv2.1, this inactivation phenotype was attributed to closed-state inactivation allosterically coupled to voltage sensor movement (Klemic *et al.*, 1998), although studies of heteromultimers of Kv2.1 with various auxiliary  $\alpha$ -subunits (Kv5.1, Kv6.1 or Kv9.3) suggest that there may also be a significant component of inactivation from the open state of Kv2.1 (Kramer *et al.*, 1998; Stocker & Kerscheneiner, 1998; Kerscheneiner & Stocker, 1999; Kerscheneiner *et al.*, 2003). Other characteristics resulting from preferential closed-state inactivation were a voltage-dependent recovery from inactivation and the phenomenon of ‘excessive cumulative inactivation’. Full-length Kv1.5 channels exhibit neither voltage-dependent inactivation (Fig. 3.5, Table 3.1) nor ‘excessive cumulative inactivation’ at any potential (Figs. 3.6, 3.7), and possess only mild voltage-dependence of recovery from inactivation (Fig. 3.8B). In contrast, the studies we have carried out on Kv1.5ΔN209 demonstrate a voltage-dependence to its inactivation similar to that seen in Kv2.1 (Figs. 3.3, 3.4, 3.5, Table 1). Kv1.5ΔN209 also shows ‘excessive cumulative inactivation’ (Figs. 3.6, 3.7) and significant voltage-dependent recovery from inactivation (Fig. 3.8C), although this is less marked than for Kv2.1 (Klemic *et al.*, 1998). The upturn of the inactivation-voltage relationship is more correctly described as a more complete inactivation of Kv1.5ΔN209 at intermediate potentials with a nadir at around -20 or -10 mV, and a relief of inactivation at more positive potentials (Fig. 3.3). Finally, these

altered properties of Kv1.5 $\Delta$ N209 result in a marked increase in accumulation of inactivation during repetitive depolarizations using a human cardiac action potential as the stimulus waveform (Fig. 3.9).

Our data suggests that the N-terminus of Kv1.5 is involved in regulating the transition between closed and closed-inactivated states of the channel. In addition to the current study, several N-terminal deletions and point mutations have been described which modulate activation gating kinetics and the voltage-dependence of activation in *Shaker* family channels, but none have characterized direct modulation of the slow inactivation gating of a *Shaker* homologue, as we have seen in Kv1.5 (Lee *et al.*, 1994; Tu *et al.*, 1996; Kobertz & Miller, 1999; Minor *et al.*, 2000; Cushman *et al.*, 2000). We have yet to characterize the effects of N-terminal deletions of other Kv1 channels, although Kv1.1, 1.2, and 1.3 all possess alternative start sites homologous to M210 in Kv1.5. Importantly, Kv1.5 $\Delta$ N209 is clearly not the only Kv channel to exhibit a U-shaped inactivation-voltage relationship. Among cloned Kv channels, this property has been reported in Kv2.1 (Klemic *et al.*, 1998), Kv3.1 (Klemic *et al.*, 2001), one study of *Shaker* (Klemic *et al.*, 2001), and Kv1.5 $\Delta$ N209 (Kurata *et al.*, 2001; Kurata *et al.*, 2002). In addition, a somewhat perplexing study of Kv1.2 has demonstrated a dramatically U-shaped inactivation-voltage relationship in oocytes injected with small doses of cRNA, but loss of inactivation with larger cRNA doses (Guillemare *et al.*, 1992). In native expression systems, K<sup>+</sup> currents exhibiting U-shaped inactivation-voltage relationships have also been reported in molluscan neurons (Aldrich *et al.*, 1979a), and in frog sympathetic neurons (Klemic *et al.*, 1998).

### ***Model of Kv1.5 $\Delta$ N209 inactivation***

To date, N-terminal disruptions of Kv1.5 remain the only mutations known to impart a U-shaped inactivation-voltage relationship in a Kv channel (Kurata *et al.*, 2002). As a result, our comparison of full-length Kv1.5 and Kv1.5 $\Delta$ N209 provided the important insight that the time course of inactivation is accelerated in Kv1.5 $\Delta$ N209 at intermediate potentials, but slows and approaches that of full-length Kv1.5 at more extreme depolarizations. A simple interpretation of this observation is that the Kv1.5 $\Delta$ N209 deletion reveals an additional pathway for inactivation, which is favored at intermediate potentials, without dramatically altering the inactivation mechanism present in full-length Kv1.5, and our kinetic model shows that this is a plausible explanation for our observations. In particular, we have shown that the inactivation-voltage relationship and ‘excessive cumulative inactivation’ of Kv1.5 $\Delta$ N209 can be reasonably reproduced by accelerating the rates of inactivation from closed-states of the channel, and allowing inactivation to proceed from the open state at rates observed in the full-length channel. The result of this model is that the truncated channel behaves similarly to full-length Kv1.5 at depolarized potentials, but inactivates more rapidly and completely (over the time intervals examined) at intermediate potentials where few channels are open. In addition, the acceleration of inactivation from closed-states predicts enhanced dissociation of the  $V_{1/2}$ s of inactivation from activation (Fig. 3.11A, D). All of these features of the model are consistent with experimental data.

Therefore, the most fundamental insight gained from our modeling, is that the N-terminus of Kv1.5 likely modulates the inactivation phenotype primarily by regulating the amount of inactivation that occurs from partially-activated closed-states. In addition, our model suggests that the mechanism for this acceleration is a shift in the allosteric coupling of

inactivation to transitions through the activation pathway, such that inactivation is increasingly favored with each forward step during channel activation. Although the mechanism implied by our model is not the only possible way to accelerate closed-state inactivation, this mechanism is also consistent with our observation of enhanced voltage-dependence of recovery in Kv1.5 $\Delta$ N209. The concept of coupling of inactivation and/or recovery to one or more closed-states in the activation pathway is implied in a number of recent models of inactivation of voltage-gated K<sup>+</sup>, Na<sup>+</sup> and Ca<sup>2+</sup> channels (Marom & Abbott, 1994; Kuo & Bean, 1994; Olcese *et al.*, 1997; Klemic *et al.*, 1998; Patil *et al.*, 1998).

Although the model structure presented here is essentially identical to that of Klemic *et al.* for Kv2.1, it is important to notice that the model makes significantly different predictions regarding state occupancy of the channel during inactivation (Fig. 3.11B; Klemic *et al.*, 1998). Most importantly, the model predicts that the bulk of inactivation occurs from the open state at depolarized potentials, primarily as a result of the faster activation rates compared with Kv2.1 (Figs. 3.10, 3.11C). This is an important departure from the model of Klemic *et al.* (1998), in which inactivation from the open state of Kv2.1 is extremely unfavorable. In their model, the rate of inactivation from the open state of Kv2.1 can be reduced 10,000-fold and substantial inactivation is still observed even at relatively extreme depolarizations, while deceleration of open state inactivation by even 10-fold in our model for Kv1.5 results in nearly complete abolition of inactivation (Fig. 3.11C). Furthermore, this model suggests that a substantial fraction of Kv1.5 $\Delta$ N209 inactivation during repetitive depolarizations occurs from the open state of the channel. Inactivation from partially-activated closed states provides an additional inactivation mechanism that accounts for the deeper inactivation observed due to increased state occupancy at intermediate depolarizations

or during repetitive pulse trains. As mentioned above, it remains unclear whether inactivation of Kv2.1 indeed occurs almost entirely from closed-states, as predicted by the model of Klemic *et al.* (1998). Characterization of heteromultimeric channels of Kv2.1 and various modulatory  $\alpha$ -subunits have shown that coexpression with auxiliary subunits has distinct effects on Kv2.1 inactivation at various voltages (Kramer *et al.*, 1998; Kerschensteiner & Stocker, 1999; Kerschensteiner *et al.*, 2003). Kv9.3, for example, dramatically accelerates inactivation at intermediate depolarizations, but inhibits inactivation at higher voltages, thereby exaggerating the inactivation-voltage relationship normally observed in WT Kv2.1 (Kerschensteiner & Stocker, 1999; Kerschensteiner *et al.*, 2003). These observations have prompted models suggesting that inactivation from the open state is a significant pathway for Kv2.1 inactivation, qualitatively resembling the model presented here for Kv1.5 $\Delta$ N209 (Kerschensteiner & Stocker, 1999; Kurata *et al.*, 2001).

An important issue for consideration is why we observe relatively minor dissociation of activation and inactivation in Kv1.5 $\Delta$ N209, in spite of the proposed rapid rates of closed-state inactivation. This differs especially from Kv4 channels, in which the  $V_{1/2}$ s of activation and inactivation are dissociated by as much as 40 mV (Jerng *et al.*, 1999). However, our results are less different from Kv2.1, where the  $V_{1/2}$ s of activation and inactivation are dissociated by only 15 to 20 mV (VanDongen *et al.*, 1990), despite the relative dominance of closed-state inactivation (Klemic *et al.*, 1998). It should be noted that a model of inactivation strictly coupled to the open state can predict substantial dissociation of the  $V_{1/2}$ s of activation and inactivation as long as the inactivation rate constant far exceeds the recovery rate constant. However, far more rapid and absorbing inactivation kinetics than those observed experimentally for Kv1.5 are required to simulate any significant dissociation of the

activation and inactivation  $V_{1/2}$ s during the 5 s depolarizations used in our experiments (eg. Fig. 3.3). Our simulations, and comparisons with recent models of Kv4 gating (Jerng *et al.*, 1999) suggest that the primary reason for the relatively small dissociation of activation and inactivation in Kv1.5 $\Delta$ N209 is the strong bias towards opening in Kv1 channels. Kv4.1 and Kv4.2, in contrast to Kv2.1 and Kv1.5, have been recently modeled with voltage-independent deactivation rates 3 times faster than the final opening rate, resulting in weak occupancy of the open state, even at very depolarized potentials (Jerng *et al.*, 1999; Bähring *et al.*, 2001). The relatively biased opening transition of Kv1 channels reduces occupancy of partially-activated closed states with strong depolarizations, resulting in less closed-state inactivation.

#### ***Mechanisms of closed-state inactivation***

It is also of some interest whether the closed state inactivation process in Kv1.5 $\Delta$ N209 occurs by a mechanism similar to inactivation in the full-length channel (ie. C-type). We have not yet thoroughly explored this question, although some experiments presented in Chapter 4 address this issue briefly. Interestingly, at the time this work was completed, a report of similar inactivation behaviour (eg. a U-shaped inactivation voltage relationship) in *Shaker* channels was also published (Klemic *et al.*, 2001). While the latter remains the only published report of a U-shaped inactivation-voltage relationship in *Shaker*, this work was accompanied by a model suggesting similar conclusions as the model presented here (Figs. 3.10-3.12). In particular, this work suggested that in *Shaker*, C-type inactivation from the open state was the predominant inactivation pathway at strongly depolarized voltages, whereas inactivation from closed states provided an additional pathway for inactivation that became more significant as voltage approached the activation  $V_{1/2}$  of the channel.

Most interestingly, their study suggested that the predominant mechanisms for closed vs. open state inactivation (which they termed 'U-type' and 'P/C-type', respectively) are distinct and mutually exclusive (Klemic *et al.*, 2001). In contrast, the model in the present study implies that inactivated states accessed through open or closed channel states can interconvert (Fig. 3.10; Kurata *et al.*, 2001). We have not examined this in detail, but a rigorous test of this difference will be to determine how the recovery kinetics are influenced by the voltage at which channels are inactivated. The model of Klemic *et al.* (2001) suggests that channels that inactivate at intermediate voltages (where closed-state inactivation is favored) will recover with different kinetics than channels inactivated with strong depolarizations (where C-type inactivation predominates). The model presented here, in contrast, suggests that the kinetics of recovery from inactivation will be insensitive to the states from which channels inactivate. Delineation of the mechanisms underlying state-dependent inactivation of Kv channels will provide an interesting avenue for future investigation.

### ***Conclusions***

The N-terminus of Kv1.5 is an important determinant of the activation and inactivation properties of the channel. This study, focused primarily on the inactivation effects of an N-terminally truncated form of Kv1.5, suggests that the N-terminus governs the propensity of the channel to inactivate from closed states. Accelerated closed state inactivation in Kv1.5 $\Delta$ N209, and allosteric coupling between closed state inactivation and voltage sensor movement, accounts for a U-shaped inactivation-voltage relationship, excessive cumulative inactivation, and enhanced voltage-dependence of recovery from inactivation.

**CHAPTER 4: AMINO-TERMINAL REGULATION OF SLOW INACTIVATION IN  
VOLTAGE-GATED K<sup>+</sup> CHANNELS**

## CHAPTER SUMMARY

Our characterization of a truncated form of Kv1.5 (Kv1.5 $\Delta$ N209) demonstrated that deletion of the N-terminus of Kv1.5 imparts a U-shaped inactivation-voltage relationship, and prompted us to investigate the N-terminus as a regulatory site for slow inactivation of Kv channels (Kurata *et al.*, 2001). In this chapter, we have examined the regulation of Kv1.5 $\Delta$ N209 inactivation by TEA<sup>+</sup> and permeant cations (K<sup>+</sup> and Cs<sup>+</sup>). The results suggest that these agents regulate the closed-state inactivation mechanism in Kv1.5 $\Delta$ N209 differently than the inactivation process in full-length Kv1.5 channels. In addition, we have characterized the macroscopic inactivation properties of several N-terminal deletion mutants of Kv1.5. Deletion of residues up to the T1 boundary (Kv1.5 $\Delta$ N19, Kv1.5 $\Delta$ N91, and Kv1.5 $\Delta$ N119) did not alter Kv1.5 inactivation. However, deletions that disrupted the T1 domain consistently exhibited inactivation phenotypes resembling Kv1.5 $\Delta$ N209. Chimeric constructs between Kv1.5 and the N-termini of Kv1.1 and Kv1.3 rescued the inactivation kinetics observed in full-length Kv1.5, again suggesting that the Kv1 T1 domain influences slow inactivation. Furthermore, disruption of intersubunit T1 contacts by mutation of residues E132 and T133 to alanines resulted in channels exhibiting a U-shaped inactivation-voltage relationship. Fusion of the N-terminus of Kv2.1 to the transmembrane segments of Kv1.5 imparted a U-shaped inactivation-voltage relationship to Kv1.5, while fusion of the N-terminus of Kv1.5 to the transmembrane core of Kv2.1 decelerated Kv2.1 inactivation and abolished the U-shaped voltage-dependence of inactivation normally observed in Kv2.1. These data suggest that intersubunit T1 domain interactions influence a U-type inactivation phenotype in Kv1 channels, and suggest a generalized influence of the T1 domain on U-type inactivation between Kv channel subfamilies.

## BACKGROUND

Data presented in Chapter 3, and studies from other groups, have distinguished a slow inactivation phenotype termed ‘U-type’ inactivation, which has been observed in several voltage-gated  $K^+$  channels, including Kv2.1 (Klemic *et al.*, 1998) and most recently in *Shaker* and Kv3.1 (Klemic *et al.*, 2001). ‘U-type’ inactivation has been named for its characteristic U-shaped inactivation-voltage relationship, as observed in Kv1.5 $\Delta$ N209, exhibiting maximal inactivation at intermediate potentials where a small fraction of channels are open, and less pronounced inactivation at more positive potentials where channel opening is favored (Klemic *et al.*, 2001). The U-shaped voltage-dependence of inactivation is likely caused by preferential channel inactivation from closed states, although the conformational changes underlying ‘U-type’ inactivation behaviour remain unclear (Klemic *et al.*, 2001; Kurata *et al.*, 2001). For this reason, at the outset of this chapter, we stress that the term ‘U-type’ inactivation remains a phenotypic description of channel behaviour. Nevertheless, several reports suggest that channels showing U-type inactivation frequently exhibit ‘paradoxical’  $K^+$  and TEA $^+$  sensitivity. That is, whereas classical C-type inactivation in *Shaker* is generally slowed by elevation of extracellular  $K^+$ , this condition generally accelerates inactivation in channels with U-type behaviour, suggesting a potentially distinct mechanism for channel inactivation (Klemic *et al.*, 1998; Klemic *et al.*, 2001).

In Chapter 3, we demonstrated that a naturally occurring N-terminally truncated form of the human cardiac potassium channel Kv1.5 (Kv1.5 $\Delta$ N209) exhibits a U-type inactivation phenotype (Attali *et al.*, 1993; Fedida *et al.*, 1993; Kurata *et al.*, 2001). This finding clearly suggests that Kv1.5 possesses machinery to exhibit both C-type and U-type inactivation phenotypes, and demonstrates that residues structurally distinct and distant from the channel

pore and transmembrane domains can regulate the slow inactivation behaviour of the channel. Therefore, in this chapter we have directed our attention toward two goals. Firstly, we present several preliminary experiments designed to functionally distinguish the closed-state inactivation process revealed in Kv1.5 $\Delta$ N209 from the inactivation mechanism present in the full-length Kv1.5 channel. Secondly, the bulk of the experimental work in this chapter is an investigation of the N-terminal structures involved in regulation of U-type inactivation characteristics in Kv1.5 and other channels. The Kv1.5 N-terminus can be roughly divided into two segments. Residues 1-119 precede the T1 domain, and are poorly conserved in other Kv channels. In Kv1.5, this region contains a proline-rich SH3 ligand domain involved in channel regulation by Src tyrosine kinase, and is also likely required for channel binding to  $\alpha$ -actinin-2 (Holmes *et al.*, 1996; Maruoka *et al.*, 2000; Nitabach *et al.*, 2001). In contrast, residues 120-250 comprise the T1 domain, which exhibits extremely high sequence identity within channel subfamilies, and high structural homology among different subfamilies (Kreusch *et al.*, 1998; Bixby *et al.*, 1999; Zhou *et al.*, 2004).

In order to investigate the molecular basis for the modulation of the slow inactivation phenotype by the Kv1.5 N-terminus, we have characterized the gating properties of a series of N-terminal deletions of human Kv1.5, and chimeric constructs in which we substituted the N-terminus of Kv1.5 with the N-terminus of other Kv1 channels. This study demonstrates that the N-terminal region responsible for modulation of slow inactivation in Kv1.5 lies within the T1 domain. Furthermore, we demonstrate that fusion of the N-terminus of Kv2.1 to the transmembrane segments of Kv1.5 imparts a U-shaped inactivation-voltage relationship to Kv1.5, while the N-terminus of Kv1.5 attenuates the U-type inactivation behavior of Kv2.1.

## RESULTS

### *Recapitulation of C-type and U-type inactivation phenotypes in Kv1.5*

In intact channels, the T1 domain is likely structurally dissociated from the transmembrane segments of the channel, forming a “hanging gondola” (Kobertz *et al.*, 2000; Sokolova *et al.*, 2001). Interestingly, disruption of the N-terminus of Kv1.5 channels can significantly affect the gating properties of the channel. As described in Chapter 3, the activation and inactivation properties of Kv1.5 $\Delta$ N209 differ substantially from those observed in full-length Kv1.5. In particular, deletion of the Kv1.5 N-terminus appeared to uncover additional pathways for inactivation, as Kv1.5 $\Delta$ N209 inactivated more completely than full-length Kv1.5 over the range of potentials examined. As a result, Kv1.5 $\Delta$ N209 exhibited a U-shaped voltage-dependence of inactivation, in which inactivation was maximal between  $-20$  and  $0$  mV and significantly less pronounced with more positive depolarizations. This shape of the inactivation-voltage relationship contrasts sharply with the flat voltage-dependence of inactivation observed in full-length Kv1.5, and more closely resembles the ‘U-type’ inactivation phenotype of Kv2.1 (Fig. 4.1). For clarity, Fig. 4.1 also describes the method used to determine the inactivation-voltage relationship throughout this chapter, which differs slightly from the method used in Chapter 3. In these experiments, cells are subjected to a triple-pulse protocol: cells are given a 100 ms control pulse to 60 mV (P1), rested for 2 s at  $-80$  mV, stepped to various conditioning in 10 mV steps for 5 s (P2), followed by a test pulse to +60 mV (P3). This allows normalization of the P3 test pulse to the P1 control pulse, to quantify the extent of inactivation during the P2 conditioning pulse.

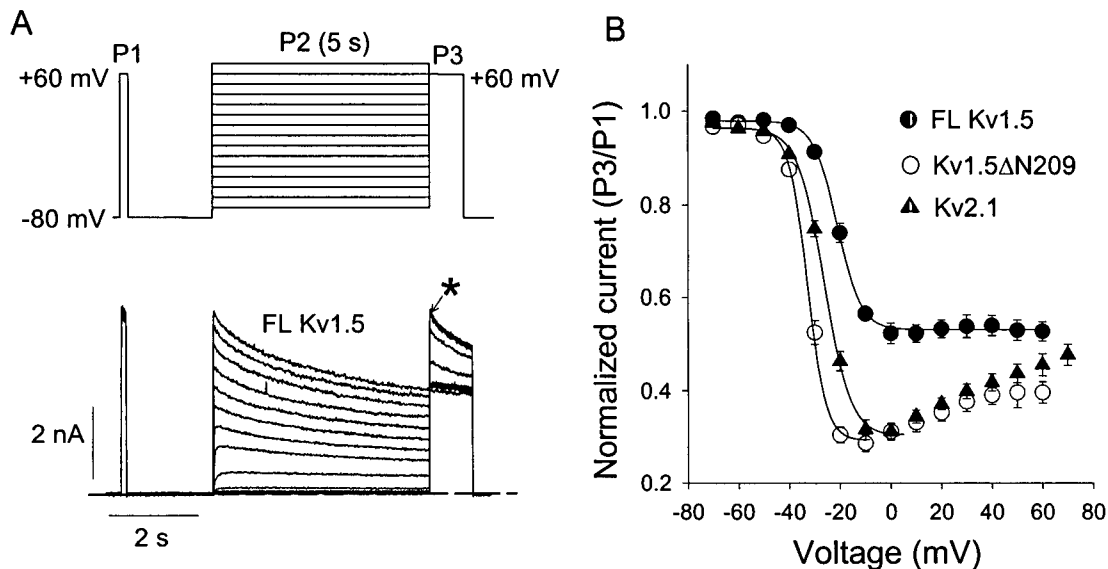


Figure 4.1. Inactivation properties of Kv1.5, Kv1.5 $\Delta$ N209, and Kv2.1. (A) To study inactivation in this chapter, cells were given a 100 ms control pulse to 60 mV (P1), rested for 2 s at  $-80$  mV, stepped from voltages between  $-70$  mV and  $+60$  mV in 10 mV steps for 5 s (P2), followed by a test pulse to  $+60$  mV (P3). The magnitude of the P3 current is proportional to the number of available channels remaining after the P2 pulse. The interpulse interval was 40 s, and the sample data shown was collected from cells expressing full-length Kv1.5. (B) Peak currents during P3 (indicated by the asterisk in panel A) were normalized to peak currents during P1, and fit with single Boltzmann equations.  $V_{1/2s}$  for inactivation in full-length Kv1.5, Kv1.5 $\Delta$ N209, and Kv2.1 were  $-21.0 \pm 1.2$  mV,  $-32.8 \pm 0.9$  mV, and  $-26.3 \pm 0.7$  mV, respectively.

#### ***Modulation of inactivation by extracellular cations***

To confirm a C-type mechanism of inactivation in Kv1.5, and to contrast the inactivation properties of Kv1.5 and Kv1.5 $\Delta$ N209, we also examined the effects of elevation of extracellular  $K^+$  on inactivation in both channels. This experiment was prompted by reports, including one characterization of *Shaker*, that other channels with a U-shaped inactivation voltage-relationship exhibited more inactivation in the presence of high extracellular  $K^+$  (Klemic *et al.*, 1998; Klemic *et al.*, 2001). This behaviour is opposite to

what would be expected based on previous studies of *Shaker* and other channels exhibiting a C-type mechanism (Lopez-Barneo *et al.*, 1993; Molina *et al.*, 1997). Inactivation was measured in both full-length Kv1.5 and Kv1.5 $\Delta$ N209, in two different extracellular K<sup>+</sup> concentrations (5 mM and 135 mM), at two different conditioning voltages (+10 mV and +60 mV in full-length Kv1.5; -20 mV and +60 mV in Kv1.5 $\Delta$ N209). The intermediate voltages (+10 mV in full-length Kv1.5 and -20 mV in Kv1.5 $\Delta$ N209) in Fig. 4.2 were selected based on the position of the ‘foot’ of the inactivation-voltage relationships for full-length Kv1.5 and Kv1.5 $\Delta$ N209 (Fig. 4.1B). To quantify inactivation, cells were given a 100 ms control pulse to 60 mV (P1), rested for 2 s at -80 mV, stepped to one of the two conditioning voltages for 5 s (P2), followed by a test pulse to +60 mV (P3). Sample data are shown normalized to the P1 test pulse, to correct for differences in current magnitude due to driving force changes in different extracellular K<sup>+</sup> conditions. Therefore, the magnitude of current in the P3 test pulse reflects the extent of inactivation during the conditioning pulse (P2). Because the effects of extracellular K<sup>+</sup> in Kv1.5 are quite small, experiments were conducted with a paired design, and summarized data is presented in the bar graphs in Fig. 4.2C. The bar graphs show the mean difference in fractional inactivation observed in 135 mM K<sup>+</sup> and 5 mM K<sup>+</sup> in full-length Kv1.5 (filled bars) and Kv1.5 $\Delta$ N209 (open bars).

In this experiment, elevation of extracellular K<sup>+</sup> resulted in a small but consistent inhibition of Kv1.5 inactivation, by between 3 and 4% at both +10 mV and +60 mV (Figs. 4.2A, 4.2C filled bars). This observation is consistent with a C-type mechanism of inactivation in full-length Kv1.5, and is consistent with previous studies on Kv1.5 and other *Shaker* homologues (Lopez-Barneo *et al.*, 1993; Rasmusson *et al.*, 1995; Fedida *et al.*, 1999). In contrast, Kv1.5 $\Delta$ N209 exhibits an opposite sensitivity to K<sup>+</sup> (Figure 4.2B, 4.2C open

bars), with 8-10% more inactivation observed in 135 mM extracellular  $K^+$  compared with the 5 mM extracellular  $K^+$  condition. The effects of extracellular  $K^+$  on inactivation of Kv1.5 $\Delta$ N209 were present at both voltages examined (-20 mV and +60 mV). Importantly, these effects are relatively minor compared with the effects observed in other channels such as Kv3.1, where elevation of extracellular  $K^+$  accelerated inactivation almost 3-fold (Klemic *et al.*, 2001). Nevertheless, this paradoxical sensitivity of inactivation to extracellular  $K^+$  appears to be a common feature of channels that exhibit a U-shaped inactivation-voltage relationship (Klemic *et al.*, 1998; Klemic *et al.*, 2001).

We have also examined experimental conditions that more potently inhibit inactivation of full-length Kv1.5 channels. We have determined the effects of these manipulations on the properties of the inactivation-voltage relationship of Kv1.5 $\Delta$ N209, to attempt to distinguish the closed-state inactivation process in Kv1.5 $\Delta$ N209 from the inactivation mechanism present in full-length Kv1.5 channels (Fedida *et al.*, 1999). Previous studies from our laboratory have suggested that substitution of  $K^+$  with  $Cs^+$  as the permeant ion can inhibit the C-type inactivation process (Fedida *et al.*, 1999). This conclusion is supported by the ability of  $Cs^+$  ions to potently prevent charge immobilization and to prevent the development of slow  $Na^+$  tail currents associated with C-type inactivation in Kv1.5 (Chen *et al.*, 1997; Fedida *et al.*, 1999; Wang & Fedida, 2002). This finding is confirmed in Fig. 4.3A, showing the inactivation of full-length Kv1.5 at +60 mV in symmetrical  $Cs^+$  (135 mM<sub>i/o</sub>) recording conditions. It is evident that, compared with  $K^+$  conditions, the extent of C-type inactivation is significantly attenuated. Inactivation-voltage relationships for full-length Kv1.5 determined in  $Cs^+$  or  $K^+$  recording conditions (using the same protocol

described in Fig. 4.1A) suggest that this inhibition by  $\text{Cs}^+$  is roughly constant at all depolarized voltages (Fig. 4.3C).

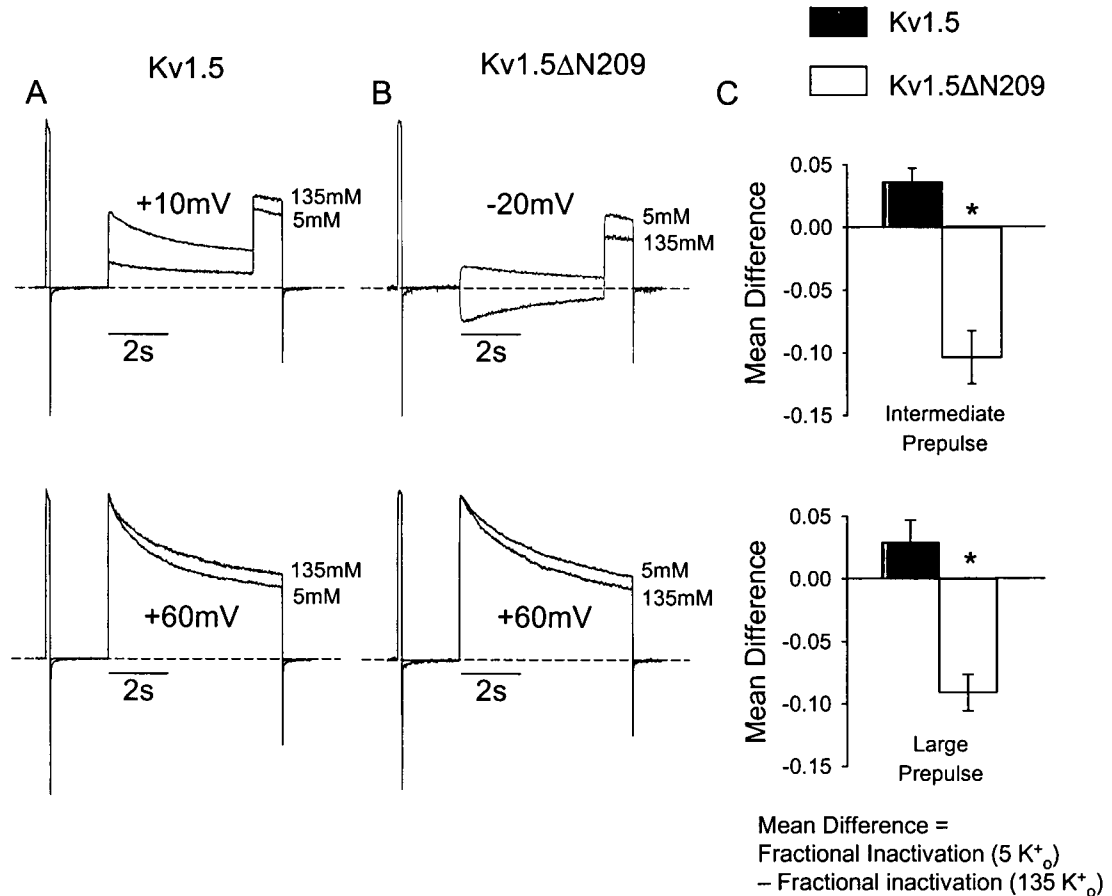


Figure 4.2. Differential effects of extracellular  $\text{K}^+$  on Kv1.5 and Kv1.5ΔN209 inactivation. To characterize inactivation, cells expressing (A) full-length Kv1.5, or (B) Kv1.5ΔN209 were given a 100 ms control pulse to 60 mV, rested for 2 s at  $-80$  mV, stepped to a large prepulse (+60 mV for both channels) or an intermediate prepulse (+10 mV for full-length Kv1.5 or  $-20$  mV for Kv1.5ΔN209) steps for 5 s, followed by a test pulse to +60 mV (P3). Experiments were conducted in either 5 mM or 135 mM extracellular  $\text{K}^+$ , as indicated on the sample traces. (C) Peak currents in the +60 mV test pulse currents were normalized to the control pulse, and the bar graphs represent the difference in fractional inactivation in 5 mM  $\text{K}^+$  vs. 135 mM  $\text{K}^+$  (positive values mean less inactivation in 135 mM  $\text{K}^+$ , negative values mean more inactivation in 135 mM  $\text{K}^+$ ). Asterisks indicate a significant difference between Kv1.5ΔN209 and full-length Kv1.5 ( $n=6$  per channel type,  $p<0.05$ ). Elevation of extracellular  $\text{K}^+$  mildly inhibits inactivation in full-length Kv1.5, but accelerates inactivation in Kv1.5ΔN209.

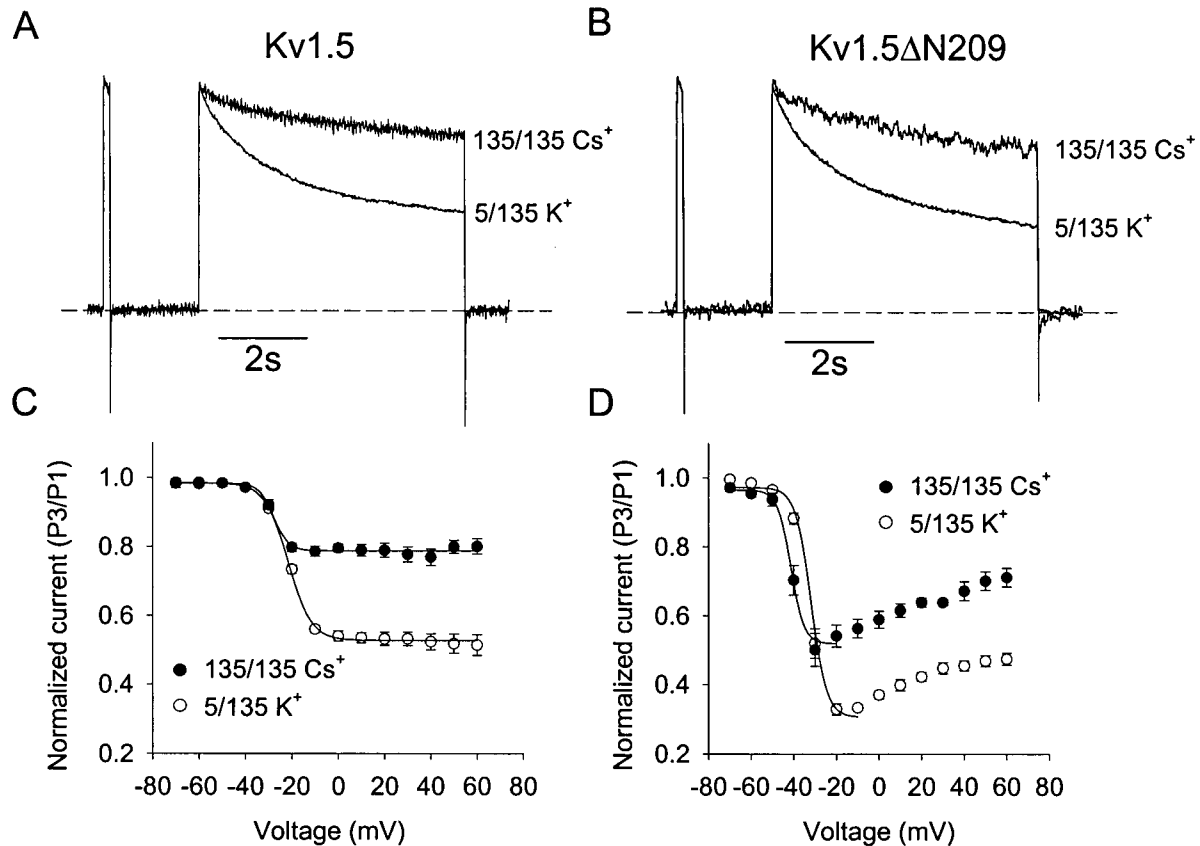


Figure 4.3. Inactivation voltage-relationships for full-length Kv1.5 and Kv1.5ΔN209 in K<sup>+</sup> and Cs<sup>+</sup> recording conditions. Inactivation voltage-relationships were recorded from cells expressing either full-length Kv1.5 (A,C) or Kv1.5ΔN209 (B,D), in K<sup>+</sup> recording conditions or in symmetrical Cs<sup>+</sup> conditions, as described in Fig. 4.1. Panels (A) and (B) depict sample traces of depolarizations to +60 mV in both recording conditions (as indicated), to illustrate slower inactivation of both full-length Kv1.5 and Kv1.5ΔN209 in the symmetrical Cs<sup>+</sup> condition. Panels (C and D) depict inactivation-voltage relationships for both channels, collected using the protocol described in Fig. 4.1, with P2 conditioning voltages between -70mV and +60 mV. The symmetrical Cs<sup>+</sup> conditions inhibit inactivation at all voltages, but do not affect the ‘upturn’ of the inactivation-voltage relationship in Kv1.5ΔN209.

Fig. 4.3B illustrates that the symmetrical Cs<sup>+</sup> condition also inhibits inactivation of Kv1.5ΔN209 channels. As for full-length Kv1.5 channels, inactivation is weaker at all voltages examined when K<sup>+</sup> is substituted with Cs<sup>+</sup>. If Cs<sup>+</sup> substitution inhibits closed-state inactivation, we would expect to see a ‘blunted’ or shallower upturn of the inactivation-

voltage relationship. However, the upturn of the Kv1.5 $\Delta$ N209 inactivation-voltage relationship is unchanged when compared with recordings in K<sup>+</sup> (Fig. 4.3D). Therefore, this result suggests that the inactivation-voltage relationship for Kv1.5 $\Delta$ N209 consists of two components: a Cs<sup>+</sup> sensitive component observed in full-length Kv1.5 (Fig. 4.3A,C), and a Cs<sup>+</sup> insensitive component that accounts for the upturn of the inactivation-voltage relationship (Fig. 4.3B,D).

The effects of extracellular TEA<sup>+</sup> application mimic the effects of K<sup>+</sup> substitution with Cs<sup>+</sup>. In *Shaker* channels, application of extracellular TEA<sup>+</sup> results in deceleration of C-type inactivation. Although residue R487 (corresponding to T449 in *Shaker*) renders wild-type Kv1.5 insensitive to extracellular TEA<sup>+</sup>, both current and inactivation in the R487T mutant of Kv1.5 or Kv1.5 $\Delta$ N209 are inhibited by TEA<sup>+</sup>. The application of extracellular TEA<sup>+</sup> diminished the peak currents observed through Kv1.5 R487T channels, with 10 mM extracellular TEA<sup>+</sup> resulting in a  $51 \pm 2\%$  (n=3) block of peak current (data not shown). Sample traces (normalized to peak current) demonstrating the effects of 10 mM extracellular TEA<sup>+</sup> on the inactivation time course at +60 mV of Kv1.5R487T  $\Delta$ N209 are shown in Fig. 4.4A. Although application of extracellular TEA<sup>+</sup> clearly inhibits inactivation through the channel, much like the effects of Cs<sup>+</sup>, this condition does not reduce the upturn of the Kv1.5R487T  $\Delta$ N209 inactivation-voltage relationship (Fig. 4.4B), as the inactivation-voltage relationships recorded in the presence or absence of extracellular TEA<sup>+</sup> are essentially parallel at positive voltages. As for Cs<sup>+</sup>, these results suggest that the component of the inactivation-voltage relationship that accounts for the upturn is not inhibited by extracellular TEA<sup>+</sup>. These results, together with the effects of Cs<sup>+</sup> in Kv1.5 $\Delta$ N209 (Fig. 4.3D) illustrate

that the closed-state inactivation process revealed by deletion of the Kv1.5 N-terminus can be differentially regulated compared to the inactivation process present in full-length Kv1.5.

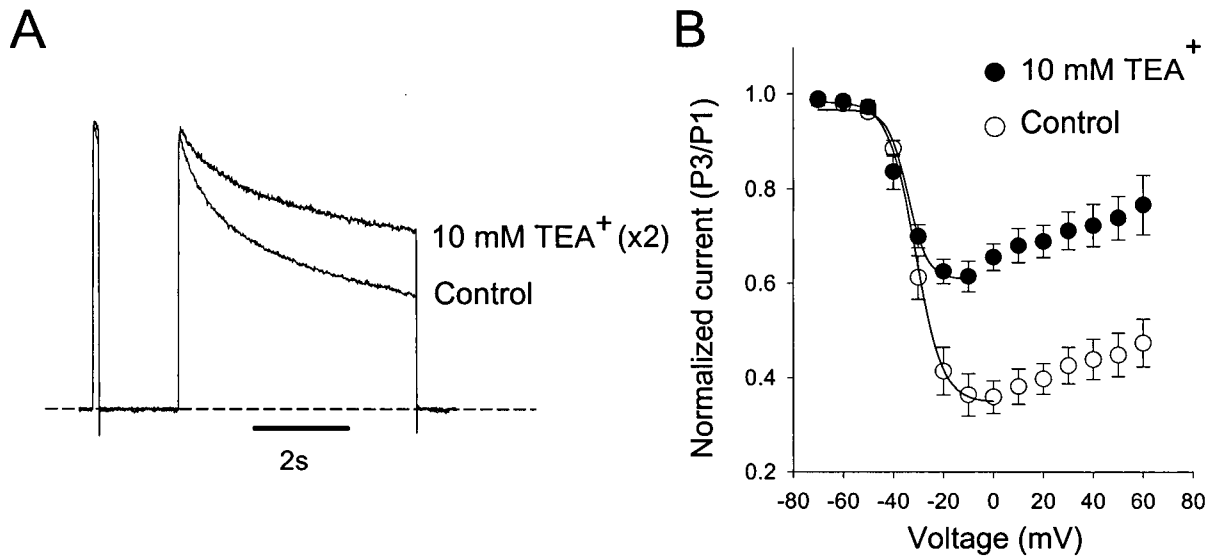


Figure 4.4. Effects of extracellular TEA<sup>+</sup> on Kv1.5R487T ΔN209 inactivation. Inactivation voltage-relationships were recorded from cells expressing Kv1.5R487T ΔN209 in standard K<sup>+</sup> recording conditions, with and without 10 mM extracellular TEA<sup>+</sup>. Panel (A) illustrates sample traces of depolarizations to +60 mV in the presence or absence of extracellular TEA<sup>+</sup> (as indicated), recorded from the same cell, to illustrate slower inactivation with TEA<sup>+</sup>. Traces in the presence of TEA<sup>+</sup> have been scaled for comparison. Panel (B) shows inactivation-voltage relationships in both conditions, at voltages between -70mV and +60 mV. As with Cs<sup>+</sup>, extracellular TEA<sup>+</sup> is able to inhibit inactivation at all voltages, but does not affect the ‘upturn’ of the inactivation-voltage relationship in Kv1.5R487T ΔN209.

### *The Kv1.5 T1 domain influences the slow inactivation phenotype*

To confirm and extend our characterization of Kv1.5 $\Delta$ N209, we have attempted to define the N-terminal region involved in altering the gating phenotype of Kv1.5. We began by constructing a series of N-terminally truncated forms of Kv1.5 (Fig. 4.5). These were transiently expressed in HEK 293 cells, and their activation and inactivation properties were examined.

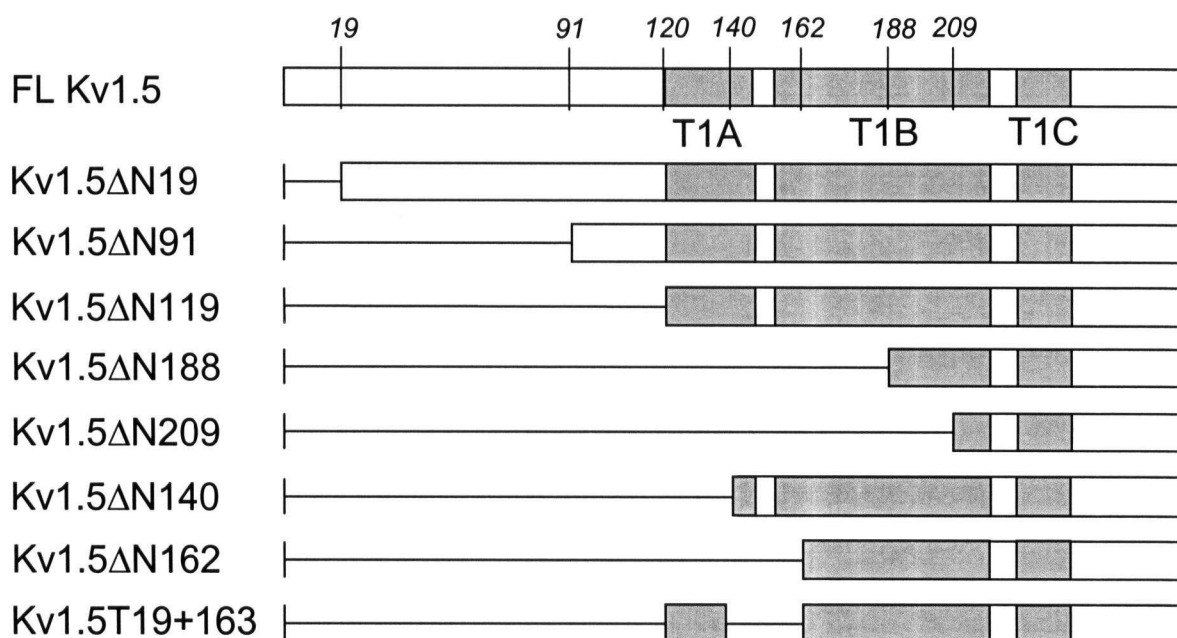


Figure 4.5. N-terminal deletion mutants of Kv1.5. N-terminal deletions of Kv1.5 were generated by either random Bal31 exonuclease digestion, PCR-based methods, or by Restriction endonuclease digestion at sites within the Kv1.5 N-terminus (see Chapter 2: Materials and Methods). Shaded boxes demarcate the cytoplasmic T1 domain, which has been subdivided into T1A, T1B, T1C (shaded regions). All mutants shown were functional and are characterized in Fig. 4.6, except Kv1.5 $\Delta$ N140 and Kv1.5 $\Delta$ N162, which did not express.

We examined three constructs comprising progressive deletions of Kv1.5 N-terminal residues up to the T1 boundary (Kv1.5 $\Delta$ N19, Kv1.5 $\Delta$ N91, Kv1.5 $\Delta$ N119, see Fig. 4.5). None of these deletion constructs exhibited any remarkable differences in activation or inactivation gating from full-length Kv1.5, although the half-inactivation voltages were slightly right-shifted in these 3 constructs relative to full-length Kv1.5 (Fig. 4.6A, C). Control data for full-length Kv1.5 channels is included in Fig. 4.6 for direct comparison. In addition, only very slight differences were observed in the level of inactivation resulting from 5 s inactivating pulses (Fig. 4.6C). Kv1.5 $\Delta$ N19, Kv1.5 $\Delta$ N91, Kv1.5 $\Delta$ N119 exhibited half-activation potentials of  $-11.0 \pm 0.6$  mV,  $-12.0 \pm 0.5$  mV, and  $-11.5 \pm 1.5$  mV, and half-inactivation potentials of  $-15.9 \pm 1.3$  mV,  $-16.0 \pm 0.5$  mV, and  $-17.0 \pm 1.5$  mV, respectively. Importantly, all three constructs exhibited a flat voltage-dependence of inactivation at positive potentials, which is consistent with the appearance of the inactivation-voltage relationship characteristic of full-length Kv1.5. These data suggest that the first 120 amino acids of Kv1.5 exert little direct effect on the activation or inactivation properties of the channel.

In contrast, a longer N-terminal deletion into the T1 domain (Kv1.5 $\Delta$ N188, Fig. 4.5) resulted in leftward shifts of both activation and inactivation, and a U-shaped inactivation-voltage relationship closely resembling that reported for Kv1.5 $\Delta$ N209 (Fig. 4.6B, D). These observations are consistent with a U-type inactivation phenotype in both Kv1.5 $\Delta$ N188 and Kv1.5 $\Delta$ N209, and demonstrate that deletions into the T1 domain are required to produce the U-shaped inactivation-voltage relationship characteristic of Kv1.5 $\Delta$ N209. Kv1.5 $\Delta$ N188 exhibited half-activation and half-inactivation potentials of  $-24.7 \pm 1.3$  mV and  $-29.9 \pm 4.0$  mV, respectively. To further characterize the influence of the T1 domain, we generated

several deletion mutants intermediate to Kv1.5 $\Delta$ N119 and Kv1.5 $\Delta$ N188, namely Kv1.5 $\Delta$ N140 and Kv1.5 $\Delta$ N162 (Fig. 4.5). Interestingly, in spite of fairly robust expression of both shorter and longer deletion constructs, repeated transfections with these intermediate deletion mutants failed to ever generate any detectable macroscopic currents. Nevertheless, the data collected suggested that the first 70 amino acids of the Kv1.5 T1 domain (between residues 119 and 188) exert a critical influence on U-type inactivation in Kv1.5.

We also examined the activation and inactivation properties of a construct in which we fused the first 19 amino acids of the Kv1.5 T1 domain to Kv1.5 $\Delta$ N162 (see Kv1.5T19+163 in Fig. 4.5). Surprisingly, this manipulation of the T1 domain sequence both restored channel expression and resulted in a U-shaped voltage-dependence of inactivation (Fig. 4.6B, D). Kv1.5T19+163 exhibited a strongly leftward-shifted half-activation potential of  $-23.8 \pm 0.7$  mV, and a half-inactivation potential of  $-32.1 \pm 1.9$  mV. These data suggested that disruption of the first 42 residues of the Kv1.5 T1 domain was sufficient to reproduce the U-type inactivation phenotype observed in Kv1.5 $\Delta$ N209. To summarize this deletion analysis, the functional mutants examined clustered very clearly into two groups. The first group comprised deletions up to the beginning of the N-terminal T1 domain, and exhibited gating parameters similar to full-length Kv1.5. The second group, in contrast, comprised deletions within the T1 domain, and exhibited gating parameters similar to Kv1.5 $\Delta$ N209.

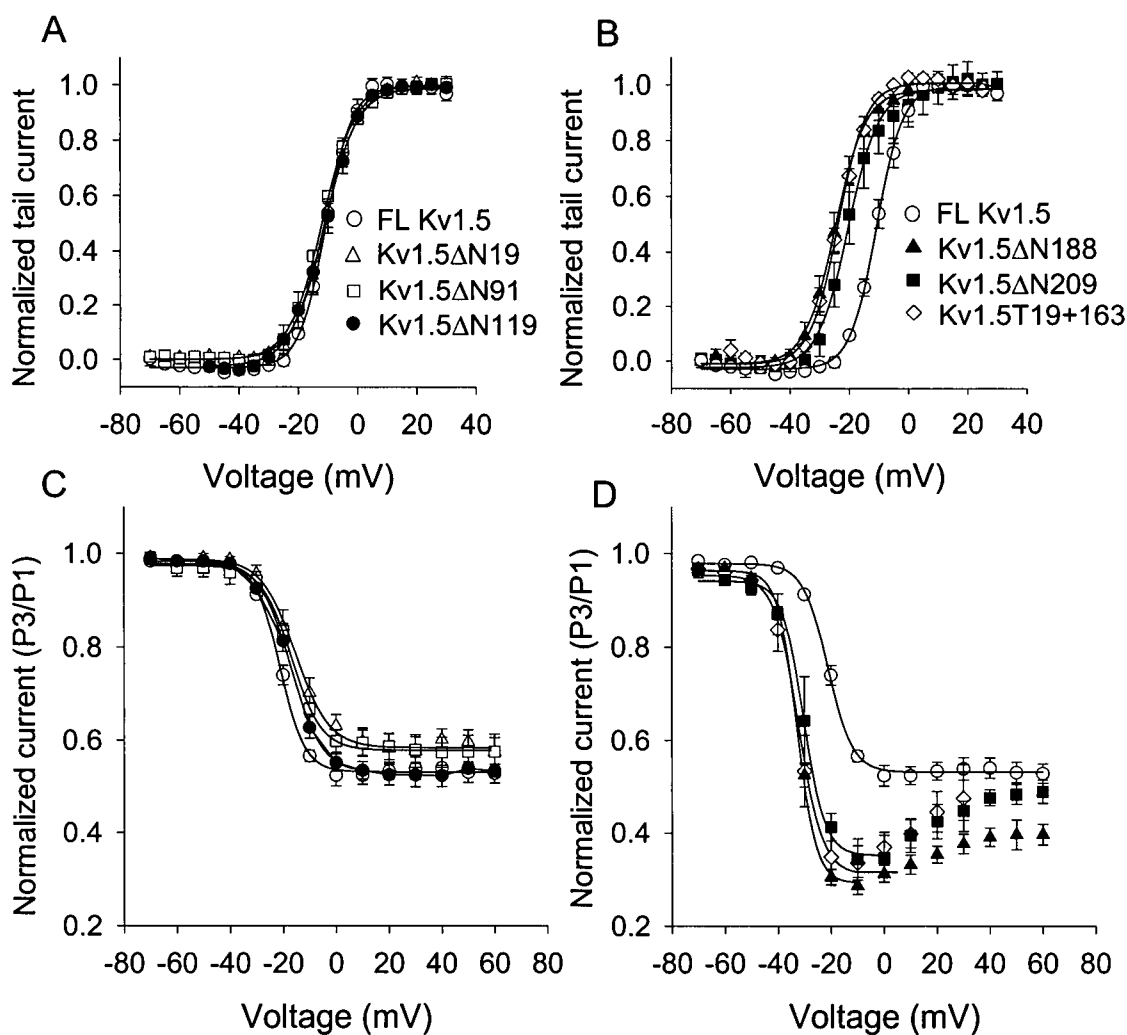


Figure 4.6. Activation and inactivation properties of N-terminal deletion mutants of Kv1.5. A series of sequential N-terminal deletion mutants of Kv1.5 were prepared (see Chapter 2: Materials and Methods, and Fig. 4.5) and their kinetic properties were examined after transient expression in HEK 293 cells. Data for full-length Kv1.5 and Kv1.5ΔN209 are included for comparison. (A, B) Activation properties were measured as described in Figure 3.2.  $V_{1/2s}$  of activation for Kv1.5ΔN19, Kv1.5ΔN91, Kv1.5ΔN119, Kv1.5ΔN188, and Kv1.5T19+163 were  $-11.0 \pm 0.6$  mV,  $-12.0 \pm 0.5$  mV,  $-11.5 \pm 1.5$  mV,  $-24.7 \pm 1.3$  mV, and  $-23.8 \pm 0.7$  mV, respectively. (C, D) Inactivation-voltage relationships were derived as described in Figure 4.1.  $V_{1/2s}$  of inactivation for Kv1.5ΔN19, Kv1.5ΔN91, Kv1.5ΔN119, Kv1.5ΔN188, and Kv1.5T19+163 were  $-15.9 \pm 1.3$  mV,  $-16.0 \pm 0.5$  mV,  $-17.0 \pm 1.5$  mV,  $-29.9 \pm 4.0$  mV, and  $-32.1 \pm 1.9$  mV, respectively.

### ***N-termini of Kv1.1 and Kv1.3 channels restore wild-type inactivation in Kv1.5***

To confirm the importance of the T1 domain, we replaced the N-terminus of Kv1.5 up to residue M210 with the corresponding N-terminal sequence of either Kv1.1 or Kv1.3 (shown in cartoon form in Fig. 4.7A), and examined activation and inactivation properties after transient expression in HEK 293 cells (Fig. 4.7). The rationale behind this experiment was that sequence alignment illustrates that channels within the Kv1 family exhibit roughly 85% sequence identity between their T1 domains, but essentially no homology in the remainder of their cytosolic N-termini (Fig. 4.7B; Kreusch *et al.*, 1998). In addition, the N-terminal sequence preceding the T1 domain differs significantly in length between different channels. In Kv1.5, this region is 120 amino acids long, compared with 38 amino acids in Kv1.1 and 53 amino acids in Kv1.3. Thus, restoration of a flat inactivation-voltage relationship in these chimeric constructs would further implicate the T1 domain in the regulation of a U-type inactivation phenotype. The Kv1.1N/Kv1.5 and Kv1.3N/Kv1.5 chimeras exhibited half-activation potentials of  $-18.0 \pm 1.1$  mV and  $-13.5 \pm 0.9$  mV, respectively (Fig. 4.7C). Most importantly, both the Kv1.1 and Kv1.3 N-termini were sufficient to rescue the inactivation properties observed in full-length Kv1.5, as both chimeric channels exhibited a flat voltage-dependence of inactivation at positive potentials, and fractional inactivation similar to that observed in full-length Kv1.5 after 5 s depolarizations (Fig. 4.7D). The half-inactivation potentials of Kv1.1N/Kv1.5 and Kv1.3N/Kv1.5 were  $-19.0 \pm 2.0$  mV and  $-21.2 \pm 1.3$  mV, respectively. Together with the data presented in Figure 4.6, and the lack of N-terminal homology outside the T1 domain of Kv1 channels, these data provide strong evidence that amino acids within the T1 domain are critical for modulating the slow inactivation phenotype in Kv1 channels.

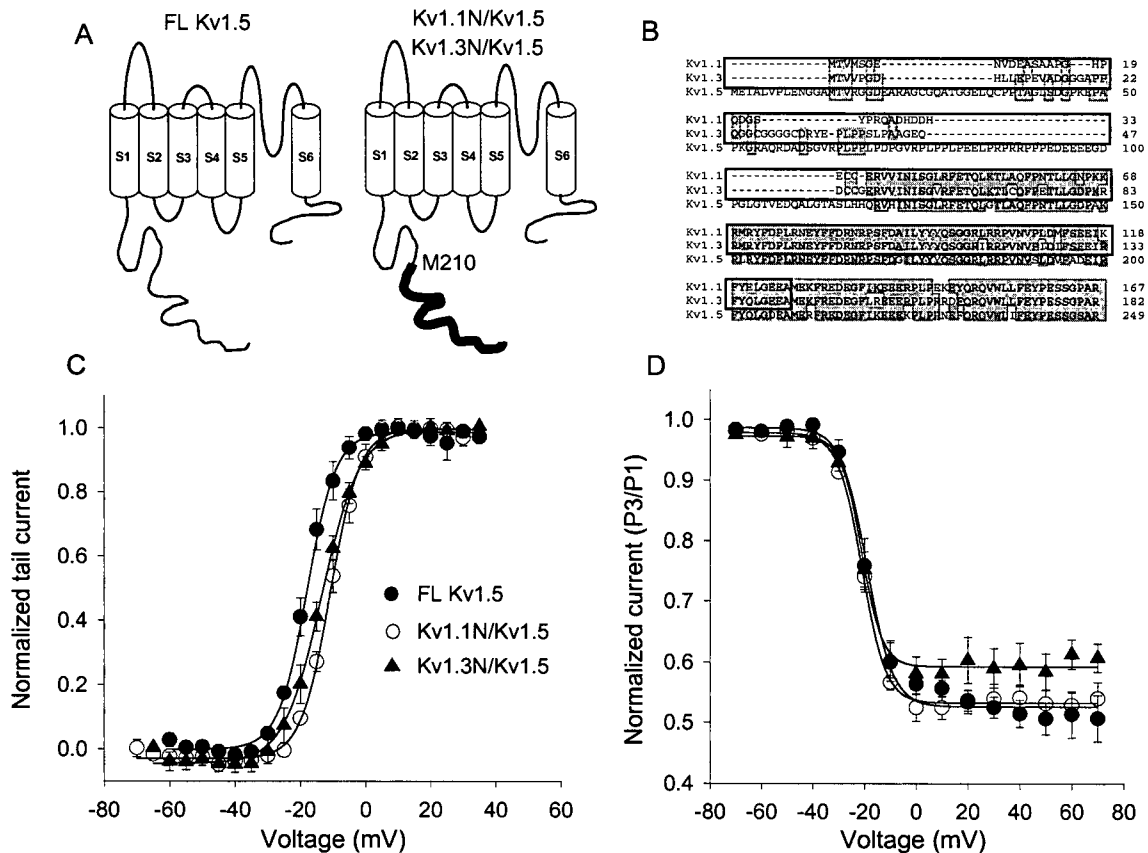


Figure 4.7. N-termini of Kv1 channels rescue the inactivation properties of full-length Kv1.5. Panel (A) illustrates construction of the Kv1.1N/Kv1.5 and Kv1.3N/Kv1.5 chimeric channels. The N-terminal amino acid sequence preceding M210 in Kv1.5 was replaced with the corresponding sequence from either Kv1.1 or Kv1.3, shown as a thick line (see Chapter 2: Materials and Methods). (B) Sequence alignment of the N-termini of Kv1.1, Kv1.3, and Kv1.5, generated with the web-based CLUSTALW sequence alignment tool (Thompson *et al.*, 1994). Blue text indicates residues making up the T1 domain, and identical amino acids in Kv1.1, Kv1.3, and Kv1.5 are shaded in gray. The segments of Kv1.1 and Kv1.3 present in the chimeric channels are boxed with a solid line, demonstrating that most N-terminal homology is restricted to the T1 domains of these Kv1 channels. (C) Activation and (D) inactivation curves were constructed as described in Figures 3.2 and 4.1, respectively, yielding  $V_{1/2}$ s of activation of  $-18.0 \pm 1.1$  mV and  $-13.5 \pm 0.9$  mV for Kv1.1N/Kv1.5 and Kv1.3N/Kv1.5, respectively.  $V_{1/2}$ s of inactivation were  $-19.0 \pm 2.0$  mV for Kv1.1N/Kv1.5 and  $-21.2 \pm 1.3$  for Kv1.3N/1.5.

### ***Disruption of the intersubunit T1 interface influences slow inactivation in Kv1.5***

Characterization of our deletion mutants of Kv1.5 (Figs. 4.5, 4.6), together with recent reports that disruption of intersubunit T1 contacts influences the activation properties of Kv1.2 (Minor *et al.*, 2000), prompted us to examine the effects of similar disruptions on the inactivation properties of Kv1.5 (Fig. 4.8). Figure 4.8A depicts amino acids in close contact at the interface formed between two adjacent T1 domains, generated from the crystal structure determined for the T1 domain of rat Kv1.2 (Minor *et al.*, 2000). The interface illustrated in Figure 4.8A is repeated four times in an intact channel, due to the rotational symmetry of the T1 tetramer. As shown in Figure 4.8A, intersubunit contacts are formed between residues throughout the crystallized region of the T1 domain, though primarily within the first 45-50 residues of T1, and are typically formed between the side chains of polar amino acids (Kreusch *et al.*, 1998; Minor *et al.*, 2000). We generated a double point mutant, Kv1.5ET/AA, by mutating two adjacent residues, E132 and T133, to alanines (backbone and side chain bonds of these residues are coloured yellow in Fig. 4.8A). Mutation of the residues homologous to either E132 or T133 in Kv1.2 results in significant shifts of activation gating (Minor *et al.*, 2000), and our double mutation should disrupt the hydrogen-bonded network of intersubunit T1 contacts near the N-terminus of the T1 domain (Fig. 4.8A). Upon transient expression in HEK 293 cells, Kv1.5ET/AA exhibited a half-activation potential of  $-21.4 \pm 1.2$  mV (Fig. 4.8B), and a half-inactivation potential of  $-32.2 \pm 3.6$  mV (Fig. 4.8C). Both parameters were left-shifted with respect to full-length Kv1.5 channels. These results were somewhat surprising, as individual mutations of homologous residues to alanine in Kv1.2 have both been shown to result in a rightward (depolarizing) shift of the activation relationship (Minor *et al.*, 2000). Most interestingly, Kv1.5ET/AA

channels consistently exhibited a U-shaped inactivation-voltage relationship (Fig. 4.8C). Kv1.5ET/AA channels inactivated maximally by  $59 \pm 3\%$  at  $-20$  mV, and only inactivated by  $48 \pm 2\%$  at  $+50$  mV. Although not as pronounced as the U-shaped inactivation-voltage relationship seen with more complete disruption of the T1 domain (eg. Kv1.5 $\Delta$ N209), this result shows that individual point mutations within the T1 domain can influence the inactivation phenotype in Kv1.5.

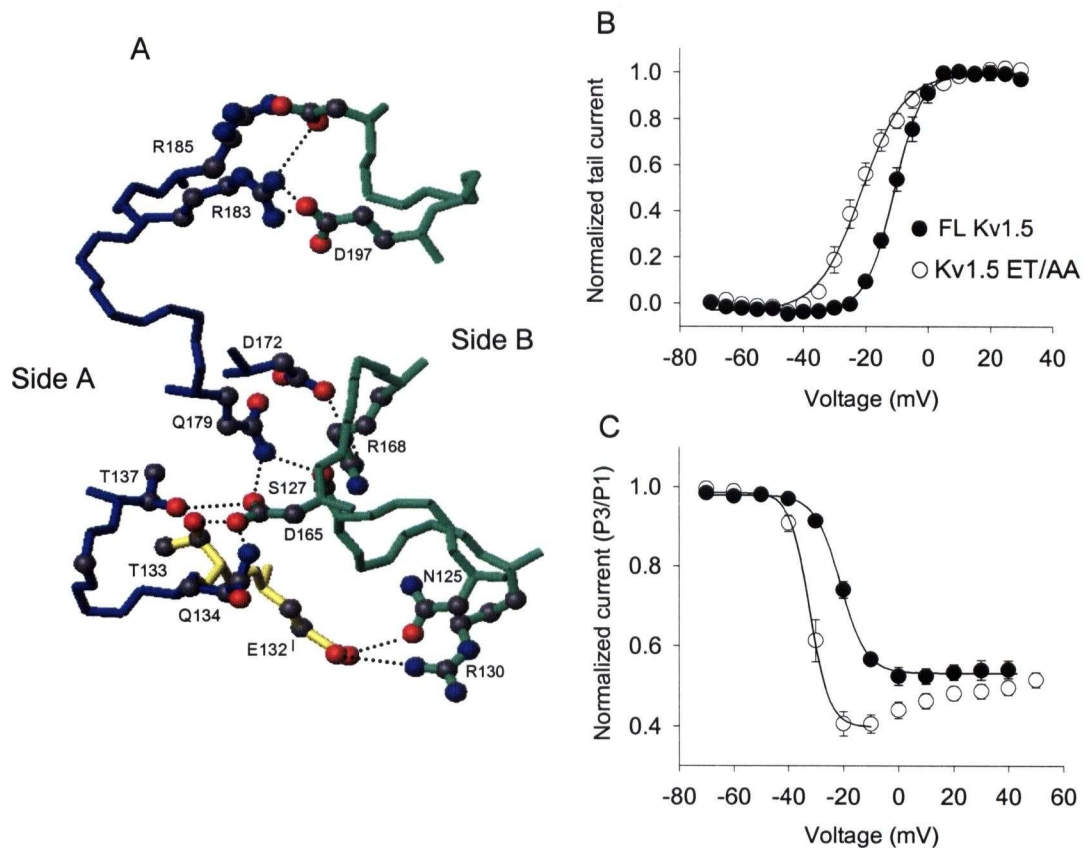


Figure 4.8. Point mutations at the intersubunit T1 interface influence Kv1.5 inactivation. (A) Diagram illustrating specific residues forming intersubunit T1 contacts, generated from the crystal structure of the human Kv1.2 T1 domain (Minor *et al.*, 2000). Ball-and-stick diagrams are shown for the sidechains of selected residues involved in intersubunit contacts. Blue and green backbone colours indicating different subunits. Intersubunit T1 contacts at residues E132 and T133 (side chain and backbone bonds are coloured yellow) were disrupted by mutating these residues to alanine. (B) Activation and (C) inactivation curves were constructed as described in Figures 3.2 and 4.1, respectively, yielding a  $V_{1/2}$  of activation of  $-21.4 \pm 1.2$  mV and a  $V_{1/2}$  of inactivation of  $-32.2 \pm 3.6$  mV for Kv1.5ET/AA. Activation and inactivation data for full-length Kv1.5 is included for comparison.

### ***Reciprocal influences of the Kv2.1 and Kv1.5 N-termini***

The data presented thus far strongly suggest that residues within the T1 domain function to prevent closed-state inactivation in full-length Kv1.5. To investigate the specificity of this interaction between the N-terminus and the transmembrane core of voltage-gated Kv channels, we generated a chimeric channel in which the N-terminus of Kv1.5 was replaced with the N-terminus of Kv2.1, a voltage-gated K<sup>+</sup> channel that exhibits a U-shaped inactivation-voltage relationship (see Kv2.1N/Kv1.5, Fig. 4.9A). The structural scaffold of the T1 domain is likely conserved among all Kv channels, however sequence alignment shows that the Kv2.1 T1 domain primary sequence exhibits roughly 37% sequence identity with the T1 domain of Kv1.5 (Fig. 4.9B; Bixby *et al.*, 1999). Again, we transiently expressed this construct in HEK 293 cells and characterized its activation and inactivation properties. Kv2.1N/Kv1.5 exhibited  $V_{1/2s}$  of activation and inactivation  $-25.5 \pm 1.1$  mV and  $-30.6 \pm 0.5$  mV, respectively (Figs. 4.9C, E). Importantly, Kv2.1N/1.5 also exhibited a marked U-shaped voltage-dependence of inactivation (Fig. 4.9E). The inactivation-voltage relationship of Kv2.1N/Kv1.5 was very similar to those observed in T1-deleted forms of Kv1.5 (Fig. 4.1B, 4.6D) and full-length Kv2.1 channels (Fig. 4.1B, 4.9E), however some slight differences were apparent. In particular, Kv2.1N/Kv1.5 did not inactivate as completely as either Kv2.1 or T1-deleted forms of Kv1.5 during the 5s pulses examined (Fig. 4.9E).

We also conducted the inverse experiment, in which the N-terminus of Kv2.1 was replaced with the N-terminus of Kv1.5 (Kv1.5N/Kv2.1, Fig. 4.9A). The half-activation and half-inactivation potentials of Kv1.5N/Kv2.1 were  $-9.3 \pm 3.3$  mV and  $-12.1 \pm 3.3$  mV, respectively (Fig. 4.9C, 4.9E). Most importantly, fusion of the Kv1.5 N-terminus to Kv2.1

resulted in complete attenuation of the U-shape normally observed in the Kv2.1 inactivation-voltage relationship (Fig. 4.1B, Fig. 4.9E). In addition, Kv1.5N/Kv2.1 exhibited weaker inactivation than observed in full-length Kv2.1, illustrated by sample traces elicited with 5 s pulses to +60 mV in cells expressing either Kv2.1 or Kv1.5N/Kv2.1 (Fig. 4.9D). During the 5s pulses employed in these experiments, maximal inactivation in wild-type Kv2.1 was  $69\% \pm 2\%$  at 0 mV, while Kv1.5N/Kv2.1 inactivated maximally by only  $34\% \pm 4\%$  at +50 mV (Fig. 4.9E). We also examined an N-terminally deleted form of Kv2.1 (Kv2.1 $\Delta$ N101), to confirm that the effects of the Kv1.5 N-terminus in the Kv1.5N/Kv2.1 chimera were not simply due to deletion of the Kv2.1 N-terminus. Based on sequence alignment, this deletion corresponds to a deletion of 181 amino-terminal residues in Kv1.5. We had difficulty expressing N-terminal deletions of Kv2.1 in our HEK cell line, however, expression of Kv2.1 $\Delta$ N101 in mouse *ltk* cells confirmed previously published data collected from *Xenopus* oocytes (VanDongen *et al.*, 1990). In particular, deletions of the T1 domain of Kv2.1 result in extreme slowing of the kinetics of activation, and essentially complete ablation of slow inactivation of the channel, evident in Figure 4.9D (VanDongen *et al.*, 1990). This contrasts sharply with currents recorded from the Kv1.5N/Kv2.1 chimera, which exhibit markedly faster kinetics of activation, and substantial inactivation during a 5s pulse (Fig. 4.9D, E). As a further control experiment, we characterized a chimeric channel consisting of the N-terminus of Kv1.5T19+163 (Fig. 4.5) fused to the transmembrane domains of Kv2.1 (T19+163/Kv2.1, Fig. 4.9D). This N-terminal construct, results in a U-shaped voltage-dependence of inactivation in Kv1.5 (Fig. 4.6D), and results in activation and inactivation kinetics in Kv2.1 which are effectively indistinguishable from the N-terminal deletion of

Kv2.1 (Fig. 4.9D). This suggests that the inactivation phenotype observed in the Kv1.5N/Kv2.1 chimera results from a specific effect of the intact Kv1.5 N-terminus.

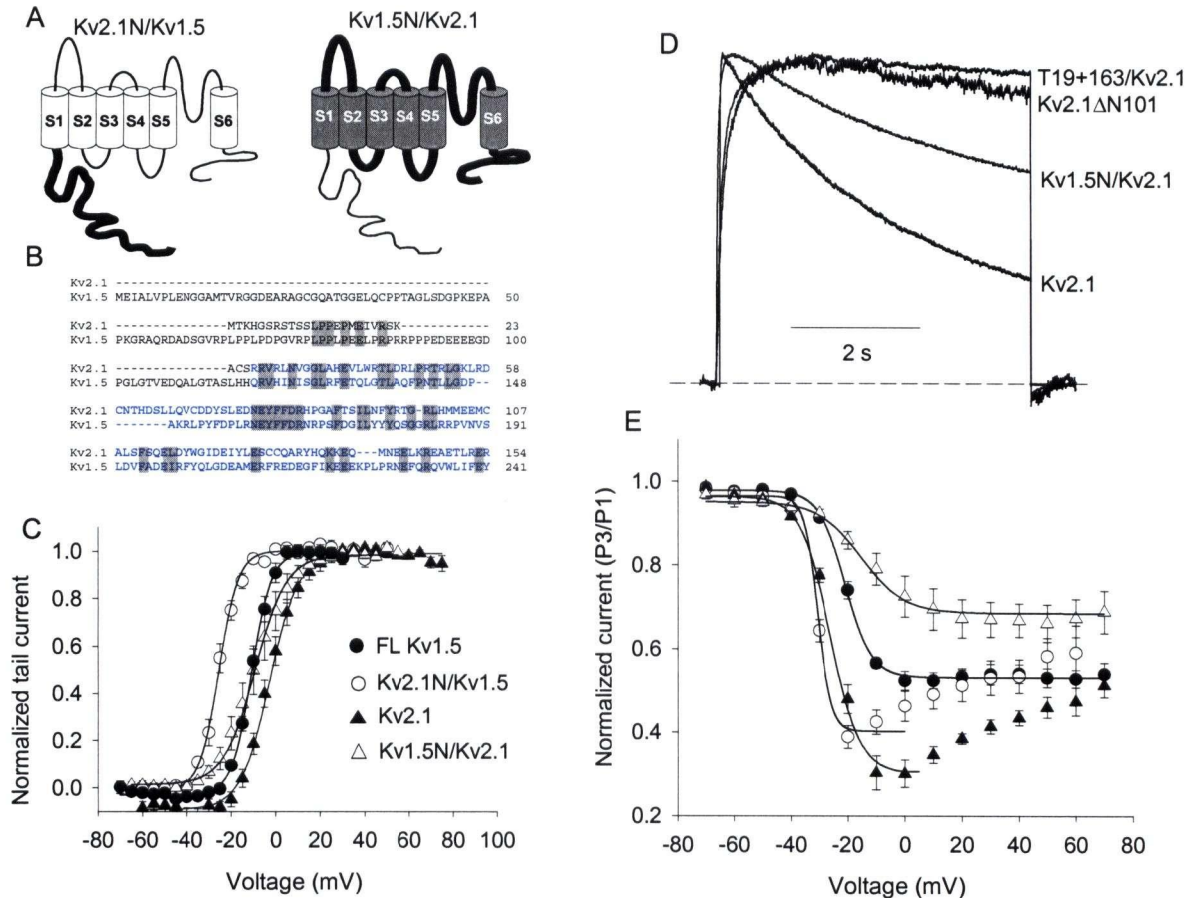


Figure 4.9. The N-termini of Kv1.5 and Kv2.1 exert reciprocal influences on Kv channel inactivation. (A) Schematic diagram of Kv1.5/Kv2.1 chimeric constructs. Amino acid sequence originating from Kv1.5 is illustrated as thin lines and non-shaded cylinders; sequence originating from Kv2.1 is illustrated as shaded cylinders and thick lines. Channels were constructed by switching the N-terminus up to residue P243 in Kv1.5 with N-terminal residues up to P180 from Kv2.1, and *vice versa*. (B) Sequence alignment of the N-termini of Kv1.5 and Kv2.1 was performed using a web-based CLUSTALW sequence alignment tool, and demonstrates a segment of the Kv2.1 N-terminus exhibiting 37% identity with the T1 domain of Kv1.5 (residues within the T1 domain are coloured blue, and identical residues are shaded). (C) Activation curves were constructed as described in Figure 3.2, yielding activation  $V_{1/2s}$  of  $-25.5 \pm 1.1$  mV and  $-9.3 \pm 3.3$  mV for Kv2.1N/Kv1.5 and Kv1.5N/Kv2.1, respectively. (D) The Kv1.5 N-terminus decelerates inactivation in Kv2.1. Sample data represent currents elicited from Kv2.1, Kv1.5N/Kv2.1, Kv2.1ΔN101, and T19+163/Kv2.1 expressed in Mouse *ltk-* cells, during 5 s pulses to +60 mV. (E) Inactivation-voltage relationships were derived as described in Figure 4.1, yielding inactivation  $V_{1/2s}$  of  $-30.6 \pm 0.5$  mV in Kv2.1N/Kv1.5 and  $-12.1 \pm 3.3$  mV in Kv1.5N/Kv2.1.

## DISCUSSION

The current 'hanging gondola' model of voltage-gated K<sup>+</sup> channel structure suggests that the T1 tetramer is structurally dissociated from membrane-bound segments of the channel (Gulbis *et al.*, 2000; Kobertz *et al.*, 2000; Zhou *et al.*, 2001a). However, it has been demonstrated that deletion mutations, and even relatively conservative point mutations, can exert strong effects on channel activation (Kobertz & Miller, 1999; Minor *et al.*, 2000; Cushman *et al.*, 2000; Strang *et al.*, 2001). This study, together with the data presented in Chapter 3, demonstrates that the T1 domain exerts equally significant effects on the inactivation properties of voltage-gated K<sup>+</sup> channels.

### *Multiple inactivation phenotypes in Kv1 channels*

The characterization of T1-deletion mutants of Kv1.5 presented here, together with recent studies in *Shaker* (Klemic *et al.*, 2001), suggest that *Shaker* family K<sup>+</sup> channels are able to exhibit at least two distinct inactivation phenotypes. As suggested by Klemic *et al.* (2001), we have referred to these here as C-type and U-type inactivation. Functionally, these two inactivation phenotypes seem to differ in the following ways. C-type inactivation occurs predominantly from the open state, is inhibited by extracellular K<sup>+</sup> or TEA<sup>+</sup>, and exhibits relatively slow and weakly voltage-dependent recovery from inactivation (Hoshi *et al.*, 1991; Rasmusson *et al.*, 1995; Rasmusson *et al.*, 1998; Klemic *et al.*, 2001). Channels exhibiting U-type inactivation properties, however, appear to exhibit preferential inactivation from partially-activated closed states, rapid and strongly voltage-dependent recovery from inactivation, and in some channel types accelerated inactivation with elevation of extracellular K<sup>+</sup> or TEA<sup>+</sup> (Klemic *et al.*, 1998; Klemic *et al.*, 2001). Experiments presented in this chapter also seem to distinguish multiple inactivation processes, since the closed-state

inactivation process in Kv1.5 $\Delta$ N209 appears to be relatively insensitive to manipulations (Cs<sup>+</sup> ions, extracellular TEA<sup>+</sup>) that slow inactivation in full-length Kv1.5 (or Kv1.5R487T) channels (Figs. 4.3, 4.4). Also, these results provide some confirmation/validation of our conclusions and modeling approach in Chapter 3, where we suggested that the inactivation mechanism of full-length Kv1.5 remains intact in Kv1.5 $\Delta$ N209. Our experiments suggest that the inactivation mechanism in full-length Kv1.5 accounts for the Cs<sup>+</sup> sensitive component of inactivation in Fig. 4.3. Deletion of the N-terminus allows inactivation via an additional (Cs<sup>+</sup> insensitive) pathway, accounting for the deeper inactivation and upturn of the inactivation-voltage relationship in Kv1.5 $\Delta$ N209 whether K<sup>+</sup> or Cs<sup>+</sup> is the permeant ion (Fig. 4.3). Unfortunately, conformational changes associated with ‘U-type’ or closed-state inactivation are poorly understood. Therefore, it remains unclear whether fundamentally distinct conformational changes underlie C-type vs. U-type inactivation behaviour, or whether their different properties reflect differences in how cations interact with open vs. closed channels.

Most importantly, our data demonstrates that the N-terminal T1 domain of Kv1.5 is a strong determinant of the slow inactivation phenotype of this channel. Full-length Kv1.5 channels exhibit no properties consistent with U-type inactivation (Fedida *et al.*, 1999), as the rate of inactivation appears to be essentially independent of voltage, inactivation is inhibited by extracellular K<sup>+</sup> and TEA<sup>+</sup> (in Kv1.5 R487T), and recovery from inactivation is weakly voltage-dependent. In addition, deletions up to the T1 border (residue 120) exert no significant effects on gating (Figs. 4.5, 4.6A, 4.6C). However, deletions within the T1 domain consistently altered both the activation and inactivation properties of Kv1.5, and resulted in a U-type inactivation phenotype in T1-deleted forms of the channel (Fig. 4.6B,D).

Using approaches of progressive channel deletion mutations (Figs. 4.5, 4.6), chimeric constructs of Kv1 channels (Fig. 4.7), and site-directed point mutations (Fig. 4.8), we have localized this function to within the Kv1 T1 domain.

The results of this study in Kv1.5 also suggest that the amino acids forming intersubunit T1 contacts may be involved in regulating the U-type inactivation phenotype, although the U-shaped inactivation-voltage relationship of the Kv1.5ET/AA construct (Fig. 4.8C) is not as marked as that observed in Kv1.5 $\Delta$ N209 or other T1 deleted forms of Kv1.5 (Figs. 4.5, 4.6D). This may be because the Kv1.5ET/AA mutation only disrupts a fraction of the intersubunit T1 interactions, as intersubunit contacts are made between multiple residues scattered throughout the T1 domain (see Fig. 4.8A). It should be noted that mutations throughout the T1 domain have been demonstrated to exert varying effects on the activation gating of Kv1 channels, including residues at the intersubunit T1 interface, residues lining the central pore of T1, and even residues in the T1-S1 linker region (Elkes *et al.*, 1997; Johnstone *et al.*, 1997; Kobertz & Miller, 1999; Cushman *et al.*, 2000). We have not yet fully characterized the effects of other T1 mutations on Kv1.5 inactivation. However, preliminary data from the Kv1.5 I126D mutant also exhibits an obviously U-shaped inactivation-voltage relationship (data not shown). Residue I126 is adjacent to N125 and S127, on side B of the intersubunit interface (both N125 and S127 are involved in multiple interactions with residues on side A of the interface, Fig. 4.8A). Also, given the number of residues able to modulate Kv channel activation, it seems likely that the gating effects of T1 are not mediated by a single locus, and that mutations at other sites in T1 will be able to mimic the inactivation effects of the E132A, T133A mutations.

### ***N-terminal regulation of inactivation in other Kv channels***

A generalized role for the N-terminus in the regulation of slow inactivation in Kv channels is also suggested by our studies of Kv1.5 and Kv2.1, which examined the effects of switching the N-termini of channels exhibiting either C-type (Kv1.5) or U-type (Kv2.1) inactivation phenotypes. Substitution of the Kv1.5 N-terminus with the Kv2.1 N-terminus resulted in channels that exhibited a U-shaped inactivation–voltage relationship, similar to the inactivation phenotype observed in Kv1.5 $\Delta$ N209 (Fig. 4.9). However, the inverse substitution resulted in a deceleration of inactivation compared with Kv2.1 (Fig. 4.9). Our interpretation of these observations is that the Kv2.1 N-terminus adopts a conformation or interacts with channels in a manner that is permissive to or promotes closed-state inactivation. In contrast, the Kv1.5 T1 domain may interact with channels in a manner that prevents closed-state inactivation, which is consistent with the absence of a U-type inactivation phenotype in Kv1.5, and the deceleration of inactivation in the Kv1.5N/Kv2.1 chimera.

Interestingly, the influence of the Kv1.5 N-terminus on the inactivation of Kv2.1 is extremely similar to the influence of Kv2.3 (also termed Kv8.1; Chiara *et al.*, 1999). In particular, coexpression of Kv2.1 and Kv2.3 results in deceleration of both Kv2.1 activation and inactivation, and studies of chimeric constructs of Kv2.1 and Kv2.3 have localized this effect to the N-terminus of Kv2.3, specifically within the C-terminal side of T1 and the T1-S1 linker (Chiara *et al.*, 1999). Similar effects are seen upon coexpression of Kv2.1 and Kv6.1, although the critical regulatory domains in Kv6.1 have not yet been determined (Kramer *et al.*, 1998). In addition, as observed in the Kv1.5N/Kv2.1 channel (Fig. 4.9), chimeric channels consisting of the N-terminal segment of Kv2.3 and the transmembrane

domains of Kv2.1 exhibit deceleration of Kv2.1 inactivation (Chiara *et al.*, 1999). These findings raise the possibility of a generalized mechanism of interaction between the N-termini and membrane-bound segments of voltage-gated K<sup>+</sup> channels. More importantly, in the context of our study these observations support the notion that the modulation of the inactivation phenotype by the N-terminus may be a general feature of voltage-gated K<sup>+</sup> channels.

### ***Coupling mechanisms between the T1 and transmembrane domains***

Studies to date have suggested several potential mechanisms of conformational coupling between T1 and the transmembrane domains of the channel. The C-terminal region of the T1 domain is thought to face the membrane-bound channel segments, and certain T1 point mutations which modulate activation gating have been shown to alter the conformation of this region of the channel, as does interaction with Kv $\beta$ -subunits (Gulbis *et al.*, 2000; Cushman *et al.*, 2000). This suggests that the conformation of the C-terminal region of the T1 domain exerts functionally significant effects on gating, possibly through the T1-S1 linkers, and this is consistent with the region of Kv2.3 involved in disruption of Kv2.1 inactivation (Chiara *et al.*, 1999). However, other T1 point mutations resulting in little global change of T1 structure have also been shown to modulate activation gating, suggesting an important role for active rearrangements of T1 during channel gating (Minor *et al.*, 2000). A further possible mechanism for the influence of T1 is through interaction with the C-terminus of Kv channels, as the N-terminal end of T1 (which faces away from the membrane-bound channel segments) and the C-terminus are sufficiently close to form disulfide bonds in intact *Shaker* channels (Schulteis *et al.*, 1996). These possibilities are discussed in more detail in Chapter 6.

## ***Conclusions***

N-terminal truncation of Kv1.5 exerts significant effects on the inactivation properties of the channel that are explained primarily by accelerated inactivation from partially-activated closed states. The closed-state inactivation process revealed in certain N-terminally deleted forms of Kv1.5 appears to be insensitive to manipulations ( $\text{Cs}^+$  and extracellular  $\text{TEA}^+$ ) that inhibit inactivation of the full-length channel. A deletion scan of the Kv1.5 N-terminus, together with data from a series of chimeric channels, has identified the T1 domain as a determinant of the state-dependence of inactivation in Kv1.5.

**CHAPTER 5: N-TERMINAL INACTIVATION DOMAIN BINDING TO C-TYPE  
INACTIVATED K<sub>v</sub> CHANNELS**

## CHAPTER SUMMARY

During recovery from C-type inactivation, several types of  $K^+$  channels transiently occupy a highly  $Na^+$  permeable state, resulting in a prominent 'recovery' tail current. In this chapter, we have exploited this unique  $Na^+$  permeation property of C-type inactivated  $K^+$  channels to characterize interactions between the N-terminal inactivation domain of Kv1.4 and the C-type inactivated state of Kv1.4 and Kv1.5. The presence of the Kv1.4 inactivation domain results in a slower decay of the  $Na^+$  tail currents normally observed through C-type inactivated channels, reduction of the peak  $Na^+$  tail current, and also a delay of the peak tail current. These effects are mimicked by internal quaternary ammonium ions. These observations demonstrate that the inactivation domain and quaternary ammonium ions can interact with the pore of C-type inactivated channels, suggesting that the Kv channel inner cavity is accessible before and after the onset of C-type inactivation. We have also examined the process of N-type inactivation under conditions where C-type inactivation is removed, to compare the interaction of the N-terminal inactivation domain with open and C-type inactivated channels. In C-type deficient forms of Kv1.4 or Kv1.5 channels, the Kv1.4 inactivation ball behaves like an open channel blocker, and the resultant slowing of deactivation tail currents is considerably weaker than observed in C-type inactivated channels. We present a kinetic model that duplicates the effects of the inactivation domain on the slow  $Na^+$  tail of C-type inactivated channels. Stable binding between the inactivation domain and the C-type inactivated state results in slower current decay, and a reduction of the  $Na^+$  tail current magnitude, due to slower transition of channels through the  $Na^+$ -permeable states traversed during recovery from inactivation.

## BACKGROUND

In channels capable of N-type inactivation, such as Kv1.4, the N-terminus acts as a tethered open-state blocker, causing rapid inactivation upon opening (Choi *et al.*, 1991; Hoshi *et al.*, 1991; Demo & Yellen, 1991). The amino terminus of a single subunit is thought to enter and occlude the central cavity of the channel as an extended peptide (MacKinnon *et al.*, 1993; Zhou *et al.*, 2001a). Occlusion of the inner pore by the inactivation domain or a quaternary ammonium ion also slows channel deactivation and causes pronounced immobilization of gating charge (Bezanilla *et al.*, 1991; Choi *et al.*, 1991; Demo & Yellen, 1991; Roux *et al.*, 1998). Other Kv1 channels, including Kv1.5, lack an N-terminal inactivation domain and inactivate exclusively by a C-type inactivation mechanism (Panyi *et al.*, 1995; Fedida *et al.*, 1999). This involves a cooperative constriction of the channel pore following evacuation of K<sup>+</sup> ions from the permeation pathway, and can be modified by point mutations in the external pore (Lopez-Barneo *et al.*, 1993; Yellen *et al.*, 1994; Ogielska *et al.*, 1995). Conformational changes of the inner pore during C-type inactivation have not been well characterized, although a recent study has suggested that C-type inactivation involves a significant constriction of the inner pore (Jiang *et al.*, 2003a).

It is well known that N-type and C-type inactivation mechanisms co-exist and interact in voltage-gated K<sup>+</sup> channels (Baukrowitz & Yellen, 1995; Rasmusson *et al.*, 1995; Baukrowitz & Yellen, 1996b). Specifically, the onset of N-type inactivation significantly speeds the onset of C-type inactivation, as demonstrated both by characterization of recovery from channel inactivation (Baukrowitz & Yellen, 1995; Rasmusson *et al.*, 1995), and fluorescent visualization of conformational changes in the outer mouth of the channel (Loots & Isacoff, 1998). The dynamics of N-terminal inactivation domain binding to the open state

have been well characterized in several studies employing experimental conditions that minimize C-type inactivation (high extracellular  $K^+$ , or pore mutations). In these experiments, unbinding of the inactivation domain allows ions to permeate open channels, resulting in a 'recovery tail' current (Demo & Yellen, 1991; Ruppertsberg *et al.*, 1991; Kuo, 1997). However, C-type inactivation renders the pore of Kv channels impermeant to  $K^+$  ions, and this impedes the study of binding of the N-terminal inactivation domain or other intracellular blockers to states other than the open state.

In this study, we have exploited the unique properties of  $Na^+$  permeation of Kv channels, particularly the  $Na^+$  permeability of C-type inactivated Kv channels, and the prominent  $Na^+$  tail observed in Kv1.5 and Kv1.4 during recovery from C-type inactivation (Starkus *et al.*, 1997; Kiss *et al.*, 1999; Wang *et al.*, 2000a), to investigate the interactions of the inactivation domain and quaternary ammonium blockers with the inner pore of C-type inactivated channels. Therefore, this experiment provides a crude probe for the conformation of the inner pore of C-type inactivated channels. We demonstrate that the Kv1.4 N-terminal inactivation domain and quaternary ammonium ions exert significant effects on  $Na^+$  tail currents in both open and C-type inactivated channels. The observations demonstrate that open as well as C-type inactivated states form patent receptor sites for the N-terminal inactivation domain. This constrains models of potential conformational rearrangements of the inner pore during C-type inactivation, suggesting that the inner cavity of Kv channels remains accessible before and after the onset of C-type inactivation. We have also constructed a kinetic model that simulates the influence of the inactivation domain on the gating of C-type inactivated channels, and suggests that the inactivation domain may bind the C-type inactivated state with greater affinity than the open state.

## RESULTS

### *Multiple mechanisms of K<sup>+</sup> channel inactivation*

We have used a double pulse protocol to illustrate the inactivation and recovery properties of WT Kv1.4 channel currents in Fig. 5.1A. From a holding potential of  $-100$  mV, cells were pulsed to  $+60$  mV for 4 seconds to observe inactivation, repolarized to  $-100$  mV for a variable recovery period, and pulsed again to  $+60$  mV to determine channel availability following the recovery period. In WT Kv1.4 channels stably expressed in HEK 293 cells, we observed very rapid current decay due to N-type inactivation. Cells stably expressing an N-terminally deleted form of Kv1.4 (Kv1.4 $\Delta$ N147) were subjected to an identical protocol in Fig. 5.1B. Deletion of the N-terminus removes N-type inactivation, and reveals the far slower process of C-type inactivation.

As mentioned, N-type and C-type inactivation mechanisms co-exist in certain channel types including Kv1.4 and *Shaker* (Baukrowitz & Yellen, 1995; Rasmusson *et al.*, 1995; Rasmusson *et al.*, 1998). Specifically, the onset of N-type inactivation is thought to accelerate the rate of C-type inactivation, such that channels C-type inactivate shortly after binding of the N-terminal ball. As a result, the full-length and N-terminally truncated forms of Kv1.4 recover from inactivation at the same rate despite a dramatic difference in their respective rates of inactivation (Fig. 5.1C; Rasmusson *et al.*, 1995). We measured virtually identical time constants of recovery of  $4.7 \pm 0.2$  s (n=10) in Kv1.4, and  $4.4 \pm 0.3$  s (n=8) in Kv1.4 $\Delta$ N147 (Fig. 5.1C).

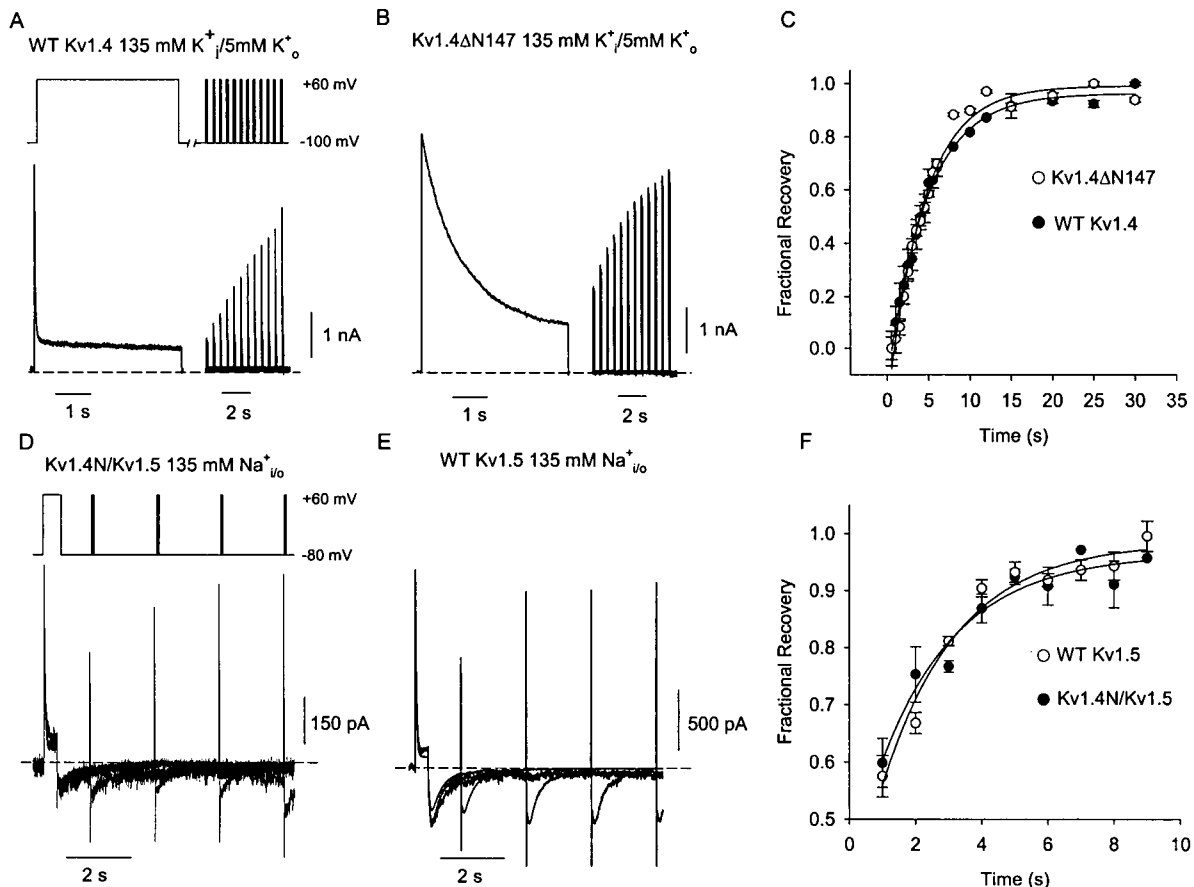


Figure 5.1. Mechanisms of N- and C-type inactivation in K<sup>+</sup> and Na<sup>+</sup> recording conditions. Currents were recorded from HEK293 cells expressing (A) WT Kv1.4 or (B) Kv1.4ΔN147 in 5 mM K<sub>o</sub><sup>+</sup>/135 mM K<sub>i</sub><sup>+</sup> recording conditions, using a double-pulse protocol. Cells were depolarized for 4 s to +60 mV to inactivate the channels, and cells were repolarized to -100 mV for a variable recovery period and briefly pulsed to +60 mV to measure recovery from inactivation. The different rates of inactivation during the 4 s depolarizing pulse reflect the presence (A) or absence (B) of N-type inactivation. The fractional recovery from inactivation is plotted against the recovery interval (C), and data points are fitted with a single exponential recovery equation. The time constants of recovery from inactivation were indistinguishable between the two constructs, measured as  $4.7 \pm 0.2$  s in WT Kv1.4 ( $n = 10$ , ●) and  $4.4 \pm 0.3$  s in Kv1.4ΔN147 ( $n = 8$ , ○). To measure inactivation and recovery in symmetrical Na<sup>+</sup> conditions, currents were recorded from HEK293 cells expressing (D) Kv1.4N/Kv1.5 chimeric channels or (E) WT Kv1.5 channels. Cells were depolarized for 400 ms to +60 mV to inactivate the channels, followed by a variable recovery period at -80 mV and a brief pulse to +60 to measure recovery from inactivation. Fractional recovery from inactivation is plotted against the recovery interval (F), and recovery time constants were measured as  $2.35 \pm 0.4$  s in Kv1.4N/Kv1.5 ( $n = 3-5$  per data point, ●) and  $2.29 \pm 0.3$  s in WT Kv1.5 ( $n = 3-8$  per data point, ○). As in K<sup>+</sup> conditions, the time course of recovery from inactivation is indistinguishable in the presence or absence of the N-terminal inactivation domain.

### ***Inactivation and recovery in Na<sup>+</sup> conditions***

We also examined the effects of the Kv1.4 inactivation domain on inactivation and recovery after substitution of all intracellular and extracellular K<sup>+</sup> ions with Na<sup>+</sup> ions. To perform these experiments, we used a chimeric construct (Kv1.4N/Kv1.5) consisting of the N-terminus of Kv1.4 fused to the channel core of Kv1.5, which transfers the rapid Kv1.4 N-type inactivation mechanism to Kv1.5. This experimental manipulation was necessary because Kv1.5 currents do not collapse when extracellular K<sup>+</sup> is completely replaced by Na<sup>+</sup> ions, whereas Kv1.4 is highly sensitive to depletion of K<sup>+</sup> ions (Pardo *et al.*, 1992; Jager *et al.*, 1998; Wang *et al.*, 2000b). From a holding potential of -80 mV, HEK 293 cells expressing either Kv1.4N/Kv1.5 or WT Kv1.5 (Fig. 5.1D, E) were pulsed to +60 mV for 400 ms, repolarized to a recovery potential of -80 mV for a variable duration, and pulsed briefly to +60 mV to determine channel availability following the recovery period. For clarity, we point out that due to the compressed time scale, the tail currents in Fig. 5.1D,E often appear to be accompanied by a rapid transient which can be mistaken for uncompensated capacity current. These rapid transients actually correspond to deactivation of open Kv1.5 channels, and are observed because the test pulses employed in Fig. 5.1D, E are too brief to completely inactivate the channels. Thus upon repolarization, there are two components to the tail current – a rapid component corresponding to deactivation of channels that remained open during the test pulse, and a slow ‘hooked’ component corresponding to channels that C-type inactivated during the test pulse. When longer test depolarizations are employed in later figures, C-type inactivation is essentially complete, and the rapid component of the tail current becomes much smaller. This biphasic nature of the Na<sup>+</sup> tail has been carefully characterized in a previous publication (Wang *et al.*, 2000a).

As in  $K^+$  conditions, the rates of recovery of outward  $Na^+$  currents in the presence or absence of the inactivation domain are very similar (Fig. 5.1F). We measured time constants of recovery of  $2.4 \pm 0.4$  s in Kv1.4N/1.5, and  $2.3 \pm 0.3$  s in WT Kv1.5. Importantly, these experimental conditions differ from those depicted in Fig. 5.1A-C because they strongly favor C-type inactivation, and therefore inactivation rates are very similar in the presence or absence of the N-terminal inactivation domain. The data in Fig. 5.1 suggest that whether in  $Na^+$  and  $K^+$  ionic conditions, the inactivation domain has little influence on the rate of recovery from inactivation, despite the dramatic effects of the inactivation ball on the time course of inactivation.

#### ***Two types of recovery tails in Kv channels***

A critically important feature of the experimental traces in Figs. 5.1D, E is the presence of inward tail currents during the recovery period, despite nearly complete inactivation of either the Kv1.4N/Kv1.5 chimera (Fig. 5.1D) or WT Kv1.5 (Fig. 5.1E). To clarify these events in more detail, Figure 5.2 distinguishes two very different types of tails that can be observed during recovery from inactivation in Kv channels. Under the physiological condition of relatively low extracellular  $K^+$ , blockade by the N-terminal inactivation domain allows evacuation of  $K^+$  from the pore, accelerating C-type inactivation, and rendering channels impermeant to  $K^+$  (Baukrowitz & Yellen, 1995). These events are illustrated in the schematic diagram accompanying Fig. 5.2A, and the sample trace illustrates that these experimental conditions preclude the observation of tail currents upon repolarization. The current understanding of unbinding of the inactivation domain has come from studies which *minimize* C-type inactivation by using high extracellular  $K^+$

concentrations or specific pore mutations (Demo & Yellen, 1991; Ruppersberg *et al.*, 1991). A representative trace of this type of experiment is depicted in Fig. 5.2B, in which currents from an HEK 293 cell transiently transfected with Kv1.4 K533V (equivalent to T449V in *Shaker*) have been recorded in the presence of 135 mM extracellular  $K^+$ . In this experiment, C-type inactivation has not occurred, and the tail currents observed during repolarization result from  $K^+$  ions passing through channels in the open state as the N-terminal inactivation domain unbinds from the pore (see Fig. 5.2B schematic). Several previous studies have demonstrated that binding of intracellular blockers, such as quaternary ammonium ions or the N-terminal inactivation domain, compete with channel closure and consequently slow tail current decay (Demo & Yellen, 1991; Choi *et al.*, 1993). Thus, the rate of tail current decay in Fig. 5.2B is influenced by the binding properties of the inactivation domain to the *open* pore.

In contrast, the traces shown in Figs. 5.1D, E, and Fig. 5.2C were collected under ionic conditions that strongly *favor* C-type inactivation, in which essentially all of the  $K^+$  ions in the recording solutions have been replaced with  $Na^+$ . In some data presented in this chapter (including Fig. 5.2C), the  $Na^+$  recording solutions have been supplemented with small amounts (up to 1 mM) of extracellular  $K^+$ . Empirically, we have found that small amounts of extracellular  $K^+$  help to maintain consistent current amplitudes from sweep to sweep (Wang *et al.*, 2000b). However, the experiments presented here have been duplicated with extracellular  $K^+$  concentrations between 0 and 1 mM.

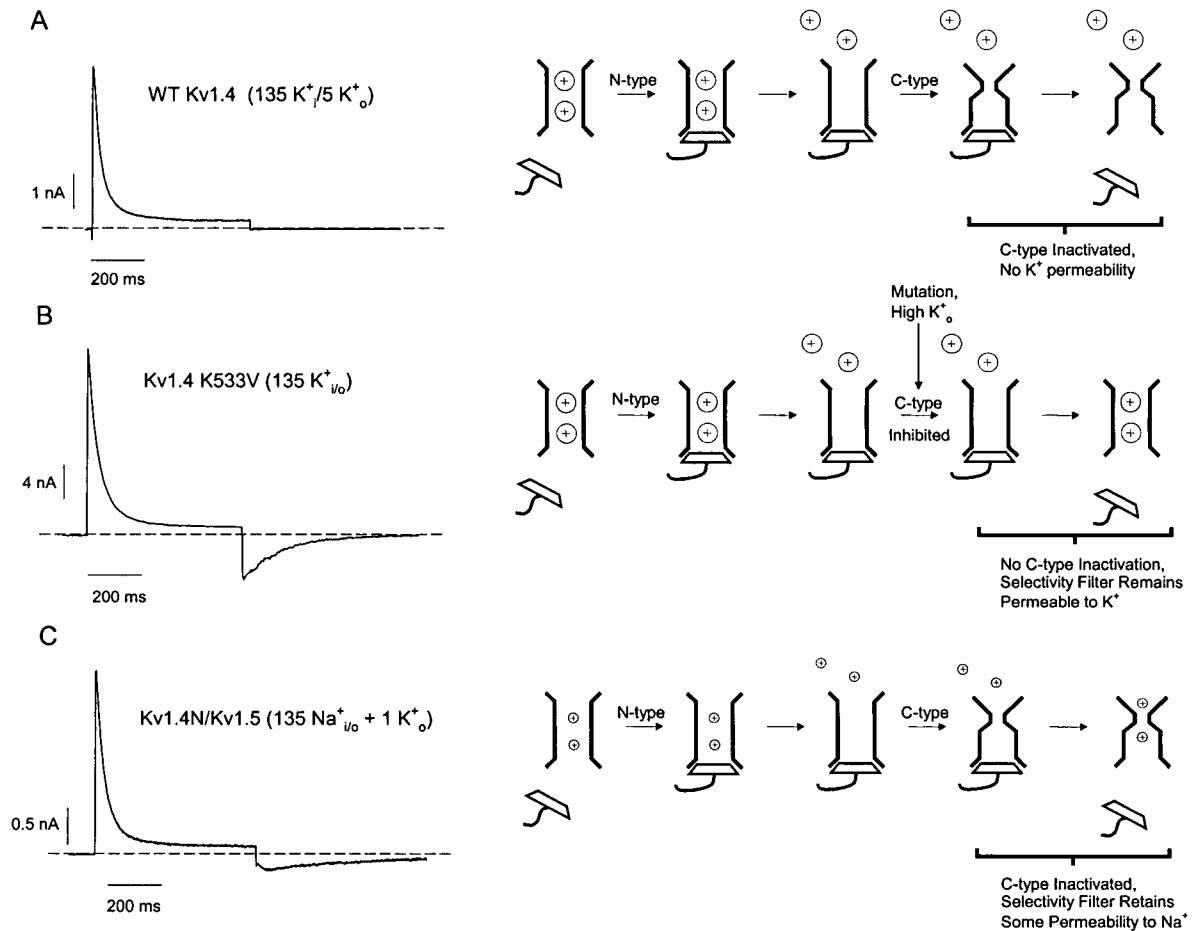


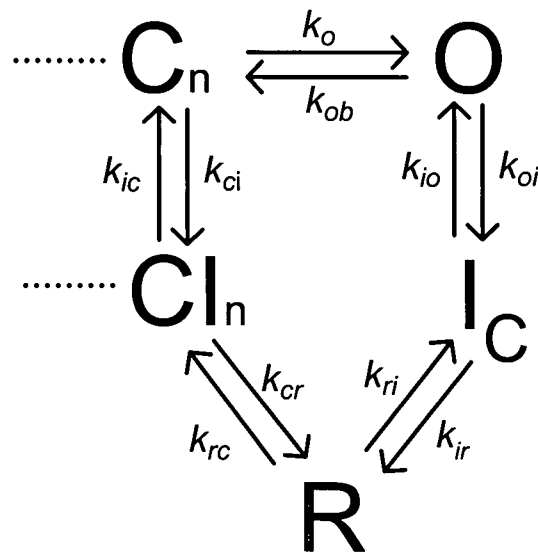
Figure 5.2. Two types of recovery tails through Kv channels. (A) Sample trace of ionic currents through WT Kv1.4 channels, in low external  $K^+$  conditions. The schematic diagram in panel (A) demonstrates that in these ionic conditions, N-type inactivation promotes C-type inactivation, which precludes the observation of ionic tail currents upon repolarization. A sample recording of recovery tails in high  $K^+$  conditions is depicted in (B). The schematic diagram in (B) shows that these experimental manipulations prevent the pore constriction of C-type inactivation, and permit the observation of  $K^+$  recovery tail currents as the inactivation domain unbinds from the open state of the channel. The schematic diagram in (C) shows that if the  $K^+$  concentration is sufficiently low, C-type inactivated Kv channels exhibit some permeability to  $Na^+$ , and this permeability increases during early stages of recovery from inactivation. This persistent  $Na^+$  permeability results in recovery tails through C-type inactivated channels, and thereby allows for the observation of the influence of the inactivation domain on the kinetics of the C-type inactivated recovery tail. A representative current trace of recovery tails through the Kv1.4N/Kv1.5 chimeric channel (exhibits both N- and C-type inactivation) is depicted in (C). In all sample traces, HEK 293 cells expressing each construct were depolarized to +60 mV for 600 ms, and repolarized to -100 mV to elicit tail currents.

Despite the strong bias towards C-type inactivation in low or zero  $K^+$  conditions, recordings with  $Na^+$  as the primary permeant ion clearly show significant inward tail currents upon repolarization (Fig. 5.1D, E; Fig. 5.2C). The schematic diagram in Figure 5.2C illustrates the origin of the recovery tails observed in  $Na^+$  recording conditions. Previous studies have shown that the conformational changes during C-type inactivation result in a change in the relative permeabilities of  $Na^+$  and  $K^+$  ions, and that C-type inactivated channels retain some permeability to  $Na^+$  (Starkus *et al.*, 1997; Kiss *et al.*, 1999; Wang *et al.*, 2000a). Critical to the present study, during recovery from inactivation, Kv1.5 channels occupy one or more states with a large  $Na^+$  permeability, allowing for the observation of significant inward  $Na^+$  tail currents (Wang *et al.*, 2000a; Wang *et al.*, 2000b). Thus, the recovery tails recorded in  $Na^+$  conditions reflect channel occupancy of  $Na^+$ -permeable states during recovery from C-type inactivation. Given the slowing effect of the N-terminal inactivation domain on the deactivation kinetics of open channels, we hypothesized that interactions between the inactivation domain and C-type inactivated channels may also influence the properties of the  $Na^+$  recovery tail current. Indeed, despite the absence of any effect of the N-terminal inactivation domain on the rate of recovery from inactivation (Fig. 5.1C, F), we noticed several dramatic effects of the inactivation domain on the  $Na^+$  recovery tail. These effects are described in the following sections, which compare the  $Na^+$  recovery tail currents of WT Kv1.5 (C-type inactivation only) and the Kv1.4N/Kv1.5 chimera (C-type and N-type inactivation).

#### ***Slowing of recovery tails by the N-terminal inactivation domain***

The representative traces in Fig. 5.3A depict  $Na^+$  tail currents recorded from WT Kv1.5 channels at voltages between  $-80$  mV and  $-120$  mV, following an 800 ms

depolarizing pulse to +60 mV. Na<sup>+</sup> tail current recordings from Kv1.5 exhibit a very prominent rising phase, followed by a slow decay taking many hundreds of milliseconds. These Na<sup>+</sup> tail currents differ dramatically from tail currents observed during deactivation of open Kv1.5 channels, which typically exhibit monoexponential decay with a time constant of a few milliseconds. In addition, the slow Na<sup>+</sup> tail currents through Kv1.5 only become apparent after the onset of C-type inactivation (Wang *et al.*, 2000a). We interpret the properties of the Na<sup>+</sup> tail currents using the state diagram shown in Scheme 5.1 (Wang *et al.*, 2000a). In this scheme, channels that undergo C-type inactivation recover primarily through a highly Na<sup>+</sup>-permeable state (R) that is distinct from the open state. During recovery from inactivation, entry of channels into the R state results in an increased Na<sup>+</sup> permeability that accounts for the prominent rising phase of the inward tail current, while deactivation of channels from the R state into closed-inactivated (CI) states accounts for the decay of the inward tail.



Scheme 5.1

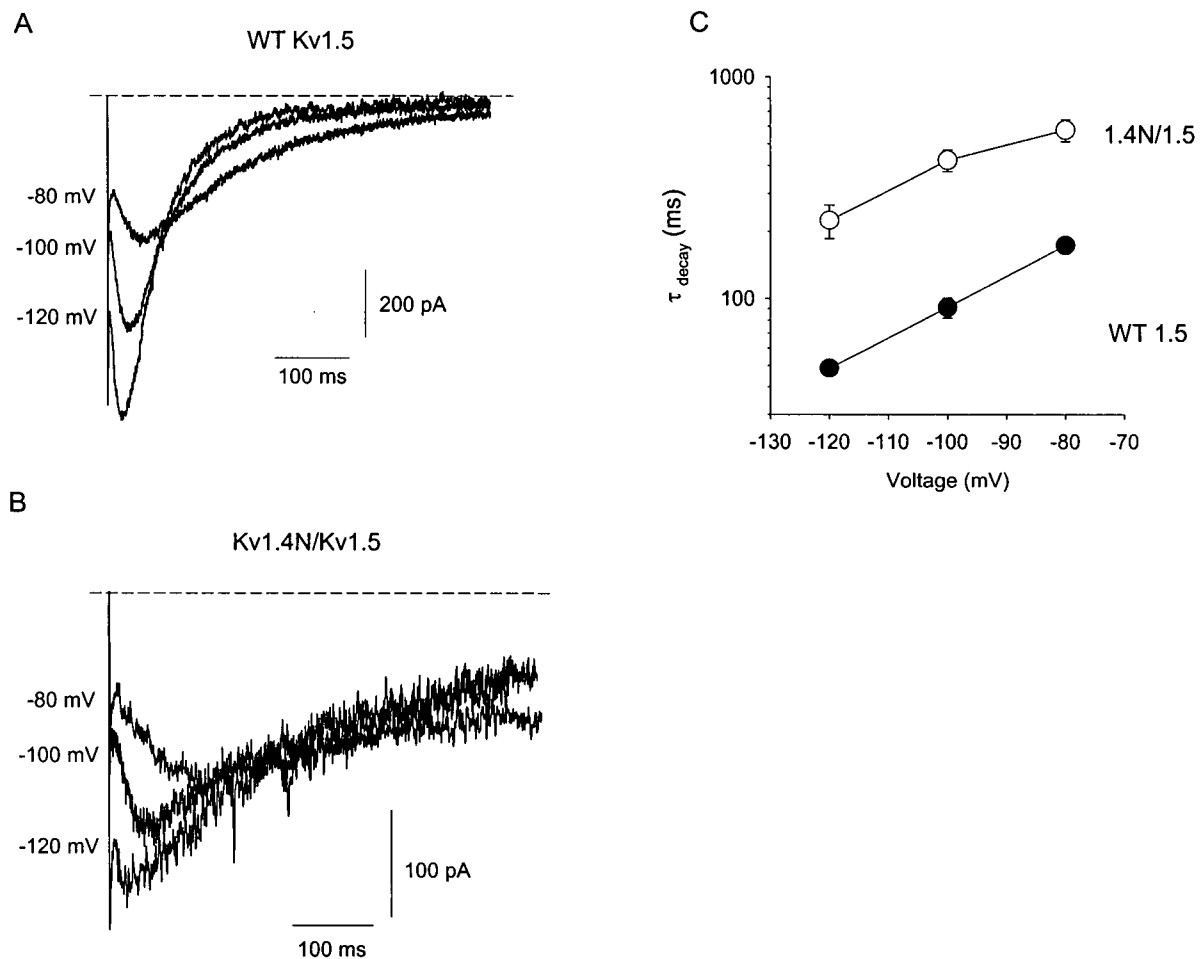


Figure 5.3. Slowing of Na<sup>+</sup> tail current decay by the Kv1.4 inactivation domain. HEK 293 cells expressing (A) WT Kv1.5 or (B) Kv1.4N/Kv1.5 were depolarized to +60 mV for 800 ms and repolarized to -80 mV, -100 mV, or -120 mV to observe Na<sup>+</sup> tail currents. Representative traces in each panel were collected from the same cell, and currents were recorded in symmetrical 135 mM Na<sup>+</sup> conditions, with 1 mM K<sup>+</sup> added to the extracellular solution. (C) The decay phase of the slow tails was fit with a single exponential function, and mean time constants (3-5 cells per point) have been compiled for Kv1.4N/Kv1.5 (○) and WT Kv1.5 channels (●). The presence of the Kv1.4 N-terminal inactivation domain results in significant slowing of the Na<sup>+</sup> tail current at all recovery potentials examined.

The first important effect of the N-terminal inactivation domain is a significant slowing of the decay time constant of the Na<sup>+</sup> tail currents. This effect is illustrated by the representative traces in Fig. 5.3B, which depict Na<sup>+</sup> tail currents recorded from the Kv1.4N/Kv1.5 chimeric channel, at recovery potentials between -80 mV and -120 mV. Na<sup>+</sup> tail current recordings from both WT Kv1.5 (Fig. 5.3A) and Kv1.4N/Kv1.5 (Fig. 5.3B) exhibit a very prominent rising phase. However, in the presence of the inactivation domain, the rate of channel closure is slowed significantly. This observation is summarized in the mean data presented in Fig. 5.3C. At all potentials examined, the rate of tail current decay was more than four-fold slower in the Kv1.4N/Kv1.5 chimera (sample tail currents in Fig. 5.3A, B have been clipped for figure preparation; longer tails were used to extract kinetic data for tail current decay). This observation suggests an interaction between the N-terminal inactivation domain and the pore of channels that have undergone C-type inactivation, suggesting that the C-type inactivated pore forms a patent receptor for the inactivation domain.

#### ***Blockade of inward Na<sup>+</sup> tails by the N-terminal inactivation domain***

A second feature of the modulation of the Na<sup>+</sup> tails by the inactivation domain is a significant reduction of the inward tail current. Data in Fig. 5.4A illustrates normalized representative current recordings from HEK 293 cells expressing either WT Kv1.5 or Kv1.4N/Kv1.5. Since Kv1.5 channels conduct a prominent outward current before inactivating, the magnitude of the inward tail current can be compared to the peak outward current to assess current blockade by the N-terminal inactivation domain. The representative traces in Figure 5.4A have been normalized to their peak outward currents, and clearly demonstrate that the peak inward tail current is smaller relative to the peak outward current

in the Kv1.4N/Kv1.5 construct. In the experiment depicted (tails were recorded at  $-100$  mV,  $135$  mM  $\text{Na}^+_{i/o}$  +  $1$  mM  $\text{K}^+_o$ ), the ratio of peak tail current/peak outward current was  $0.43 \pm 0.04$  in WT Kv1.5 ( $n = 6$ ), and  $0.12 \pm 0.01$  in Kv1.4N/Kv1.5 ( $n=5$ ) (Figure 5.4B). Thus, interaction of the channel with the N-terminal inactivation domain in Kv1.4N/Kv1.5 results in a roughly 70% reduction of the magnitude of the inward  $\text{Na}^+$  tail current. Also evident in Fig. 5.4A is a crossover of tail currents from WT Kv1.5 and Kv1.4N/Kv1.5 channels (marked with an asterisk), illustrating the slowing of tail current kinetics by the N-terminal inactivation domain described in Figure 5.3.

#### ***Delayed peak of the slow $\text{Na}^+$ tail***

As shown in the previously described current recordings, the inward  $\text{Na}^+$  recovery tail exhibits a prominent rising phase, which reflects entry into a highly  $\text{Na}^+$  permeable state (R in Scheme 5.1) during recovery from inactivation. Figure 5.4C illustrates representative tail current recordings from WT Kv1.5 and Kv1.4N/Kv1.5, enlarged to show the region of peak  $\text{Na}^+$  tail current. These recordings show that the presence of the N-terminal inactivation domain results in a delay in the time to peak of the inward tail current. This superimposition of tail currents also reinforces that unbinding of the inactivation domain is not solely responsible for the rising phase of the  $\text{Na}^+$  tail current, since the tail current is 'hooked' in both WT Kv1.5 and Kv1.4N/Kv1.5 (Fig. 5.3A). However, the presence of the N-terminal inactivation domain mildly prolongs the rising phase. In this experimental condition (tails at  $-100$  mV,  $135$  mM  $\text{Na}^+_{i/o}$  +  $1$  mM  $\text{K}^+_o$ ), the presence of the inactivation ball delays the time to peak current roughly two-fold, increasing the time to peak current from  $38 \pm 6$  ms in WT Kv1.5 ( $n=6$ ) to  $82 \pm 21$  ms ( $n=5$ ) in Kv1.4N/Kv1.5 (Figure 5.4D).

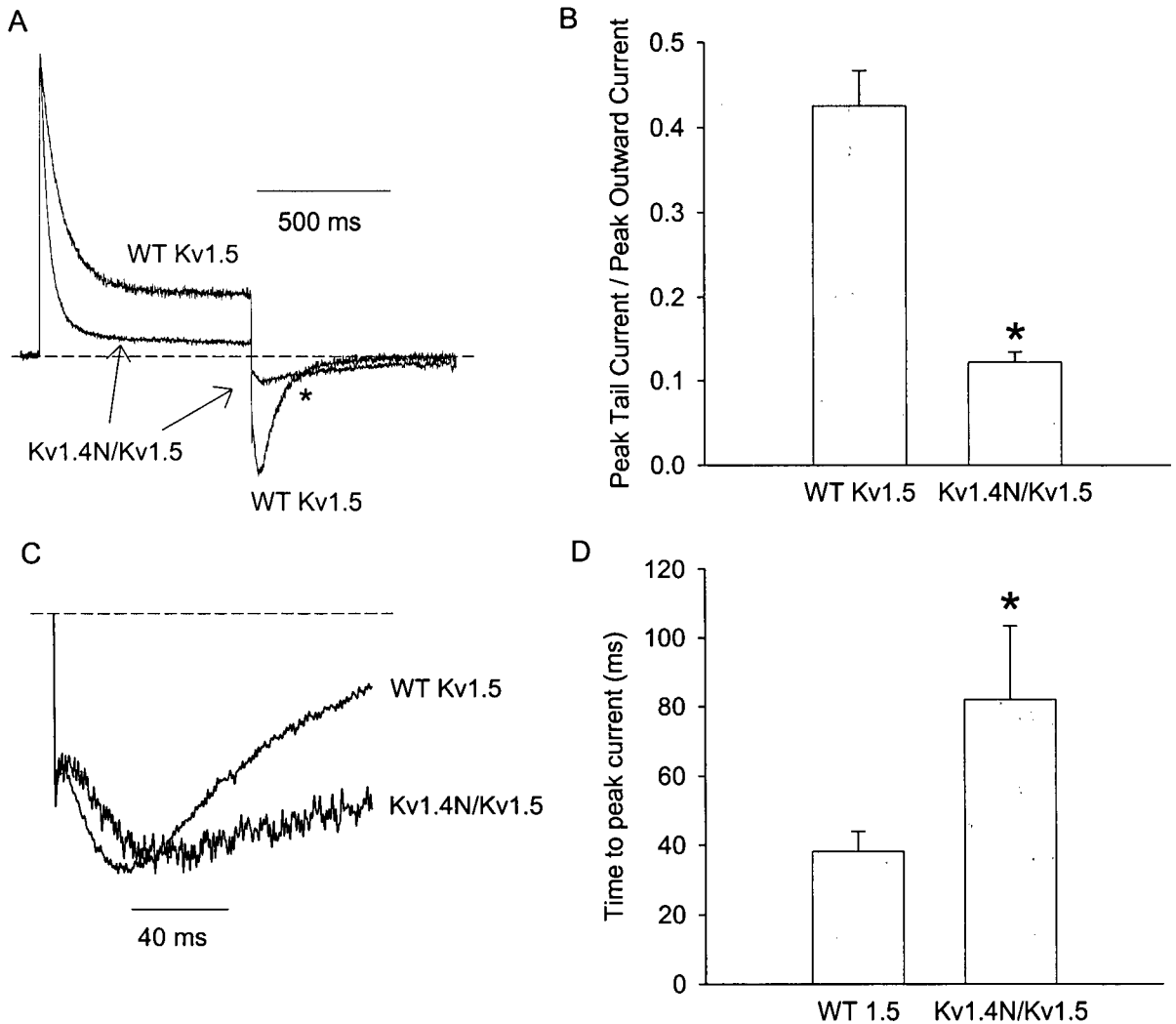


Figure 5.4. Blockade and delay of peak tail current by the Kv1.4 inactivation domain. HEK 293 cells expressing WT Kv1.5 or Kv1.4N/Kv1.5 were depolarized to +60 mV for 500 ms and repolarized to -100 mV to observe Na<sup>+</sup> tail currents. Representative traces depicted in (A) have been normalized to their respective peak outward current, to illustrate the different magnitude of the inward tail current relative to the peak outward tail current. (B) Mean data in which the magnitude of the inward tail current has been normalized to the peak outward current in cells expressing Kv1.4N/Kv1.5 or WT Kv1.5 under identical recording conditions. This reduction of the inward tail current magnitude was observed at all recovery potentials examined (-80 mV, -100 mV and -120 mV) and in the presence or absence of 1 mM extracellular K<sup>+</sup>. Tail currents depicted in (C) have been normalized to the peak tail current, and expanded around the region of the peak tail current. The Kv1.4N/Kv1.5 chimeric channel consistently exhibited a prolonged delay to the peak tail current, compared with the WT Kv1.5 channel. Panel (D) illustrates mean data of the delay to the peak inward tail current in Kv1.4N/Kv1.5 or WT Kv1.5. In panel (C) and (D), asterisks denote a statistically significant difference (Student's *t*-test,  $p < 0.05$ ).

### ***Common effects of the N-terminal inactivation domain in Kv1.5 and Kv1.4***

The features of the slow Na<sup>+</sup> tail described thus far have all been characterized in the Kv1.4N/Kv1.5 chimeric channel – this permits the convenient measurement of both outward and inward currents, and allows for normalization of tail current magnitude to peak outward current. Importantly, we have also observed similar effects of the Kv1.4 inactivation domain in the native background of the Kv1.4 channel (Fig. 5.5A). Cells expressing Kv1.4 in symmetrical Na<sup>+</sup> conditions were pulsed to +60 mV for 2 ms or 800 ms, and repolarized to -100 mV for tail current measurement – the inward Na<sup>+</sup> tails have been normalized to the peak tail current (Fig. 5.5A). Interestingly, slow Na<sup>+</sup> tail currents resembling those observed after C-type inactivation of Kv1.5 appear after even very brief depolarizations of Kv1.4 (Fig. 5.5A, 2 ms pulse). In addition, the Na<sup>+</sup> tail current kinetics observed following brief depolarizations of Kv1.4 are very similar to Na<sup>+</sup> tail currents observed in the N-terminally deleted Kv1.4ΔN147 channel (data not shown), suggesting that the 2 ms depolarizing pulse (Fig. 5.5A) is not sufficiently long to allow any appreciable binding of the N-terminal inactivation domain. Longer depolarizations (Fig. 5.5A, 800 ms pulse) that allow time for the inactivation domain to bind to the channel result in Na<sup>+</sup> tail currents qualitatively similar to those observed in the Kv1.4N/Kv1.5 chimera (compare Fig. 5.5A and Fig. 5.5B). After the onset of inactivation ball binding, the Kv1.4 Na<sup>+</sup> tail currents exhibited a slower rising phase resulting in a delayed peak tail current, and a significantly slower rate of tail current decay (Fig. 5.5A, 800 ms pulse). We could not reproducibly quantify the blockade of the inward tail current by the inactivation ball as was done for Kv1.5 (Fig. 5.4), because Kv1.4 did not conduct any outward currents to allow normalization of traces.

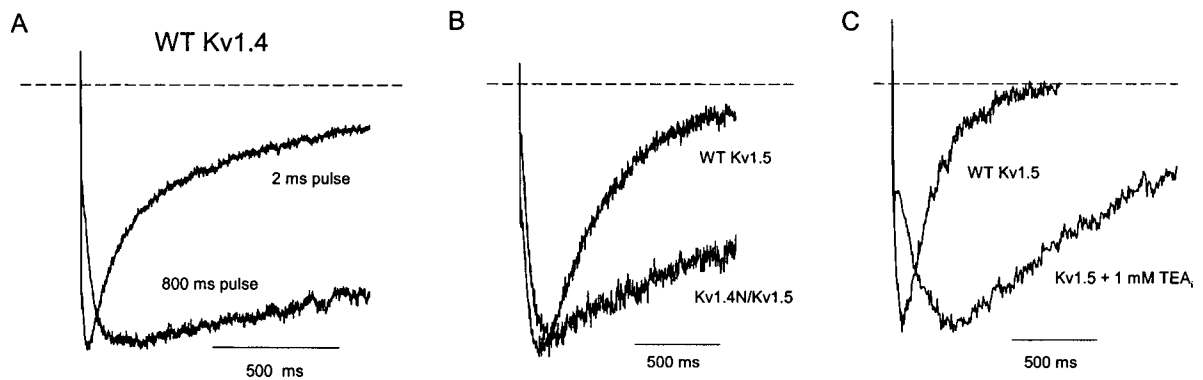


Figure 5.5. Common effects of the N-terminal inactivation domain and quaternary ammonium ions in Kv1.4 and Kv1.5. (A) Cells expressing WT Kv1.4 were pulsed to +60 mV for either 2 ms or 800 ms and repolarized to  $-100$  mV to observe tail currents. Tail currents have been expanded and normalized to the peak of the inward tail current. Slowing of tail current decay is apparent with longer depolarizations that allow binding of the inactivation domain. (B) Currents were recorded from cells expressing either WT Kv1.5 or Kv1.4N/Kv1.5 in  $135$  mM  $\text{Na}^+_{i/o}$ . Cells were depolarized to +60 mV for 400 ms, followed by repolarization to  $-100$  mV. Tail currents have been expanded and again normalized to the peak tail current to illustrate the time course of decay in the presence and absence of the inactivation ball. (C)  $\text{Na}^+$  tail currents recorded from WT Kv1.5 in the presence or absence of  $1$  mM  $\text{TEA}^+$  have been normalized to peak current to observe the slowing of tail current resulting from interactions of the C-type inactivated channel with intracellular quaternary ammonium ions.

We also emphasize an important difference between the tail currents recorded from Kv1.4N/Kv1.5 (Fig. 5.5B) and Kv1.4 (Fig. 5.5A), as binding of the N-terminal inactivation domain likely occurs in different channel states in these two constructs. Kv1.5 readily conducts outward  $\text{Na}^+$  current through the open state upon depolarization, and thus is subjected to N-type inactivation from the open state (Fig. 5.1 D, E; Fig. 5.4A). Although no extracellular  $\text{K}^+$  was present in the recordings in Fig. 5.5B or C, qualitatively similar slowing of the  $\text{Na}^+$  tail kinetics was observed with  $1$  mM extracellular  $\text{K}^+$ , as demonstrated in Figs. 5.3 and 5.4. This is an important consideration, as the inclusion of small amounts of  $\text{K}^+$  in

the extracellular solution slows C-type inactivation (Kiss & Korn, 1998; Wang *et al.*, 2000b), ensuring that the N-terminal inactivation domain binds primarily to the open state in the Kv1.4N/Kv1.5 chimera (Fig. 5.4A).

In contrast, Kv1.4 conducts minimal outward Na<sup>+</sup> current upon depolarization, because this channel is very sensitive to reductions in extracellular K<sup>+</sup> concentration (Pardo *et al.*, 1992). Also, since slow Na<sup>+</sup> tail currents appear after even very brief depolarizations of Kv1.4 (Fig. 5.5A, 2 ms pulse), it is likely that in 0 K<sup>+</sup> conditions Kv1.4 is either predominantly C-type inactivated at rest, or undergoes C-type inactivation almost instantaneously upon depolarization (Jager *et al.*, 1998). This is also consistent with the failure to observe any rapid tail currents corresponding to deactivation of open channels when Kv1.4 is examined in Na<sup>+</sup> conditions (Fig. 5.5A). In either case, the early appearance of the slow Na<sup>+</sup> tail suggests that in 0 K<sup>+</sup> conditions, Kv1.4 channels enter a C-type inactivated state before the N-terminal inactivation domain binds to the pore (Fig. 5.5A). Similar rapid development of Na<sup>+</sup> tail currents is seen in Kv1.5 when recordings are made at low pH, a condition that accelerates Kv1.5 inactivation (Zhang *et al.*, 2003b). Also, sensitivity to K<sup>+</sup> depletion in Kv1.4 is abolished by the K533V mutation (equivalent to *Shaker* T449V; Fig. 5.7), which has been identified as an important determinant of C-type inactivation in many prior studies (Busch *et al.*, 1991; Lopez-Barneo *et al.*, 1993; Baukrowitz & Yellen, 1995; Kupper *et al.*, 1995; Rasmusson *et al.*, 1998). Therefore, in Na<sup>+</sup> recording conditions, the inactivation ball likely binds primarily to the C-type inactivated state of Kv1.4. Nevertheless, the effects of the inactivation domain on the C-type inactivated Na<sup>+</sup> tail currents are similar in the Kv1.4N/Kv1.5 and Kv1.4 channels, suggesting that the N-terminal inactivation domain is able to bind to both the open and C-type inactivated states.

Inclusion of quaternary ammonium ions in the pipette filling solution mimics the slowing of the  $\text{Na}^+$  tail current decay caused by the N-terminal inactivation domain (Fig. 5.5C). The representative traces depict tail currents recorded from HEK 293 cells expressing WT Kv1.5 channels, in the presence and absence of 1 mM intracellular tetraethylammonium ( $\text{TEA}^+$ ). In the presence of intracellular  $\text{TEA}^+$ , the inward  $\text{Na}^+$  tails are slowed considerably, and the time to peak current is significantly delayed. Similar findings were observed with other quaternary ammonium blockers in both WT Kv1.5 and WT Kv1.4 channels (10  $\mu\text{M}$  tetrabutylammonium, 10  $\mu\text{M}$  tetrapentylammonium, data not shown). These data clearly illustrate an interaction between the Kv1.4 inactivation domain, or quaternary ammonium ions, and the pore of channels that have undergone C-type inactivation.

As mentioned previously, by using  $\text{Na}^+$  recording conditions in our experimental approach, we are able to infer some properties of binding of the N-terminal inactivation domain to C-type inactivated channels. With an understanding of the effects of the inactivation domain on the slow  $\text{Na}^+$  tail, we generated two further objectives. Firstly, we have used C-type inactivation-deficient channel mutants to compare N-terminal inactivation domain binding to open channels vs. channels with an intact C-type inactivation mechanism. Secondly, we have used a kinetic model and simulations to evaluate possible mechanisms underlying our observations, and explore steps involved in recovery from N- and C-type inactivation.

***C-type inactivation deficient channels exhibit incomplete N-type inactivation in  $\text{Na}^+$  recording conditions***

Previous studies have suggested that recovery from C-type inactivation remains limiting in Kv1.4 even in conditions (e.g. high extracellular  $\text{K}^+$ ) designed to minimize the

onset of C-type inactivation (Rasmusson *et al.*, 1995). To ensure separation of the effects of C-type inactivation from those of N-type inactivation, we have used mutations in Kv1.4 (K533V) and Kv1.5 (R487V) that are equivalent to the T449V mutation in *Shaker*, and have been shown to significantly reduce C-type inactivation (Lopez-Barneo *et al.*, 1993). Importantly, we have observed empirically that the slowing of inactivation by these mutations is very dramatic when recordings are performed in symmetrical Na<sup>+</sup> conditions (in the absence of any permeating K<sup>+</sup>; Wang *et al.*, 2000a). Confirming this result in Kv1.4, data in Fig. 5.6 illustrates the absence of inactivation in the Kv1.4 K533V mutant with Na<sup>+</sup> as the permeant ion. Unlike the  $\Delta$ N147 deleted (N-type inactivation removed) forms of WT Kv1.4 or Kv1.4 K533V in K<sup>+</sup> conditions, the Na<sup>+</sup> condition dramatically reduces the extent of slow inactivation, and we have reported a similar effect in the equivalent Kv1.5 R487V mutant (Fig. 5.6; Wang *et al.*, 2000a). Thus, we are confident that the Kv1.5 R487V or Kv1.4 K533V mutations provide an effective means of reducing C-type inactivation, particularly when Na<sup>+</sup> is the permeating ion. Importantly, even with prolonged depolarizations in symmetrical Na<sup>+</sup> conditions, the Kv1.5 R487V or Kv1.4 K533V  $\Delta$ N147 channels never develop the slowly decaying hooked Na<sup>+</sup> tails associated with the onset of C-type inactivation (Starkus *et al.*, 1997; Wang *et al.*, 2000a). This feature of the tail currents provides a valuable experimental index of the state of the pore: the absence of a slow Na<sup>+</sup> tail current confirms that channels have not undergone C-type inactivation. We have used these C-type inactivation deficient systems to examine the influence of the N-terminal inactivation domain on the open pore, in ionic conditions identical to those used earlier to characterize ball binding to C-type inactivated channels.

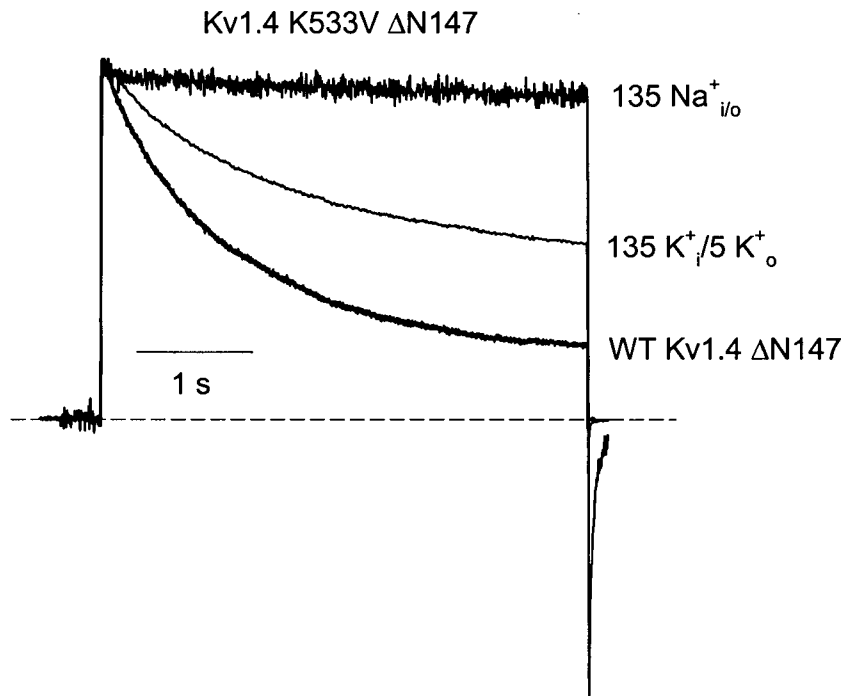


Figure 5.6. A Kv1.4 C-type inactivation deficient channel mutant. C-type inactivation was removed from Kv1.4 with the K533V mutation. HEK 293 cells expressing Kv1.4 K533V  $\Delta$ N147 were depolarized for 4 s at +60 mV, from a holding potential of  $-100$  mV, in the ionic conditions indicated in the Figure. In  $135\text{K}^+_{i}/5\text{K}^+_{o}$ , the K533V mutation attenuates the decay of outward current. In  $135\text{Na}^+_{i/o}$ , the K533V mutation essentially abolishes any decay of outward current. Representative currents exhibiting C-type inactivation in WT Kv1.4 $\Delta$ N147 ( $135\text{K}^+_{i}/5\text{K}^+_{o}$ ) are also shown for reference.

When the full-length Kv1.4 K533V channel (with an intact N-terminal inactivation domain) was depolarized in symmetrical  $\text{Na}^+$  (Fig. 5.7A), a rapidly decaying current was observed, confirming the persistence of N-type inactivation. However, we made the surprising observation that the N-type inactivation process left a much larger steady-state current than is usually observed when the same channel is studied in  $\text{K}^+$  conditions (compare Figs. 5.7A and 5.2B, C). C-type inactivation deficient Kv1.4 K533V channels appeared to

inactivate by only  $71 \pm 2\%$  ( $n=6$ ) when  $\text{Na}^+$  was the permeant ion, compared with the  $>90\%$  inactivation routinely observed in WT Kv1.4 channels or K533V channels permeating  $\text{K}^+$  (Fig. 5.2A, B). This effect was slightly more pronounced in a chimeric channel consisting of the N-terminus of Kv1.4 fused to the Kv1.5 R487V channel, which exhibited only  $63 \pm 2\%$  ( $n=6$ ) inactivation in this experiment (Fig. 5.7B).

The Kv1.4 K533V or Kv1.5 R487V mutations did not markedly affect the rate of current decay due to N-type inactivation in  $\text{Na}^+$  conditions. This observation is consistent with previous reports, which have demonstrated insignificant effects of these and similar mutations on the rate of N-type inactivation by the Kv1.4 inactivation domain (Baukrowitz & Yellen, 1995; Rasmusson *et al.*, 1995). However, others have not reported the weaker steady-state block that we observe here, suggesting that it may be a unique feature of the  $\text{Na}^+$  recording conditions used in our experiments (Figs. 5.7A, B). One intriguing explanation is that the R487V or K533V mutations do not completely abolish C-type inactivation in  $\text{K}^+$  conditions, and that a residual inactivation process contributes to the enhanced steady-state block seen in  $\text{K}^+$  conditions. In support of this, Fig. 5.6 clearly demonstrates that the Kv1.4 K533V mutant inactivates markedly more slowly in  $\text{Na}^+$  conditions compared with  $\text{K}^+$  conditions, and similar results are observed in Kv1.5 (Wang *et al.*, 2000a). In addition, the R487V mutation of Kv1.5 and even the T449V mutant of *Shaker* both exhibit an appreciable degree of slow inactivation in  $\text{K}^+$  conditions. As shown here for Kv1.4 K533V  $\Delta\text{N147}$ , this current decay is essentially abolished when  $\text{Na}^+$  is substituted for  $\text{K}^+$  (Fig. 5.6; Wang *et al.*, 2000a; Starkus *et al.*, 2003). A second possible explanation for this observation is an ion-dependence of the affinity between the N-terminal inactivation domain and the channel, possibly arising from slight conformational changes of the open state when  $\text{K}^+$  is replaced

with  $\text{Na}^+$  is the primary permeant ion. Importantly, since the Kv1.4 K533V (compare Fig. 5.2A and 5.2B) or Kv1.4 K533Y mutations (Rasmusson *et al.*, 1995) have no apparent effect on the affinity for the N-terminal inactivation domain when  $\text{K}^+$  is the permeant ion, it seems likely that our observation of weaker steady-state block is due to the altered ionic conditions, and not the outer pore mutation. However, our experiments have not excluded the possibility of a unique interaction between the  $\text{Na}^+$  recording conditions and the R487V or K533V mutation.

N-type inactivation in the C-type inactivation deficient channels also resulted in slowing of the deactivation tails. In the Kv1.4 K533V channel, the time constant of deactivation was  $42.1 \pm 6.7$  ms following a brief depolarization (10 ms in Fig. 5.7A), but was slowed to  $65.5 \pm 6.1$  ms following the onset of N-type inactivation. Similarly in the Kv1.4N/Kv1.5 R487V chimeric channel, time constants of deactivation were  $8.4 \pm 0.8$  ms after a brief depolarization and  $28.7 \pm 1.7$  ms following the onset of N-type inactivation (Fig. 5.7B). This slowing of deactivation is consistent with unbinding of the inactivation domain limiting the rate of channel closure (Demo & Yellen, 1991). Furthermore, the deactivation tail currents following N-type inactivation exhibit mild biphasic kinetics in Kv1.4 K533V, with a very brief rising phase preceding tail current decay (Fig. 5.7A inset, Fig. 5.7C). This feature resembles the 'hooked tails' previously observed due to unbinding of the N-terminal inactivation domain during *Shaker* deactivation in high  $\text{K}^+$  conditions (Demo & Yellen, 1991). Tail currents recorded from the Kv1.4N/Kv1.5 R487V chimeric channel exhibited no significant 'hook' or biphasic kinetics, but were clearly slowed by the onset of N-type inactivation (Fig. 5.7B, inset)

In the K533V mutant channel, C-type inactivation appears to be essentially eliminated in the symmetrical Na<sup>+</sup> condition (Fig. 5.6). Consequently, the rate of recovery from N-type inactivation in this condition should be very similar to the rate of tail current relaxation, as both should be limited by the rate of unbinding of the N-terminal inactivation domain. We have examined this relationship in the double-pulse experiment in Fig. 5.7C, in which cells expressing Kv1.4 K533V channels were depolarized to +60 mV for 600 ms followed by a variable recovery period and a test pulse to +60 mV to observe the extent of recovery from inactivation (eg. unbinding of the inactivation domain from the pore). In four cells tested, we confirmed this idea by showing that peak current recovery of Kv1.4 K533V occurred with a time constant of  $53.5 \pm 5.5$  ms (Fig. 5.7D), while tail current recovery following N-type inactivation occurred with a time constant of  $62.3 \pm 3.1$  ms. Similar correlation between the rates of deactivation and recovery from inactivation were also observed in the Kv1.4N/Kv1.5 R487V chimeric channel. It is noteworthy that we also consistently observed a slow component to recovery in these channels, although we are unsure of the mechanism underlying this process (Fig. 5.7D). We have included only a fit of the rapid component of recovery, because this represents the largest component of recovery, and mirrors the kinetics of tail current decay in both Kv1.5 K533V and Kv1.4N/Kv1.5 R487V. This analysis of the Kv1.4 K533V and Kv1.5 R487V channels provides a benchmark with which to compare the effects of the inactivation domain on the slow Na<sup>+</sup> tail currents of Kv1.4 and Kv1.5.

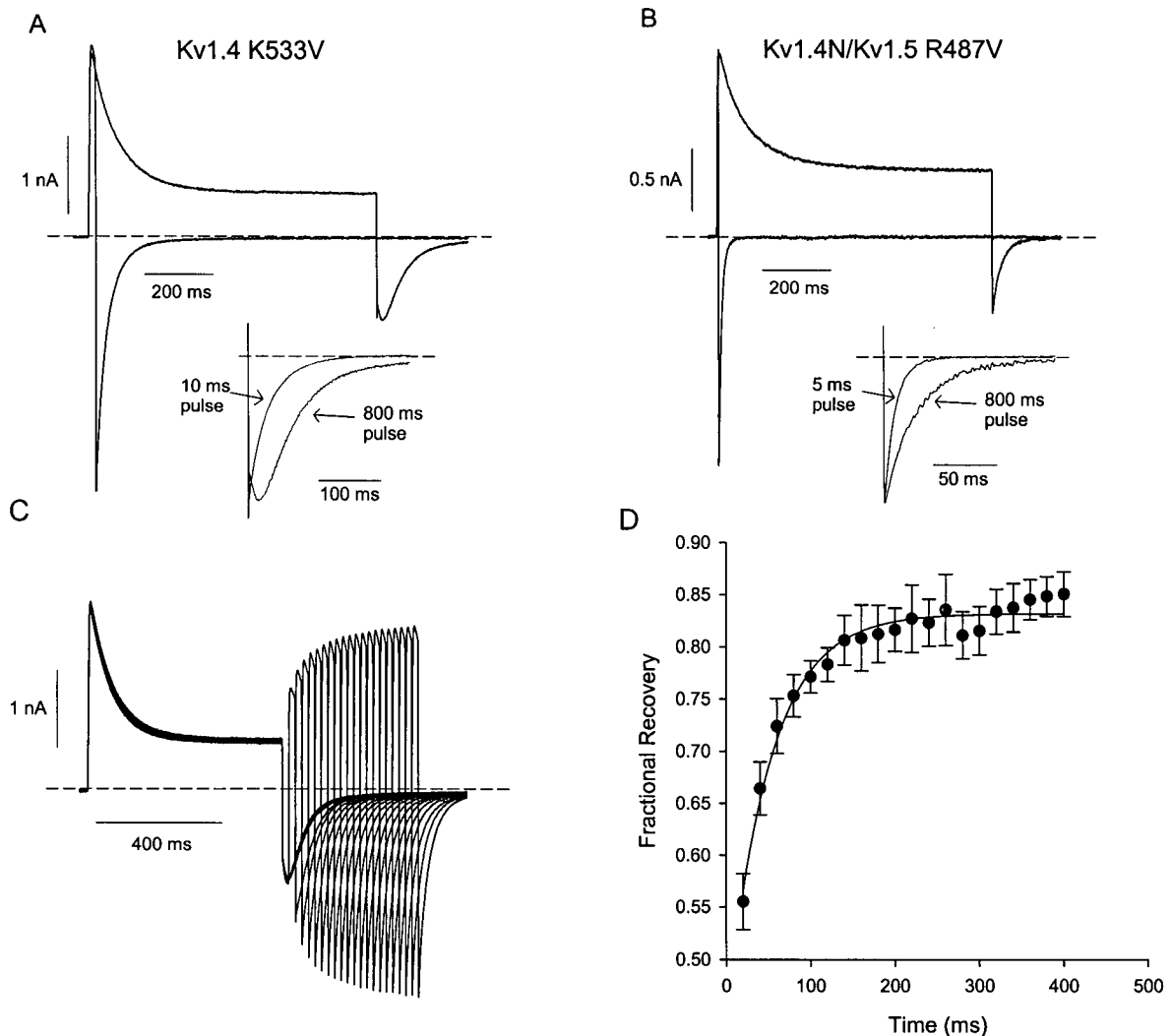


Figure 5.7. N-type inactivation in C-type inactivation-deficient Kv channels. Currents were recorded from cells expressing (A) Kv1.4 K533V or (B) a chimeric construct of Kv1.5 R487V and the N-terminus of Kv1.4, in symmetrical  $\text{Na}^+$  recording conditions. Cells were depolarized to +60 mV from a holding potential of -100 mV for a brief pulse (5-10 ms) or 800 ms, and repolarized to -100 mV. Current tracings from the short and long protocols are overlaid in each panel. The insets in (A) and (B) depict normalized tail currents after the brief and long depolarizing pulses, illustrating the slowing of tail currents after binding of the inactivation domain. (C) Recovery from N-type inactivation in a C-type deficient channel (Kv1.4 K533V) was measured with a double pulse protocol, consisting of a 600 ms depolarizing prepulse to +60 mV, followed by a variable recovery period at -100 mV and a brief test pulse to +60 mV. Experiments were conducted in symmetrical  $\text{Na}^+$  recording conditions. (D) The envelope of peak test pulse currents in (C) was fit with a single exponential equation yielding a mean time constant of  $53.5 \pm 5.5$  ms ( $n=4$ ). Tail current decay in this experiment had a mean time constant of  $62.3 \pm 3.1$  ms ( $n=4$ ).

### ***Summary and model of the slow Na<sup>+</sup> tail***

The data presented thus far illustrates three major effects of the Kv1.4 inactivation domain on the slow Na<sup>+</sup> tails of Kv1.4 or Kv1.5: a dramatic slowing of tail current decay, a blockade of the peak inward tail current, and a slowing of the rising phase of the Na<sup>+</sup> tail current. These experiments clearly suggest an interaction between the N-terminal inactivation domain and the C-type inactivated pore, and qualitatively resemble the effects of the inactivation domain on channel deactivation from the open state. We have used our characterization of inactivation ball binding to the open and C-type inactivated channel states to construct a kinetic model and to investigate the steps involved in recovery from inactivation.

Our kinetic model is based upon previously published versions describing the pathway of recovery from inactivation of Kv1.5, shown in Scheme 5.1 (Wang *et al.*, 2000a; Zhang *et al.*, 2003b). Although likely an oversimplification of the steps involved in inactivation and recovery, the model in Figure 5.8A reasonably duplicates our experimental results, and illustrates the most important conclusion of our modeling, which is that binding of the N-terminal inactivation domain to the C-type state is required to explain its effects on the C-type inactivated Na<sup>+</sup> tail current. In Fig. 5.8A, we have added two additional states to Scheme 5.1: an N-type inactivated state ( $I_N$ ), and a state which has undergone both C-type and N-type inactivation ( $I_{N,C}$ ). The state diagram in Fig. 5.8A explains the slower tail current decay (Fig. 5.5B, C) and the delayed time to peak current (Fig. 5.4C, D) as follows. Stable inactivation domain binding to the  $I_C$  state results in slow exit of channels from the  $I_{N,C}$  state to the  $I_C$  state, and consequently slower transit of channels through the highly Na<sup>+</sup>-permeable R state. This slower transit of channels through the R state also accounts for the observed

reduction of the peak inward  $\text{Na}^+$  tail current (Fig. 5.4A, B), because there is a lower occupancy of the R state throughout recovery.

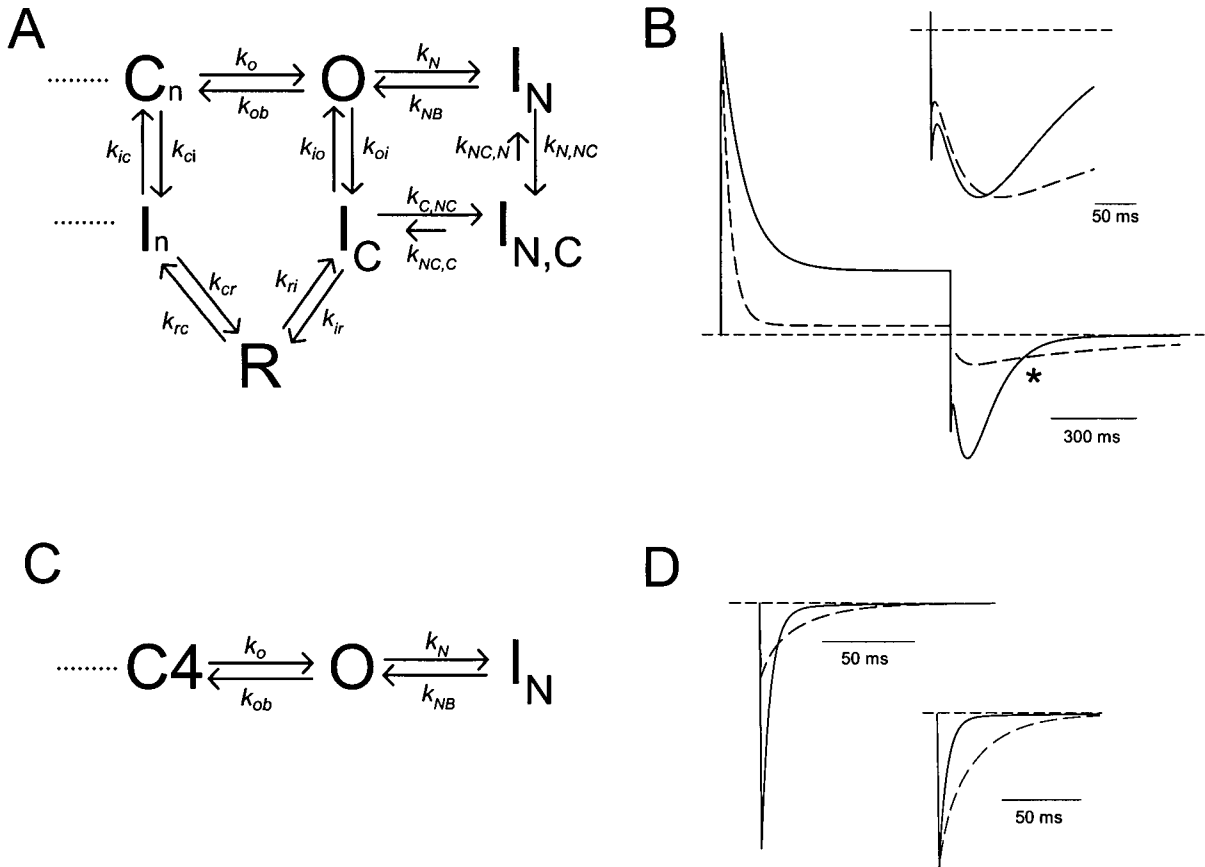


Figure 5.8. Kinetic model of  $\text{Na}^+$  permeation through N- and C-type inactivated  $\text{K}^+$  channels. (A) State diagram illustrating a mechanism for the apparent blockade and slowing of  $\text{Na}^+$  tail currents by N-type inactivation. Rates for N-type and C-type inactivation were governed by the voltage-independent rate constants (in  $\text{ms}^{-1}$ )  $k_N = 0.025$ ,  $k_{NB} = 0.0125$ ,  $k_{N,NC} = 0.1$ ,  $k_{NC,N} = 0.006$ ,  $k_{io} = 0.0025$ ,  $k_{oi} = 0.01$ ,  $k_{C,NC} = 0.0167$ ,  $k_{NC,C} = 0.002$ ,  $k_{ic} = 0.000055$ ,  $k_{ci} = 0.00008$ . All other rates depicted were governed by exponential functions of voltage. Rate constants at 0 mV were (in  $\text{ms}^{-1}$ )  $k_o = 0.31$ ,  $k_{ob} = 0.011$ ,  $k_{ir} = 0.001$ ,  $k_{ri} = 0.0072$ ,  $k_{rc} = 0.017$ ,  $k_{cr} = 0.185$ , and equivalent valences were  $z_o = 0.60$ ,  $z_{ob} = -0.70$ ,  $z_{ir} = -0.65$ ,  $z_{ri} = 0.55$ ,  $z_{rc} = -0.05$ ,  $z_{cr} = 0.05$ . Rates in the activation pathway (not shown in this diagram) were the same as in our previous models of Kv1.5 (Kurata *et al.*, 2001; Zhang *et al.*, 2003b; see Fig. 3.10). (B) Simulations of WT Kv1.5 (solid trace) and Kv1.4N/Kv1.5 (dashed trace) currents recorded in 135 mM  $\text{Na}^+_{i/o}$  + 1 mM  $\text{K}^+_o$ . Currents were simulated using a 800 ms depolarization to +60 mV, followed by a 800 ms repolarization to -100 mV, reproducing the experiment depicted in Fig. 5.4A. To simulate Kv1.4N/Kv1.5, all the rates described in panel (A) were used. To

simulate Kv1.5, transitions to and from N-type inactivated states ( $k_N$ ,  $k_{NB}$ ,  $k_{C,NC}$ ,  $k_{NC,C}$ ) were removed from the model. (Inset) The tail currents in panel (B) have been expanded and normalized to peak current, to illustrate the prolonged delay and slower decay of the simulated Na<sup>+</sup> tail caused by N-type inactivation. (C) All transitions to and from the C-type inactivated states have been removed from the state diagram in (A), to simulate currents through C-type inactivation deficient channels (eg. Kv1.4N/Kv1.5 R487V). (D) Tail currents at -100 mV simulated using the state diagram in (C). Solid traces were simulated with an initial condition of 100% of channels in the open state, while the dashed traces were simulated with an initial condition of 30% of channels open, and 70% of channels in the N-type inactivated state. Rate constants were (in ms<sup>-1</sup>)  $k_N = 0.025$ ,  $k_{NB} = 0.05$ ,  $k_o = 0.31$ , and  $k_{ob} = 0.011$ , with associated valences of  $z_o = 0.60$ , and  $z_{ob} = -0.70$ . (Inset) The tail currents in (D) have been normalized to peak current, to illustrate slowing of tail currents after the onset of N-type inactivation.

We have used this kinetic scheme to generate the simulations presented in Fig. 5.8B, which duplicate the experimental features of the slow Na<sup>+</sup> tail current characterized in Figs. 5.3-5.4. Currents depicted by the solid trace represent simulations of WT Kv1.5, in the absence of N-type inactivation, whereas currents depicted by the dashed traces represent simulations of the Kv1.4N/Kv1.5 chimera (N-type and C-type inactivation). These data demonstrate the reduction of Na<sup>+</sup> tail current magnitude resulting from slow unbinding of the inactivation ball from the C-type inactivated state, and also exhibit the tail current crossover observed in Fig. 5.4A. Tail currents from both simulations have been expanded and normalized in the inset to Fig. 5.8B, showing that the model also duplicates the considerable slowing of Na<sup>+</sup> tail current decay resulting from interactions between N- and C-type inactivation (compare with Fig. 5.3 and Fig. 5.5), and the slightly prolonged time to peak of the Na<sup>+</sup> tail current (Fig. 5.4C).

Many of the rate constants describing ball binding/unbinding are constrained by experimental data. The rates  $k_N$  and  $k_{NB}$  were estimated based on the inactivation kinetics of ball binding in C-type inactivation deficient channels (Fig. 5.7A, D). The rates  $k_{io}$  and  $k_{oi}$  were determined based on the rates of C-type inactivation in WT Kv1.5 (Fig. 5.4A). We

have also observed that the time course of the onset of deceleration of the inward  $\text{Na}^+$  tail is slow ( $\tau \sim 60\text{-}100$  ms) in Kv1.4 (which undergoes C-type inactivation extremely rapidly in the absence of  $\text{K}^+$ ), suggesting that binding of the inactivation ball to the C-type inactivated state is slightly slower than binding to the open state (data not shown). This observation allowed us to roughly estimate the rate  $k_{C,NC}$ , which describes the rate of ball binding to the C-type inactivated channel. However, it should be noted that the absolute value of the  $k_{C,NC}$  rate has little bearing on the altered kinetics or apparent blockade of  $\text{Na}^+$  tails by the N-terminal inactivation domain. Rather, the ratio of the rates  $k_{C,NC}$  and  $k_{NC,C}$  predominantly determines the extent of blockade and tail slowing (all rate constants and valencies used for simulations are summarized in the legend to Fig. 5.8).

#### ***Simulation of tail currents in C-type deficient channels***

Fig. 5.8C shows a state diagram in which the transitions to the C-type inactivated state have been removed. Given the absence of any current decay in  $\text{Na}^+$  recordings of Kv1.5 R487V or Kv1.4 K533V  $\Delta\text{N147}$  channels (Fig. 5.6; Wang *et al.*, 2000a), this is likely an adequate description of gating for the C-type deficient channels. In this model, binding of the N-terminal inactivation domain competes with closure of the activation gate, and therefore slows deactivation tail currents, analogous to the effects of intracellular quaternary ammonium ions and the N-terminal inactivation domain in *Shaker* (Demo & Yellen, 1991; Choi *et al.*, 1993). Figure 5.8D illustrates tail current decay simulated at  $-100$  mV in two different initial conditions. The solid trace represents the time course of tail current decay with an initial condition of all channels occupying the open state, to approximate the short pulses in Fig. 5.7A, B, where channels have opened but not substantially inactivated. The dashed traces represent the time course of tail current decay with an initial condition of 30%

of channels occupying the open state, and 70% occupying the N-type inactivated state, to approximate the conditions following 800 ms pulses to +60 mV (Fig. 5.7A, B). The onset of N-type inactivation results in slower tail current decay, because unbinding of the N-terminal inactivation domain is required before channels can close (Fig. 5.8C; Demo & Yellen, 1991; Choi *et al.*, 1993).

In order to reasonably simulate the extent of tail current deceleration observed experimentally in the Kv1.4N/Kv1.5 R487V chimera (Fig. 5.7B), this model required acceleration of the unbinding rate of the inactivation domain ( $k_{NB}$ ) compared to the value required to accurately simulate inactivation of outward currents. This arises from an effective voltage-dependence of unbinding of the N-terminal inactivation domain, likely caused by a ‘knock-off’ effect of inward ionic currents, as previously described by Demo and Yellen (1991), among others. To reproduce the extent of N-type inactivation of outward currents (Fig. 5.8B), the unbinding rate of the N-terminal inactivation domain ( $k_{NB}$ ) was set to be 50% of the binding rate ( $k_N$ ). However, to simulate the tail current decay in Fig. 5.8D, the unbinding rate ( $k_{NB}$ ) was set to be double the binding rate ( $k_N$ ). In contrast, our simulation of the Na<sup>+</sup> tail currents through channels with intact N- and C-type inactivation (Kv1.4N/Kv1.5) were most representative of the data with an unbinding rate from the C-type inactivated state ( $k_{NC,C}$ , Fig. 5.8A) of four- to eight-fold smaller than the binding rate ( $k_{C,NC}$ ) to reasonably simulate the deceleration and blockade of the C-type inactivated Na<sup>+</sup> recovery tail current.

This approach allows for some preliminary considerations of the affinity between the inactivation domain and the pore of open *vs.* C-type inactivated channels. As mentioned above, simulations suggest that binding of the inactivation domain to the C-type inactivated pore in Kv1.5 exhibits a binding rate ( $k_{C,NC}$ ) four-fold to eight-fold larger than the unbinding

rate. It is probably most appropriate and conservative to compare these values to the rate constants estimated for binding of the inactivation domain to the open channel (eg. Kv1.4N/Kv1.5 R487V) at depolarized voltages (Fig. 5.8B, +60 mV), rather than the tail currents simulated above (Fig. 5.8D, at -100 mV). This is because at depolarized voltages, there is little or no influence of cations permeating in the inward direction (ie. no 'knock-off' effect), so the observed off-rate of the inactivation domain is minimized (Demo & Yellen, 1991; Kuo, 1997). Therefore, this situation probably more closely reflects the influence of cations on unbinding of the inactivation domain from the C-type inactivated channel, because the permeability of the Kv1.5 C-type inactivated state to Na<sup>+</sup> is lower than in the open state (Wang *et al.*, 2000a; Wang *et al.*, 2000b). In open, C-type inactivation deficient channels permeating Na<sup>+</sup> (Kv1.4N/Kv1.5 R487V), the binding constant ( $k_N$ ) of the inactivation domain is roughly double the unbinding constant ( $k_{NB}$ ) at +60 mV, to reproduce the 65-70% steady-state block observed in these conditions (Fig. 5.7A, B and Fig 5.8, legend). Although quantitative estimates of affinity are not possible (because the effective concentration of the N-terminal inactivation domain at the intracellular mouth of the pore is unknown), ratios of these binding and unbinding rates can be used to estimate relative changes in affinity between the N-terminal inactivation domain and the inner pore of the channel. Based on the rate constants just discussed, the model predicts that the onset of C-type inactivation in Kv1.4N/Kv1.5 slightly enhances the affinity between the inactivation domain and the pore by two- to four-fold.

### ***Interactions of the N-terminal inactivation domain with the R state***

To investigate the interactions of the N-terminal inactivation domain with the R state (Scheme 5.1) during channel recovery, we subjected channels to the double pulse protocol shown in Fig. 5.9. Cells expressing WT Kv1.5 or Kv1.4N/Kv1.5 were pulsed to +60 mV for 800 ms and repolarized to -100 mV for 100 ms, followed by a second depolarization to +60 mV. In WT Kv1.5, the second depolarizing pulse elicits an outward current that decays much more slowly than the first (Fig. 5.9A; Wang *et al.*, 2000a). We have previously suggested that this current decay is likely governed by the transition from the R state to the C-type inactivated state (Scheme 5.1; Wang *et al.*, 2000). In the Kv1.4N/Kv1.5 chimera, with intact N-type inactivation, the current decay in the second pulse is more rapid (Fig. 5.9A). To illustrate this observation more clearly, currents from the second depolarizing pulse have been normalized and magnified in Fig. 5.9C. These data demonstrate that the presence of the N-terminal inactivation domain increases the decay rate of currents through the R state, suggesting that the inactivation domain can bind to the R state and block currents through this state.

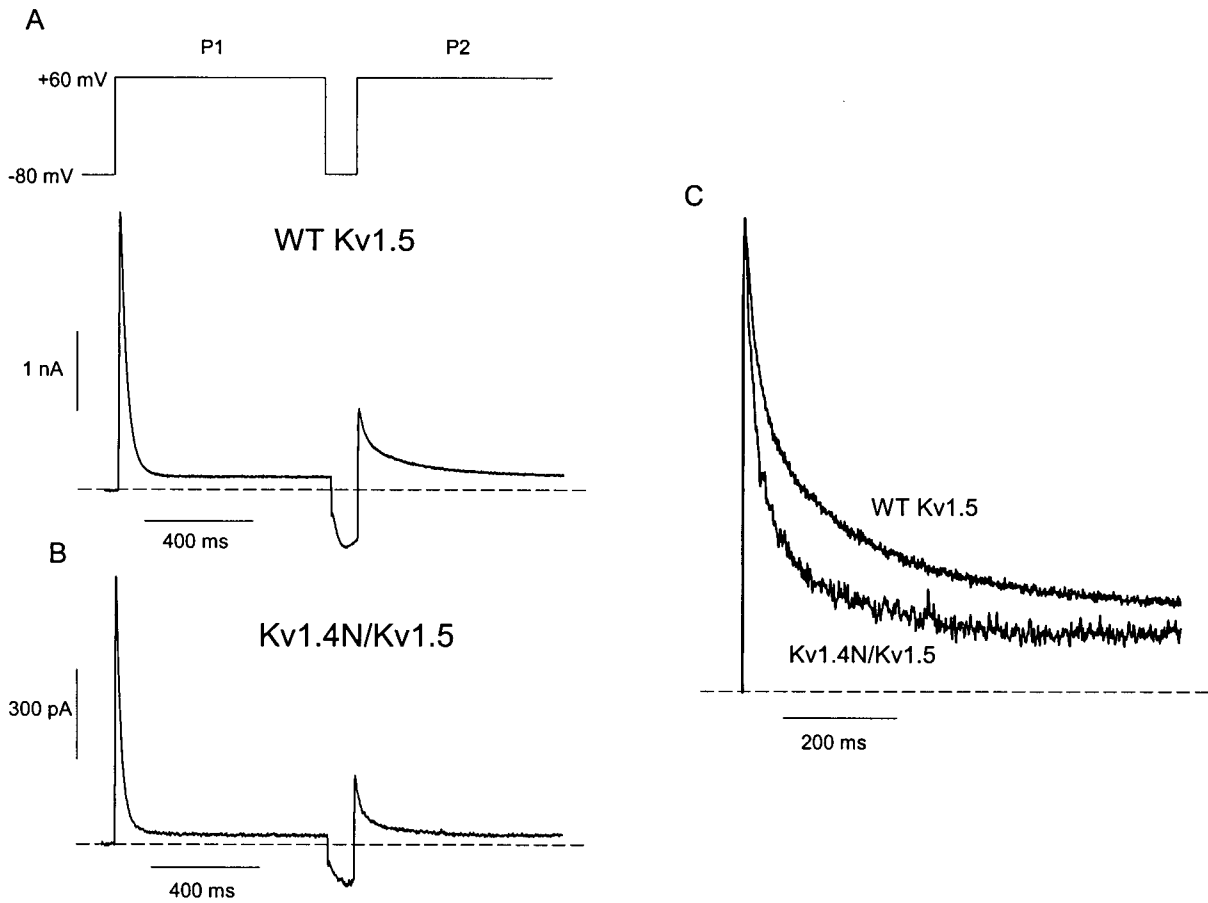
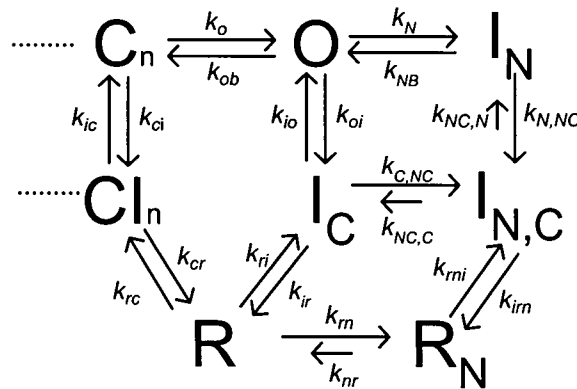


Figure 5.9. Interactions between the R state and the N-terminal inactivation domain. Cells were subjected to a double pulse protocol to elicit currents through the R state. From a holding potential of  $-80$  mV, cells expressing (A) WT Kv1.5 or (B) Kv1.4N/Kv1.5 were pulsed to  $+60$  mV for 800 ms (P1) and repolarized to  $-100$  mV for 100 ms, followed by a second depolarization to  $+60$  mV (P2). (C) The currents elicited during the second depolarizing pulse (P2) have been normalized and magnified, to illustrate the accelerated current decay in Kv1.4N/Kv1.5. Recordings were made in  $135 \text{ Na}^+_{i/o}$ .

The experimental data in Fig. 5.9 suggest a more complete version of the model used in our simulations (Fig. 5.8). This is depicted in Scheme 5.2, in which the N-terminal inactivation domain is also permitted to bind the R state during recovery from inactivation. This scheme may be more correct than the scheme in Fig. 5.8A, for two reasons. Firstly, the activation gates are very likely open in the R state, otherwise ions would be occluded from the permeation pathway, and no  $\text{Na}^+$  tail would be apparent. The open activation gate leaves the inner vestibule accessible, exposing the binding site for the N-terminal inactivation domain. Secondly, Scheme 5.2 might account for the results of the double pulse experiment in Fig. 5.9, which suggests an interaction between the inactivation domain and the R state.

Scheme 5.2



## DISCUSSION

In the current study, we have examined binding of the Kv1.4 N-terminal inactivation domain to open and C-type inactivated channels by exploiting the properties of Na<sup>+</sup> permeation through K<sup>+</sup> channels, particularly the ability of inactivated K<sup>+</sup> channels to conduct Na<sup>+</sup> currents. This experimental approach offers insight into the structural changes associated with C-type inactivation and recovery, and contrasts the binding properties of the N-terminal inactivation domain to the open state and the C-type inactivated state of the channel.

### *Mechanism of slowing of the Na<sup>+</sup> tail by the N-terminal inactivation domain*

We observed that the Kv1.4 N-terminal inactivation domain and quaternary ammonium ions exert effects on C-type inactivated Na<sup>+</sup> tail currents in both Kv1.4 and Kv1.5, recapitulating the well-known effects of these agents on the deactivating tail currents of open channels (Armstrong, 1971; Demo & Yellen, 1991; Choi *et al.*, 1993). That is, these agents were shown to reduce and delay the peak tail current (intracellular blockers often impart 'hooked' deactivation tail currents), and slow the decay of the C-type inactivated Na<sup>+</sup> tail. Importantly, the mechanism underlying the effects of the N-type inactivation domain on the C-type inactivated Na<sup>+</sup> tail currents is subtly different from its effects on deactivation tail currents from open channels, as they result from binding to the C-type inactivated conformation of the channel pore. In the model presented in Fig. 5.8, this stable binding delays entry of channels into the highly Na<sup>+</sup>-permeable state (R) normally occupied during recovery from inactivation, and slower transit of channels into the Na<sup>+</sup>-permeable R state results in a reduction and slower decay of the inward Na<sup>+</sup> tail current (Wang *et al.*, 2000a). A direct interaction of the inactivation domain or quaternary ammonium ions with the C-type

inactivated channel pore is required to explain these effects on the tail current. Models that preclude binding of the N-terminal inactivation domain to the C-type inactivated state, and only permit binding to the R state in the recovery pathway, fail to duplicate the delayed peak tail current consistently observed in our experiments (Figs. 5.4, 5.5).

***Inactivation ball binding to the C-type inactivated state – structural considerations***

The first important insight provided by our experiments relates to binding of the inactivation ball to the C-type inactivated state of the channel. It is known that inhibition of C-type inactivation by high extracellular  $K^+$  conditions allows for the observation of ‘recovery tails’ (reopening of channels during recovery from N-type inactivation) in both *Shaker* and Kv1.4 channels (Demo & Yellen, 1991; Ruppertsberg *et al.*, 1991), in which slow unbinding of the N-terminal inactivation domain results in a reduction of deactivation tail currents, and slower tail current decay. All of these features are explained by the ‘ball and chain’ model of N-type inactivation, in which the N-terminal inactivation domain is thought to bind as an extended peptide within the inner cavity of the  $K^+$  channel pore (Zhou *et al.*, 2001a). Previous studies of binding properties of the N-terminal inactivation domain within the pore have relied upon experimental manipulations that inhibit C-type inactivation, and are therefore limited to characterization of interactions between the inactivation domain and the open state of the pore (Demo & Yellen, 1991; Ruppertsberg *et al.*, 1991; Kuo, 1997). In contrast, our experiments have been carried out in conditions where C-type inactivation is favourable. Our demonstration that the N-terminal inactivation domain is able to influence  $Na^+$  tail currents suggests that the inactivation domain can bind and modify pore dynamics in C-type inactivated Kv1.5 and Kv1.4 channels.

There is some uncertainty in the literature regarding the conformational changes underlying C-type inactivation. Considerable evidence suggests conformational changes in the selectivity filter and the outer pore mouth during C-type inactivation (Liu *et al.*, 1996; Starkus *et al.*, 1997; Kiss & Korn, 1998; Loots & Isacoff, 1998; Ogielska & Aldrich, 1999; Gandhi *et al.*, 2000). However, little is known about the conformation of the inner pore mouth, and recent structural advances have not explicitly addressed the process of C-type inactivation. Based on changes in the C-type inactivation properties of Kv1.4 in response to altered intracellular tonicity, one recent study has suggested that the inner pore mouth undergoes a significant constriction during C-type inactivation, similar in magnitude to the volume change associated with deactivation (Jiang *et al.*, 2003a). This structural description of C-type inactivation is difficult to resolve with the data presented here, for several reasons. In particular, our experiments demonstrate that the N-terminal inactivation domain, and quaternary ammonium ions, exert similar effects on the Na<sup>+</sup> tail current whether they first bind to open (Kv1.4N/Kv1.5, Figs. 5.4A, 5.5B) or C-type inactivated (Kv1.4) channels (Figure 5.5). These experiments suggest that the binding site for quaternary ammonium ions and the N-terminal inactivation domain is accessible in both open and C-type inactivated channels. Given the strong structural (Zhou *et al.*, 2001a) and biophysical/mutagenic (Yellen *et al.*, 1991; Choi *et al.*, 1993) evidence that the quaternary ammonium binding site lies deep in the inner cavity near the selectivity filter, these results suggest that the activation gates are open and the inner pore is accessible to cytosolic compounds before and after C-type inactivation. Furthermore, in *Shaker* and other Kv1 channels, deactivation is not favoured if a quaternary ammonium ion is in the pore. TEA<sup>+</sup>, TBA<sup>+</sup> and other quaternary ammonium derivatives are very poorly trapped by Kv1 channels, and generally compete with closure of

open channels (Choi *et al.*, 1993; Holmgren *et al.*, 1997). Thus, if C-type inactivation involves a conformational change of the inner vestibule similar to deactivation (Jiang *et al.*, 2003a), one might expect intracellular quaternary ammonium ions or the N-terminal inactivation domain to antagonize C-type inactivation, much like they antagonize deactivation (Demo & Yellen, 1991; Choi *et al.*, 1993). The opposite is clearly true, with quaternary ammonium ions typically accelerating C-type inactivation of *Shaker* and other Kv1 channels (Baukrowitz and Yellen, 1996).

***Inactivation domain binding to the C-type inactivated state – gating considerations***

Although the demonstration of binding of the N-terminal inactivation domain to C-type inactivated channels may not be entirely surprising, to our knowledge it has not yet been demonstrated experimentally, because the techniques and understanding allowing for the measurement of currents through inactivated channels are still being developed (Starkus *et al.*, 1997; Starkus *et al.*, 1998; Wang *et al.*, 2000a). An obvious consequence of this finding is that reopening of K<sup>+</sup> channels is not obligatory during recovery from N-type inactivation. It has been demonstrated that as the extracellular K<sup>+</sup> concentration is reduced, N-type inactivation results in a stronger bias towards C-type inactivation of Kv channels, so channel reopenings upon repolarization become very infrequent and recovery from inactivation is limited by the recovery rate from C-type inactivation (Demo & Yellen, 1991; Baukrowitz & Yellen, 1995; Rasmusson *et al.*, 1995). Our data and modeling are consistent with the hypothesis that the pore of channels that are both C-type and N-type inactivated recover without revisiting the open state, via the same pathway (albeit more slowly) as channels that are only C-type inactivated.

A second interesting issue is that despite the apparent effects of the N-terminal inactivation domain and quaternary ammonium ions on the kinetics of the C-type inactivated Na<sup>+</sup> tail currents (Figs. 5.3-5.5), the effects on the overall rate of recovery from inactivation are clearly quite innocuous, whether Na<sup>+</sup> or K<sup>+</sup> is the primary permeant ion (Fig. 5.1C, F). A possible simple explanation for this is that even in the presence of the N-terminal inactivation domain, the time course of the Na<sup>+</sup> tail current is quite brief ( $\tau$  on the order of hundreds of milliseconds, Fig. 5.3C) compared with the overall time course of recovery from inactivation, which can take 15 s or longer to approach completion (Fig. 5.1C). In addition, the kinetics of the C-type inactivated Na<sup>+</sup> tail are more voltage-dependent (Fig. 5.3A, see also Fig. 7 in Wang *et al.*, 2000a) than the kinetics of recovery from C-type inactivation in Kv1.5 (Kurata *et al.*, 2001). These observations suggest that one or more rate-limiting steps during recovery from C-type inactivation dominate the overall rate of recovery and minimize the effects of the N-terminal inactivation domain on pore closure observed in our experiments. As an example, in the model presented in Chapter 3, it is the transitions between the closed-inactivated and closed states that govern the rate of recovery from inactivation.

Though speculative, another possible explanation arises from a prior observation that gating processes in the pore are not necessarily rigidly coupled to gating processes elsewhere in the channel, especially after the onset of C-type inactivation (Wang & Fedida, 2002). We have previously demonstrated that during recovery from C-type inactivation in Kv1.5, complete recovery of gating charge occurs long before decay of the Na<sup>+</sup> tail is complete, suggesting that the channel pore can become functionally dissociated from the voltage sensor after C-type inactivation (Wang & Fedida, 2002). Thus, a second possible explanation for the very minor effects of the N-terminal inactivation domain on recovery from inactivation is

that there are several independent processes occurring in parallel during recovery from inactivation, and that the recovery of pore conformation influenced by the inactivation domain is not rate-limiting. In this vein, it should be noted that N-terminal inactivation domains are not always without influence on recovery from inactivation. Recent characterization of multiple 'tandem' inactivation domains in Kv1.4 has shown that after deletion of the first inactivation domain, a second inactivation domain (an alanine rich region comprising amino acids 39-50) can impart N-type inactivation kinetics virtually identical to the WT channel, but slows recovery from inactivation dramatically, resulting in a recovery time constant of  $\sim 300$  s (Wissmann *et al.*, 2003). Thus, in the Kv1.4 $\Delta$ N39 mutant channel, it is possible that the inactivation domain dissociates from the pore extremely slowly, and this dissociation becomes the limiting step in recovery from inactivation.

#### ***Kinetic effects of binding of the N-terminal inactivation domain***

Since  $K^+$  channels become highly permeable to  $Na^+$  during recovery from inactivation, our experiments performed in low or zero  $K^+$  conditions provide new insights into the kinetics of binding/unbinding of the N-terminal inactivation domain with C-type inactivated channels. Surprisingly, kinetic modeling predicted a slightly greater affinity of the inactivation domain for the C-type state than the open state (Fig. 5.8). This interpretation arises primarily from our fitting of the simulated  $Na^+$  tail currents to experimental data, and at this stage it is appropriate to stress that this finding remains based on a model that is likely a simplified representation of the actual gating mechanism. Therefore, we are currently exploring a number of experimental approaches to confirm this finding independently. Nevertheless, we found that our model required considerably slower unbinding of the N-terminal inactivation domain from the C-type inactivated state relative to the open state in

order to adequately reproduce the effects of the inactivation domain on the slow Na<sup>+</sup> tail currents of Kv1.5. This translated into an estimated two- to four-fold increase in affinity for the inactivation domain in C-type inactivated channels. Interestingly, altered affinity for the inactivation domain after the onset of C-type inactivation is also consistent with concerns of maintaining microscopic reversibility in the model (Fig. 5.8A). That is, if binding of the N-terminal inactivation domain to the open state is considered to promote C-type inactivation, satisfaction of microscopic reversibility requires that the C-type inactivated state have a greater affinity than the open state for the inactivation domain.

This finding may have important implications regarding the mechanism(s) underlying promotion of C-type inactivation following blockade by the N-terminal inactivation domain or intracellular quaternary ammonium ions. Multiple mechanisms of coupling between N-type and C-type inactivation have been proposed (Rasmusson *et al.*, 1998). The most clearly and quantitatively understood mechanism of coupling is the demonstration of the link between permeation and C-type inactivation, in which evacuation of K<sup>+</sup> ions from the selectivity filter under conditions of intracellular blockade results in accelerated C-type inactivation (Baukrowitz & Yellen, 1995; Baukrowitz & Yellen, 1996b). However, it is recognized that blockade of K<sup>+</sup> permeation is not the only the mechanism of coupling between intracellular blockade and C-type inactivation, and that different open channel blockers can also exhibit a spectrum of allosteric effects on C-type inactivation (Baukrowitz & Yellen, 1996a; Baukrowitz & Yellen, 1996b; Rasmusson *et al.*, 1998). A frequently cited example of this phenomenon is 4-AP, which appears to antagonize C-type inactivation in *Shaker* and mammalian Kv1 channels despite its prolonged dwell time in the pore and blockade of K<sup>+</sup> flux (Castle *et al.*, 1994; Russell *et al.*, 1994; Rasmusson *et al.*, 1998). In

addition, different quaternary ammonium derivatives have been shown to either inhibit or promote C-type inactivation in the absence of effects on permeating ions (Baukrowitz & Yellen, 1996a; Baukrowitz & Yellen, 1996b). Presumably, this variability arises from detailed differences in the structural interactions between various blockers and the inner Kv channel pore, and it has been suggested that certain intracellular blockers may bind the inner vestibule of the pore and 'orient' the channel to favour C-type inactivation (Rasmusson *et al.*, 1998; Wang *et al.*, 2003; Bett & Rasmusson, 2004), however the mechanistic/structural basis underlying allosteric interactions between blockers and C-type inactivation remains poorly understood. In the present study, our results raise the possibility that interactions between the N-terminal inactivation domain and the inner Kv channel pore are stabilized by the onset of C-type inactivation. This stabilized interaction between the inactivation domain and the C-type inactivated pore may underlie, at least in part, the promotion of C-type inactivation after binding of the inactivation domain.

### ***Conclusion***

We have shown that the Kv1.4 inactivation domain exerts significant effects on the C-type inactivated Na<sup>+</sup> tail currents of Kv1.4 and Kv1.5, including slowing of tail current kinetics, and a reduction in peak tail current magnitude. These effects are observed whether the inactivation domain binds to open channels or to C-type inactivated channels, suggesting that the inner vestibule of Kv channels is accessible to the cytosol before, and after, the onset of C-type inactivation. Kinetic modeling suggests that the N-terminal inactivation domain binds stably to the pore of C-type inactivated channels, delaying transitions through Na<sup>+</sup>-permeable states traversed during recovery from inactivation.

## **CHAPTER 6: CONCLUSIONS AND GENERAL DISCUSSION**

The principal focus of the experimental work presented in this thesis is the mechanisms by which the cytosolic N-terminus of a Kv channel can interact with the transmembrane domains and regulate slow inactivation gating. The mechanisms examined can be divided into two themes: regulation of the state-dependence of inactivation by the Kv1.5 T1 domain (Chapters 3 and 4; Kurata *et al.*, 2001; Kurata *et al.*, 2002), and interactions between intracellular pore blockers, such as the N-terminal inactivation domain, with the pore of C-type inactivated channels (Chapter 5; Kurata *et al.*, 2004).

#### ***Regulation of state-dependence of inactivation by the Kv1.5 N-terminus***

Work presented in Chapters 3 and 4 demonstrates that the N-terminus of Kv1.5 plays a significant role in modulating the inactivation phenotype of the channel. Most importantly, N-terminal truncation confers an apparent voltage-dependence to Kv1.5 inactivation, and this effect has been attributed to an alteration in the state-dependence of channel inactivation (Kurata *et al.*, 2001). Deletion analysis of the Kv1.5 N-terminus delimited the gating effects observed in Kv1.5 $\Delta$ N209 to the T1 domain. The involvement of the T1 domain was also confirmed by several chimeric constructs, and the identification of point mutations near the T1 domain intersubunit interface that recapitulate many of the gating features of T1 deletion mutants (Kurata *et al.*, 2002).

#### ***Potential physiological roles of N-terminally truncated channels***

From a physiological perspective, it is of particular interest that N-terminally truncated forms of Kv1.5 have been identified in neonatal murine and fetal human cardiac myocytes, and may arise from an unusual splicing mechanism within the Kv1.5 gene structure (Tamkun *et al.*, 1991; Attali *et al.*, 1993; Fedida *et al.*, 1993). Since there remains

uncertainty with regards to the genotypes underlying the various  $K^+$  currents in heart and vasculature, the altered phenotype of short forms of Kv1.5 suggests a potential mechanism by which  $K^+$  current diversity may be generated in many tissues. Apart from the unique gating properties of Kv1.5 $\Delta$ N209 (Kurata *et al.*, 2001), another potential mechanism underlying diversity could be inter-subfamily heteromultimerization, since Kv1.5 $\Delta$ N209 lacks the structural determinants necessary for subfamily specificity during Kv channel assembly (Li *et al.*, 1992; Shen & Pfaffinger, 1995; Xu *et al.*, 1995). Importantly, another N-terminally truncated channel isoform isolated from myocardium, particularly truncated forms of KvLQT1, appears to exert a dominant negative function (Jiang *et al.*, 1997). Although we have not yet characterized the effects of co-expression of full-length Kv1.5 and Kv1.5 $\Delta$ N209, the functionality of Kv1.5 $\Delta$ N209 homotetramers suggests that they will not exert a dominant negative effect.

Since our data suggest that deletion of the N-terminus affects the depth of inactivation, it is possible that differential expression of this channel could alter the properties of outward  $K^+$  currents in tissues such as cardiac muscle and vascular smooth muscle. For example, the expression of Kv1.5 $\Delta$ N209 could decrease the sensitivity of action potential duration to heart rate, as inactivation of Kv1.5 $\Delta$ N209 is enhanced by repetitive depolarizations (Figs. 3.6, 3.7), and during action potential clamp experiments (Fig. 3.9). Also, maximal inactivation of Kv1.5 $\Delta$ N209 occurs at potentials near the plateau of the cardiac action potential, so small physiological or pathophysiological changes in action potential shape could significantly affect inactivation of the channel. In addition, the Kv1.5 $\Delta$ N209 isoform lacks binding sites for  $\beta$ -subunits (Accili *et al.*, 1997) and  $\alpha$ -actinin-2 (Maruoka *et al.*, 2000), as well as several potential phosphorylation sites within the N-

terminus. All these differences suggest that the short form of the channel may be subject to different regulation than full-length Kv1.5 channels. Finally, a general understanding of the mechanisms governing accumulation of inactivation in K<sup>+</sup> channels is of significant interest, particularly in the study of tissues where repetitive firing takes place. In various neuronal and artificial systems, changes in K<sup>+</sup> channel availability due to accumulation of inactivation have been shown to affect action potential duration and the rate/frequency of firing during bursts of action potentials (Aldrich *et al.*, 1979b; Hsu *et al.*, 1993). The different inactivation phenotypes of Kv1.5 and Kv1.5ΔN209 suggest that mechanisms regulating the state-dependence of channel inactivation could significantly alter the properties of rapidly firing neurons.

#### ***Regulation of channel gating by the T1 domain***

My personal interests are centered more in the realm of molecular mechanisms of ion channel function. In this context, the most important implication of results in Chapters 3 and 4 is that functions of the Kv channel T1 domain extend far beyond channel assembly. Rather, the T1 domain plays an additional important role in controlling both activation and inactivation gating in Kv channels. Work presented in Chapters 3 and 4 helps to confirm reports by many groups demonstrating the influence of mutations in the T1 domain on the activation properties of *Shaker* family K<sup>+</sup> channels (Elkes *et al.*, 1997; Johnstone *et al.*, 1997; Pascual *et al.*, 1997; Kobertz & Miller, 1999; Minor *et al.*, 2000; Cushman *et al.*, 2000; Strang *et al.*, 2001; Kurata *et al.*, 2001; Rosenthal & Bezanilla, 2002; Kurata *et al.*, 2002; Ju *et al.*, 2003). More importantly, this experimental work remains the only detailed characterization of the influence of the T1 domain on *Shaker* family inactivation. However, despite the structural determination of T1 domains from multiple channel subtypes, and for

multiple *Shaker* family T1 mutants, our understanding of the role of the T1 domain in channel gating is incomplete.

Delineation of a structural understanding of the mechanism of T1 regulation of channel function will require several elements. Although several studies suggest that conformational changes of the T1 domain play a role in channel gating, the precise nature of these conformational changes remain very poorly understood (Minor *et al.*, 2000). Several reports have described significant gating effects of T1 mutations with minor effects on the structure of the T1 domain. Notably, Minor *et al.* (2000) demonstrated that the Kv1.2 T46V T1 domain mutant exhibited a significant 20 mV depolarizing shift of the activation  $V_{1/2}$ , but a T1 domain structure essentially indistinguishable from WT Kv1.2, leading to the hypothesis that the T1 domain is conformationally coupled to channel activation. Other studies of T1 domain mutants, or of the T1/Kv $\beta$ 2 complex, have shown small alterations in the structure of the C-terminal side of the T1 domain, which is generally thought to face the transmembrane domains of channel (Gulbis *et al.*, 2000; Cushman *et al.*, 2000). In addition, the first publication of the T1 domain structure presented data from multiple crystal forms, not distorted by packing interactions, that exhibited structural differences on the C-terminal side of the tetramer (Kreusch *et al.*, 1998). These observations have led to some speculation that the C-terminal side of the T1 domain is conformationally flexible or mobile, and that conformational changes in this region may be involved in regulation of channel activation (Minor *et al.*, 2000). Other preliminary work (in abstract form) has hinted at changes in accessibility of Zn<sup>2+</sup>-binding cysteine residues within the Kv4.2 T1 domain during inactivation, suggesting that inactivation may also involve conformational changes within the T1 domain (Shahidullah *et al.*, 2003). Nevertheless, at present there is no detailed model of

potential conformational states of the T1 domain, apart from the crystallized structures. Again, there seems to be general consensus in the literature that the T1 domain undergoes conformational changes during gating, but the nature of these changes is unknown.

Also of great importance is some elucidation of a mechanism of coupling between the cytosolic T1 domain and the transmembrane gating elements of Kv channels. In other words, how are conformational changes communicated between the apparently structurally distinct cytosolic and transmembrane modules of an intact channel (Sokolova *et al.*, 2001; Sokolova *et al.*, 2003; Orlova *et al.*, 2003)? While an understanding of this communication is important in the development of structural models of gating comprising the entire channel, it is also critically important for an understanding of the transduction of cytoplasmic signals to the gating machinery of the channel. Various Kv channels exhibit diverse responses to multiple intracellular signals, which target the cytoplasmic domains of the channel (Huang *et al.*, 1993; Huang *et al.*, 1994; Holmes *et al.*, 1996; Jing *et al.*, 1999; Nitabach *et al.*, 2001). Also, the demonstration that point mutations in the T1 domain can alter the properties of Kv1.5 inactivation raises the possibility that cytoplasmic signals may modulate slow inactivation of Kv channels, although very few instances have been identified to date (Fadool *et al.*, 1997). With the exception of certain processes regulating N-type inactivation (reviewed briefly in Chapter 1; Drain *et al.*, 1994; Beck *et al.*, 1998; Kwak *et al.*, 1999; Antz *et al.*, 1999; Encinar *et al.*, 2002; Padanilam *et al.*, 2002), the molecular mechanisms underlying the gating effects of channel phosphorylation, assembly with auxiliary subunits, or other post-translational modifications are generally unknown.

One obvious potential mode of interaction between the T1 domain and the transmembrane domains of the channel is a direct mechanism through the T1-S1 linkers.

Indeed mutations or chimeric substitutions in this region have been shown to affect activation and inactivation properties in a number of channels (Elkes *et al.*, 1997; Johnstone *et al.*, 1997; Chiara *et al.*, 1999; Kerschensteiner *et al.*, 2003). Other insights into this problem might arise from the general observation that disruptions of the T1 domain produce a spectrum of effects in different channels. As demonstrated here, deletion of the Kv1.5 N-terminus exerted marginal effects on the kinetics of channel activation (Kurata *et al.*, 2001; Kurata *et al.*, 2002). In contrast, deletions of similar magnitude in Kv2.1 (as shown in Chapter 4) or *Shaker* channels resulted in very significant slowing of the time course of activation (VanDongen *et al.*, 1990; Kobertz & Miller, 1999). In addition, all of the Kv1.5 T1 domain disruptions tested in our study consistently exhibited a ~10 mV hyperpolarizing shift of the  $V_{1/2}$  of channel activation (Figs. 4.6, 4.8, 4.9; Kurata *et al.*, 2002). This observation contrasts with data from Kv1.2, in which point mutations near the intersubunit interface predominantly (18 out of 27 mutants tested) resulted in depolarizing shifts of the voltage-dependence of channel activation (Minor *et al.*, 2000). More detailed comparisons also reveal differences between these channels. For example, the Kv1.5 ET/AA (E132A, T133A) mutation examined in Chapter 4 resulted in a 10 mV hyperpolarizing shift of the activation  $V_{1/2}$ , whereas in Kv1.2, the T46A mutation (equivalent to Kv1.5 T133A) resulted in a shift of comparable magnitude, but in the reverse direction.

These disparate effects of T1 domain disruption in different channels occur despite considerable structural homology of T1 domains between different channel subfamilies, and nearly perfect primary sequence identity of T1 domains within subfamilies (Kreusch *et al.*, 1998). Thus, one possibility is that the gating effects of mutations within the T1 domain depend, at least in part, on determinants elsewhere in the channel. That is, the T1 domain

may be coupled to transmembrane gating domains through other structural elements that differ between channels. The most frequent suggestion in this regard is that the Kv channel N- and C-termini may associate to form a functional complex that allows conformational changes to be communicated between the cytosolic and transmembrane domains of the channel. In this hypothesis, the C-terminus (as a direct extension of the S6 activation gate) acts as an 'adaptor' between the channel pore and the T1 domain (Minor *et al.*, 2000; Ju *et al.*, 2003; Wray, 2003). Differences in structure of the C-terminus, which exhibits considerable sequence variability even within Kv channel subfamilies, could conceivably transduce similar disruptions or conformational changes of the T1 domain into different effects on the gating properties of the pore (a cartoon illustrating this suggested arrangement is shown in Fig. 6.1, adapted from similar cartoons in Minor *et al.*, 2000; Wray, 2002).

By analogy with multiple Kv channel relatives, the C-terminus provides an interesting potential mechanism for transduction of cytoplasmic signals to the transmembrane core of the channel. A role of the C-terminus is implicated in the control of gating properties by cytoplasmic factors in many channels. In the 6 transmembrane domain CNG or HCN channels, C-terminal binding of cyclic nucleotides alters the open-closed equilibrium (Wainger *et al.*, 2001; Kaupp & Seifert, 2002; Robinson & Siegelbaum, 2003). In the Ca<sup>2+</sup> gated channel MthK, the regulatory domains controlling gating are also direct extensions of the M2 helix (homologous to the S6 helix in Kv channels), although Ca<sup>2+</sup> regulation by the C-terminus of BK channel remains controversial (Jiang *et al.*, 2001; Piskorowski & Aldrich, 2002; Jiang *et al.*, 2002a). Even in ligand-gated Kir channels (eg. GIRK channels formed by Kir3.1/3.4 or K<sub>ATP</sub> channels formed by Kir6 subunits), the C-terminus generally forms a significant component of the ligand-binding domains that regulate to channel gating (Nishida

& MacKinnon, 2002). Therefore, as the direct cytoplasmic extension of the pore-lining S6 transmembrane helix, the C-terminus is uniquely positioned to play a role in regulating pore dynamics of Kv channels.

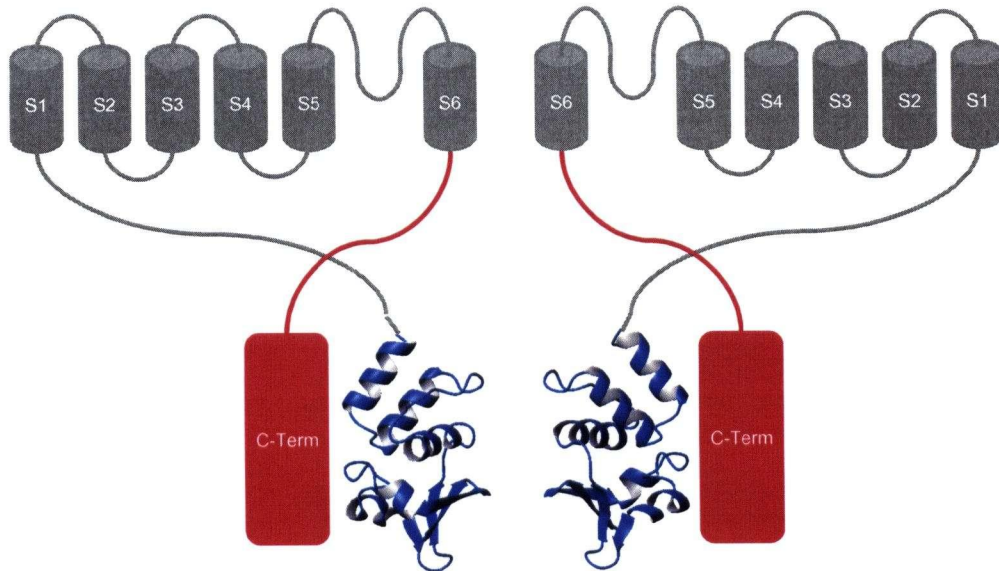


Figure 6.1. Schematic diagram illustrating a potential mechanism of communication between the cytosolic and membrane bound domains of a Kv channel. Multiple lines of evidence suggest that the Kv channel T1 domain (ribbon structure) and C-terminus (red box, C-term) lie in close proximity. As a direct extension of the pore-lining S6 helix, the C-terminus domain may act as an adaptor domain and transduce conformational changes of the T1 domain into measurable effects on the kinetics of activation or inactivation.

There is also evidence that the N- and C-termini of Kv channels lie very close to one another in an intact Kv channel. In *Shaker* channels, the N-terminal side of the T1 domain and C-termini of adjacent subunits reach close enough proximity to form disulfide bonds, although significant gating effects of coupling between the N- and C-termini of the channel have not been demonstrated in this channel (Schulteis *et al.*, 1996). Furthermore, single molecule electron microscope images of *Shaker* channels have suggested that the N- and C-termini form a close complex. Although these images are inadequate to discern individual amino acids, difference maps between full-length *Shaker* and C-terminally deleted *Shaker*

channels indicate that a portion of the C-terminus is nestled in grooves at each intersubunit T1 domain interface (Sokolova *et al.*, 2003). Finally, in contrast to the polar intersubunit T1 domain interface, the outer surface of the T1 tetramer is relatively hydrophobic, suggesting that it may serve as a binding interface for other proteins or potentially other channel domains (Kreusch *et al.*, 1998; Minor *et al.*, 2000). Evidence for a functional interaction between the N- and C-termini has been demonstrated in Kv 2.1, in which residues in the C-terminus of human vs. rat forms of Kv2.1 modify the effects of mutations at two solution-exposed residues within the T1 domain (Ju *et al.*, 2003). This complementarity between the N- and C-termini in Kv2.1, and their interaction in a GST-pulldown assay, suggests that these domains are in close proximity in an intact channel, and that their interaction may underlie the gating effects of mutations in the T1 domain (Ju *et al.*, 2003; Wray, 2003). A functional interaction between the N- and C-termini also appears to play a role in governing the time course of inactivation in Kv4 channels (Jerng & Covarrubias, 1997; Jerng *et al.*, 1999). Clear elucidation of the structural basis for the involvement of cytoplasmic domains in channel gating remains an important challenge.

### ***Structural determinants of state-dependent inactivation***

N-type inactivation of Kv channels exhibits a well-defined state-dependence, as channels must open before the N-terminal inactivation domain can bind. The structural correlate of this state-dependence is well understood to be the steric gate formed by the cytoplasmic ends of the S6 transmembrane helices, which occlude entry of the inactivation domain into the inner cavity of closed channels (Liu *et al.*, 1997; Del Camino & Yellen, 2001; Aldrich, 2001; Zhou *et al.*, 2001a). In contrast, characterization of the inactivation properties of several Kv channel types, in Chapters 3 and 4 of this thesis, and elsewhere, has

suggested a range of state-dependencies of slow inactivation mechanisms in Kv channels (Klemic *et al.*, 1998; Jerng *et al.*, 1999; Klemic *et al.*, 2001; Kurata *et al.*, 2001; Bähring *et al.*, 2001; Kurata *et al.*, 2002).

In most recently published kinetic models of Kv channel inactivation, there is a common implication that slow inactivation is somehow coupled to movement of voltage-sensors into their activated conformation (Marom & Abbott, 1994; Olcese *et al.*, 1997; Klemic *et al.*, 2001; Olcese *et al.*, 2001; Kurata *et al.*, 2001). The structural model of Larsson and Elinder for the role of E418 in *Shaker* inactivation (Larsson & Elinder, 2000), together with the demonstration that the S4 segment and residues near E418 approach one another very closely (Gandhi *et al.*, 2000; Elinder *et al.*, 2001a; Elinder *et al.*, 2001b; Laine *et al.*, 2003; Gandhi *et al.*, 2003), provides a hypothetical structural mechanism by which conformational changes of the voltage-sensor can influence the conformation of the outer pore (Loots & Isacoff, 1998; Loots & Isacoff, 2000). Also important is the demonstration that formation of a disulfide bond between cysteines introduced at E418 and V451 in a *single subunit* is sufficient to promote inactivation in *Shaker* (Larsson & Elinder, 2000). Since this disulfide bond formation may mimic the conformational change induced by close contact of the S4 domain and the pore in a single subunit, their observation supports the basic kinetic model structures presented here and elsewhere, in which channel inactivation becomes increasingly favorable with each progressive step along the activation pathway (Olcese *et al.*, 1997; Klemic *et al.*, 1998; Kurata *et al.*, 2001).

While the possibility that activation of voltage sensors somehow promotes C-type inactivation seems likely, this does not provide an obvious explanation for the most basic distinction of state-dependence during inactivation, which is the relative ease with which

channels inactivate from the open state vs. closed states. Clearly, in some Kv channel types the conformational changes accompanying opening of the pore must affect the propensity of the pore to inactivate. Changes in ionic selectivity during activation/deactivation suggest that activation includes rearrangements around the selectivity filter, and these may differentially impact the ability to C-type inactivate in different channel types (Zheng & Sigworth, 1997; Zheng & Sigworth, 1998). A second possibility is that interactions between the extracellular pore and the extracellular end of S4 may influence C-type inactivation by promoting conformational changes of the extracellular pore (Loots & Isacoff, 2000). Of course, in the context of this thesis, the question that remains is how deletions or point mutations in the cytoplasmic N-terminus of Kv1.5 can affect the state-dependence of inactivation. An influence of N-terminal residues on pore conformation is not without precedent, as N-terminal deletions of Kv1.3 have been shown to alter both the single-channel conductance and charybdotoxin affinity of the channel (Segal *et al.*, 1999; Yao *et al.*, 2000). Similarly, various N-terminal splice variants of *Shaker* exhibit altered sensitivity to TEA<sup>+</sup>, 4-AP, and charybdotoxin (Stocker *et al.*, 1990). However, the structural basis for these effects is unknown.

### ***Mechanisms of Kv Channel Slow Inactivation***

It is evident that slow inactivation mechanisms of Kv channels exhibit great diversity in their respective state-dependencies and sensitivity to extracellular K<sup>+</sup>. A frequently mentioned example thus far is that while inactivation of *Shaker* is clearly inhibited by elevation of extracellular K<sup>+</sup> or TEA<sup>+</sup> concentrations (Lopez-Barneo *et al.*, 1993), these same manipulations *accelerate* inactivation of Kv2.1 and Kv3.1 (Klemic *et al.*, 1998; Klemic *et al.*, 2001). Despite this difference, some reports suggest that inactivation is accompanied by

similar changes in selectivity in various channel types that exhibit apparently different regulation by cations, including Kv2.1, *Shaker*, *Shaker* A463C, and a Kv1.3/Kv2.1 chimeric channel (Gross *et al.*, 1994; Starkus *et al.*, 1997; Kiss *et al.*, 1999). Therefore, despite differences in sensitivity to extracellular cations, these channels may converge on a similar terminal mechanism of inactivation involving constriction of the selectivity filter.

Additionally, several mutations have been identified that appear to shift the K<sup>+</sup>-dependence of inactivation of various Kv channels. The Kv1.4 V561A mutant, for instance, exhibits accelerated inactivation in elevated extracellular K<sup>+</sup> concentrations (Li *et al.*, 2003; Bett & Rasmusson, 2004), whereas WT Kv1.4 inactivation (as for *Shaker*) is inhibited by extracellular K<sup>+</sup> (Rasmusson *et al.*, 1995), and we observed a similar effect in Kv1.5 vs. Kv1.5ΔN209 in Chapter 4. Similarly, the Kv2.1 I369L mutation also appears to reverse the K<sup>+</sup> dependence of inactivation in Kv2.1 (De Biasi *et al.*, 1993). In both Kv1.4 and Kv1.5, we have shown that mutations equivalent to *Shaker* T449V (K533V and R487V, respectively) also dramatically alter the effects of K<sup>+</sup> on C-type inactivation (Wang *et al.*, 2000a; Kurata *et al.*, 2004). Much like Kv2.1, these mutants exhibit significantly more rapid inactivation in K<sup>+</sup> conditions than when Na<sup>+</sup> is the only permeant ion (Fig. 5.6; Immke *et al.*, 1999; Wang *et al.*, 2000a; Kurata *et al.*, 2004). Finally, apart from regulating K<sup>+</sup> sensitivity, our studies in Kv1.5 and Kv1.5ΔN209 have demonstrated that N-terminal deletions and specific mutations at the intersubunit T1 interface can also alter the state-dependence of channel inactivation (Kurata *et al.*, 2001). In summary, results such as these suggest that Kv channels possess elements allowing for multiple inactivation behaviours. Given that inactivation properties, particularly the response to extracellular cations, can be switched by minor alterations of the primary sequence (even in regions structurally distinct from the pore), it seems plausible that

these processes are not markedly different. However, it remains unclear whether the range of inactivation phenotypes observed in Kv channels truly reflects multiple distinct inactivation mechanisms, or an incomplete understanding of the regulation of a generalized mechanism of inactivation mediated by the selectivity filter.

In some instances, it has been suggested that differences in state-dependence and  $K^+$ -sensitivity of inactivation do indeed reflect multiple distinct mechanisms. For example, in their study of *Shaker* channel inactivation, Klemic *et al.* (2001) reported two components of recovery from slow inactivation, whose relative magnitudes were sensitive to extracellular  $K^+$  and the voltage at which channels were inactivated. They observed that the recovery kinetics in *Shaker* are determined by the conditions during the inactivating pulse, and interpreted this to mean that multiple, mutually-exclusive, slow inactivation mechanisms (termed 'U-type' and 'P/C-type') can occur simultaneously in *Shaker* channels. Importantly, it should be noted that similar observations of the influence of extracellular  $K^+$  and prepulse voltage on the kinetics of recovery from inactivation were reported earlier in Kv1.3, but with a significantly different interpretation that voltage-dependent  $K^+$  occupancy of a modulatory site during inactivation modifies subsequent recovery kinetics, as opposed to promoting a distinct inactivation process (Levy & Deutsch, 1996a; Levy & Deutsch, 1996b).

An alternative scenario is that permeant ions may differentially regulate the conformational state of the outer pore in different channel types, resulting in disparate effects on inactivation. It is well described in Kv2.1 that the  $K^+$  content of recording solutions affects the conformation of the outer pore sufficiently to dramatically alter block by extracellular TEA<sup>+</sup> (Ikeda & Korn, 1995). Interestingly, experimental conditions that favor binding of extracellular TEA<sup>+</sup> also promote inactivation of Kv2.1, suggesting that  $K^+$  ions are

in fact required for Kv2.1 inactivation, and that  $K^+$ -dependent conformations of the outer pore thereby alter the kinetics of inactivation (Immke *et al.*, 1999). In this scenario, variations in extracellular  $K^+$  concentrations could alter the distribution of channels in different extracellular pore conformations, and consequently alter the rate of inactivation or recovery.

At present, however, our ability to address this issue is hindered by the paucity of experimental data explicitly addressing conformational changes of slow inactivation mechanisms in any channel other than *Shaker*. Clearly, a satisfactory resolution will likely require studies directed towards understanding the conformational changes in multiple channels, with varying sensitivity to  $K^+$ , TEA<sup>+</sup>, or other 'classical' modifiers of C-type inactivation. Studies that have been particularly informative of the conformational changes during *Shaker* C-type inactivation include accessibility and fluorescence studies of outer pore residues, and delineation of the role of residues corresponding to *Shaker* E418 (which is highly conserved among Kv channels)(Yellen *et al.*, 1994; Liu *et al.*, 1996; Larsson & Elinder, 2000).

#### ***N-terminal regulation of Kv channel expression***

An additional interesting observation arising from our deletion scan of the Kv1.5 N-terminus is that intermediate deletion mutations ( $\Delta N140$ ,  $\Delta N162$ ) within the T1 domain abolished current expression, while progressively longer deletions ( $\Delta N188$ ,  $\Delta N209$ ) significantly restored current expression. This phenomenon was mentioned only briefly in Chapter 4, but is a very interesting and puzzling observation. The different expression profile between intermediate deletions ( $\Delta N140$ ,  $\Delta N162$ ) vs. longer deletions ( $\Delta N188$ ,  $\Delta N209$ ) into the T1 domain is difficult to resolve on the basis of channel tetramerization,

because there is no reason *a priori* to expect aggressive deletions of the tetramerization domain to assemble more efficiently than shorter deletions. One possibility currently being explored is that the progressive deletions of the Kv1.5 N-terminus are affecting current expression by revealing or deleting amino acid motifs involved in channel export or retention. In this hypothesis, trafficking signals for ER retention, or binding elements for proteins involved in reverse trafficking of channels may be present in the Kv1.5 $\Delta$ N140 or Kv1.5 $\Delta$ N162 channels, but deleted by the  $\Delta$ N188 or  $\Delta$ N209 truncations. In support of this hypothesis, we have observed that co-expression with the prototypical PDZ protein PSD-95 does not alter expression of full-length Kv1.5, but dramatically enhances the efficiency and expression level of Kv1.5 $\Delta$ N209 (Eldstrom *et al.*, 2002). These observations suggest that a binding domain or a reverse trafficking signal in the N-terminus may negate the effects of PSD-95 in full-length Kv1.5, but is deleted in the Kv1.5 $\Delta$ N209. As a potential candidate, the N-terminus of Kv1.5 is critical for coupling of the channel to the actin cytoskeleton through an interaction with  $\alpha$ -actinin-2, and disruption of this interaction has been shown to dramatically increase Kv1.5 expression in heterologous expression systems (Maruoka *et al.*, 2000). Furthermore, a number of candidate RXR motifs, which have been shown to regulate the surface expression of multiple Kir channels (Zerangue *et al.*, 1999; Ma & Jan, 2002; Shikano & Li, 2003), have been identified in the Kv1.5 N-terminus and are currently being evaluated for a functional role.

### ***Conformational changes of the inner pore during C-type inactivation***

In the second group of studies presented in this thesis (Chapter 5), we used the N-terminal inactivation domain of Kv1.4 to probe the conformational changes of the inner mouth of Kv channels during C-type inactivation. The role of N-terminal inactivation

domains in channels such as Kv1.4 and *Shaker* is well understood as an important mediator of N-type inactivation. Upon opening of the channel, the N-terminal inactivation domain is able to bind within the pore and occlude ion permeation (Aldrich, 2001).

The most straightforward result presented in Chapter 5 is that the Kv1.4 inactivation domain influences the Na<sup>+</sup> tail currents observed through C-type inactivated Kv1.4 or Kv1.5 channels. The effects of the inactivation domain on the C-type inactivated Na<sup>+</sup> tail current draws interesting parallels with previously characterized effects on tail currents through open channels (Demo & Yellen, 1991). In both instances, the N-terminal inactivation domain appears to inhibit channel closure, and imparts (or enhances) a 'hook' to the tail current decay kinetics (Fig. 5.7; Demo & Yellen, 1991). A simple interpretation of these results is that the binding site for the N-terminal inactivation domain remains accessible whether a channel is open or C-type inactivated. This finding contributes to the understanding of conformational changes that accompany C-type inactivation, particularly at the inner mouth of the channel. Conformational changes in this region of the channel have not yet been examined with the same rigor as the conformational changes in the outer pore (Liu *et al.*, 1996; Loots & Isacoff, 1998). Only one previous study has explicitly studied the conformational changes of the inner pore of a *Shaker* family channel during C-type inactivation, demonstrating that hyperosmotic intracellular solutions (that favor smaller conformations of the inner pore) accelerate C-type inactivation of Kv1.4. The authors suggested that the inner cavity of Kv1.4 undergoes a significant reduction in volume during C-type inactivation, and likened this conformational change to a constriction of the inner cavity similar to deactivation (Jiang *et al.*, 2003a). As discussed to some extent in Chapter 5, the hypothesis of a constriction of the inner pore is at odds with our demonstration that the

Kv1.4 N-terminal inactivation domain and quaternary ammonium ions can access their binding site in channels that have C-type inactivated (Fig. 5.5). A possible resolution of this conflict may be that volume change detected by Jiang et al. (2003) arises from an effective 'shortening' of the permeation pathway during C-type inactivation, as opposed to the decrease in cross-sectional area (or constriction) of the inner pore that they proposed. Our observations suggest that the Kv channel inner cavity remains accessible to various cytosolic agents after C-type inactivation, suggesting that C-type inactivation does not require significant constriction of the inner cavity.

Other evidence also suggests that C-type inactivation is not accompanied by a constriction of the inner pore. Notably, the ability of inactivated *Shaker* channels to remain permeable to Na<sup>+</sup> ions suggests that the cytoplasmic S6 gate of the channel remains open following inactivation, since closure of this gate is able to strongly impede cations with ionic radii similar to Na<sup>+</sup> (Starkus *et al.*, 1997; Wang *et al.*, 2000a; Del Camino & Yellen, 2001). Furthermore, characterization of Na<sup>+</sup> currents through *Shaker* channels has demonstrated that C-type inactivated channels can activate and deactivate in response to changes in transmembrane voltage (Starkus *et al.*, 1997). These results clearly distinguish the C-type inactivation gate from the activation gate formed by the S6 transmembrane helices, and demonstrate that motions of the activation gate remain possible after channels have C-type inactivated. Finally, as mentioned in Chapter 5, the well-characterized interaction between intracellular quaternary ammonium blockade and C-type inactivation in *Shaker* family channels argues against a constriction of the inner cavity during C-type inactivation (Kurata *et al.*, 2004). In particular, it is clear that intracellular quaternary ammonium blockade and N-type inactivation can promote C-type inactivation (Demo & Yellen, 1991; Baukrowitz &

Yellen, 1995), however both processes compete with channel deactivation (Demo & Yellen, 1991; Choi *et al.*, 1993). These two observations seem to conflict if C-type inactivation requires a constriction of the inner cavity akin to deactivation.

While our data seems to exclude the possibility of a significant constriction of the inner cavity during C-type inactivation, they do not rule out other potential conformational changes at the inner mouth of the channel. Indeed, conformational changes in this region of the channel have been suggested in other channel types. For example, in hERG channels, reports have suggested that C-type inactivation plays a role in modulating the potency of methanesulfonanilide blockers such as dofetilide (Ficker *et al.*, 2001). It has been suggested that this phenomenon is related to a rotation of the pore-lining S6 helix during inactivation, leading to exposure of multiple aromatic residues required for high-affinity methanesulfonanilide drug binding (Mitcheson *et al.*, 2000; Chen *et al.*, 2002). Furthermore, various intracellular blockers can exert distinct effects on C-type inactivation of Kv channels: quaternary ammonium ions and quinidine can accelerate C-type inactivation (Baukrowitz & Yellen, 1995; Baukrowitz & Yellen, 1996b; Wang *et al.*, 2003; Bett & Rasmusson, 2004), whereas 4-AP blockade and C-type inactivation seem to be mutually inhibitory (Castle *et al.*, 1994; Russell *et al.*, 1994). These differences may reflect differing structural interactions of these compounds with the inner pore of open or C-type inactivated Kv channels. Finally, our results in Chapter 5 suggest that binding affinity between the N-terminal inactivation ball and the inner pore may be slightly enhanced by the onset of C-type inactivation, and this might also reflect conformational rearrangements of the inner pore during C-type inactivation (Kurata *et al.*, 2004).

Hopefully, further development of the methods and reasoning presented in Chapter 5 will contribute to a broader understanding of the interactions between various blockers and the pore of C-type inactivated Kv channels. At the moment, these insights have all arisen from indirect studies that correlate the effects of mutations on C-type inactivation and drug affinity (Ficker *et al.*, 2001; Wang *et al.*, 2003; Bett & Rasmusson, 2004). However, as we have shown, the Na<sup>+</sup> permeability that develops during recovery from C-type inactivation in certain Kv channels may be used to report upon interactions between blockers and the pore (Kurata *et al.*, 2004). Interestingly, in *Shaker*, the Na<sup>+</sup> permeability that persists after C-type inactivation is substantially larger than in Kv1.5, and so similar studies in *Shaker* may permit direct measurements of blocker interactions with C-type inactivated channels, without relying upon the development of Na<sup>+</sup> permeation during recovery from inactivation that is seen in Kv1.5 (Starkus *et al.*, 1997). Further examination of blockers and inactivation domains/peptides of varying potency, as well as blockers that appear to compete with C-type inactivation, will hopefully contribute to development and validation of our studies using Na<sup>+</sup> permeation, and offer new insights into mechanisms of interaction between channel blockade and gating.

#### ***Steps in recovery from inactivation***

A final important consideration of the findings in Chapter 5 relates to the steps involved in recovery of channels from both C-type and N-type inactivation. A frequently encountered assumption in the literature, based on early demonstrations of reopening tail currents during recovery from N-type inactivation of both Kv1.4 and *Shaker* (Demo & Yellen, 1991; Ruppertsberg *et al.*, 1991), is that recovery from N-type inactivation is always accompanied by channel reopening (Gebauer *et al.*, 2004). In fact, as demonstrated by Demo

and Yellen (1991) in *Shaker* channels, reopening during recovery from N-type inactivation likely only occurs in a subset of experimental conditions in which C-type inactivation is inhibited. For example, in high extracellular  $K^+$  conditions, C-type inactivation is minimal, and channel reopening is frequently observed upon repolarization (Demo & Yellen, 1991; Ruppersberg *et al.*, 1991; Kuo, 1997). However, low extracellular  $K^+$  conditions are permissive for C-type inactivation, and in these conditions C-type inactivation becomes limiting in the recovery process and reopenings are rarely observed (Demo & Yellen, 1991; Rasmusson *et al.*, 1995). The experiments in Chapter 5 highlight this distinction, by demonstrating that channels that are both N-type and C-type inactivated can recover through the C-type inactivated state, without revisiting the open state (Kurata *et al.*, 2004). This is evident from the dramatically different  $Na^+$  tail current kinetics in open vs. C-type inactivated channels (Figs. 5.5, 5.7), and is consistent with reports that C-type inactivation limits the time course of channel recovery after N-type inactivation or quaternary ammonium blockade (Baukrowitz & Yellen, 1995; Rasmusson *et al.*, 1995; Baukrowitz & Yellen, 1996b).

### ***Summary***

The work described in this thesis examined the influence of N-terminal domains on the inactivation properties of Kv channels. N-terminal truncations of Kv1.5 deleting portions of the T1 domain consistently imparted a U-shaped inactivation-voltage relationship to the channel, and this was attributed to a shift in the state-dependence of inactivation. Therefore, the cytosolic T1 domain plays an important role in regulating both activation and slow inactivation of Kv channels. We also demonstrate that the N-type inactivation domain of Kv1.4 is able to bind the pore of C-type inactivated channels, suggesting that the inner pore remains open and accessible to the cytosol after the onset of C-type inactivation.

## **APPENDICES**

These appendices contain code used for the kinetic models constructed in Chapters 3 and 5. Simulation programs were generated using ScoP software (version 3.11, see Materials and Methods). The source code has been annotated here for clarity (notes are shown as blue text).

## APPENDIX A1: SOURCE CODE FOR CLOSED-STATE INACTIVATION MODEL OF Kv1.5 AND Kv1.5ΔN209

TITLE Kv1.5 Closed-State Inactivation Model

:Declaration of rates, valences, and constants. Values in black are for both Kv1.5 and Kv1.5ΔN209. Values in red were changed for simulation of Kv1.5Δ209 (see legend for Fig. 3.10). Names for rate constants are assigned to match the names used in Fig. 3.10 (ie. Ratekci corresponds to kci in Fig. 3.10).

```

PARAMETER      {
Ratekci = 0.00008 (0.0013)      Rate constants for inactivation transitions.
All rate constants in the model are in ms-1.
Ratekoi = 0.00017
Ratekic = 0.000055 (0.0000054)
inacratio = 0.35
g = 1.39 (0.11)
f = 0.64 (0.3)
e = 1.6E-19
T = 295
k = 1.38E-23
KF = 0.4                :Rate constants (@ 0 mV) for activation transitions
KB = 0.065
KO = 0.31
KOB = 0.017
ZV = 1.4                :Valences associated with activation transitions
ZB = 0.35
ZO = 0.38
ZOB = 0.70
height = 140           :Values defining 'perpulse' pulse command routine.
'perpulse' is a versatile command embedded in the ScOP software that can
generate repetitive pulses, and was useful for generating most of the
simulations described in the text.
duration = 300
delay = 400
lag = 0
recpot = -80
delta_time = 0.1
EK=-80
}
ASSIGNED          { :declaration of rates solved @ runtime.
v
RateKF
RateKB
Rateko
Ratekob
current
Ratekio
}

INDEPENDENT      { :declaration of independent variable time

```

```

time FROM 0 TO 1000 WITH 1000
}
STATE      { :declaration of model states
numC0 FROM 0 TO 1 START 1      :defines initial condition, all channels
occupy C0
numC1 FROM 0 TO 1 START 0
numC2 FROM 0 TO 1 START 0
numC3 FROM 0 TO 1 START 0
numC4 FROM 0 TO 1 START 0
numO FROM 0 TO 1 START 0
numIA FROM 0 TO 1 START 0
numI1 FROM 0 TO 1 START 0
numI2 FROM 0 TO 1 START 0
numI3 FROM 0 TO 1 START 0
numI4 FROM 0 TO 1 START 0
numI FROM 0 TO 1 START 0
}
PLOT numO VS time      :directive for plotting simulations

DERIVATIVE changes      {:rate equations defining occupancy of each state
numC0' = (numC1*RateKB+numIA*Ratekic/(f^4)) -
(numC0*4*RateKF+numC0*Ratekci*(f^4))
numC1' = (numC0*4*RateKF+numC2*2*RateKB+numI1*Ratekic/(f^3)) -
(numC1*RateKB+numC1*Ratekci*(f^3)+numC1*3*RateKF)
numC2' = (numC1*3*RateKF+numC3*3*RateKB+numI2*Ratekic/(f^2)) -
(numC2*2*RateKB+numC2*Ratekci*(f^2)+numC2*2*RateKF)
numC3' = (numC2*2*RateKF+numC4*4*RateKB+numI3*Ratekic/(f)) -
(numC3*3*RateKB+numC3*RateKF+numC3*(f)*Ratekci)
numC4' = (numC3*RateKF+numO*Ratekob+numI4*Ratekic) -
(numC4*4*RateKB+numC4*Rateko+numC4*Ratekci)
numO' = (numC4*Rateko+numI*Ratekio) - (numO*Ratekob+numO*Ratekoi)
numIA' = (numC0*Ratekci*(f^4)+numI1*RateKB*(f)) -
(numIA*Ratekic/(f^4)+numIA*4*RateKF/(f))
numI1' = (numIA*4*RateKF/(f)+numC1*Ratekci*(f^3)+numI2*2*(f)*RateKB) -
(numI1*(f)*RateKB+numI1*Ratekic/(f^3)+numI1*3*RateKF/(f))
numI2' = (numI1*3*RateKF/(f)+numI3*3*RateKB*(f)+numC2*Ratekci*(f^2)) -
(numI2*2*(f)*RateKB+numI2*2*RateKF/(f)+numI2*Ratekic/(f^2))
numI3' = (numI2*2*RateKF/(f)+numI4*4*(f)*RateKB+numC3*Ratekci*(f)) -
(numI3*3*(f)*RateKB+numI3*RateKF/(f)+numI3*Ratekci/(f))
numI4' = (numI3*RateKF/(f)+numI*Ratekob/g+numC4*Ratekci) -
(numI4*4*(f)*RateKB+numI4*Rateko*g+numI4*Ratekic)
numI' = (numO*Ratekoi+numI4*Rateko*g) - (numI*Ratekio+numI*Ratekob/g)

:equations defining rates solved @ runtime

RateKF = KF*(exp(ZV*e*v/(k*T*1000)))
RateKB = KB*(exp((-ZB)*e*v/(k*T*1000)))
Rateko = KO*(exp(ZO*e*v/(k*T*1000)))
Ratekob = KOB*(exp((-ZOB)*e*v/(k*T*1000)))
Ratekio = Ratekoi * inacratio
v = recpot + perpulse (time, lag, height, duration, delay)
current = (v-EK)*(numO)
}
BREAKPOINT      {
SOLVE changes
}

```

## APPENDIX A2: SOURCE CODE FOR MODEL OF Na<sup>+</sup> TAILS THROUGH Kv1.5

TITLE Kv1.5 Na<sup>+</sup> Tails Model

:declaration of rates, valences, and constants. Names for rate constants are assigned to match the names used in Fig. 5.8 (ie. RatekN corresponds to kN in Fig. 5.8).

```
PARAMETER {
Ratekci = 0.00008      :Rate constants for inactivation transitions. All
rate constants in the model are in ms-1.
Ratekoi = 0.01
RatekN = 0.025
inacratio = 0.25
ninacratio = 0.5
f = 0.64
e = 1.6E-19
T = 295
k = 1.38E-23
KF = 0.4              :Rate constants (@ 0 mV) for activation transitions
KB = 0.045
KO = 0.31
KOB = 0.034
KNNC = 0.1
KNCN = 0.005
KCNC = 0.01
KNCC = 0.00095
KIR = 0.000323
KRI = 0.0072
KCR = 0.185
KRC = 0.00855
ZF = 1.4              :Valences associated with activation transitions
ZB = 0.5
ZO = 0.60
ZOB = 0.70
ZIR = 0.65
ZRI = 0.55
ZCR = 0.05
ZRC = 0.05
height = 140          :Values defining 'perpulse' pulse command routine
duration = 300
delay = 400
lag = 0
recpot = -80
Ratekic = 0.000055
delta_time = 0.1
ENa=0
}

ASSIGNED { :declaration of rates and other parameters determined
(voltage, current) @ runtime.
```

```

v
RateKF
RateKB
Rateko
Ratekob
current
Ratekio
RatekNB
RateKIR
RateKRI
RateKRC
RateKCR
}

INDEPENDENT      { :declaration of independent variable time
time FROM 0 TO 1000 WITH 1000
}

STATE            { :declaration of model states
numC0 FROM 0 TO 1 START 1      :defines initial condition, all channels
occupy C0
numC1 FROM 0 TO 1 START 0
numC2 FROM 0 TO 1 START 0
numC3 FROM 0 TO 1 START 0
numC4 FROM 0 TO 1 START 0
numO FROM 0 TO 1 START 0
numIA FROM 0 TO 1 START 0
numI1 FROM 0 TO 1 START 0
numI2 FROM 0 TO 1 START 0
numI3 FROM 0 TO 1 START 0
numI4 FROM 0 TO 1 START 0
numI FROM 0 TO 1 START 0
numIN FROM 0 TO 1 START 0
numINC FROM 0 TO 1 START 0
numR FROM 0 TO 1 START 0
}

PLOT current VS time      :directive for plotting simulations

DERIVATIVE changes      { :rate equations defining occupancy of each state
numC0' = (numC1*RateKB+numIA*Ratekic/(f^4)) -
(numC0*4*RateKF+numC0*Ratekci*(f^4))
numC1' = (numC0*4*RateKF+numC2*2*RateKB+numI1*Ratekic/(f^3)) -
(numC1*RateKB+numC1*Ratekci*(f^3)+numC1*3*RateKF)
numC2' = (numC1*3*RateKF+numC3*3*RateKB+numI2*Ratekic/(f^2)) -
(numC2*2*RateKB+numC2*Ratekci*(f^2)+numC2*2*RateKF)
numC3' = (numC2*2*RateKF+numC4*4*RateKB+numI3*Ratekic/(f)) -
(numC3*3*RateKB+numC3*RateKF+numC3*(f)*Ratekci)
numC4' = (numC3*RateKF+numO*Ratekob+numI4*Ratekic) -
(numC4*4*RateKB+numC4*Rateko+numC4*Ratekci)
numO' = (numC4*Rateko+numI*Ratekio+numIN*RatekNB) -
(numO*Ratekob+numO*Ratekoi+numO*RatekN)
numIA' = (numC0*Ratekci*(f^4)+numI1*RateKB*(f)) -
(numIA*Ratekic/(f^4)+numIA*4*RateKF/(f))
numI1' = (numIA*4*RateKF/(f)+numC1*Ratekci*(f^3)+numI2*2*(f)*RateKB) -
(numI1*(f)*RateKB+numI1*Ratekic/(f^3)+numI1*3*RateKF/(f))

```

```

numI2' = (numI1*3*RateKF/(f)+numI3*3*RateKB*(f)+numC2*Ratekci*(f^2))-
(numI2*2*(f)*RateKB+numI2*2*RateKF/(f)+numI2*Ratekic/(f^2))
numI3' = (numI2*2*RateKF/(f)+numI4*4*(f)*RateKB+numC3*Ratekci*(f))-
(numI3*3*(f)*RateKB+numI3*RateKF/(f)+numI3*Ratekic/(f))
numI4' = (numI3*RateKF/(f)+numR*RateKRC+numC4*Ratekci)-
(numI4*4*(f)*RateKB+numI4*RateKCR+numI4*Ratekic)
numI' = (numINC*KNCC+numO*Ratekoi+numR*RateKRI)-
(numI*Ratekio+numI*KCNC+numI*RateKIR)
numIN' = (numO*RatekN+numINC*KNCN) - (numIN*RatekNB+numIN*KNNC)
numINC' = (numIN*KNNC+numI*KCNC) - (numINC*KNCC+numINC*KNCN)
numR' = (numI*RateKIR+numI4*RateKCR) - (numR*RateKRI+numR*RateKRC)

```

```

:equations defining rates solved @ runtime

```

```

RateKF = KF*(exp(ZF*e*v/(k*T*1000)))
RateKB = KB*(exp((-ZB)*e*v/(k*T*1000)))
Rateko = KO*(exp(ZO*e*v/(k*T*1000)))
Ratekob = KOB*(exp((-ZOB)*e*v/(k*T*1000)))
Ratekio = Ratekoi * inacratio
RatekNB = RatekN * ninacratio
RateKIR = KIR*(exp(-ZIR*e*v/(k*T*1000)))
RateKRI = KRI*(exp(ZRI*e*v/(k*T*1000)))
RateKRC = KRC*(exp(-ZRC*e*v/(k*T*1000)))
RateKCR = KCR*(exp(ZCR*e*v/(k*T*1000)))
v = recpot + perpulse (time, lag, height, duration, delay)

```

```

current = (v-ENa)*(numO + numR + 0.05*numI)

```

```

}

```

```

BREAKPOINT {

```

```

SOLVE changes

```

```

}

```

## REFERENCES

- Accili, E. A., Kiehn, J., Yang, Q., Wang, Z. G., Brown, A. M., & Wible, B. A. (1997). Separable Kv $\beta$  subunit domains alter expression and gating of potassium channels. *Journal of Biological Chemistry* **272**, 25824-25831.
- Adda, S., Fleischmann, B. K., Freedman, B. D., Yu, M. F., Hay, D. W. P., & Kotlikoff, M. I. (1996). Expression and function of voltage-dependent potassium channel genes in human airway smooth muscle. *Journal of Biological Chemistry* **271**, 13239-13243.
- Aggarwal, S. K. & MacKinnon, R. (1996). Contribution of the S4 segment to gating charge in the *Shaker* K<sup>+</sup> channel. *Neuron* **16**, 1169-1177.
- Ahern, C. A. & Horn, R. (2004a). Specificity of charge-carrying residues in the voltage sensor of potassium channels. *J.Gen.Physiol* **123**, 205-216.
- Ahern, C. A. & Horn, R. (2004b). Stirring up controversy with a voltage sensor paddle. *Trends Neurosci.* **27**, 303-307.
- Albagli, O., Dhordain, P., Deweindt, C., Lecocq, G., & Leprince, D. (1995). The BTB/POZ domain: a new protein-protein interaction motif common to DNA- and actin-binding proteins. *Cell Growth Differ.* **6**, 1193-1198.
- Aldrich, R. W. (1981). Inactivation of voltage-gated delayed potassium current in molluscan neurons. A kinetic model. *Biophys. J.* **36**, 519-532.
- Aldrich, R. W. (2001). Fifty years of inactivation. *Nature* **411**, 643-644.
- Aldrich, R. W., Getting, P. A., & Thompson, S. H. (1979a). Inactivation of delayed outward current in molluscan neurone somata. *J.Physiol* **291**, 507-530.
- Aldrich, R. W., Getting, P. A., & Thompson, S. H. (1979b). Mechanism of frequency-dependent broadening of molluscan neurone soma spikes. *J.Physiol* **291**, 531-544.
- Antz, C., Bauer, T., Kalbacher, H., Frank, R., Covarrubias, M., Kalbitzer, H. R., Ruppersberg, J. P., Baukrowitz, T., & Fakler, B. (1999). Control of K<sup>+</sup> channel gating by

protein phosphorylation: structural switches of the inactivation gate. *Nat.Struct.Biol.* **6**, 146-150.

Armstrong, C. M. (1971). Interaction of tetraethylammonium ion derivatives with the potassium channels of giant axon. *Journal of General Physiology* **58**, 413-437.

Attali, B., Lesage, F., Ziliani, P., Guillemare, E., Honoré, E., Waldmann, R., Hugnot, J.-P., Mattéi, M.-G., Lazdunski, M., & Barhanin, J. (1993). Multiple mRNA isoforms encoding the mouse cardiac Kv1.5 delayed rectifier K<sup>+</sup> channel. *Journal of Biological Chemistry* **268**, 24283-24289.

Ayer, R. K., Jr. & Sigworth, F. J. (1997). Enhanced closed-state inactivation in a mutant Shaker K<sup>+</sup> channel. *Journal of Membrane Biology* **157**, 215-230.

Bahring, R., Boland, L. M., Varghese, A., Gebauer, M., & Pongs, O. (2001). Kinetic analysis of open- and closed-state inactivation transitions in human Kv4.2 A-type potassium channels. *J.Physiol* **535**, 65-81.

Baker, O. S., Larsson, H. P., Mannuzzu, L. M., & Isacoff, E. Y. (1998). Three transmembrane conformations and sequence-dependent displacement of the S4 domain in Shaker K<sup>+</sup> channel gating. *Neuron* **20**, 1283-1294.

Baukrowitz, T. & Yellen, G. (1995). Modulation of K<sup>+</sup> current by frequency and external [K<sup>+</sup>]: A tale of two inactivation mechanisms. *Neuron* **15**, 951-960.

Baukrowitz, T. & Yellen, G. (1996a). Two functionally distinct subsites for the binding of internal blockers to the pore of voltage-activated K<sup>+</sup> channels. *Proceedings of the National Academy of Sciences of the USA* **93**, 13357-13361.

Baukrowitz, T. & Yellen, G. (1996b). Use-dependent blockers and exit rate of the last ion from the multi-ion pore of a K<sup>+</sup> channel. *Science* **271**, 653-656.

Beck, E. J., Sorensen, R. G., Slater, S. J., & Covarrubias, M. (1998). Interactions between multiple phosphorylation sites in the inactivation particle of a K<sup>+</sup> channel - *Insights into the molecular mechanism of protein kinase C action*. *Journal of General Physiology* **112**, 71-84.

Berneche, S. & Roux, B. (2001). Energetics of ion conduction through the K<sup>+</sup> channel. *Nature* **414**, 73-77.

Bett, G. C. & Rasmusson, R. L. (2004). Inactivation and recovery in Kv1.4 K<sup>+</sup> channels: lipophilic interactions at the intracellular mouth of the pore. *J.Physiol* **556**, 109-120.

Bezanilla, F. (2000). The voltage sensor in voltage-dependent ion channels. *Physiological Reviews* **80**, 555-592.

Bezanilla, F., Perozo, E., Papazian, D. M., & Stefani, E. (1991). Molecular basis of gating charge immobilization in *Shaker* potassium channels. *Science* **254**, 679-683.

Bezanilla, F., Perozo, E., & Stefani, E. (1994). Gating of *Shaker* K<sup>+</sup> channels: II. The components of gating currents and a model of channel activation. *Biophysical Journal* **66**, 1011-1021.

Bixby, K. A., Nanao, M. H., Shen, N. V., Kreuzsch, A., Bellamy, H., Pfaffinger, P. J., & Choe, S. (1999). Zn<sup>2+</sup>-binding and molecular determinants of tetramerization in voltage-gated K<sup>+</sup> channels. *Nature Structural Biology* **6**, 38-43.

Brandt, M. C., Priebe, L., Böhle, T., Südkamp, M., & Beuckelmann, D. J. (2000). The ultrarapid and the transient outward K<sup>+</sup> current in human atrial fibrillation. Their possible role in postoperative atrial fibrillation. *Journal of Molecular and Cellular Cardiology* **32**, 1885-1896.

Brehm, P. & Eckert, R. (1978). Calcium entry leads to inactivation of calcium channel in *Paramecium*. *Science* **202**, 1203-1206.

Busch, A. E., Hurst, R. S., North, R. A., Adelman, J. P., & Kavanaugh, M. P. (1991). Current inactivation involves a histidine residue in the pore of the rat lymphocyte potassium channel RGK5. *Biochem.Biophys.Res.Commun.* **179**, 1384-1390.

Castle, N. A., Fadous, S. R., Logothetis, D. E., & Wang, G. K. (1994). 4-Aminopyridine binding and slow inactivation are mutually exclusive in rat Kv1.1 and *Shaker* potassium channels. *Mol.Pharmacol.* **46**, 1175-1181.

Cha, A. & Bezanilla, F. (1997). Characterizing voltage-dependent conformational changes in the *Shaker* K<sup>+</sup> channel with fluorescence. *Neuron* **19**, 1127-1140.

Cha, A. & Bezanilla, F. (1998). Structural implications of fluorescence quenching in the *Shaker* K<sup>+</sup> channel. *Journal of General Physiology* **112**, 391-408.

Cha, A., Ruben, P. C., George, A. L., Jr., Fujimoto, E., & Bezanilla, F. (1999a). Voltage sensors in domains III and IV, but not I and II, are immobilized by Na<sup>+</sup> channel fast inactivation. *Neuron* **22**, 73-87.

Cha, A., Snyder, G. E., Selvin, P. R., & Bezanilla, F. (1999b). Atomic scale movement of the voltage-sensing region in a potassium channel measured via spectroscopy. *Nature* **402**, 809-813.

Cha, A., Zerangue, N., Kavanaugh, M., & Bezanilla, F. (1998). Fluorescence techniques for studying cloned channels and transporters expressed in *Xenopus* oocytes. *Methods Enzymol.* **296**, 566-578.

Chanda, B. & Bezanilla, F. (2002). Tracking voltage-dependent conformational changes in skeletal muscle sodium channel during activation. *J.Gen.Physiol* **120**, 629-645.

Chapman, M. L., VanDongen, H. M. A., & VanDongen, A. M. J. (1997). Activation-dependent subconductance levels in the *drk1* K<sup>+</sup> channel suggest a subunit basis for ion permeation and gating. *Biophysical Journal* **72**, 708-719.

Chen, F. S. P., Steele, D., & Fedida, D. (1997). Allosteric effects of permeating cations on gating currents during K<sup>+</sup> channel deactivation. *Journal of General Physiology* **110**, 87-100.

Chen, J., Seebohm, G., & Sanguinetti, M. C. (2002). Position of aromatic residues in the S6 domain, not inactivation, dictates cisapride sensitivity of HERG and eag potassium channels. *Proc.Natl.Acad.Sci.U.S.A* **99**, 12461-12466.

Chiara, M. D., Monje, F., Castellano, A., & Lopez-Barneo, J. (1999). A small domain in the N terminus of the regulatory alpha-subunit Kv2.3 modulates Kv2.1 potassium channel gating. *Journal of Neuroscience* **19**, 6865-6873.

Choi, K. L., Aldrich, R. W., & Yellen, G. (1991). Tetraethylammonium blockade distinguishes two inactivation mechanisms in voltage-activated K<sup>+</sup> channels. *Proceedings of the National Academy of Sciences of the USA* **88**, 5092-5095.

Choi, K. L., Mossman, C., Aubé, J., & Yellen, G. (1993). The internal quaternary ammonium receptor site of *Shaker* potassium channels. *Neuron* **10**, 533-541.

Clapham, D. E. (1999). Unlocking family secrets: K<sup>+</sup> channel transmembrane domains. *Cell* **97**, 547-550.

Clément-Chomienne, O., Ishii, K., Walsh, M. P., & Cole, W. C. (1999). Identification, cloning and expression of rabbit vascular smooth muscle Kv1.5 and comparison with native delayed rectifier K<sup>+</sup> current. *Journal of Physiology* **515**, 653-667.

Cohen, B. E., Grabe, M., & Jan, L. Y. (2003). Answers and questions from the KvAP structures. *Neuron* **39**, 395-400.

Collins, T., Stone, J. R., & Williams, A. J. (2001). All in the family: the BTB/POZ, KRAB, and SCAN domains. *Mol. Cell Biol.* **21**, 3609-3615.

Cushman, S. J., Nanao, M. H., Jahng, A. W., DeRubeis, D., Choe, S., & Pfaffinger, P. J. (2000). Voltage dependent activation of potassium channels is coupled to T1 domain structure. *Nat. Struct. Biol.* **7**, 403-407.

De Biasi, M., Hartmann, H. A., Drewe, J. A., Taglialatela, M., Brown, A. M., & Kirsch, G. E. (1993). Inactivation determined by a single site in K<sup>+</sup> pores. *Pflugers Archiv* **422**, 354-363.

Del Camino, D., Holmgren, M., Liu, Y., & Yellen, G. (2000). Blocker protection in the pore of a voltage-gated K<sup>+</sup> channel and its structural implications. *Nature* **403**, 321-325.

Del Camino, D. & Yellen, G. (2001). Tight steric closure at the intracellular activation gate of a voltage-gated K<sup>+</sup> channel. *Neuron* **32**, 649-656.

Demo, S. D. & Yellen, G. (1991). The inactivation gate of the *Shaker* K<sup>+</sup> channel behaves like an open-channel blocker. *Neuron* **7**, 743-753.

Dobrzynski, H., Rothery, S. M., Marples, D. D. R., Coppen, S. R., Takagishi, Y., Honjo, H., Tamkun, M. M., Henderson, Z., Kodama, I., Severs, N. J., & Boyett, M. R. (2000). Presence of the Kv1.5 K<sup>+</sup> channel in the sinoatrial node. *Journal of Histochemistry and Cytochemistry* **48**, 769-780.

Doyle, D. A., Cabral, J. M., Pfuetzner, R. A., Kuo, A. L., Gulbis, J. M., Cohen, S. L., Chait, B. T., & MacKinnon, R. (1998). The structure of the potassium channel: Molecular basis of K<sup>+</sup> conduction and selectivity. *Science* **280**, 69-77.

Drain, P., Dubin, A. E., & Aldrich, R. W. (1994). Regulation of *Shaker* K<sup>+</sup> channel inactivation gating by the cAMP-dependent protein kinase. *Neuron* **12**, 1097-1109.

Eisenman, G., Latorre, R., & Miller, C. (1986). Multi-ion conduction and selectivity in the high-conductance  $\text{Ca}^{2+}$ -activated  $\text{K}^+$  channel from skeletal muscle. *Biophysical Journal* **50**, 1025-1034.

Eldstrom, J., Doerksen, K. W., Steele, D. F., & Fedida, D. (2002). N-terminal PDZ-binding domain in Kv1 potassium channels. *FEBS Lett.* **531**, 529-537.

Elinder, F. & Århem, P. (1999). Role of individual surface charges of voltage-gated K channels. *Biophysical Journal* **77**, 1358-1362.

Elinder, F., Århem, P., & Larsson, H. P. (2001a). Localization of the extracellular end of the voltage sensor S4 in a potassium channel. *Biophysical Journal* **80**, 1802-1809.

Elinder, F., Männikkö, R., & Larsson, H. P. (2001b). S4 charges move close to residues in the pore domain during activation in a K channel. *Journal of General Physiology* **118**, 1-10.

Elkes, D. A., Cardozo, D. L., Madison, J., & Kaplan, J. M. (1997). *egl-36* Shaw channels regulate *C. elegans* egg-laying muscle activity. *Neuron* **19**, 165-174.

Encinar, J. A., Fernandez, A. M., Molina, M. L., Molina, A., Poveda, J. A., Albar, J. P., Lopez-Barneo, J., Gavilanes, F., Ferrer-Montiel, A. V., & Gonzalez-Ros, J. M. (2002). Tyrosine phosphorylation of the inactivating peptide of the *Shaker* B potassium channel: a structural-functional correlate. *Biochemistry* **41**, 12263-12269.

Fadool, D. A., Holmes, T. C., Berman, K., Dagan, D., & Levitan, I. B. (1997). Tyrosine phosphorylation modulates current amplitude and kinetics of a neuronal voltage-gated potassium channel. *J. Neurophysiol.* **78**, 1563-1573.

Fedida, D., Bouchard, R., & Chen, F. S. (1996). Slow gating charge immobilization in the human potassium channel Kv1.5 and its prevention by 4-aminopyridine. *J. Physiol* **494**, 377-387.

Fedida, D., Maruoka, N. D., & Lin, S. (1999). Modulation of slow inactivation in human cardiac Kv1.5 channels by extra- and intra-cellular permeant cations. *J. Physiol.* **515**, 315-329.

Fedida, D., Wible, B., Wang, Z., Fermini, B., Faust, F., Nattel, S., & Brown, A. M. (1993). Identity of a novel delayed rectifier current from human heart with a cloned  $\text{K}^+$  channel current. *Circulation Research* **73**, 210-216.

Ficker, E., Jarolimek, W., & Brown, A. M. (2001). Molecular determinants of inactivation and dofetilide block in ether a-go-go (*eag*) channels and *eag*-related K<sup>+</sup> channels. *Mol.Pharmacol.* **60**, 1343-1348.

Flynn, G. E. & Zagotta, W. N. (2001). Conformational changes in S6 coupled to the opening of cyclic nucleotide-gated channels. *Neuron* **30**, 689-698.

Frazier, C. J., George, E. G., & Jones, S. W. (2000). Apparent change in ion selectivity caused by changes in intracellular K<sup>+</sup> during whole-cell recording. *Biophysical Journal* **78**, 1872-1880.

Gandhi, C. S., Clark, E., Loots, E., Pralle, A., & Isacoff, E. Y. (2003). The orientation and molecular movement of a K<sup>+</sup> channel voltage-sensing domain. *Neuron* **40**, 515-525.

Gandhi, C. S., Loots, E., & Isacoff, E. Y. (2000). Reconstructing voltage sensor-pore interaction from a fluorescence scan of a voltage-gated K<sup>+</sup> channel. *Neuron* **27**, 585-595.

Gebauer, M., Isbrandt, D., Sauter, K., Callsen, B., Nolting, A., Pongs, O., & Bähring, R. (2004). N-type inactivation features of Kv4.2 channel gating. *Biophysical Journal* **86**, 210-223.

Glauner, K. S., Mannuzzu, L. M., Gandhi, C. S., & Isacoff, E. Y. (1999). Spectroscopic mapping of voltage sensor movement in the *Shaker* potassium channel. *Nature* **402**, 813-817.

Goldstein, S. A. (1996). A structural vignette common to voltage sensors and conduction pores: canaliculi. *Neuron* **16**, 717-722.

Gomez-Lagunas, F. & Armstrong, C. M. (1995). Inactivation in *Shaker* B K<sup>+</sup> channels: a test for the number of inactivating particles on each channel. *Biophysical Journal* **68**, 89-95.

Grissmer, S. & Cahalan, M. (1989). TEA prevents inactivation while blocking open K<sup>+</sup> channels in human T lymphocytes. *Biophysical Journal* **55**, 203-206.

Gross, A., Abramson, T., & MacKinnon, R. (1994). Transfer of the scorpion toxin receptor to an insensitive potassium channel. *Neuron* **13**, 961-966.

Guillemare, E., Honore, E., Pradier, L., Lesage, F., Schweitz, H., Attali, B., Barhanin, J., & Lazdunski, M. (1992). Effects of the level of mRNA expression on biophysical properties,

sensitivity to neurotoxins, and regulation of the brain delayed-rectifier K<sup>+</sup> channels Kv1.2. *Biochemistry* **31**, 12463-12468.

Gulbis, J. M., Zhou, M., Mann, S., & MacKinnon, R. (2000). Structure of the cytoplasmic  $\beta$  subunit - T1 assembly of voltage-dependent K<sup>+</sup> channels. *Science* **289**, 123-127.

Harris, R. E., Larsson, H. P., & Isacoff, E. Y. (1998). A permanent ion binding site located between two gates of the *Shaker* K<sup>+</sup> channel. *Biophysical Journal* **74**, 1808-1820.

Hartmann, H. A., Kirsch, G. E., Drewe, J. A., Tagliatela, M., Joho, R. H., & Brown, A. M. (1991). Exchange of conduction pathways between two related K<sup>+</sup> channels. *Science* **251**, 942-944.

Hashimoto, Y., Nunoki, K., Kudo, H., Ishii, K., Taira, N., & Yanagisawa, T. (2000). Changes in the inactivation of rat Kv1.4 K<sup>+</sup> channels induced by varying the number of inactivation particles. *Journal of Biological Chemistry* **275**, 9358-9362.

Heginbotham, L., Lu, Z., Abramson, T., & MacKinnon, R. (1994). Mutations in the K<sup>+</sup> channel signature sequence. *Biophysical Journal* **66**, 1061-1067.

Heginbotham, L. & MacKinnon, R. (1993). Conduction properties of the cloned *Shaker* K<sup>+</sup> channel. *Biophysical Journal* **65**, 2089-2096.

Hille, B. & Schwarz, W. (1978). Potassium ions as multi-ion single file pores. *Journal of General Physiology* **72**, 409-442.

Hodgkin, A. L. & Keynes, R. D. (1955). The potassium permeability of a giant nerve fibre. *Journal of Physiology* **128**, 61-88.

Hollerer-Beitz, G., Schonherr, R., Koenen, M., & Heinemann, S. H. (1999). N-Terminal deletions of rKv1.4 channels affect the voltage dependence of channel availability. *Pflugers Archiv* **438**, 141-146.

Holmes, T. C., Fadool, D. A., Ren, R., & Levitan, I. B. (1996). Association of Src tyrosine kinase with a human potassium channel mediated by SH3 domain. *Science* **274**, 2089-2091.

Holmgren, M., Smith, P. L., & Yellen, G. (1997). Trapping of organic blockers by closing of voltage-dependent K<sup>+</sup> channels - *Evidence for a trap door mechanism of activation gating*. *Journal of General Physiology* **109**, 527-535.

Horn, R. (2000). Conversation between voltage sensors and gates of ion channels. *Biochemistry* **39**, 15653-15658.

Hoshi, T., Zagotta, W. N., & Aldrich, R. W. (1990). Biophysical and molecular mechanisms of *Shaker* potassium channel inactivation. *Science* **250**, 533-538.

Hoshi, T., Zagotta, W. N., & Aldrich, R. W. (1991). Two types of inactivation in *Shaker* K<sup>+</sup> channels: Effects of alterations in the carboxy-terminal region. *Neuron* **7**, 547-556.

Hoshi, T., Zagotta, W. N., & Aldrich, R. W. (1994). *Shaker* potassium channel gating. I: Transitions near the open state. *Journal of General Physiology* **103**, 249-278.

Hsu, H., Huang, E., Yang, X. C., Karschin, A., Labarca, C., Figl, A., Ho, B., Davidson, N., & Lester, H. A. (1993). Slow and incomplete inactivations of voltage-gated channels dominate encoding in synthetic neurons. *Biophysical Journal* **65**, 1196-1206.

Huang, X. Y., Morielli, A. D., & Peralta, E. G. (1993). Tyrosine kinase-dependent suppression of a potassium channel by the G protein-coupled m1 muscarinic acetylcholine receptor. *Cell* **75**, 1145-1156.

Huang, X. Y., Morielli, A. D., & Peralta, E. G. (1994). Molecular basis of cardiac potassium channel stimulation by protein kinase A. *Proc.Natl.Acad.Sci.U.S.A* **91**, 624-628.

Ikeda, S. R. & Korn, S. J. (1995). Influence of permeating ions on potassium channel block by external tetraethylammonium. *J.Physiol* **486 ( Pt 2)**, 267-272.

Immke, D., Wood, M., Kiss, L., & Korn, S. J. (1999). Potassium-dependent changes in the conformation of the Kv2.1 potassium channel pore. *J.Gen.Physiol* **113**, 819-836.

Isacoff, E. Y., Jan, Y. N., & Jan, L. Y. (1990). Evidence for the formation of heteromultimeric potassium channels in *Xenopus* oocytes. *Nature* **345**, 530-534.

Islas, L. D. & Sigworth, F. J. (2001). Electrostatics and the gating pore of *Shaker* potassium channels. *J.Gen.Physiol* **117**, 69-89.

Jager, H., Rauer, H., Nguyen, A. N., Aiyar, J., Chandy, K. G., & Grissmer, S. (1998). Regulation of mammalian *Shaker*-related K<sup>+</sup> channels: evidence for non-conducting closed and non-conducting inactivated states. *J.Physiol* **506** ( Pt 2), 291-301.

Jahng, A. W., Strang, C., Kaiser, D., Pollard, T., Pfaffinger, P., & Choe, S. (2002). Zinc mediates assembly of the T1 domain of the voltage-gated K channel 4.2. *Journal of Biological Chemistry* **277**, 47885-47890.

Jerng, H. H. & Covarrubias, M. (1997). K<sup>+</sup> channel inactivation mediated by the concerted action of the cytoplasmic N- and C-terminal domains. *Biophysical Journal* **72**, 163-174.

Jerng, H. H., Shahidullah, M., & Covarrubias, M. (1999). Inactivation gating of Kv4 potassium channels - *Molecular interactions involving the inner vestibule of the pore*. *Journal of General Physiology* **113**, 641-659.

Jiang, M., Tseng-Crank, J., & Tseng, G. N. (1997). Suppression of slow delayed rectifier current by a truncated isoform of KvLQT1 cloned from normal human heart. *Journal of Biological Chemistry* **272**, 24109-24112.

Jiang, X., Bett, G. C., Li, X., Bondarenko, V. E., & Rasmusson, R. L. (2003a). C-type inactivation involves a significant decrease in the intracellular aqueous pore volume of Kv1.4 K<sup>+</sup> channels expressed in *Xenopus* oocytes. *J.Physiol* **549**, 683-695.

Jiang, Y., Lee, A., Chen, J., Cadene, M., Chait, B. T., & MacKinnon, R. (2002a). Crystal structure and mechanism of a calcium-gated potassium channel. *Nature* **417**, 515-522.

Jiang, Y., Lee, A., Chen, J., Cadene, M., Chait, B. T., & MacKinnon, R. (2002b). The open pore conformation of potassium channels. *Nature* **417**, 523-526.

Jiang, Y., Lee, A., Chen, J., Ruta, V., Cadene, M., Chait, B. T., & MacKinnon, R. (2003b). X-ray structure of a voltage-dependent K<sup>+</sup> channel. *Nature* **423**, 33-41.

Jiang, Y. & MacKinnon, R. (2000). The barium site in a potassium channel by x-ray crystallography. *J.Gen.Physiol* **115**, 269-272.

Jiang, Y., Pico, A., Cadene, M., Chait, B. T., & MacKinnon, R. (2001). Structure of the RCK domain from the E. coli K<sup>+</sup> channel and demonstration of its presence in the human BK channel. *Neuron* **29**, 593-601.

Jiang, Y., Ruta, V., Chen, J., Lee, A., & MacKinnon, R. (2003c). The principle of gating charge movement in a voltage-dependent K<sup>+</sup> channel. *Nature* **423**, 42-48.

Jing, J., Chikvashvili, D., Singer-Lahat, D., Thornhill, W. B., Reuveny, E., & Lotan, I. (1999). Fast inactivation of a brain K<sup>+</sup> channel composed of K<sub>v</sub>1.1 and K<sub>v</sub>β1.1 subunits modulated by G protein βγ-subunits. *EMBO Journal* **18**, 1245-1256.

Johnson, J. P., Jr. & Zagotta, W. N. (2001). Rotational movement during cyclic nucleotide-gated channel opening. *Nature* **412**, 917-921.

Johnstone, D. B., Wei, A., Butler, A., Salkoff, L., & Thomas, J. H. (1997). Behavioral defects in *C. elegans egl-36* mutants result from potassium channels shifted in voltage-dependence of activation. *Neuron* **19**, 151-164.

Jones, S. W. & Marks, T. N. (1989). Calcium currents in bullfrog sympathetic neurons. II. Inactivation. *J.Gen.Physiol* **94**, 169-182.

Ju, M., Stevens, L., Leadbitter, E., & Wray, D. (2003). The Roles of N- and C-terminal determinants in the activation of the Kv2.1 potassium channel. *Journal of Biological Chemistry* **278**, 12769-12778.

Kaupp, U. B. & Seifert, R. (2002). Cyclic nucleotide-gated ion channels. *Physiol Rev.* **82**, 769-824.

Kerschensteiner, D., Monje, F., & Stocker, M. (2003). Structural determinants of the regulation of the voltage-gated potassium channel Kv2.1 by the modulatory alpha-subunit Kv9.3. *Journal of Biological Chemistry* **278**, 18154-18161.

Kerschensteiner, D. & Stocker, M. (1999). Heteromeric assembly of Kv2.1 with Kv9.3: Effect on the state dependence of inactivation. *Biophysical Journal* **77**, 248-257.

Kim, L. A., Furst, J., Gutierrez, D., Butler, M. H., Xu, S., Goldstein, S. A., & Grigorieff, N. (2004). Three-dimensional structure of I<sub>to</sub>; Kv4.2-KChIP2 ion channels by electron microscopy at 21 Å resolution. *Neuron* **41**, 513-519.

Kirsch, G. E., Pascual, J. M., & Shieh, C.-C. (1995). Functional role of a conserved aspartate in the external mouth of voltage-gated potassium channels. *Biophysical Journal* **68**, 1804-1813.

Kiss, L., Immke, D., LoTurco, J., & Korn, S. J. (1998). The interaction of Na<sup>+</sup> and K<sup>+</sup> in voltage-gated potassium channels - Evidence for cation binding sites of different affinity. *Journal of General Physiology* **111**, 195-206.

Kiss, L. & Korn, S. J. (1998). Modulation of C-type inactivation by K<sup>+</sup> at the potassium channel selectivity filter. *Biophysical Journal* **74**, 1840-1849.

Kiss, L., LoTurco, J., & Korn, S. J. (1999). Contribution of the selectivity filter to inactivation in potassium channels. *Biophysical Journal* **76**, 253-263.

Klemic, K. G., Kirsch, G. E., & Jones, S. W. (2001). U-type inactivation of Kv3.1 and *Shaker* potassium channels. *Biophysical Journal* **81**, 814-826.

Klemic, K. G., Shieh, C. C., Kirsch, G. E., & Jones, S. W. (1998). Inactivation of Kv2.1 potassium channels. *Biophysical Journal* **74**, 1779-1789.

Kobertz, W. R. & Miller, C. (1999). K<sup>+</sup> channels lacking the 'tetramerization' domain: implications for pore structure. *Nature Structural Biology* **6**, 1122-1125.

Kobertz, W. R., Williams, C., & Miller, C. (2000). Hanging gondola structure of the T1 domain in a voltage-gated K<sup>+</sup> channel. *Biochemistry* **39**, 10347-10352.

Kondoh, S., Ishii, K., Nakamura, Y., & Taira, N. (1997). A mammalian transient type K<sup>+</sup> channel, rat Kv1.4, has two potential domains that could produce rapid inactivation. *Journal of Biological Chemistry* **272**, 19333-19338.

Korn, S. J. & Ikeda, S. R. (1995). Permeation selectivity by competition in a delayed rectifier potassium channel. *Science* **269**, 410-412.

Kramer, J. W., Post, M. A., Brown, A. M., & Kirsch, G. E. (1998). Modulation of potassium channel gating by coexpression of Kv2.1 with regulatory Kv5.1 or Kv6.1  $\alpha$ -subunits. *Am.J.Physiol.Cell Physiol.* **274**, C1501-C1510.

Kreusch, A., Pfaffinger, P. J., Stevens, C. F., & Choe, S. (1998). Crystal structure of the tetramerization domain of the *Shaker* potassium channel. *Nature* **392**, 945-948.

Kuo, A., Gulbis, J. M., Antcliff, J. F., Rahman, T., Lowe, E. D., Zimmer, J., Cuthbertson, J., Ashcroft, F. M., Ezaki, T., & Doyle, D. A. (2003). Crystal structure of the potassium channel KirBac1.1 in the closed state. *Science* **300**, 1922-1926.

Kuo, C. C. (1997). Deactivation retards recovery from inactivation in *Shaker* K<sup>+</sup> channels. *Journal of Neuroscience* **17**, 3436-3444.

Kuo, C. C. & Bean, B. P. (1994). Na<sup>+</sup> channels must deactivate to recover from inactivation. *Neuron* **12**, 819-829.

Kupper, J., Bowlby, M. R., Marom, S., & Levitan, I. B. (1995). Intracellular and extracellular amino acids that influence C-type inactivation and its modulation in a voltage-dependent potassium channel. *Pflugers Archiv* **430**, 1-11.

Kurata, H. T., Soon, G. S., Eldstrom, J. R., Lu, G. W., Steele, D. F., & Fedida, D. (2002). Amino-terminal determinants of U-type inactivation of voltage-gated K<sup>+</sup> channels. *Journal of Biological Chemistry* **277**, 29045-29053.

Kurata, H. T., Soon, G. S., & Fedida, D. (2001). Altered state dependence of C-type inactivation in the long and short forms of human Kv1.5. *J.Gen.Physiol* **118**, 315-332.

Kurata, H. T., Wang, Z., & Fedida, D. (2004). NH<sub>2</sub>-terminal inactivation peptide binding to C-type-inactivated Kv channels. *J.Gen.Physiol* **123**, 505-520.

Kwak, Y. G., Hu, N. N., Wei, J., George, A. L., Grobaski, T. D., Tamkun, M. M., & Murray, K. T. (1999). Protein kinase A phosphorylation alters Kvβ1.3 subunit-mediated inactivation of the Kv1.5 potassium channel. *Journal of Biological Chemistry* **274**, 13928-13932.

Labro, A. J., Raes, A. L., Bellens, I., Ottschytsch, N., & Snyders, D. J. (2003). Gating of *Shaker*-type channels requires the flexibility of S6 caused by prolines. *Journal of Biological Chemistry* **278**, 50724-50731.

Laine, M., Lin, M. C., Bannister, J. P., Silverman, W. R., Mock, A. F., Roux, B., & Papazian, D. M. (2003). Atomic proximity between S4 segment and pore domain in *Shaker* potassium channels. *Neuron* **39**, 467-481.

Laine, M., Papazian, D. M., & Roux, B. (2004). Critical assessment of a proposed model of *Shaker*. *FEBS Lett.* **564**, 257-263.

- Larsson, H. P., Baker, O. S., Dhillon, D. S., & Isacoff, E. Y. (1996). Transmembrane movement of the *Shaker* K<sup>+</sup> channel S4. *Neuron* **16**, 387-397.
- Larsson, H. P. & Elinder, F. (2000). A conserved glutamate is important for slow inactivation in K<sup>+</sup> channels. *Neuron* **27**, 573-583.
- Lee, T. E., Philipson, L. H., Kuznetsov, A., & Nelson, D. J. (1994). Structural determinant for assembly of mammalian K<sup>+</sup> channels. *Biophysical Journal* **66**, 667-673.
- Lee, T. E., Philipson, L. H., & Nelson, D. J. (1996). N-type inactivation in the mammalian *Shaker* K<sup>+</sup> channel Kv1.4. *Journal of Membrane Biology* **151**, 225-235.
- Levy, D. I. & Deutsch, C. (1996a). A voltage-dependent role for K<sup>+</sup> in recovery from C-type inactivation. *Biophysical Journal* **71**, 3157-3166.
- Levy, D. I. & Deutsch, C. (1996b). Recovery from C-type inactivation is modulated by extracellular potassium. *Biophysical Journal* **70**, 798-805.
- Li, M., Isacoff, E., Jan, Y. N., & Jan, L. Y. (1993). Assembly of potassium channels. *Ann.NY Acad.Sci.* **707**, 51-59.
- Li, M., Jan, Y. N., & Jan, L. Y. (1992). Specification of subunit assembly by the hydrophilic amino-terminal domain of the *Shaker* potassium channel. *Science* **257**, 1225-1230.
- Li, X., Bett, G. C., Jiang, X., Bondarenko, V. E., Morales, M. J., & Rasmusson, R. L. (2003). Regulation of N- and C-type inactivation of Kv1.4 by pH<sub>o</sub> and K<sup>+</sup>: evidence for transmembrane communication. *Am.J.Physiol Heart Circ.Physiol* **284**, H71-H80.
- Li-Smerin, Y., Hackos, D. H., & Swartz, K. J. (2000). A localized interaction surface for voltage-sensing domains on the pore domain of a K<sup>+</sup> channel. *Neuron* **25**, 411-423.
- Liman, E. R., Hess, P., Weaver, F., & Koren, G. (1991). Voltage-sensing residues in the S4 region of a mammalian K<sup>+</sup> channel. *Nature* **353**, 752-756.
- Liu, J. & Siegelbaum, S. A. (2000). Change of pore helix conformational state upon opening of cyclic nucleotide-gated channels. *Neuron* **28**, 899-909.

- Liu, Y., Holmgren, M., Jurman, M. E., & Yellen, G. (1997). Gated access to the pore of a voltage-dependent K<sup>+</sup> channel. *Neuron* **19**, 175-184.
- Liu, Y., Jurman, M. E., & Yellen, G. (1996). Dynamic rearrangement of the outer mouth of a K<sup>+</sup> channel during gating. *Neuron* **16**, 859-867.
- Loots, E. & Isacoff, E. Y. (1998). Protein rearrangements underlying slow inactivation of the *Shaker* K<sup>+</sup> channel. *Journal of General Physiology* **112**, 377-389.
- Loots, E. & Isacoff, E. Y. (2000). Molecular coupling of S4 to a K<sup>+</sup> channel's slow inactivation gate. *Journal of General Physiology* **116**, 623-635.
- Lopez-Barneo, J., Hoshi, T., Heinemann, S. H., & Aldrich, R. W. (1993). Effects of external cations and mutations in the pore region on C-type inactivation of *Shaker* potassium channels. *Receptors and Channels* **1**, 61-71.
- Lu, Z., Klem, A. M., & Ramu, Y. (2001). Ion conduction pore is conserved among potassium channels. *Nature* **413**, 809-813.
- Lu, Z., Klem, A. M., & Ramu, Y. (2002). Coupling between voltage sensors and activation gate in voltage-gated K<sup>+</sup> channels. *J.Gen.Physiol* **120**, 663-676.
- Ma, D. & Jan, L. Y. (2002). ER transport signals and trafficking of potassium channels and receptors. *Curr.Opin.Neurobiol.* **12**, 287-292.
- MacKinnon, R. (1991). Determination of the subunit stoichiometry of a voltage-activated potassium channel. *Nature* **350**, 232-235.
- MacKinnon, R. (2003). Potassium channels. *FEBS Lett.* **555**, 62-65.
- MacKinnon, R., Aldrich, R. W., & Lee, A. W. (1993). Functional stoichiometry of *Shaker* potassium channel inactivation. *Science* **262**, 757-759.
- Mannuzzu, L. M., Moronne, M. M., & Isacoff, E. Y. (1996). Direct physical measurement of conformational rearrangement underlying potassium channel gating. *Science* **271**, 213-216.
- Marom, S. & Abbott, L. F. (1994). Modeling state-dependent inactivation of membrane currents. *Biophysical Journal* **67**, 515-520.

- Maruoka, N. D., Steele, D. F., Au, B. P. Y., Dan, P., Zhang, X., Moore, E. D. W., & Fedida, D. (2000).  $\alpha$ -Actinin-2 couples to cardiac Kv1.5 channels, regulating current density and channel localization in HEK cells. *FEBS Letters* **473**, 188-194.
- Miller, C. (2000). Ion channels: doing hard chemistry with hard ions. *Curr. Opin. Chem. Biol.* **4**, 148-151.
- Milligan, C. J. & Wray, D. (2000). Local movement in the S2 region of the voltage-gated potassium channel hKv2.1 studied using cysteine mutagenesis. *Biophysical Journal* **78**, 1852-1861.
- Minor, D. L. Jr., Lin, Y. F., Mobley, B. C., Avelar, A., Jan, Y. N., Jan, L. Y., & Berger, J. M. (2000). The polar T1 interface is linked to conformational changes that open the voltage-gated potassium channel. *Cell* **102**, 657-670.
- Mitcheson, J. S., Chen, J., Lin, M., Culberson, C., & Sanguinetti, M. C. (2000). A structural basis for drug-induced long QT syndrome. *Proc. Natl. Acad. Sci. U.S.A* **97**, 12329-12333.
- Molina, A., Castellano, A. G., & Lopez-Barneo, J. (1997). Pore mutations in *Shaker* K<sup>+</sup> channels distinguish between the sites of tetraethylammonium blockade and C-type inactivation. *J. Physiol* **499 ( Pt 2)**, 361-367.
- Morales, M. J., Castellino, R. C., Crews, A. L., Rasmusson, R. L., & Strauss, H. C. (1995). A novel  $\beta$  subunit increases rate of inactivation of specific voltage-gated potassium channel  $\alpha$  subunits. *Journal of Biological Chemistry* **270**, 6272-6277.
- Murrell-Lagnado, R. D. & Aldrich, R. W. (1993a). Energetics of *Shaker* K channels blocked by inactivation peptides. *Journal of General Physiology* **102**, 977-1004.
- Murrell-Lagnado, R. D. & Aldrich, R. W. (1993b). Interactions of the amino terminal domains of *Shaker* K channels with a pore blocking site studied with synthetic peptides. *Journal of General Physiology* **102**, 949-976.
- Neyton, J. & Miller, C. (1988a). Discrete Ba<sup>2+</sup> block as a probe of ion occupancy and pore structure in the high-conductance Ca<sup>2+</sup>-activated K<sup>+</sup> channel. *Journal of General Physiology* **92**, 569-586.
- Neyton, J. & Miller, C. (1988b). Potassium blocks barium permeation through a calcium-activated potassium channel. *J. Gen. Physiol* **92**, 549-567.

Nguyen, T. P. & Horn, R. (2002). Movement and crevices around a sodium channel S3 segment. *J.Gen.Physiol* **120**, 419-436.

Nishida, M. & MacKinnon, R. (2002). Structural basis of inward rectification: cytoplasmic pore of the G protein-gated inward rectifier GIRK1 at 1.8 Å resolution. *Cell* **111**, 957-965.

Nitabach, M. N., Llamas, D. A., Araneda, R. C., Intile, J. L., Thompson, I. J., Zhou, Y. I., & Holmes, T. C. (2001). A mechanism for combinatorial regulation of electrical activity: Potassium channel subunits capable of functioning as Src homology 3-dependent adaptors. *Proc.Natl.Acad.Sci.U.S.A* **98**, 705-710.

Noda, M., Shimizu, S., Tanabe, T., Takai, T., Kayano, T., Ikeda, T., Takahashi, H., Nakayama, H., Kanaoka, Y., Minamino, N., & . (1984). Primary structure of Electrophorus electricus sodium channel deduced from cDNA sequence. *Nature* **312**, 121-127.

Ogielska, E. M. & Aldrich, R. W. (1998). A mutation in S6 of shaker potassium channels decreases the K<sup>+</sup> affinity of an ion binding site revealing ion-ion interactions in the pore. *Journal of General Physiology* **112**, 243-257.

Ogielska, E. M. & Aldrich, R. W. (1999). Functional consequences of a decreased potassium affinity in a potassium channel pore - *Ion interactions and C-type inactivation* . *Journal of General Physiology* **113**, 347-358.

Ogielska, E. M., Zagotta, W. N., Hoshi, T., Heinemann, S. H., Haab, J., & Aldrich, R. W. (1995). Cooperative subunit interactions in C-type inactivation of K channels. *Biophysical Journal* **69**, 2449-2457.

Olcese, R., Latorre, R., Toro, L., Bezanilla, F., & Stefani, E. (1997). Correlation between charge movement and ionic current during slow inactivation in *Shaker* K<sup>+</sup> channels. *Journal of General Physiology* **110**, 579-589.

Olcese, R., Sigg, D., Latorre, R., Bezanilla, F., & Stefani, E. (2001). A conducting state with properties of a slow inactivated state in a *Shaker* K<sup>+</sup> channel mutant. *Journal of General Physiology* **117**, 149-163.

Orlova, E. V., Papakosta, M., Booy, F. P., van Heel, M., & Dolly, J. O. (2003). Voltage-gated K<sup>+</sup> channel from mammalian brain: 3D structure at 18Å of the complete  $\alpha_4\beta_4$  complex. *J.Mol.Biol.* **326**, 1005-1012.

Overturf, K. E., Russell, S. N., Carl, A., Vogalis, F., Hart, P. J., Hume, J. R., Sanders, K. M., & Horowitz, B. (1994). Cloning and characterization of a  $K_v1.5$  delayed rectifier  $K^+$  channel from vascular and visceral smooth muscles. *Am.J.Physiol.Cell Physiol.* **267**, C1231-C1238.

Padanilam, B. J., Lu, T., Hoshi, T., Padanilam, B. A., Shibata, E. F., & Lee, H. C. (2002). Molecular determinants of intracellular pH modulation of human  $K_v1.4$  N-type inactivation. *Mol.Pharmacol.* **62**, 127-134.

Panyi, G., Sheng, Z., Tu, L., & Deutsch, C. (1995). C-type inactivation of a voltage-gated  $K^+$  channel occurs by a cooperative mechanism. *Biophysical Journal* **69**, 896-903.

Papazian, D. M., Schwarz, T. L., Tempel, B. L., Jan, Y. N., & Jan, L. Y. (1987). Cloning of genomic and complementary DNA from *Shaker*, a putative potassium channel gene from *Drosophila*. *Science* **237**, 749-753.

Papazian, D. M., Shao, X. M., Seoh, S.-A., Mock, A. F., Huang, Y., & Wainstock, D. H. (1995). Electrostatic interactions of S4 voltage sensor in *Shaker*  $K^+$  channel. *Neuron* **14**, 1293-1301.

Papazian, D. M., Timpe, L. C., Jan, Y. N., & Jan, L. Y. (1991). Alteration of voltage-dependence of *Shaker* potassium channel by mutations in the S4 sequence. *Nature* **349**, 305-310.

Pardo, L. A., Heinemann, S. H., Terlau, H., Ludewig, U., Lorra, C., Pongs, O., & Stuhmer, W. (1992). Extracellular  $K^+$  specifically modulates a rat brain  $K^+$  channel. *Proc.Natl.Acad.Sci.U.S.A* **89**, 2466-2470.

Pascual, J. M., Shieh, C. C., Kirsch, G. E., & Brown, A. M. (1997). Contribution of the  $NH_2$  terminus of  $K_v2.1$  to channel activation. *Am.J.Physiol* **273**, C1849-C1858.

Patil, P. G., Brody, D. L., & Yue, D. T. (1998). Preferential closed-state inactivation of neuronal calcium channels. *Neuron* **20**, 1027-1038.

Perozo, E., MacKinnon, R., Bezanilla, F., & Stefani, E. (1993). Gating currents from a non-conducting mutant reveal open-closed conformation in *Shaker*  $K^+$  channels. *Neuron* **11**, 353-358.

Perozo, E., Santacruz-Tolozza, L., Stefani, E., Bezanilla, F., & Papazian, D. M. (1994). S4 mutations alter gating currents of *Shaker* K channels. *Biophysical Journal* **66**, 345-354.

- Peterson, B. Z., DeMaria, C. D., Adelman, J. P., & Yue, D. T. (1999). Calmodulin is the  $\text{Ca}^{2+}$  sensor for  $\text{Ca}^{2+}$ -dependent inactivation of L-type calcium channels. *Neuron* **22**, 549-558.
- Phillips, L. R., Enkvetchakul, D., & Nichols, C. G. (2003). Gating dependence of inner pore access in inward rectifier  $\text{K}^+$  channels. *Neuron* **37**, 953-962.
- Phillips, L. R. & Nichols, C. G. (2003). Ligand-induced closure of inward rectifier Kir6.2 channels traps spermine in the pore. *J.Gen.Physiol* **122**, 795-804.
- Piskorowski, R. & Aldrich, R. W. (2002). Calcium activation of  $\text{BK}_{\text{Ca}}$  potassium channels lacking the calcium bowl and RCK domains. *Nature* **420**, 499-502.
- Pongs, O., Leicher, T., Berger, M., Roeper, J., Bähring, R., Wray, D., Giese, K. P., Silva, A. J., & Storm, J. F. (1999). Functional and molecular aspects of voltage-gated  $\text{K}^+$  channel  $\beta$  subunits. *Annals of the New York Academy of Sciences* **868**, 344-355.
- Proks, P., Antcliff, J. F., & Ashcroft, F. M. (2003). The ligand-sensitive gate of a potassium channel lies close to the selectivity filter. *EMBO Rep.* **4**, 70-75.
- Rasmusson, R. L., Morales, M. J., Castellino, R. C., Zhang, Y., Campbell, D. L., & Strauss, H. C. (1995). C-type inactivation controls recovery in a fast inactivating cardiac  $\text{K}^+$  channel ( $\text{Kv}1.4$ ) expressed in *Xenopus* oocytes. *Journal of Physiology* **489**, 709-721.
- Rasmusson, R. L., Morales, M. J., Wang, S., Liu, S., Campbell, D. L., Brahmajothi, M. V., & Strauss, H. C. (1998). Inactivation of voltage-gated cardiac  $\text{K}^+$  channels. *Circulation Research* **82**, 739-750.
- Rehm, H. & Lazdunski, M. (1988). Purification and subunit structure of a putative  $\text{K}^+$ -channel protein identified by its binding properties for dendrotoxin I. *Proceedings of the National Academy of Sciences of the USA* **85**, 4919-4923.
- Rettig, J., Heinemann, S. H., Wunder, F., Lorra, C., Parcej, D. N., Dolly, J. O., & Pongs, O. (1994). Inactivation properties of voltage-gated  $\text{K}^+$  channels altered by presence of  $\beta$ -subunit. *Nature* **369**, 289-294.
- Robinson, R. B. & Siegelbaum, S. A. (2003). Hyperpolarization-activated cation currents: from molecules to physiological function. *Annu.Rev.Physiol* **65**, 453-480.

- Rosenthal, J. J. & Bezanilla, F. (2002). Extensive editing of mRNAs for the squid delayed rectifier K<sup>+</sup> channel regulates subunit tetramerization. *Neuron* **34**, 743-757.
- Roux, B. & MacKinnon, R. (1999). The cavity and pore helices in the KcsA K<sup>+</sup> channel: electrostatic stabilization of monovalent cations. *Science* **285**, 100-102.
- Roux, M. J., Olcese, R., Toro, L., Bezanilla, F., & Stefani, E. (1998). Fast inactivation in *Shaker* K<sup>+</sup> channels - Properties of ionic and gating currents. *Journal of General Physiology* **111**, 625-638.
- Ruppertsberg, J. P., Frank, R., Pongs, O., & Stocker, M. (1991). Cloned neuronal I<sub>K<sub>A</sub></sub> channels reopen during recovery from inactivation. *Nature* **353**, 657-660.
- Russell, S. N., Publicover, N. G., Hart, P. J., Carl, A., Hume, J. R., Sanders, K. M., & Horowitz, B. (1994). Block by 4-aminopyridine of a Kv1.2 delayed rectifier K<sup>+</sup> current expressed in *Xenopus* oocytes. *J. Physiol* **481**, 571-584.
- Ruta, V., Jiang, Y., Lee, A., Chen, J., & MacKinnon, R. (2003). Functional analysis of an archaeobacterial voltage-dependent K<sup>+</sup> channel. *Nature* **422**, 180-185.
- Sasaki, Y., Ishii, K., Nunoki, K., Yamagishi, T., & Taira, N. (1995). The voltage-dependent K<sup>+</sup> channel (Kv1.5) cloned from rabbit heart and facilitation of inactivation of the delayed rectifier current by the rat β subunit. *FEBS Lett.* **372**, 20-24.
- Scannevin, R. H., Wang, K., Jow, F., Megules, J., Kopsco, D. C., Edris, W., Carroll, K. C., Lu, Q., Xu, W., Xu, Z., Katz, A. H., Olland, S., Lin, L., Taylor, M., Stahl, M., Malakian, K., Somers, W., Mosyak, L., Bowlby, M. R., Chanda, P., & Rhodes, K. J. (2004). Two N-terminal domains of Kv4 K<sup>+</sup> channels regulate binding to and modulation by KCHIP1. *Neuron* **41**, 587-598.
- Schaffer, P., Pelzmann, B., Bernhart, E., Lang, P., Lokebo, J. E., Mächler, H., Rigler, B., & Koidl, B. (1998). Estimation of outward currents in isolated human atrial myocytes using inactivation time course analysis. *Pflugers Archiv* **436**, 457-468.
- Schlieff, T., Schonherr, R., & Heinemann, S. H. (1996). Modification of C-type inactivating *Shaker* potassium channels by chloramine-T. *Pflugers Archiv* **431**, 483-493.
- Schoppa, N. E., McCormack, K., Tanouye, M. A., & Sigworth, F. J. (1992). The size of gating charge in wild-type and mutant *Shaker* potassium channels. *Science* **255**, 1712-1715.

- Schoppa, N. E. & Sigworth, F. J. (1998a). Activation of *Shaker* potassium channels I. Characterization of voltage-dependent transitions. *Journal of General Physiology* **111**, 271-294.
- Schoppa, N. E. & Sigworth, F. J. (1998b). Activation of *Shaker* potassium channels III. An activation gating model for wild-type and V2 mutant channels. *Journal of General Physiology* **111**, 313-342.
- Schulteis, C. T., Nagaya, N., & Papazian, D. M. (1996). Intersubunit interaction between amino- and carboxyl-terminal cysteine residues in tetrameric *Shaker* K<sup>+</sup> channels. *Biochemistry* **35**, 12133-12140.
- Segal, A. S., Yao, X., & Desir, G. V. (1999). The T0 domain of rabbit Kv1.3 regulates steady state channel protein level. *Biochem.Biophys.Res. Commun.* **254**, 54-64.
- Seoh, S. A., Sigg, D., Papazian, D. M., & Bezanilla, F. (1996). Voltage-sensing residues in the S2 and S4 segments of the *Shaker* K<sup>+</sup> channel. *Neuron* **16**, 1159-1167.
- Sewing, S., Roeper, J., & Pongs, O. (1996). Kv $\beta$ 1 subunit binding specific for *Shaker*-related potassium channel  $\alpha$  subunits. *Neuron* **16**, 455-463.
- Shahidullah, M., Rocha, C., & Covarrubias, M. (2003). The intersubunit Zn<sup>2+</sup> binding site in the T1 domain as a putative locus of inactivation gating in Kv4 channels. *Biophysical Journal* **84**, 77A.
- Shen, N. V., Chen, X., Boyer, M. M., & Pfaffinger, P. J. (1993). Deletion analysis of K<sup>+</sup> channel assembly. *Neuron* **11**, 67-76.
- Shen, N. V. & Pfaffinger, P. J. (1995). Molecular recognition and assembly sequences involved in the subfamily-specific assembly of voltage-gated K<sup>+</sup> channel subunit proteins. *Neuron* **14**, 625-633.
- Sheng, M., Liao, Y. J., Jan, Y. N., & Jan, L. Y. (1993). Presynaptic A-current based on heteromultimeric K<sup>+</sup> channels detected in vivo. *Nature* **365**, 72-75.
- Sheng, Z. F., Skach, W., Santarelli, V., & Deutsch, C. (1997). Evidence for interaction between transmembrane segments in assembly of Kv1.3. *Biochemistry* **36**, 15501-15513.

Shikano, S. & Li, M. (2003). Membrane receptor trafficking: evidence of proximal and distal zones conferred by two independent endoplasmic reticulum localization signals. *Proc.Natl.Acad.Sci.U.S.A* **100**, 5783-5788.

Smith, P. L., Baukrowitz, T., & Yellen, G. (1996). The inward rectification mechanism of the HERG cardiac potassium channel. *Nature* **379**, 833-836.

Sokolova, O., Accardi, A., Gutierrez, D., Lau, A., Rigney, M., & Grigorieff, N. (2003). Conformational changes in the C terminus of *Shaker* K<sup>+</sup> channel bound to the rat Kvβ2-subunit. *Proc.Natl.Acad.Sci.U.S.A* **100**, 12607-12612.

Sokolova, O., Kolmakova-Partensky, L., & Grigorieff, N. (2001). Three-dimensional structure of a voltage-gated potassium channel at 2.5 nm resolution. *Structure* **9**, 215-220.

Stampe, P., Arreola, J., Pérez-Cornejo, P., & Begenisich, T. (1998). Nonindependent K<sup>+</sup> movement through the pore in IRK1 potassium channels. *Journal of General Physiology* **112**, 475-484.

Stampe, P. & Begenisich, T. (1996). Unidirectional K<sup>+</sup> fluxes through recombinant *Shaker* potassium channels expressed in single *Xenopus* oocytes. *Journal of General Physiology* **107**, 449-457.

Starace, D. M. & Bezanilla, F. (2004). A proton pore in a potassium channel voltage sensor reveals a focused electric field. *Nature* **427**, 548-553.

Starace, D. M., Stefani, E., & Bezanilla, F. (1997). Voltage-dependent proton transport by the voltage sensor of the *Shaker* K<sup>+</sup> channel. *Neuron* **19**, 1319-1327.

Starkus, J. G., Kuschel, L., Rayner, M. D., & Heinemann, S. H. (1997). Ion conduction through C-type inactivated *Shaker* channels. *Journal of General Physiology* **110**, 539-550.

Starkus, J. G., Kuschel, L., Rayner, M. D., & Heinemann, S. H. (1998). Macroscopic Na<sup>+</sup> currents in the "nonconducting" *Shaker* potassium channel mutant W434F. *Journal of General Physiology* **112**, 85-93.

Starkus, J. G., Varga, Z., Schonherr, R., & Heinemann, S. H. (2003). Mechanisms of the inhibition of *Shaker* potassium channels by protons. *Pflugers Archiv* **447**, 44-54.

- Stefani, E., Toro, L., Perozo, E., & Bezanilla, F. (1994). Gating of *Shaker* K<sup>+</sup> channels: I. Ionic and gating currents. *Biophysical Journal* **66**, 996-1010.
- Steidl, J. V. & Yool, A. J. (1999). Differential sensitivity of voltage-gated potassium channels Kv1.5 and Kv1.2 to acidic pH and molecular identification of pH sensor. *Mol.Pharmacol.* **55**, 812-820.
- Stocker, M. & Kerschensteiner, D. (1998). Cloning and tissue distribution of two new potassium channel  $\alpha$ -subunits from rat brain. *Biochem.Biophys.Res.Commun.* **248**, 927-934.
- Stocker, M., Stuhmer, W., Wittka, R., Wang, X., Muller, R., Ferrus, A., & Pongs, O. (1990). Alternative *Shaker* transcripts express either rapidly inactivating or noninactivating K<sup>+</sup> channels. *Proc.Natl.Acad.Sci.U.S.A* **87**, 8903-8907.
- Strang, C., Cushman, S. J., DeRubeis, D., Peterson, D., & Pfaffinger, P. J. (2001). A central role for the T1 domain in voltage-gated potassium channel formation and function. *Journal of Biological Chemistry* **276**, 28493-28502.
- Sun, Z. P., Akabas, M. H., Goulding, E. H., Karlin, A., & Siegelbaum, S. A. (1996). Exposure of residues in the cyclic nucleotide-gated channel pore: P region structure and function in gating. *Neuron* **16**, 141-149.
- Tagliatela, M., Champagne, M. S., Drewe, J. A., & Brown, A. M. (1994). Comparison of H5, S6, and H5-S6 exchanges on pore properties of voltage-dependent K<sup>+</sup> channels. *Journal of Biological Chemistry* **269**, 13867-13873.
- Tamkun, M. M., Knoth, K. M., Walbridge, J. A., Kroemer, H., Roden, D. M., & Glover, D. H. (1991). Molecular cloning and characterization of two voltage-gated K<sup>+</sup> channel cDNAs from human ventricle. *FASEB Journal* **5**, 331-337.
- Tempel, B. L., Papazian, D. M., Schwarz, T. L., Jan, Y. N., & Jan, L. Y. (1987). Sequence of a probable potassium channel component encoded at *Shaker* locus of *Drosophila*. *Science* **237**, 770-775.
- Thompson, J. D., Higgins, D. G., & Gibson, T. J. (1994). CLUSTAL W: improving the sensitivity of progressive multiple sequence alignment through sequence weighting, position-specific gap penalties and weight matrix choice. *Nucleic Acids Res.* **22**, 4673-4680.

Tiwari-Woodruff, S. K., Lin, M. A., Schulteis, C. T., & Papazian, D. M. (2000). Voltage-dependent structural interactions in the *Shaker* K<sup>+</sup> channel. *J.Gen.Physiol* **115**, 123-138.

Tiwari-Woodruff, S. K., Schulteis, C. T., Mock, A. F., & Papazian, D. M. (1997). Electrostatic interactions between transmembrane segments mediate folding of *Shaker* K<sup>+</sup> channel subunits. *Biophysical Journal* **72**, 1489-1500.

Tristani-Firouzi, M., Chen, J., & Sanguinetti, M. C. (2002). Interactions between S4-S5 linker and S6 transmembrane domain modulate gating of HERG K<sup>+</sup> channels. *Journal of Biological Chemistry* **277**, 18994-19000.

Tu, L., Wang, J., Helm, A., Skach, W. R., & Deutsch, C. (2000). Transmembrane biogenesis of Kv1.3. *Biochemistry* **39**, 824-836.

Tu, L. W., Santarelli, V., Sheng, Z. F., Skach, W., Pain, D., & Deutsch, C. (1996). Voltage-gated K<sup>+</sup> channels contain multiple intersubunit association sites. *Journal of Biological Chemistry* **271**, 18904-18911.

Van Wagoner, D. R., Pond, A. L., McCarthy, P. M., Trimmer, J. S., & Nerbonne, J. M. (1997). Outward K<sup>+</sup> current densities and Kv1.5 expression are reduced in chronic human atrial fibrillation. *Circulation Research* **80**, 772-781.

VanDongen, A. M. J., Frech, G., Drewe, J. A., Joho, R. H., & Brown, A. M. (1990). Alteration and restoration of K<sup>+</sup> channel function by deletions at the N- and C-termini. *Neuron* **5**, 433-443.

Vergara, C., Alvarez, O., & Latorre, R. (1999). Localization of the K<sup>+</sup> lock-In and the Ba<sup>2+</sup> binding sites in a voltage-gated calcium-modulated channel. Implications for survival of K<sup>+</sup> permeability. *J.Gen.Physiol* **114**, 365-376.

Wagoner, P. K. & Oxford, G. S. (1987). Cation permeation through the voltage-dependent potassium channel in the squid axon. Characteristics and mechanisms. *J.Gen.Physiol* **90**, 261-290.

Wainger, B. J., DeGennaro, M., Santoro, B., Siegelbaum, S. A., & Tibbs, G. R. (2001). Molecular mechanism of cAMP modulation of HCN pacemaker channels. *Nature* **411**, 805-810.

- Wang, S., Morales, M. J., Qu, Y. J., Bett, G. C., Strauss, H. C., & Rasmusson, R. L. (2003). Kv1.4 channel block by quinidine: evidence for a drug-induced allosteric effect. *J. Physiol* **546**, 387-401.
- Wang, Z. & Fedida, D. (2001). Gating charge immobilization caused by the transition between inactivated states in the Kv1.5 channel. *Biophysical Journal* **81**, 2614-2627.
- Wang, Z. & Fedida, D. (2002). Uncoupling of gating charge movement and closure of the ion pore during recovery from inactivation in the Kv1.5 channel. *J. Gen. Physiol* **120**, 249-260.
- Wang, Z., Fermini, B., & Nattel, S. (1993). Delayed rectifier outward current and repolarization in human atrial myocytes. *Circulation Research* **73**, 276-285.
- Wang, Z., Hesketh, J. C., & Fedida, D. (2000a). A High-Na<sup>+</sup> conduction state during recovery from inactivation in the potassium channel Kv1.5. *Biophysical Journal* **89**, 23-45.
- Wang, Z., Zhang, X., & Fedida, D. (2000b). Regulation of transient Na<sup>+</sup> conductance by intra- and extracellular K<sup>+</sup> in the human delayed rectifier K<sup>+</sup> channel Kv1.5. *Journal of Physiology* **523 Pt 3**, 575-591.
- Webster, S. M., Del Camino, D., Dekker, J. P., & Yellen, G. (2004). Intracellular gate opening in *Shaker* K<sup>+</sup> channels defined by high-affinity metal bridges. *Nature* **428**, 864-868.
- Wissmann, R., Bildl, W., Oliver, D., Beyermann, M., Kalbitzer, H. R., Bentrop, D., & Fakler, B. (2003). Solution structure and function of the "tandem inactivation domain" of the neuronal A-type potassium channel Kv1.4. *Journal of Biological Chemistry* **278**, 16142-16150.
- Wray, D. (2003). The roles of intracellular regions in the activation of voltage-dependent potassium channels. *Eur. Biophys. J.*
- Xiao, J., Zhen, X. G., & Yang, J. (2003). Localization of PIP<sub>2</sub> activation gate in inward rectifier K<sup>+</sup> channels. *Nat. Neurosci.* **6**, 811-818.
- Xu, J., Yu, W. F., Jan, Y. N., Jan, L. Y., & Li, M. (1995). Assembly of voltage-gated potassium channels - Conserved hydrophilic motifs determine subfamily-specific interactions between the  $\alpha$ -subunits. *Journal of Biological Chemistry* **270**, 24761-24768.

- Xu, J., Yu, W. F., Wright, J. M., Raab, R. W., & Li, M. (1998). Distinct functional stoichiometry of potassium channel  $\beta$  subunits. *Proceedings of the National Academy of Sciences of the USA* **95**, 1846-1851.
- Yang, N., George, A. L., Jr., & Horn, R. (1996). Molecular basis of charge movement in voltage-gated sodium channels. *Neuron* **16**, 113-122.
- Yang, N. & Horn, R. (1995). Evidence for voltage-dependent S4 movement in sodium channels. *Neuron* **15**, 213-218.
- Yang, Y., Yan, Y., & Sigworth, F. J. (1997). How does the W434F mutation block current in *Shaker* potassium channels? *J.Gen.Physiol* **109**, 779-789.
- Yao, X., Liu, W., Tian, S., Rafi, H., Segal, A. S., & Desir, G. V. (2000). Close association of the N terminus of Kv1.3 with the pore region. *Journal of Biological Chemistry* **275**, 10859-10863.
- Yellen, G. (1998). The moving parts of voltage-gated ion channels. *Q.Rev.Biophys.* **31**, 239-295.
- Yellen, G. (2001). Keeping  $K^+$  completely comfortable. *Nat.Struct.Biol.* **8**, 1011-1013.
- Yellen, G. (2002). The voltage-gated potassium channels and their relatives. *Nature* **419**, 35-42.
- Yellen, G., Jurman, M. E., Abramson, T., & MacKinnon, R. (1991). Mutations affecting internal TEA blockade identify the probable pore-forming region of a  $K^+$  channel. *Science* **251**, 939-942.
- Yellen, G., Sodickson, D., Chen, T.-Y., & Jurman, M. E. (1994). An Engineered cysteine in the external mouth of a  $K^+$  channel allows inactivation to be modulated by metal binding. *Biophysical Journal* **66**, 1068-1075.
- Yool, A. J. & Schwarz, T. L. (1991). Alteration of ionic selectivity of a  $K^+$  channel by mutation of the H5 region. *Nature* **349**, 700-704.
- Yu, W., Xu, J., & Li, M. (1996). NAB domain is essential for the subunit assembly of both  $\alpha$ - $\alpha$  and  $\alpha$ - $\beta$  complexes of *Shaker*-like potassium channels. *Neuron* **16**, 441-453.

Zagotta, W. N., Hoshi, T., & Aldrich, R. W. (1990). Restoration of inactivation in mutants of *Shaker* potassium channels by a peptide derived from ShB. *Science* **250**, 568-571.

Zagotta, W. N., Hoshi, T., & Aldrich, R. W. (1994a). *Shaker* potassium channel gating. III: Evaluation of kinetic models for activation. *Journal of General Physiology* **103**, 321-362.

Zagotta, W. N., Hoshi, T., Dittman, J., & Aldrich, R. W. (1994b). *Shaker* potassium channel gating. II: Transitions in the activation pathway. *Journal of General Physiology* **103**, 279-319.

Zerangue, N., Jan, Y. N., & Jan, L. Y. (2000). An artificial tetramerization domain restores efficient assembly of functional *Shaker* channels lacking T1. *Proceedings of the National Academy of Sciences of the United States of America* **97**, 3591-3595.

Zerangue, N., Schwappach, B., Jan, Y. N., & Jan, L. Y. (1999). A new ER trafficking signal regulates the subunit stoichiometry of plasma membrane  $K_{ATP}$  channels. *Neuron* **22**, 537-548.

Zhang, S., Kehl, S. J., & Fedida, D. (2003a). Modulation of human ether-a-go-go-related  $K^+$  (HERG) channel inactivation by  $Cs^+$  and  $K^+$ . *J.Physiol* **548**, 691-702.

Zhang, S., Kurata, H. T., Kehl, S. J., & Fedida, D. (2003b). Rapid induction of P/C-type inactivation is the mechanism for acid-induced  $K^+$  current inhibition. *J.Gen.Physiol* **121**, 215-225.

Zheng, J. & Sigworth, F. J. (1997). Selectivity changes during activation of mutant *Shaker* potassium channels. *Journal of General Physiology* **110**, 101-117.

Zheng, J. & Sigworth, F. J. (1998). Intermediate conductances during deactivation of heteromultimeric *Shaker* potassium channels. *Journal of General Physiology* **112**, 457-474.

Zhou, M., Morais-Cabral, J. H., Mann, S., & MacKinnon, R. (2001a). Potassium channel receptor site for the inactivation gate and quaternary amine inhibitors. *Nature* **411**, 657-661.

Zhou, W., Qian, Y., Kunjilwar, K., Pfaffinger, P. J., & Choe, S. (2004). Structural insights into the functional interaction of KChIP1 with *Shal*-type  $K^+$  channels. *Neuron* **41**, 573-586.

Zhou, Y. & MacKinnon, R. (2004). Ion Binding Affinity in the Cavity of the KcsA Potassium Channel. *Biochemistry* **43**, 4978-4982.

Zhou, Y., Morais-Cabral, J. H., Kaufman, A., & MacKinnon, R. (2001b). Chemistry of ion coordination and hydration revealed by a K<sup>+</sup> channel-Fab complex at 2.0 Å resolution. *Nature* **414**, 43-48.